UNIVERSITY OF OKLAHOMA

GRADUATE COLLEGE

EXPERIMENTAL AND ADVANCED COMPUTATIONAL MODELLING STUDY OF DOWNHOLE ELASTOMER SEAL ASSEMBLIES

A DISSERTATION

SUBMITTED TO THE GRADUATE FACULTY

in partial fulfilment of the requirements for the

Degree of

DOCTOR OF PHILOSOPHY

By

HARSHKUMAR PATEL
Norman, Oklahoma
2020

EXPERIMENTAL AND ADVANCED COMPUTATIONAL MODELLING STUDY OF DOWNHOLE ELASTOMER SEAL ASSEMBLIES

A DISSERTATION APPROVED FOR THE
MEWBOURNE SCHOOL OF PETROLEUM AND GEOLOGICAL ENGINEERING

BY THE COMMITTEE CONSISTING OF

Dr. Saeed Salehi, Chair

Dr. Ramadan Ahmed, Co-Chair

Dr. Harold Stalford

Dr. Subhash Shah

Dr. Deepak Devegowda

To my loving family and teachers

Acknowledgement

Foremost, I would like to express my utmost gratitude to my PhD advisor Dr. Saeed Salehi for his invaluable academic guidance and relentless support throughout my doctoral studies. Words fall short in describing how much I have learnt from him! He showed great confidence in my abilities and trusted me with increasing responsibilities to shape me as a confident and independent researcher. He constantly introduced me to various opportunities to advance my professional career and helped me excel at them. I owe my scholarly achievements and research successes to his immense knowledge, constant encouragement, professional guidance, and financial support. I am profoundly grateful to have a mentor like him.

I am immensely grateful to my PhD co-chair Dr. Ramadan Ahmed for providing constant mentorship throughout my MS and PhD years. His insightful suggestions during research projects taught me valuable skills and greatly improved quality of my work. His cooperative nature and constant guidance greatly facilitated my journey as a scholar. I am also very thankful to him for admitting me into the PhD program and providing financial support during early year of my PhD.

I am deeply honored to have Dr. Subhash Shah as my mentor and PhD committee member. He identified my potential while I was in undergraduate studies, and provided me financial support and the opportunity to work under him during my MS degree. I am very grateful to him for shaping my early graduate years and preparing me for successful PhD studies. His immense knowledge, vast industry experience, and mentorship have greatly influenced my academic journey over the years.

I would like to sincerely thank Dr. Deepak Devegowda for providing valuable comments to improve the quality of this dissertation work. I am also thankful to him for providing continuous

academic and administrative guidance throughout my graduate studies. I am truly grateful to Dr. Harold Stalford for taking interest in my research work and providing valuable feedback from mechanical engineering perspective to enhance technical aspects of this research.

I am grateful to Bureau of Safety and Environmental Enforcement for partial financial support to this dissertation work. I am sincerely grateful to the office of the provost at University of Oklahoma for supporting this work through Nancy Mergler Dissertation completion fellowship. I would also like to thank Dr. Catalin Teodoriu for providing help and support during the project in the lab. I am extremely grateful to my colleagues Dr. Chinedum Ezeakacha, George Kwatia, and Shawgi Ahmed for supporting this dissertation work through help in experiments. Special thanks to my colleagues and friends Jeff McCaskill, Raj, Mustafa, Yuxing, Musaab, Feyi, Vineet, Soham, and Abhishek for making the workplace feel like home.

I am immensely grateful to the University of Oklahoma especially Mewbourne School of Petroleum and Geological Engineering for providing resources, financial support, and scholarly recognitions to support my graduate studies. I am deeply thankful to my industry mentors especially Dr. Hari Hariharan and colleagues at Shell and McDermott for teaching me valuable skills and preparing me for a successful career ahead.

Many thanks to Bella didi, Himanshu uncle, Vimlesh, Anuj, and Himani for being the family away from home. Special thanks to my friends at OU and back in India especially Varun, Deep, Parth, and Viral for giving me fondest memories during my academic journey. I would also like to thank all my teachers who have directly or indirectly helped me throughout my academic years.

I owe special thanks to my family without whom I wouldn't have made it so far. I am profoundly grateful to my wife Jainisha for always believing in me and standing by my side through thick and thin. I attribute my success to her constant love, support, and encouragement. I am deeply thankful to my parents Rajeshbhai and Chandrikaben for their love, blessings, and support in all my decisions. I will always be indebted to them for the sacrifices they have made to help me reach where I am today. I am deeply grateful to my father-in-law Amitbhai, mother-in-law Rakshaben, and brother-in-law Yug for their constant inspiration, love, and care. Many thanks goes to my entire extended family for looking after my parents while I have been away all these years.

Above all, my deepest gratitude and "vandan" to my Sadhgurus Maa and Bapu for being the divine force in my life without which nothing in my life is ever possible! I dedicate this dissertation to you!

Table of Contents

List of Tables

List of Figures

Abstract

Elastomers seals are widely used in various drilling, completion, and production equipment. One such equipment is liner hanger which has become integral part of modern well designs. Failure of liner hanger seal assembly can compromise well integrity, and lead to severe health, safety, and environmental consequences. Concerns regarding reliability of elastomer seals in liner hanger assemblies have been raised by the regulators as well as industry.

This dissertation work provides detailed investigation of design, and failure of downhole elastomer seal assemblies using experimentally supported advanced computational modeling techniques. This work is partially supported by Bureau of Safety and Environmental Enforcement (BSEE) and it is set in the context of liner hanger assemblies. However, major outcomes of this research also applies to other downhole seal assemblies. Specific objectives of this dissertation are - (i) investigate performance of liner hanger seal assembly under various design, operational, and failure scenarios, (ii) develop operating envelops and identify critical parameters influencing performance of the elastomer seal assembly, (iii) develop a modelling tool for predicting leakage through elastomer seal interface considering surface characteristics, (iv) generate guidelines for design and qualification of elastomer seals and provide regulatory recommendations.

Novel technical aspects of this research work are – (i) studying material behavior of different elastomer material (NBR, EPDM, FKM, FEPM, FFKM, PTFE) under normal and downhole conditions, (ii) using the elastomer material data in true-scale finite element (FEA) models to evaluate equipment level performance of seal, (iii) scaled laboratory tests and analytical calculations to validate FEA models, and (iv) development of a leakage modelling tool that can predict leakage rates as a function of surface topography of seal interface and operating conditions.

Results from this dissertation indicate that type and design of seal equipment determines which elastomer properties need to be qualified. Hardness and elastic modulus alone may not be good predictors of fitness-for-service of seal assembly. For example, performance of expandable liner hanger seal assembly primarily depends on seal dimensions and elastomer shear modulus while performance of conventional liner hanger seal assembly mainly depends on elastomer bulk modulus. Selection of appropriate elastomer material for a certain application depends not only on chemical environment and temperature but also on assembly design, operational constraints, and thermal changes. Comparative evaluation demonstrated that conventional liner hanger seal assembly outperforms expandable liner hanger seal assembly in terms of contact pressure generated per unit energization but it is more prone to failure than expandable assembly.

Contact pressure at seal-pipe interface, as predicted by macro-scale FEA models, does not accurately indicate fluid pressure that can be effectively sealed. Leakage modelling studies demonstrated that surface characteristics of elastomer and fluid properties determines the contact pressure needed to achieve complete sealability. Leakage modelling approach developed in this work can be an invaluable tool in seal design workflow for determining target seal energization needed for complete sealability.

Chapter 1: Introduction

1.1 Background

Elastomers are widely used in well construction as seal components in various drilling, completion, and wellhead equipment. Commonly used equipment containing elastomer seal components are – wellhead assemblies, blowout preventers, liner hangers, subsurface-safety valves, completion packers, bridge plugs, etc. Primary purpose of elastomer seal components in these equipment is to isolate and contain fluids within pipe, and/or annular section of wells and prevent communication with downhole and surface environment. Industry professionals consider seal design as a top technological challenge for future unconventional and High Pressure – High Temperature (HPHT) oil & gas exploration activities (Oil & Gas iQ 2015). Review of past loss of well control events (discussed in chapter 2) indicate that failure in seal containing equipment are responsible for almost half (46%) of the failures in secondary barrier (Patel et al. 2019a).

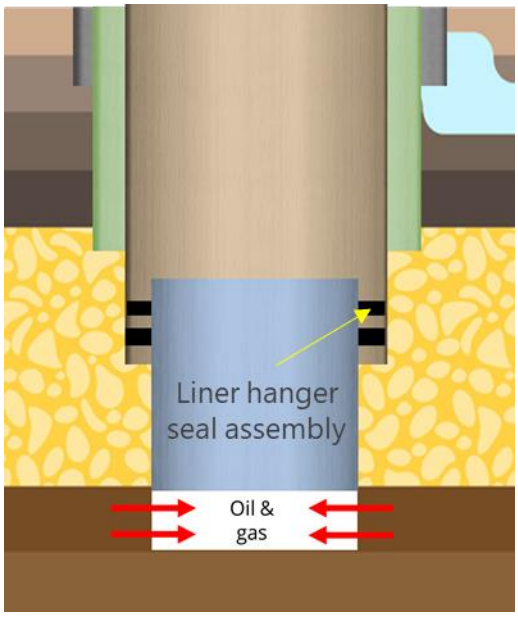

Figure 1.1: Schematic of well design with liner

One such equipment is liner hanger which has become integral part of modern well construction. Liners enable deeper well designs by eliminating the size constraints resulting from full casing strings ran all the way to surface. Plus, liner also saves overall costs by minimizing casing material needs. Unlike full casing string, which is suspended and isolated at the wellhead, liner string needs to be suspend from previous casing string and the liner-casing overlap needs to be isolated from fluids (**Figure 1.1**). These two requirements were originally addressed by the industry by running liner string with a hanger assembly and installing a liner top packer separately to isolate annular space. To minimize complexities and improve operational efficiency, industry developed and started deploying liner hangers with integrated seal assembly.

1.2 Motivation and Hypotheses

Unlike surface wellhead spool assembly used for full casing string, liner hanger assembly needs to operate in downhole conditions. Hence, maintaining reliability of liner hanger seal assembly become critical and relatively challenging. Failure of liner hanger seal assembly can compromise well integrity. Loss of well control, if not mitigated, can lead to severe health, safety, and environmental consequences (**Figure 1.2**).

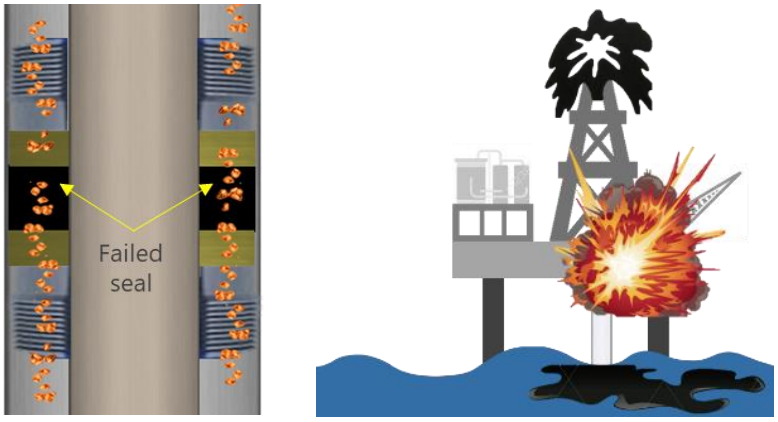

Figure 1.2: Failure in seal assembly can lead to catastrophic health, safety, and environmental consequences

Issue of reliability in liner hanger seal assemblies has been acknowledged by the industry since 2000s. An informal survey of several Gulf of Mexico operators indicated that about 30% to 50% of the pressure seals in liner overlaps failed (Lohoefer et al. 2000). A 2009 report indicates that as many as 18% of offshore wells worldwide are estimated to have some form of weakness or uncertainty in seal assemblies and the record of failures of critical liner-hanger seals in HPHT completions, for example, has become a large concern (Van Dort 2009). Although industry is gradually moving towards arguably more robust design of expandable liner hanger assembly, concerns with reliability of elastomer seal assemblies persist as acknowledged by the regulatory agency - Bureau of Safety and Environmental Enforcement (BSEE) in a technical report (BSEE 2014). The agency investigated loss of well control event in Gulf of Mexico (BSEE 2014) and recommended further investigations into design, reliability, industry standards, and fitness-for-service assessment of elastomer seal assemblies for liner hanger applications (BSEE 2014). As analyzed in the next chapter of dissertation, industry did not even have a dedicated standard for liners until July 2019 (API 2019).

Detailed literature review (discussed in Chapter 2 and also published in Patel et al. 2019a), leads to hypothesis that some of the major reliability issues of liner hanger seal assemblies can be mitigated by extending research efforts beyond lab-scale standardized material testing to equipment level assessment like design, function, and scale of seal assembly. However, most research in the industry has been focused on laboratory scale standardized testing of elastomer material. Two major knowledge gaps exist in the current literature that this dissertation work aims to address.

First, it is not completely understood whether compliance with standard shaped laboratory scale elastomer material testing is representative of qualification of larger and varying seal

geometries installed in the actual equipment (**Figure 1.3a**). It is understandable that testing true-scale seal geometries in laboratory environment may not be practically or economically feasible. However, the qualification criteria used to assess elastomer material can be customized as per end-application and equipment design. This dissertation work fills this gap by evaluating performance of commonly used elastomer materials at equipment level with varying assembly designs, and operational and failure scenarios.

Second major research gap is the unknown seal energization criteria. There is no consensus on whether contact pressure generated at seal-pipe interface due to seal energization indicates actual fluid pressure the seal can hold without permitting leakage (**Figure 1.3b**). Through leakage modelling, this dissertation work presents a design tool to identify target contact pressure i.e. seal energization to seal different fluids at different pressure.

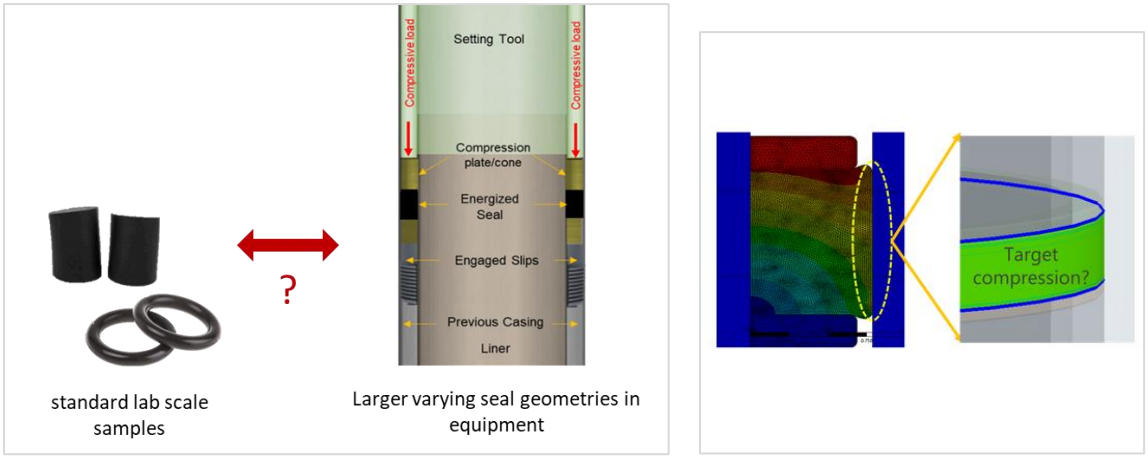

(a) **(b)**

Figure 1.3: This dissertation addresses two major research gaps: (a) need for elastomer qualification criteria to be customized as per equipment design, and (b) ideal seal energization to achieve complete sealability

1.3 Objectives

This dissertation work provides detailed investigation of design, and failure of downhole elastomer seal assemblies using experimentally supported advanced computational modeling techniques. This work is partially supported by Bureau of Safety and Environmental Enforcement (BSEE) and it is set in the context of liner hanger assemblies. However, major outcomes of this research also applies to other downhole seal assemblies. Following are the specific objectives of this dissertation work:

1. Investigate performance of liner hanger seal assembly under various design, operational, and failure scenarios.
2. Develop operating envelops and identify critical parameters influencing performance of the elastomer seal assembly.
3. Develop a modelling tool for predicting leakage through elastomer seal interface considering surface characteristics.
4. Generate guidelines for design and qualification of elastomer seals and provide regulatory recommendations.

Novel technical aspects of this research work are – (i) studying material behavior of different elastomer material (NBR, EPDM, FKM, FEPM, FFKM, PTFE) under normal and downhole conditions, (ii) using the elastomer material data in true-scale finite element (FEA) models to evaluate equipment level performance of seal, (iii) scaled laboratory tests and analytical calculations to validate FEA models, and (iv) development of a leakage modelling tool that can predict leakage rates as a function of surface topography of seal interface and operating conditions.

1.4 Research Methodology

To achieve aforementioned objectives, this comprehensive study was divided into four major tasks – theoretical analysis, experimental study, finite element modelling, and development of leakage modelling tools. Graphical overview of the technical approach employed in this work is shown in **Figure 1.4.**

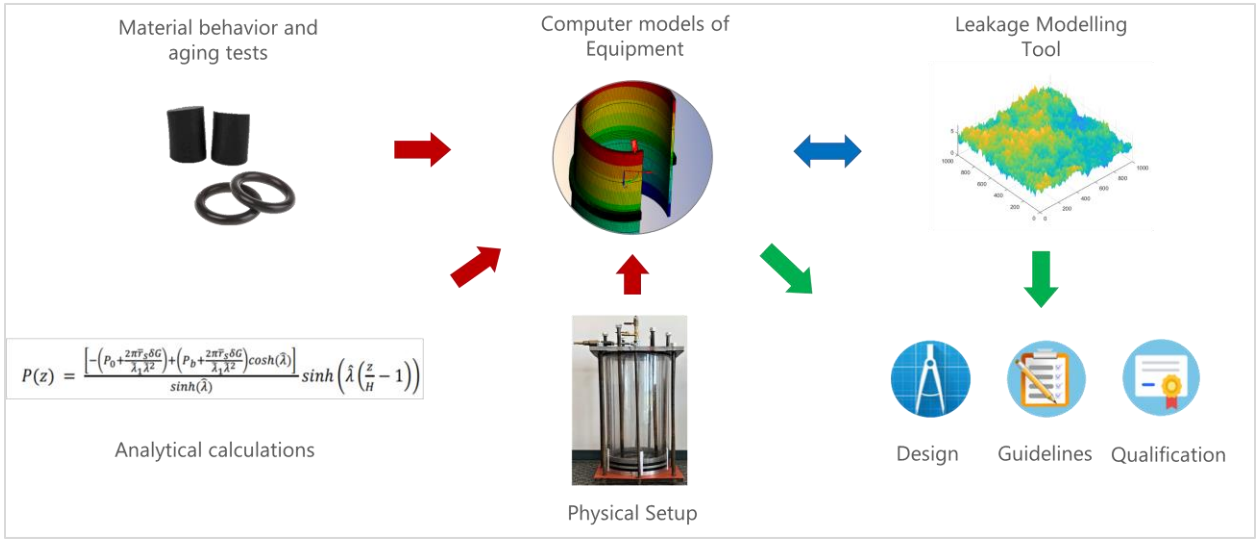

Figure 1.4: Overview of research methodology employed in this dissertation work

1.4.1 Theoretical analysis

Theoretical analysis (Chapter 2) was conducted at the beginning of the project to identify major research gaps and determine the approach and scope of the undertaken research. Extensive literature review was conducted to identify influential parameters, common failure mechanisms, and existing research gaps relevant to elastomer seal assemblies. Gap analysis of relevant industry standards such as API, ISO, NACE, ASTM, NORSOK, etc. was conducted to recognize existing qualification guidelines and their limitations. Relevant analytical/empirical models were reviewed and modified for validating some of the FEA modelling predictions.

1.4.2 Experimental Study

The purpose of experimental work (Chapter 3) was to obtain material behavior and aging data for use in FEA models and for validating some of the observations/trends predicted by FEA models. Two types of laboratory experiments were conducted in this work. First, standardized elastomer material tests were conducted to measure elastomer hardness and deformation behavior under various temperature and downhole chemical conditions. Second, sealability tests were conducted using a laboratory scale apparatus representative of liner hanger seal assembly.

1.4.3 Finite Element Modelling

True-scale finite element models of liner hanger seal assembly were developed using ANSYS® software (Chapter 4). Seal energization process similar to actual equipment installations were simulated. Performance of seal assembly was quantified in terms of contact pressure generated at the seal-pipe interface after energization. Some FEA models were validated by theoretical calculations and experimental observations to improve confidence in predictions. Using verified models, parametric and sensitivity analyses were conducted by simulating various design, operating, and failure scenarios.

1.4.4 Development of Leakage Model

Unlike metallic seals, it is believed that elastomer seal's performance is not highly dependent on its surface characteristics. However, evidences suggest that elastomer surface quality or defects like wear, blistering, etc. can impact fluid penetration risk and leakage. Finite element modelling using commercial software is not capable of accurately simulating leakage since it assumes perfectly smooth sealing interfaces. It is computationally challenging to combine microscopic surface model with true-scale FEA model. Hence, in this study, a novel leakage model was

developed (Chapter 5) that can take surface characteristics of elastomer as an input and predict leakage rates through seal interface as a function of contact pressure and microscopic contact gaps. Contact mechanics and fluid flow theories were used in development of this leakage model. The model codes were written in MATLAB.

1.5 Scope of Study

Six type of commonly used elastomer material have been investigated in this work. This includes – NBR, EPDM, FKM, FEPM, FFKM, and PTFE. Hardness and compression behavior data have been measured. Additionally, both linear elastic and hyperelastic type material behavior have been examined. Material data used encompasses effect of temperature (75°F, 212°F, and 350°F), and effect of chemicals exposure (CO_2, CH_4, H_2S, and mixture of the gases; with and without presence of brine, 1 and 7 days, 120°F, and 180°F, 1000 psi).

Currently, two types of liner hanger assemblies are used in the industry - conventional and expandable type. Both assemblies have been modelled and studied in this work. Various design, operational, and failure scenarios investigated include – quality of seal energization, energization method, effect of seal dimensions, effect of elastomer type, seal containment quality, over-energization/extrusion failure, thermal effects, and chemical exposure.

Sealability tests were limited up to 40 psi of N_2 injection because of limited rating of the setup. EPDM elastomer before and after CO_2 aging was evaluated at different energization using the sealability apparatus. Sealability tests serve to validate seal energization behavior and effect of CO_2 aging predicted by the FEA model. Analytical calculations were also performed to further validate contact pressure value predicted by FEA model.

Current state of leakage modelling tool developed in this work is only applicable to Newtonian fluids. The model considered isothermal condition and rigid smooth pipe surface. The primary purpose of the tool is to examine effects of surface RMS, surface topography, and elastomer type on target contact pressure needed to achieve complete sealability. Experimental validation of the leakage modelling tool and leakage of compressible fluid flow demand separate future study and hence, beyond the scope of this dissertation.

1.6 Overview of Dissertation

This dissertation is divided into 10 chapters.

- First chapter provides overview of the research work including background, motivation, objectives, methodology, and scope.
- Second chapter discusses theoretical background necessary to understand the methodology and results of this work. The discussion includes - types of elastomer material and their properties, failure mechanisms, critical review of relevant industry standards, and review of relevant studies and analytical models.
- Third chapter provides overview of experimental setup, equipment used, and results of material testing.
- Fourth chapter discusses steps in development of FEA models including their schematic, boundary conditions, meshing, model verification, and model validation.
- Chapter five presents the novel approach used to develop leakage modelling tool. The chapter discusses details of the contact mechanics and fluid mechanics models developed.
- Chapter six discusses results related to assembly design. Specifically, it discusses effects of equipment type, energization method, seal dimensions, seal geometry, and elastomer material.

- Chapter seven presents result from failure scenarios investigated. This includes extrusion, over-energization, thermal degradation, chemical exposure, and support component failures.
- Chapter eight presents result from sensitivity analysis and ranks various parameters in terms of individual impact on performance of seal assembly.
- Chapter nine presents results from leakage modelling and discuses effects of elastomer type, surface roughness, and surface topography on the leakage criteria i.e. contact pressure vs leakage rate relationship.
- Chapter ten summarizes all results obtained in this dissertation work.
- Last chapter presents major conclusions from this work, and provides recommendations for design and qualification of seal assemblies. At the end, some important future work to further improve research in this area are discussed.

Chapter 2: Literature Review, Industry Standards, Research Gaps, and Preliminary Work

2.1 Elastomer Material

Elastomer is a cross-linked network of natural or synthetic polymers. Its characteristics property of deforming and recovering under load (elasticity and resilience) make them arguably one of the most important engineering materials with versatile applications. Polymer chains typically consists of 300,000 or more monomer or repeating units (James Walker 2017). Some elastomers are co-polymers, a combination of two different monomers, or consists of three monomers (terpolymer). Most types of elastomers are thermosets which gain most of their strength through vulcanization – a process of irreversible crosslinking of polymer chains under pressure and heat. The other type of elastomers is thermoplastic which exhibits weaker cross-linking. Thermoplastics can be molded, deformed, and extruded like plastic materials while still having typical elastic properties. In addition to elasticity and resilience, elastomers possess several useful properties such as – low permeability, good electrical/thermal insulation, good mechanical properties, and the ability to adhere to different metal, plastics, and other materials.

Elastomers in the oil & gas industry are primarily used for sealing applications. The most common elastomer materials used in the industry can be classified into five groups – NBR, HNBR, FKM, FEPM, and FFKM. Chemical and mechanical properties of each of these elastomers are a function of type of monomer, molecular weight, number, and type of crosslinks. Within each of the elastomer group, properties can notably vary as manufacturers use different formulations, types and ratio of monomers, degree of cross-linking, etc. to attain necessary resistance for desired application. Moreover, various additives such as fillers, accelerators, curatives, activators, desiccants, plasticizers, etc. are frequently used to improve mechanical or chemical properties

(Elhard et al. 2017). Chemical composition and important characteristics of each of the elastomer groups has been summarized in **Table 2.1**. Their relative comparison in terms of temperature robustness, mechanical properties, and chemical resistance is provided in **Table 2.2**.

It is clear from the **Table 2.2** that as a general rule, fluoroelastomers and perfluoroelastomers (FKM, FEPM, and FFKM) are more expensive and demonstrate greater chemical resistance and higher operating temperatures. However, they typically struggle at lower temperatures compared to NBR, EPDM, and HNBR. Less expensive elastomers such as NBR, exhibit better mechanical properties than fluoroelastomers but they are limited by low resistance to chemicals and heat. Hydrogenated NBR (HNBR) improves temperature range and some chemical resistance but also adds cost.

Table 2.1: Chemical composition and important characteristics of common oil field elastomers

(Information compiled from Elhard et al. 2017, James Walker elastomer engineering guide 2017, and Apple Rubber material selection guide 2017)

NBR (Nitrile)	**EPDM** (Ethylene Propylene Diene)
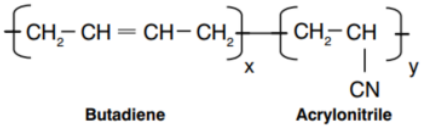	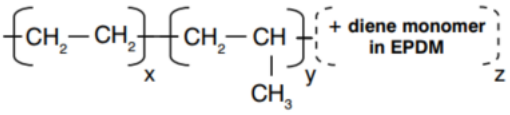
• Suitable with aliphatic hydrocarbon oils/fuels, lower alcohols • Not compatible with Aromatic hydrocarbons, ketones, acids and bases, ketones, ethers, aldehydes, chlorinated solvents, phosphate esters • Limited weathering and UV resistance • Modest temperature resistance	• Excellent resistance to ozone/weathering, hot water, steam • Good resistance to inorganic and polar organic chemicals • Low resistance to hydrocarbons

HNBR (Hydrogenated nitrile)	**FKM** (Fluorocarbon)
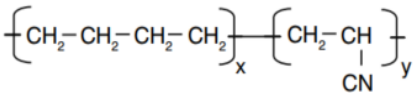	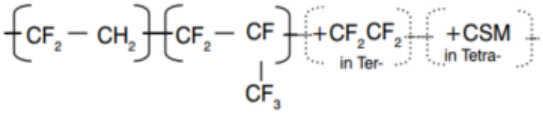
• Good oil/fuel, and chemical resistance • Suitable with aliphatic hydrocarbon oils/fuels, lower alcohols • Excellent mechanical properties including tensile strength, tear, modulus, elongation at break and abrasion • High cost • Not compatible with aromatic hydrocarbons, ketones, ethers, phosphate esters • Limited weathering and UV resistance • Modest temperature resistance	• Excellent resistance to ozone/weathering • Good resistance to heat • Suitable for Hydrocarbon fuels, oil, aliphatic and aromatic chemicals • Limited resistance to steam, hot water, and polar fluids (Except tetra-), high pH caustic, amines, low molecular weight carbonyls, light oxygenates (MeOH), and mineral acids • Limited low temperature capabilities • Properties vary significantly with type
FEPM (Tetrafluoroethylene propylene)	**FFKM** (Perfluorocarbon)
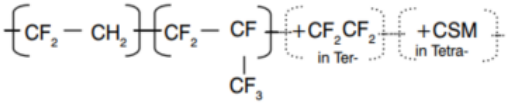	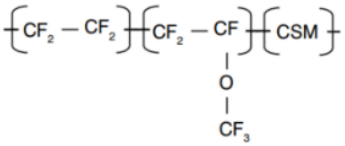
• Good resistance to heat • Overall good chemical resistance • Excellent resistance to ozone/weathering, steam, and radiation • Suitable with strong acids, bases, steam, light oxygenates (MeOH), and amines • Limited resistance to esters, ketones, light oils, gasoline, chlorinated and hydrocarbon solvents	• Ultimate in heat and chemical resistance • Suitable with fuels, oils, solvents, alcohols, ketones, mineral acids and bases • Very expensive • Some concern with hot water and amines • Moderate mechanical properties deteriorate rapidly at elevated temperatures, and at temperatures below 0°C

• High compression set and high glass transition temperature. • Difficult to process • Poor extrusion resistance especially at high temperatures	

Table 2.2: Comparison of oil-field elastomers in terms of mechanical properties and chemical compatibility (Grading: 1-Poor, 2-Fair, 3-Good, 4-Excellent)

Property	NBR	EPDM	HNBR	FKM	FEPM	FFKM
ASTM D1418-17 Class	R	M	R	M	M	M
Economy	4	4	2	2	1	1
Low Temp. Resistance	-50°C (-58°F) to -5°C (23°F)	-45°C (-49°F)	-30°C (-22°F)	-30°C (-22°F) to -8°C (18°F)	-12°C (10°F) to -3°C (27°F)	-5°C (23°F)
High Temp. Resistance	100°C (248°F) to 130°C (266°F)	150°C (302°F) to 180°C (356°F)	150°C (302°F) to 180°C (356°F)	204°C (400°F) to 250°C (482°F)	230°C (446°F) to 260°C (500°F)	220°C (428°F) to 327°C (621°F)
Tensile Strength	3	3	3-4	2	2	2-3
Max. Elongation (%)	600	600	340	300	400	120-190
Hardness Range Shore A	40-90	40-95	50-90	55-90	60-90	65-90
Resilience	3	3	NA	2-3	2-3	3
Compression Set	3	2-3	3-4	3	2-3	2
Adhesion to metals	3-4	2-3	NA	2-3	2	3-4
Abrasion Resistance	3-4	3	3-4	3	3	3-4
Tear Resistance	3	2-3	3	2-3	2	2

Weather Resistance	1-2	4	3	4	4	4
Ozone Resistance	1	4	3	4	4	4
Water Swell Resistance	3	4	3	3	3	3
Steam Resistance under 300F	1	4	1	1	4	4
Gas Impermeability	3-4	2	3	3-4	3	3-4
Acid Resistance	2-3	4	2-3	4	3	4
Alkali Resistance	3	4	1-3	1	4	3
Alcohols	3-4	4	4	2-3	3	4
Lubricating Oils	4	1	4	4	3	4
Aliphatic Hydrocarbons	3-4	1	3-4	4	2	4
Aromatic Hydrocarbons	2-3	1	2-1	4	2-3	4
Halogenated Hydrocarbons	2-1	1	1	4	1-2	1
Phosphate Ester	1	4	1	1	3	4
Polar Solvents	1	4	1	1	2	1

Source of information**:**

Elhard et al. 2017; James Walker elastomer engineering guide 2017; Apple Rubber material selection guide 2017

NA: Clear relative comparison not clear or not available

2.1.1 Material Properties

Elastomer material can be characterized using several properties. Selection of properties to measure and control for strongly depends on the type of application. Some of the commonly measured material properties, in no particular order, are as follows.

2.1.1.1 Cure Characteristics

A rheometer is typically used to measure how elastomer cures over time. An oscillating rotor is places in contact with elastomer compound as it cures between hot platens. Torque measurements are obtained with time. As compound cures, the resistance to torque increases and ideally plateaus eventually. The torque vs time chart is known as rheograph (**Figure 2.1**). For some compounds, the curing may take longer as characterized by "marching modulus in the **Figure 2.1** (James Walker 2017). For some material, especially natural rubber, heat breaking of polymer chains instead of cross-linking may reverse the curing process.

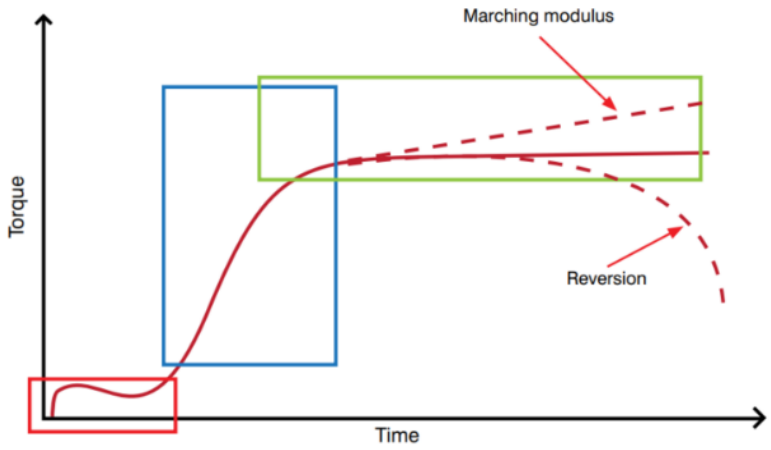

Figure 2.1: Typical rheography profile for curing elastomer compound (James Walker 2017)

2.1.1.2 Hardness

Hardness is a quick measurement of elastomer's resistance to indentation. It is typically measured using Shore durometer (**Figure 2.2**) and a standard sample of elastomer as prescribed in ASTM D2240, BS ISO 48, or other equivalent standards. There are several scales of durometer but the most common scale for elastomers is type A. Higher Shore A number indicates higher material

hardness. Typical values of hardness and Shore grade used for common oil & gas elastomers is provided in **Table 2.2**.

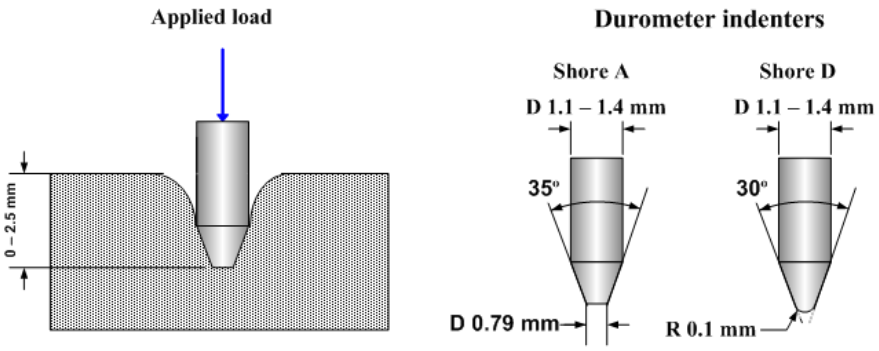

Figure 2.2: Schematic of durometer hardness test (Substech 2018)

2.1.1.3 Tensile Strength and Elongation at Break

This is a measure of the tensile stress required to rupture a standard sample of elastomer. Tensile strength is frequently used as a quick indicator of quality check during multi-batch manufacturing. Temperature has notable impact on tensile strength, and hence, measurement at operating condition would be a more meaningful indicator. It should be noted, however, that tensile strength does not indicate extrusion resistance. Elongation at break is more common and practical measurement. It refers to the percentage strain measured at the point of rupture. Its requirement would typically depend on amount of gap seal has to fill-in during energization.

2.1.1.4 Modulus

Unlike metals, elastomer material typically exhibits non-linear relationship between stress and strain (**Figure 2.3**). Hence, in elastomer terminology, modulus is defined as the stress at a particular strain or elongation (**Figure 2.3**). Typically, elastic modulus is reported at 25%, 50%, 100%, 200%, and 300% elongation or strain. Modulus value tends to increase with increase in Hardness of the material.

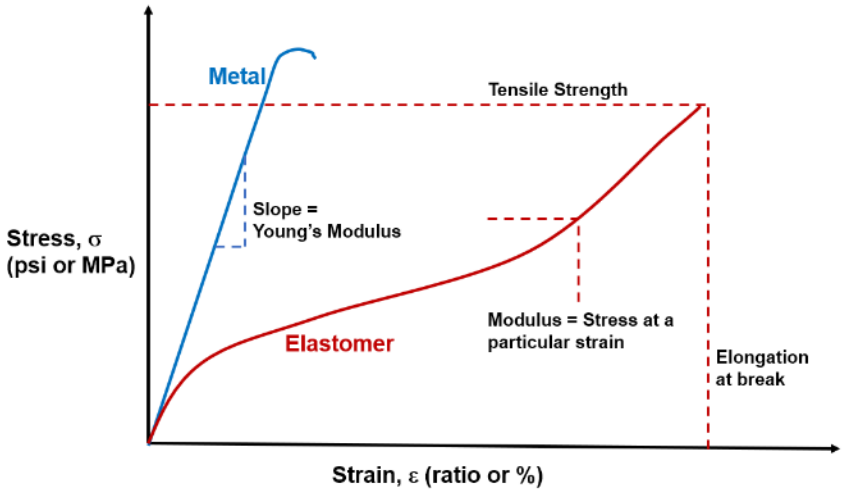

Figure 2.3: Comparing modulus of metal and elastomer materials (not to scale)

2.1.1.5 Compression Set

Compression set refers to elastomer's ability to recover the original volume after unloading. It is important parameter to assess for sealing applications. As shown in **Figure 2.4**, a standard sample is compressed, exposed for a fixed time, at a fixed temperature, and then allowed to recover (typically for 30 minutes). Compression set is expressed in terms of percentage of the original deformation not recovered after the recovery period. Full recovery is represented by 0% compression set while 100% indicates no recovery. Compression set is typically higher at extremes of elastomers operating capability.

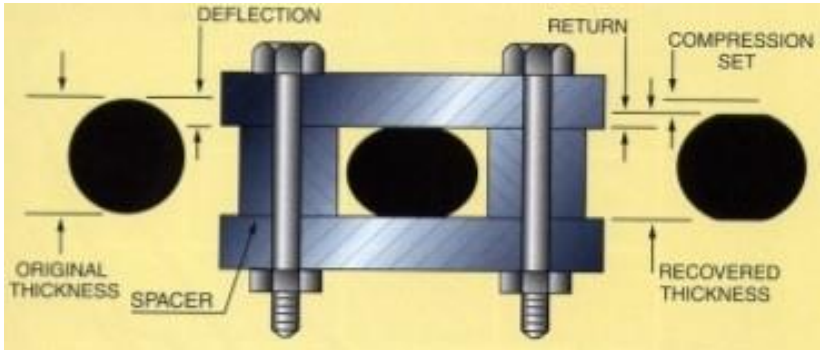

Figure 2.4: Schematic of compression set testing (K.C. Seals Inc. 2018)

2.1.1.6 Compression Stress Relaxation

The basic principle is to compress test sample between two rigid plates and held them at a constant strain (**Figure 2.5**). The top plate is connected to a sensor that measures residual sealing force at the elastomer-plate interface. This setup is typically known as compression jigs. The instrument can be placed in various environment to obtain more practical and meaningful measurements. As compression set increases, sealing force decreases (**Figure 2.6**).

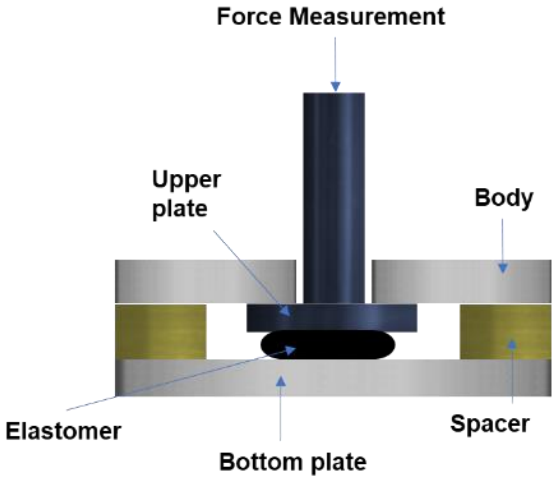

Figure 2.5: Compression jig used for stress relaxation measurement

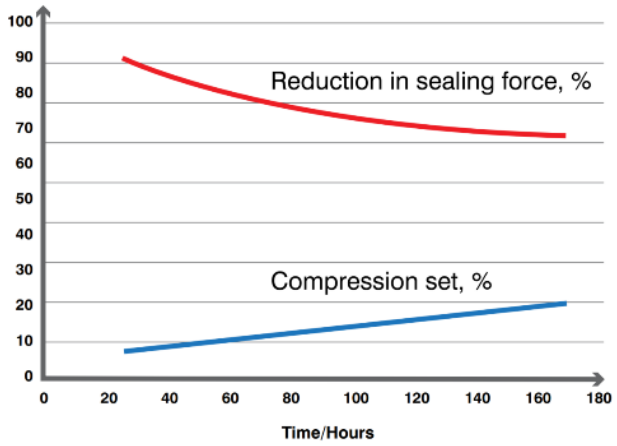

Figure 2.6: Compression set and corresponding reduction in sealing force for nitrile elastomer sample at 100°C (James Walker 2017)

2.1.1.7 Fluid Resistance

Elastomer's resistance to liquid chemical exposure is typically measured by immersion of sample in various fluids at different temperatures. Change in properties such as volume, hardness, tensile strength, or any other property relevant to particular application is measured before and after exposure to determine degree of resistance.

A useful property for chemical resistance is solubility parameter (δ). It is a thermodynamic property that measures energy or attraction between molecules. If a fluid has a solubility parameter close to that of an elastomer then it can result in high mixing potential and eventually volumetric swell. Hansen three-dimensional solubility parameters is a useful equation that incorporates factors for non-polar dispersive interactions (represented as δ_d), polar interactions (δ_p), and hydrogen bonding interactions (δ_h), with a total parameter determined according to following equation (Rodriguez et al. 2003). Polymers exposed to liquids with similar values for their δ_d, δ_p, and δ_h terms are more likely to experience polymer swelling.

$$\delta_{total}^2 = \delta_d^2 + \delta_p^2 + \delta_h^2 \quad \text{(2.1)}$$

2.1.1.8 Torsion Modulus

The torsional test consists of twisting a standard elastomer specimen under the action of torque applied at one end while keeping the other one fixed. It is typically a part of low temperature testing of elastomer wherein torsion tests are conducted at different reduced temperatures to obtain temperature modulus curve. This set of procedures is termed as Gehman test. An important outcome from this test, is temperature value at which elastomer reaches the limit of technically useful flexibility which is 70 MPa (10,153 psi) (James Walker 2017).

2.1.1.9 Tear and Abrasion Resistance

Tear strength indicates the resistance of elastomer to tearing. It is measured using a tensile test machine operating at a constant rate of traverse until the sample breaks (**Figure 2.7a**).

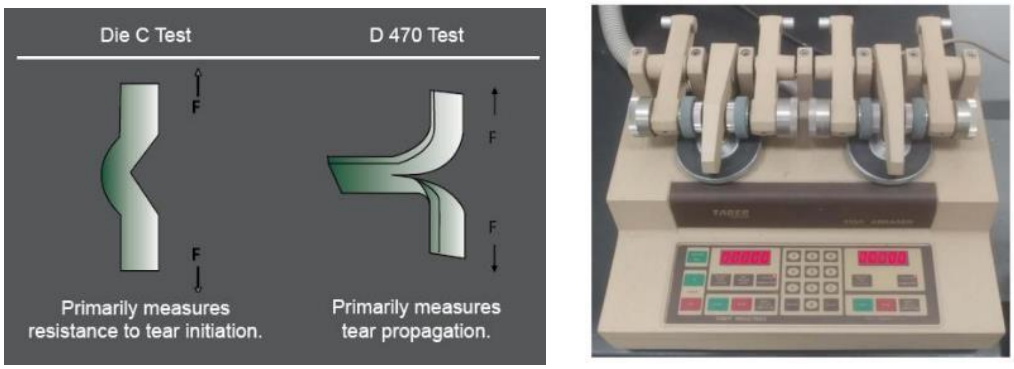

(a) **(b)**

Figure 2.7: Tear resistance test specimens (Era polymers 2019), and (b) rotary platform type abrasion tester (Denison et al. 2018)

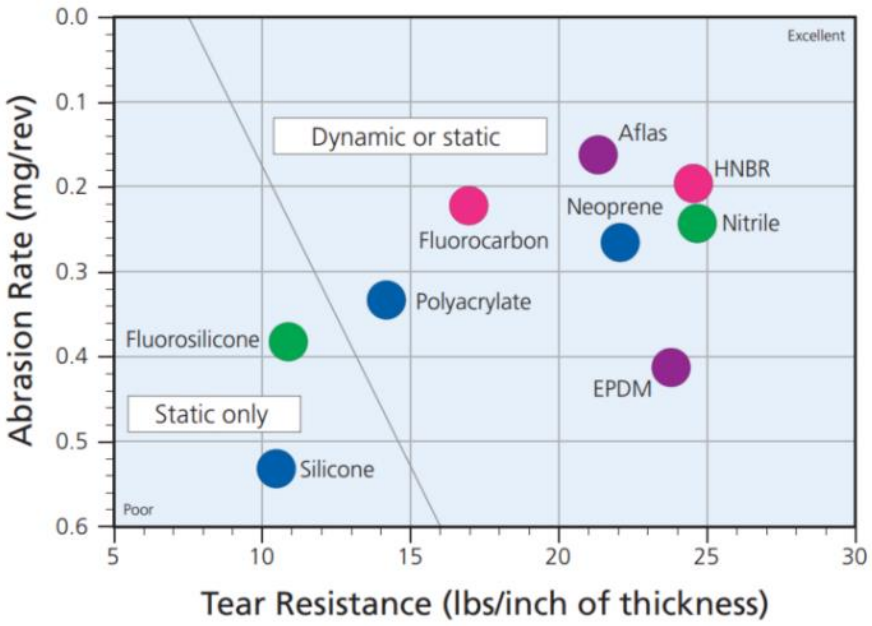

Figure 2.8: Abrasion and tear resistance of medium-hardness elastomers (Parco Inc. 2013)

Abrasion resistance of elastomer material indicates robustness to damage against abrasive counter surface. Standard abrasion resistance measurement includes generating relative motion

between elastomer and abrasive surface pressed together by a predetermined force. There are different standardized machines available for such tests. One such equipment is shown in **Figure 2.7b**. Abrasion resistance is mainly dependent on polymer type and composition. High modulus and high tear strength may indicate better abrasion resistance, but the relationship is not strict and can be reverse. Abrasion and tear resistance of medium-hardness elastomers is shown in **Figure 2.8.**

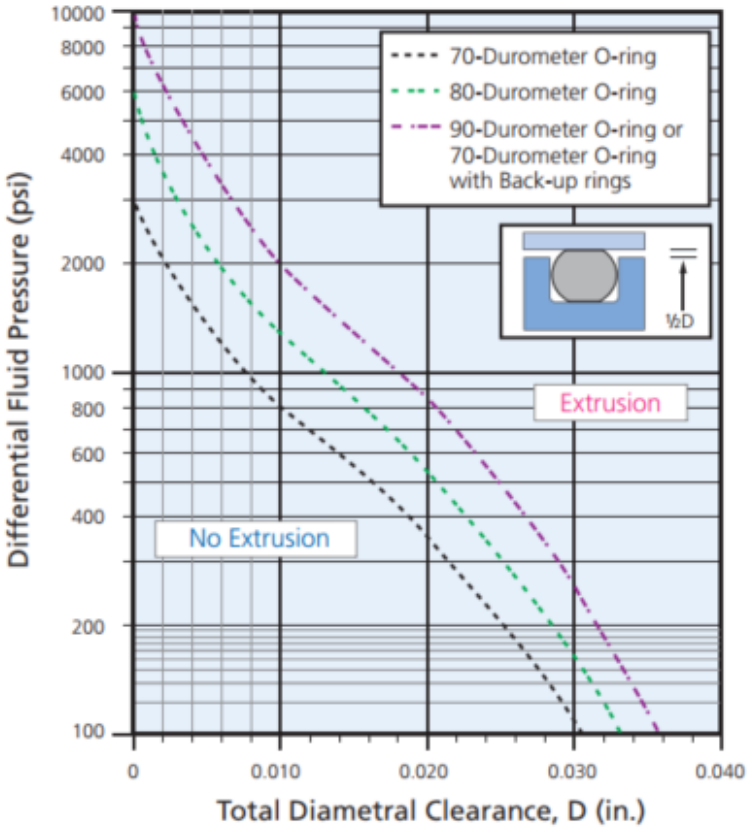

Figure 2.9: Example of extrusion resistance curve (Parco Inc. 2013)

2.1.1.10 Extrusion Resistance

Extrusion resistance is an important parameter from the perspective of functional performance of elastomer. It measures elastomer's capability to resist differential pressure that tends to extrude the seal across the assembly gap. There are different types of testing devices available depending

on the application type. A typical extrusion resistance plot for O-ring along with schematic of test configuration is shown in **Figure 2.9**. Typically, backup rings or some type of anti-extrusion device is installed against the extrusion gap to prevent elastomer extrusion. Elastomer seal with high modulus and hardness are typically more resistant to extrusion.

2.1.1.11 Permeability

Permeability of elastomer sample can be a useful property for sealing applications. It is measured by applying a constant pressure at one end of standard test specimen and measuring volume of gas permeating out of the low pressure side.

There are several other elastomer material properties used to characterize its quality or performance. Discussing each of them is beyond the scope of this document.

2.1.2 Material Models

2.1.2.1 Linear Elastic Model

The most fundamental material model known to engineers is Hook's law or linear elastic model,

$$\sigma = E \cdot \varepsilon \quad \text{(2.2)}$$

In this equation, the proportionality constant E between stress (σ) and strain (ε) is Young's modulus or modulus of elasticity of the material. In three-dimensional system, Hook's law can be represented in terms of three principle strains as following:

$$\varepsilon_1 = \frac{1}{E}[\sigma_1 - \nu(\sigma_2 + \sigma_3)] \quad \text{(2.3)}$$

$$\varepsilon_2 = \frac{1}{E}[\sigma_2 - \nu(\sigma_1 + \sigma_3)] \quad \text{(2.4)}$$

$$\varepsilon_1 = \frac{1}{E}[\sigma_3 - \nu(\sigma_1 + \sigma_2)] \quad \text{(2.5)}$$

Where σ_i, and ε_i are orthogonal principle stresses and principle strain respectively. ν is Poisson's ratio. The strain energy density of uniaxially loaded linear elastic material is calculated as:

$$W = \frac{1}{2}\sigma\varepsilon = \frac{1}{2}E\varepsilon^2 \quad \text{……………………………………………………… (2.6)}$$

This is exactly the area below the stress-strain curve.

If the strain is below approximately 10% then, for many applications, the simple linear elastic model assumption is enough for elastomers (Jakel 2010). For higher strains, a hyperelastic material models are necessary.

2.1.2.2 Hyperelastic Model

A hyperelastic material is still an elastic material and returns to its original shape after unloading. However, it is Cauchy-elastic meaning that stress is determined by current state of deformation and not the path or history of deformation. Another difference to linear elastic material is that the stress-strain relationship in hyperelastic material derives from strain energy density function and not a constant factor. The loading and unloading curves for hyperelastic material are not the same and depends on various factors such as time, frequency, dynamic loading, etc. However, typical hyperelastic material models ignores this viscous behavior.

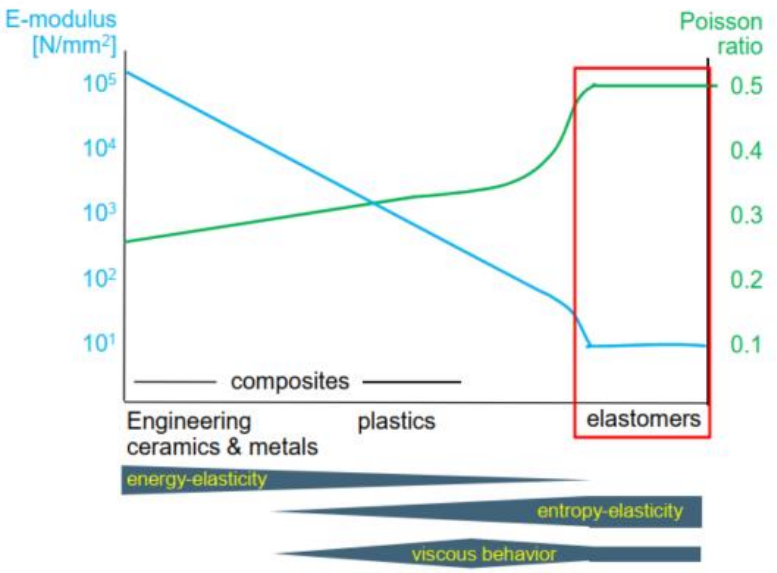

Figure 2.10: Comparison of elasticity between metals, plastics, and elastomers (Jakel 2010)

As shown in **Figure 2.10**, elastomers exhibit entropy-elasticity compared to energy-elasticity in metals. In metals, distance among atoms changes during loading/unloading and internal energy correspondingly increases/decreases. In elastomers, polymer chains ball up if unloaded and stretch/untangles during loading. After unloading, the unordered state or entropy appears again. Elastomers also exhibit some viscous behavior which indicates retention of small deformation after every loading-unloading

In general, the strain energy density function in hyperelastic material is a function of the stretch invariants (I) or principle stretch ratio (λ). Stretch ratio is defined as deformed length divided by the original length. That is,

$$\lambda = \frac{l_1}{l_0} = \frac{l_1 - l_0 + l_0}{l_0} = \varepsilon + 1 \quad \text{……...……..……..……...…..…..…} \quad (2.7)$$

Analogous to three principle strains in Hook's law, three principle stretch ratios (λ_1, λ_2, λ_3) can be obtained from principle axis transformation. The three stretch invariants are independent from coordinate system and are defined as,

$$I_1 = \lambda_1^2 + \lambda_2^2 + \lambda_3^2 \quad \ldots\ldots (2.8)$$

$$I_1 = \lambda_1^2\lambda_2^2 + \lambda_2^2\lambda_3^2 + \lambda_1^2\lambda_3^2 \quad \ldots\ldots (2.9)$$

$$\lambda = \lambda_1^2\lambda_2^2\lambda_3^2 = 1 + \left(\frac{\Delta V}{V}\right)^2 = J^2 \quad \ldots\ldots (2.10)$$

Where J is total volumetric ratio which equals to 1 for incompressible material with Poisson's ratio of 0.5.

For typical hyperelastic models, the general equation for strain energy function is following:

$$W = \sum_{i+j=1}^{N} C_{ij}\,(I_1 - 3)^i (I_2 - 3)^j + \sum_{k=1}^{N} \frac{1}{D_k}(J-1)^{2k} \quad \ldots\ldots (2.11)$$

Where C_{ij} and D_k are material constant to be determined by material tests. The function has a polynomial form. Depending on the order, one or more inflection points in the stress-strain curve may appear.

Neo-Hookean Model

It is the simplest hyperelastic model that is a function of only one stretch invariant. It is defined as,

$$W = \mathrm{C}_{10}(I_1 - 3) + \frac{1}{D_1}(J-1)^2 \quad \ldots\ldots (2.12)$$

Constants C_{10} and D_1 are related to initial shar and initial bulk modulus by following expressions:

$$\mathrm{G}_0 = 2\,\mathrm{C}_{10} \quad \ldots\ldots (2.13)$$

$$G_0 = \frac{2}{D_1} \quad \text{(2.14)}$$

Mooney-Rivlin Model

It is the earliest model for hyperelasticity and uses first and second stretch invariants. Neo-Hookean is a special case of this model.

$$W = C_{10}(I_1 - 3) + C_{01}(I_2 - 3) \ + \frac{1}{D_1}(J-1)^2 \quad \text{(2.15)}$$

In this model, initial shear modulus becomes $G_0 = 2\ (C_{10}+C_{01})$

Ogden Model

Ogden defined strain energy density function directly in terms of three principle stretch ratios. The model is expressed as,

$$W = \sum_{i=1}^{N} \frac{2\mu}{\alpha_i^2}(\lambda_1^{\alpha i} + \lambda_2^{\alpha i} + \lambda_3^{\alpha i} - 3) + \sum_{i=1}^{N} \frac{1}{D_i}(J-1)^2 \quad \text{(2.16)}$$

Yeoh Model

Yeoh proposed not to use the second invariant term because it is more difficult to measure and provides less accurate data fit for limited test data points. This special form of reduced polynomial model is expressed as,

$$W = C_{10}(I_1 - 3) + C_{20}(I_1 - 3)^2 + C_{30}(I_1 - 3)^3 + \frac{1}{D_1}(J-1)^2 + \frac{1}{D_2}(J-1)^4 + \frac{1}{D_3}(J-1)^6 \quad \text{(2.17)}$$

There are several other phenomenological, micromechanical, response function etc. type hyperelastic models. They are readily available in literature and beyond the scope of this work.

Accurate material test data is critical to model hyperelastic elastomer materials. There six major type of tests - uniaxial tension, uniaxial compression, biaxial tension (circular or rectangular specimen), planar shear, simple shear, and volumetric test (button specimen). Data from at least two of these tests are required to use the simplest hyperelastic model that is Neo-Hookean. If more data is available, then progressively higher order models can be utilized.

2.2 Seal Assemblies and Failure Statistics

There four types of critical elastomer seal assemblies used in oil & gas wells – packers, blowout preventers, sub-surface safety valves, and wellhead assemblies.

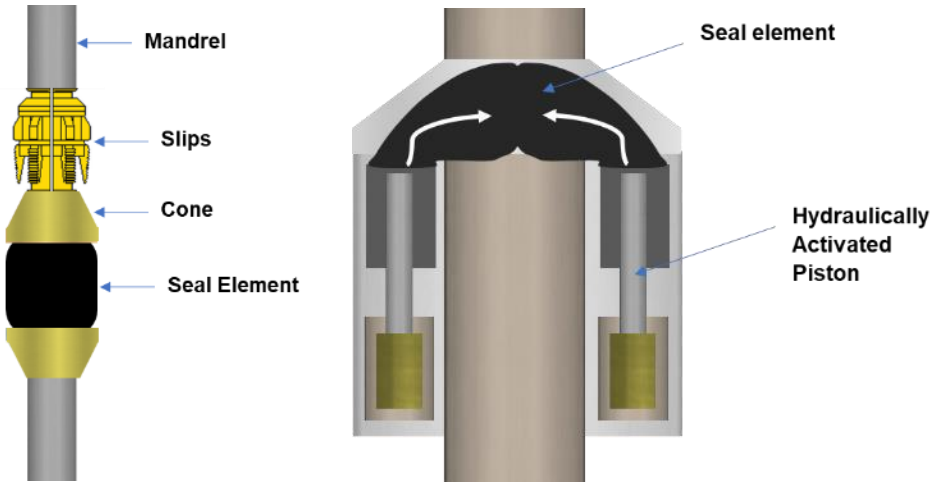

Figure 2.11: Elastomer seal components (black color) in (a) packer, and (b) blowout preventer after closure (Patel et al. 2019a)

Packers are typically used to isolate production zones or to seal off annular space between production tubing and completion. They are available in numerous variants with a typical configuration shown in **Figure 2.11a**. The elastomer element is energized by compressing it through mechanical/hydraulic means or using swellable elastomer material. The elastomer must

be compatible with producing fluid and should be able to withstand in-situ temperature/pressure conditions. Blowout preventer is a critical wellhead equipment designed to act as a secondary barrier or failsafe in the event of loss of well control such as a formation kick or blowout. As shown in **Figure 2.11b**, it consists of a solid donut shaped elastomer component which is compressed around the drill pipe using hydraulic pressure to seal off the well opening around the drill string. In the event of a potential event of kick, hydraulic pressure is applied to the donut, forcing it to conform tightly around the drill pipe. The elastomer element is directly exposed to the formation fluid pressure and required to seal against it. Sub-surface safety valve is installed downhole with the objective to stop flow in the event of emergency. The hydraulic pressure is released and the ball or flapper type safety valve closes and seals off the well.

As discussed in chapter 1, the proposed dissertation work is focused on liner hanger seal assemblies as they are a common equipment used in modern well designs. Present discussion will focuse more on the types of wellhead assemblies particularly casing/liner hangers.

Whether drilling a well on land or offshore, casing/liner hanger with seal is an important component of wellhead system. The primary purpose of seal assembly is pressure containment. Typically, seals are made outside of each individual casing or liner string to seal off the individual annuli. The traditional “build as you go” spool wellhead system uses a slip-and-seal assembly which is landed on casing heads. This assembly supports next casing/liner string by transferring its weight to conductor and also provides annular seal via energized weight-set elastomeric seal. There are two types of common hanger systems: a slip-and-seal casing-hanger assembly and a mandrel style casing hanger. The slip-and-seal assembly (**Figure 2.12a**) has outer diameter that matches with the internal profile of previous casing head and intermediate casing spools. The assembly has a set of slips with serrated teeth. The seal assembly is set mechanically by applying

predetermined weight. As the weight is applied, the slips travel down and engages the pipe. A load is placed on the elastomer element which expands radially by compression and seals the annulus pressure below the hanger from the wellbore. In the offshore jack up drilling application with mudline, weight-set slip-and-seal assembly is not used because the weight of the well sits at the seabed. In such cases, a mechanical set seal assembly (**Figure 2.12b**) is used in which cap screws are made up with a wrench against the compression plate to energize the seal element. If a unitized wellhead system having one-piece body is used instead of a spool system, then the mandrel type hanger assembly is used (**Figure 2.12c**). A casing string with mandrel hanger at the top is run first and once it is cemented, seal assembly is run through the BOP stack on a drillpipe running tool. Subsea wellhead systems consist of such mandrel type hangers and seal assembly.

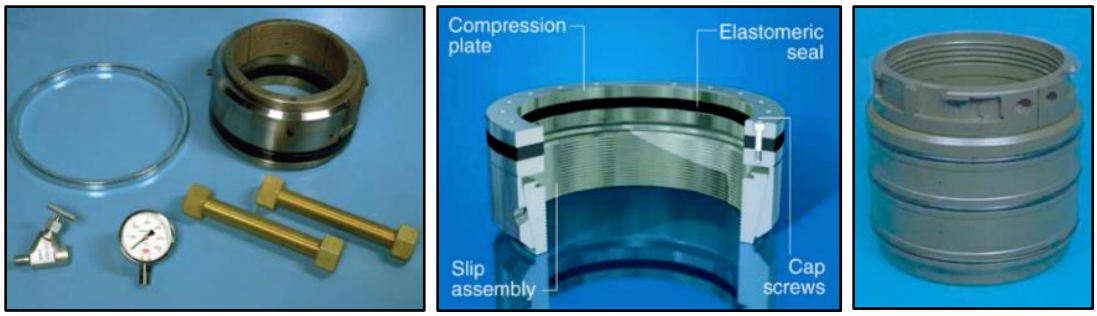

(a) **(b)** **(c)**

Figure 2.12: Different types of elastomer hanger seal assemblies: (a) weight-set slip-and-seal assembly with casing head installation components, (b) mechanical-set slip-and-seal assembly in sub-mudline liner hanger assembly, and (c) mandrel type hanger seal assembly (Speer 2006)

In offshore wells, as drilling depth increases, it is a common practice for operators to run a liner string instead of running a full casing string back to the wellhead. The liner is typically hung from the previous casing and/or cemented in place. Conventionally, liner hanger systems used to rely only upon the cement to provide sealing between liner/casing overlap and maintain well integrity. The challenges associated with obtaining a good quality primary cementing and financial incentive in not running the cement throughout the overlap up to the liner hanger

necessitated a backup sealing mechanism or a barrier (Smith and Williford 2006). This led to development of liner-top packer or liner hanger with integrated seal assembly.

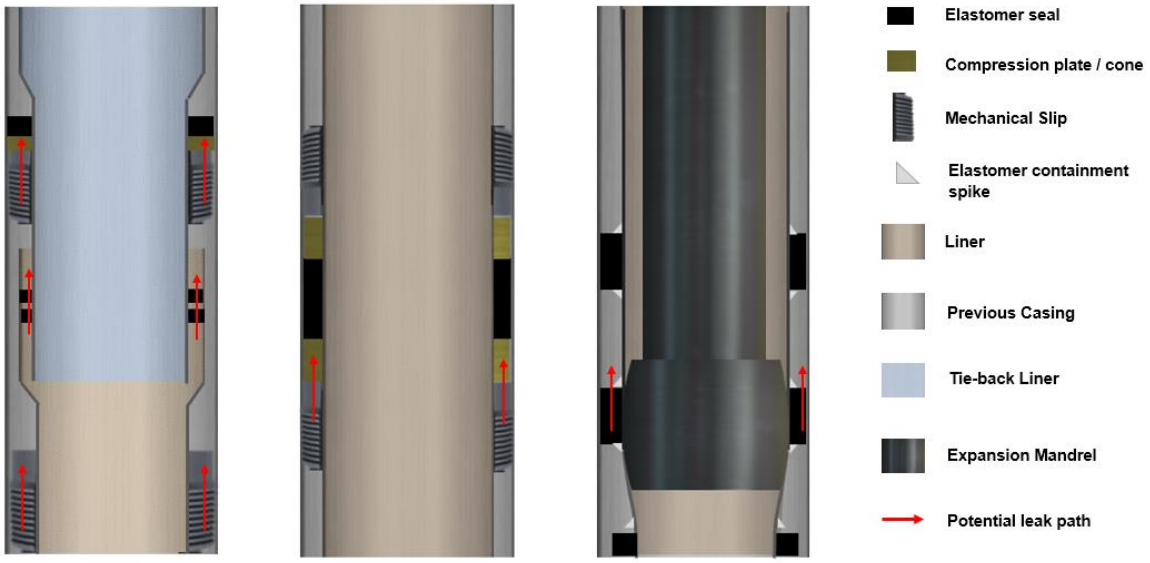

Figure 2.13: Comparison among (a) liner top packer assembly, (b) integral liner hanger seal, and (c) expandable liner hanger seal assembly (Patel et al. 2019a)

The conventional liner hanger consists of cone and slips components to hang the liner. The slip has serrated teeth on it and the cone acts as a guide to redirect the slips toward casing for engagement during the setting process. The seal assembly is either integral to the liner running tool or can be installed later requiring second trip. The assembly is set either mechanically or hydraulically applying required setting force resulting in engaging of the slips followed by seal energization. The schematic of conventional liner hanger with seal assembly is provided in **Figure 2.13a** and **Figure 2.13b.**

Expandable liner hanger is a new technology whose application is gaining momentum in the industry. Expandable liner hanger consists of a smooth body with no moving parts and elastomer elements bonded to its outer profile (**Figure 2.13c**). The idea is to expand the liner either

hydraulically by applying internal pressure or mechanically by running in a solid mandrel having larger outer dimeter than the internal diameter of hanger. Expansion of hanger body leads elastomer elements to compress against the casing resulting in seal energization. The seals not only provide hydraulic integrity but also act as anchor for the liner. The advantages of expandable liner hangers over the conventional hangers is readily available in the literature (Mullins 2016; Mccormick et al. 2012; Walvekar and Jackson 2007; Smith and Williford 2006; Lohoefer et al. 2000).

It has been observed that the failure of a seal assembly is often responsible for well control incidents. A QC-FIT evaluation report on a recent shallow gas incident (BSEE 2014) revealed failure in seal assembly as one of the potential causes. An informal survey of several Gulf of Mexico operators indicated that about 30% to 50% of the pressure seals in overlaps failed (Lohoefer et al. 2000). Another report indicates that as many as 18% of offshore wells worldwide are estimated to have some form of weakness or uncertainty in seal assemblies and the record of failures of critical liner-hanger seals in HP/HT completions, for example, has become a large concern. (Van Dort 2009).

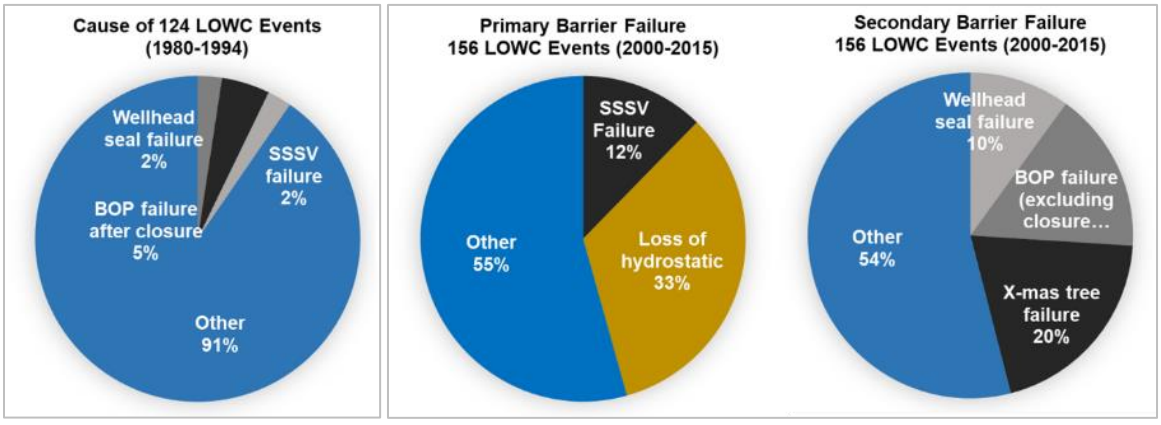

(a) **(b)**

Figure 2.14: Causes of loss of well control (LOWC) events occurred during (a) 1980-1994, and (b) 2000-2015. Black and gray shades represent causes likely related to seal and/or supporting component failures (From Patel et al. 2019a based on data of Elhard et al. 2017 and Holand 2017)

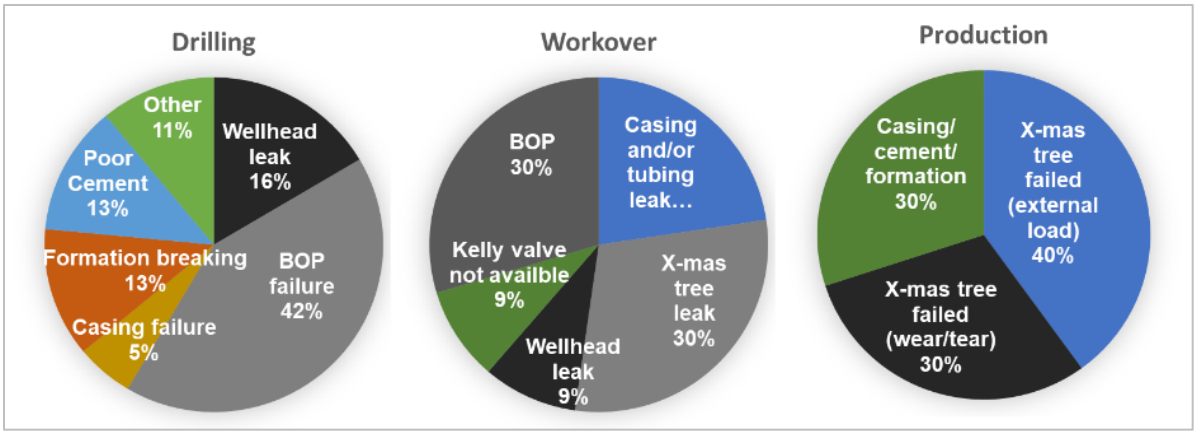

(a) **(b)** **(c)**

Figure 2.15: Causes of secondary barrier failure during (a) drilling, (b) workover, and (c) production in 156 LWOC events occurred between 2000-2015. Black and gray shades represent causes likely related to seal failures (From Patel et al. 2019a based on data of Elhard et al. 2017 and Holand 2017)

SINTEF keeps a database of well blowouts and loss of well control (LWOC) events and reports that most blowouts occur during drilling, followed by workover, completion, and production. Based on review of SINTEF LWOC data provided in Holand (2017) and Elhard et al. (2017), statistical analysis was performed to identify frequency of potential seal related causes. Causes of LOWC events occurred during the period of 1980-1994, and 2000-2015 are presented in **Figure 2.14**. In the pie charts, black and gray shades represent causes likely related to failures in seal and/or supporting components such as - wellhead leak, sub surface safety valve failure, x-mas tree failure, and BOP failure after successful closure. Charts clearly indicate almost half (46%) of the failures in secondary barrier originate in seal containing components. The secondary barrier failures were further categorizing into drilling, workover, and production activity (**Figure 2.15**). It is clear that BOP, x-mas tree, and wellhead leaks are the top three causes of failure in secondary failure.

With the increasing global energy demand and dwindling of conventional resources, High-Pressure High-Temperature (HPHT) wells have become increasingly commonplace. Recent data

by (Oil & Gas iQ 2015) indicates that seal is considered as one of the biggest technological challenge associated with HPHT oil & gas exploration (**Figure 2.16**)

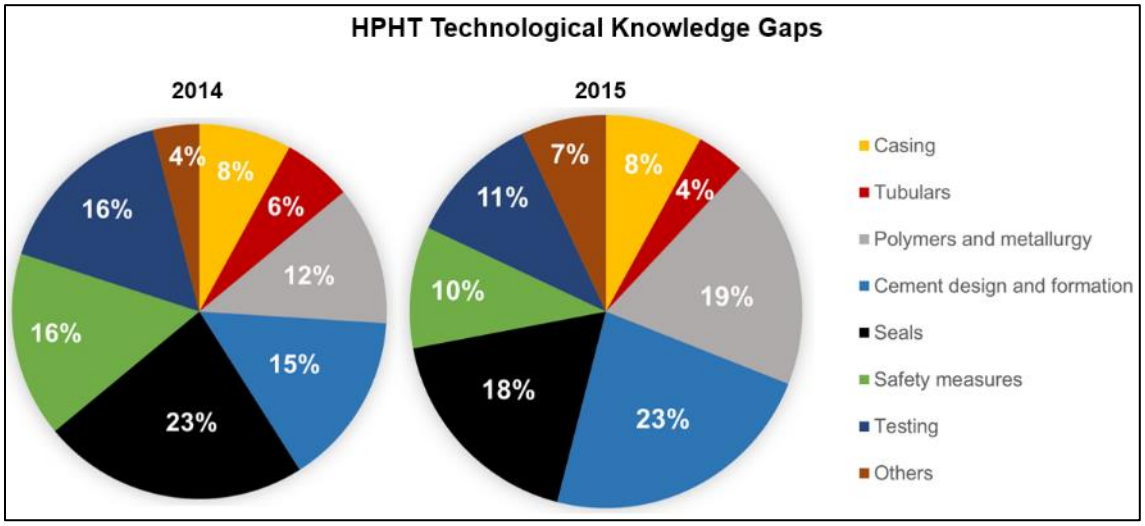

Figure 2.16: Technological knowledge gaps for high pressure high temperature (HPHT) well construction (source of data: Oil & Gas iQ 2015)

Table 2.3: Likelihood of elastomer seal bearing equipment being present in the well during a blowout. "X" indicates "expectation" of equipment being present while "P" indicates "possibility" of presence (Elhard et al. 2017)

	Well Activity					
Likely HSE Equipment	**Drilling**	**Completion**	**Workover**	**Production without external cause**	**Wireline**	**Likelihood of being present during a blowout**
BOP	x	x	x		x	94.0
SSSV			p	x		27.3
Packer		p	p	x	p	35.3
Wellhead	x	x	x	x	x	100.0

These elastomer seal bearing equipment can be ordered in terms of likelihood of presence during different well activity (Elhard et al. 2017). **Table 2.3** indicates that the wellhead followed by BOP are far more likely to be present when a blowout occurs in comparison to the packer and

SSSV. Present report and proposed dissertation work will be focused on wellhead and casing/liner hanger assemblies. Majority of discussion, literature review, elastomer material properties, and some of the function aspects will also be applicable to other equipment such as BOP, packer, and SSSV.

2.3 Failure Mechanisms

2.3.1 Operating Conditions

Before analyzing failure mechanisms, it is important to understand the typical operating conditions that elastomer seals must endure. As per 2012 estimate, over 50% of proven oil and gas reserves in the US lie below 14,000 ft (Shadravan and Amani 2012). American Petroleum Institute (API) defines High-Pressure High-Temperature (HPHT) condition as operating pressure and temperature of greater than 15,000 psi and 350°F respectively.

Table 2.4: High-Pressure High-Temperature (HPHT) conditions defined by regulators (API, NORSOK) and service companies

HPHT	HPHT Tier 1	HPHT Tier 2	Source
>15,000 psi > 350°F	-	-	API
15,000 – 20,000 psi 350-400°F	20,000 – 30,000 psi 400-500°F	>30,000 psi > 500°F	Baker Hughes
10,000 – 15,000 psi 300-350°F	15,000 – 20,000 psi 350-400°F	>20,000 psi > 400°F	Halliburton
>10,000 psi > 300°F	-	-	NORSOK
10,000 – 15,000 psi 300-400°F	20,000 – 35,000 psi 400-500°F	35,000 – 40,000 psi 500-600°F	Schlumberger

As shown in **Table 2.4**, the description of HPHT condition varies depending on regulators and operating/service companies. Most of the HPHT operations in shale plays and many of the HPHT deepwater wells, particularly in the Gulf of Mexico, fall into Tier I (Shadravan and Amani 2012).

Elastomer seal during the service life encounters variety of chemicals. In addition to liquid and gaseous hydrocarbon, a typical well may encounter hydrogen sulfide, carbon dioxide, mercaptans, etc. These sour and corrosive gases can notably impact elastomer material. Moreover, because of such corrosive downhole environment, corrosion inhibitors are frequently added to drilling fluid, fracturing fluid, completion fluid, packer fluids, etc. In addition to corrosion inhibitors, solvents, surfactants, acids, etc. chemical are widely used for various purposes such as reducing formation damage, enhancing production, improving wellbore stability, etc. Elastomer seals particularly the ones used in wellhead, SSSV, and packer must withstand and maintain sealability under such complex chemical environment.

2.3.2 Material Failures

As discussed previously failure in seal assembly is a larger concern for the industry. Such failures not only reduce the effectiveness of the applications for which the liners are intended, but they also increase well costs because of the remedial operations that must be undertaken. Furthermore, if such failures go undetected then it can greatly compromise the well's process safety, resulting in loss of well control with greater environmental, safety, and business consequences. Failure in seal assembly can be categorized into (i) material failure of the elastomer seal component, and (ii) operational and hardware failure.

Extensive literature is available on elastomer material failure as elastomer is a widely used seal material in several industries. The elastomer material has several limitations in terms of

maximum differential pressure, temperature, chemical, and gas resistance. Elastomer can fail in several ways but some of the major modes of failure are rapid gas decompression, temperature and chemical degradation, extrusion and nibbling, compression set, wear, spiral failure etc. (Elhard et al. 2017).

2.3.2.1 Physical Failure

Rapid Gas Decompression (RGD) or gasification or explosive decompression (**Figure 2.17a**) is one of the most common mode of seal failure. In downhole high-pressure environment, seal may come into contact with gas which gradually absorbs into molecular voids of the elastomer material. If the surround pressure suddenly decreases, then the absorbed gas expands and tries to rapidly diffuse out of the material resulting in development of cracks and eventual 'explosion' (**Figure 2.17a**). Elastomers with less hardness and elastic modulus are more prone to RGD (Marco Rubber & Plastic Inc. 2018). The risk of decompression increases at elevated temperature or very low temperature when elastomer becomes brittle. The term 'explosive' is misleading as decompression damage can occur when pressure decreases gradually over several hours similar to the time associated with tripping out operation (Mackenzie and Garfield 2007).

Temperature degradation (**Figure 2.17c**) is another common risk associated with elastomers. At high temperatures or temperature changes, elastomer seal may exhibit radial cracks and/or sign of softening. It is becoming increasingly common to drill and operate in high pressure high temperature (HPHT) conditions. It is challenging to seal with elastomer in temperatures beyond 250-300°F (Mackenzie and Garfield 2007).

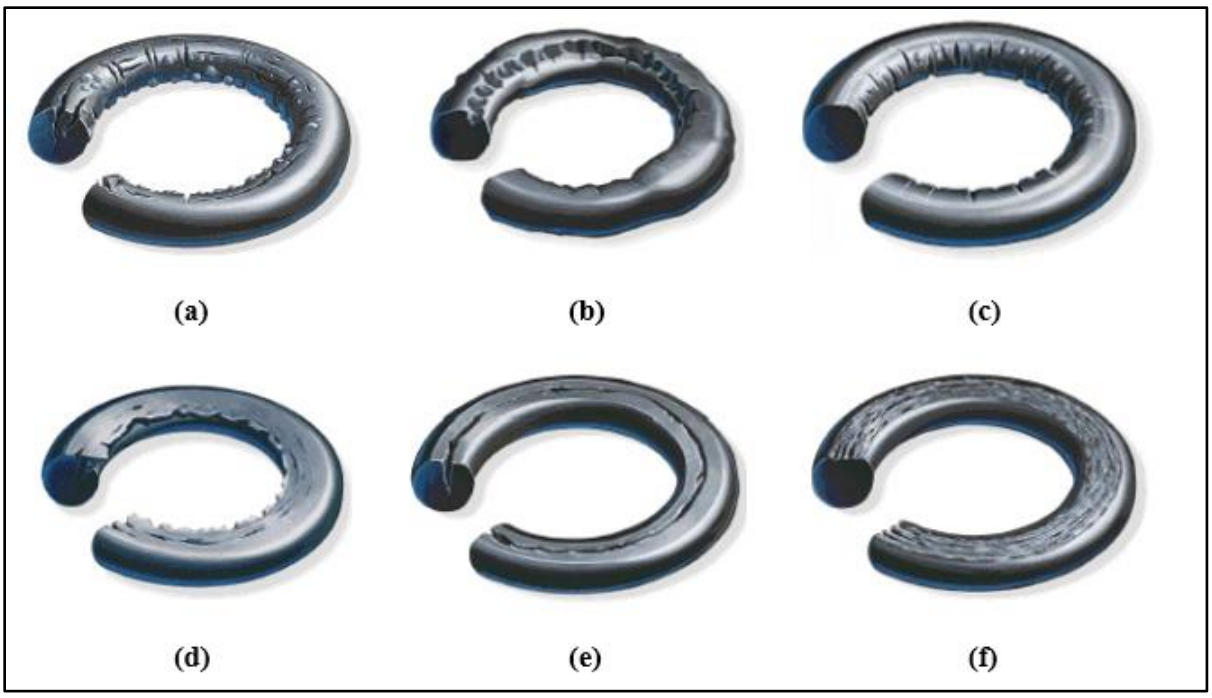

Figure 2.17: Type of material failures in elastomer: (a) explosive decompression, (b) chemical degradation, (c) Thermal degradation, (d) extrusion, (e) compression set, and (f) abrasion-friction (image source: Marco Rubber & Plastics Inc.)

Extrusion and nibbling (**Figure 2.17d**) is a type of mechanical failure which can degrade the sealability of elastomer. It occurs when an elastomer seal is sealing against moving surfaces with friction or static interfaces with pulsating or cyclic movements gets pulled or nibbled resulting in loss of material. Failure can also occur due to shearing of seal element across the extrusion gap. High pressure differential, thermal stress or other operational load induced movement at the frictional interface between elastomer and casing can lead to such failure. The extrusion failure can not only affect sealability but also makes the service tool or equipment difficult to retrieve.

Compression set is one of the more commonly observed failure modes. This failure (**Figure 2.17e**) typically arise due to improper dimensioning of the seal element (Elhard et al. 2017). This can result in permanent deformation of seal or pre-mature extrusion of seals (Daemar Inc. 2015). Abrasion or wear type failure (**Figure 2.17f**) can occur during storage, handling, or installation.

Primary causes can be improper lubrication, uneven contact surfaces, presence of debris/solids at sealing interface etc. This failure mechanism can be important for tools that are moved or reciprocated frequently during downhole operation.

2.3.2.2 Chemical Degradation

Chemical degradation is a major factor affecting seal performance. During the service, elastomer may come into contact with different fluids such as drilling, completion, fracturing, formation brine, or production fluid containing various solvents, caustics, acids or corrosive chemicals. Leaching of these chemicals into elastomer can weaken its polymer structure (Campion et al. 2005). The leaching becomes more severe as temperature increases. The absorption of fluid can also lead to swelling increasing the risk of other types of failure such as abrasion or extrusion (Elhard et al. 2017). Moreover, presence of oxidation agents (such as ozone) during service or storage and transportation can lead to scission reaction within elastomer resulting in weakened molecular structure and increased risk of degradation (Campion et al. 2005). Increasing temperature makes chemical degradation faster and worse. Fernández and Castaño (2016) studied effect of crude oil on elastomers at 150°F and 1000 psi for 168 hours. They observed reduction in tensile strength and elongation at break. Aging also affected hardness and compression set, and caused volumetric swelling. Crude oil with high percentage of saturates and aromatic caused more severe degradation.

The three major gases typically encountered in oil & gas wells are Hydrogen Sulfide (H_2S), Carbon Dioxide (CO_2), and Methane (CH_4). CO_2 and H_2S can lead to severe chemical degradation of elastomers. However, CH_4 typically does not react chemically with elastomer but it can permeate through the material and cause other physical alterations.

Effect of H_2S

Sour oil reservoir can lead to high hydrogen sulfide content in operating environment. H_2S is known to cause notable deterioration in elastomer physical properties. Cong et al. (2013) conducted aging experiments using HNBR samples in aqueous solutions of H_2S at 1000±100 psi pressure and 212°F temperature. They observed reduction in tensile strength, hardness, and elongation capability of the elastomer. Degradation in HNBR sample can be attributed to homolysis or heterolysis reactions. In aqueous solution, H2S dissociates into H+ and HS-ions. H+ causes hydrolysis of the C≡N group in HNBR (**Figure 2.18**) while HS- attacks C=O. This results in C=S and C-C=S groups. In homolysis, mercapto radicals from H2S (H• and HS•) causes reaction with elastomer polymer and results in macromolecule radical. This radical then to react with another mercapto radical. This chain reaction continues, dissociates triple and double bonds, and eventually results in saturated C-S-C bonds. These processes notable altera physical properties of elastomer. Fernández and Castaño (2016) studied effect of H2S concentration on NBR elastomer and observed development of brittle fracture surfaces with increase in concentration (**Figure 2.19**). They also observed that increase in H2S concentration reduces tensile strength, elongation break, and resilience.

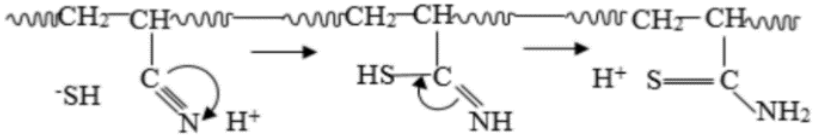

Figure 2.18: Nucleophilic reaction mechanism showing breaking of acrylonitrile group in HNBR (Cong et al. 2013)

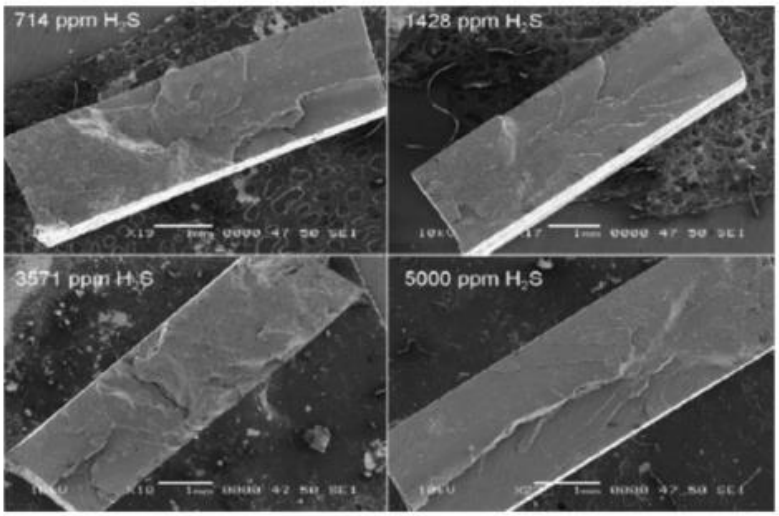

Figure 2.19: SEM images of NBR samples aged with different concentration of H_2S for 168 hours at 203°F (Fernandez and Castano 2016)

Tynan (2016) compared reactivity of various elastomers to H_2S with their glass transition temperature and high temperature performance (**Table 2.5**). It was shown that the decreasing order of H_2S resistance is - FFKM > FKM > FEPM > HNBR > NBR.

Table 2.5: H_2S resistance, glass transition temperature, and high service temperature of various elastomers (Carrol 2016)

Elastomer Type	Resistant to H_2S	Glass Transition (Tg) °F	Upper Service Temp. °F
NBR	Most reactive	-22	248
Low Temp. HNBR	Most reactive	-40	320
HNBR	Less reactive	-22	356
FEPM	Non-reactive	41	482
Low Temp. FKM	Less reactive	-40	437
FKM	Most reactive	1.4	437

Low Temp. FFKM	Non-reactive	-22	464
FFKM	Non-reactive	32	500

Effect of CO_2

Carbon dioxide is stable, inert, and non-toxic under normal conditions. Its carbon-oxygen double bond is very stable with high dissociation energy of 732 KJ/mol. Typically, it would not cause chemical reaction with elastomer material. However, in presence of aqueous medium such as water or brine, it can form carbonic acid. In large quantities, this weak acid can become corrosive and cause chemical reactions with elastomers. This irreversible reaction is caused by dissociation of weak C≡N bond in NBR and results in amine groups. The C=C double bond in EPDM exhibits relatively higher resistance to dissociation. The C-F bond in Fluorocarbon elastomer is highly stable bond with very high dissociation energy and hence, FKM exhibits more resistance to CO_2 degradation.

Fernández and Castaño (2016) demonstrated that increase in CO_2 concentration increases volumetric swelling and permanent deformation in NBR elastomer. The increase in permanent deformation plateaus at very high concentration of CO_2. The SEM images show decrease in brittle fracture surface with increase in CO_2 concentration in NBR (**Figure 2.20**). Dajiang et al. (2017) studied aging of mechanically compressed NBR and HNBR samples in presence of liquid and gaseous CO_2. They observed increase in elastomer weight after aging in comparison to control samples. They also observed reduction in hardness which was more severe in gaseous containment compared to liquid CO_2. Furthermore, their results indicate that mechanical loading increases the degradation in presence of CO_2. Based on SEM and energy dispersive spectroscopy (EDS), they

concluded that swelling and damage of elastomer increases with increase in compression load (**Figure 2.21**). This damage is more severe in liquid CO_2 compared to gaseous.

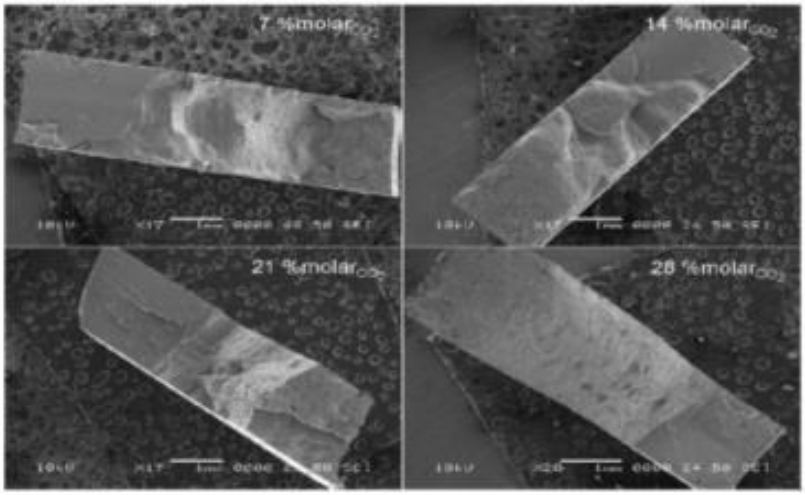

Figure 2.20: SEM images of NBR aged in presence of carbon dioxide at 203°F for 168 hours (Fernández and Castaño 2016)

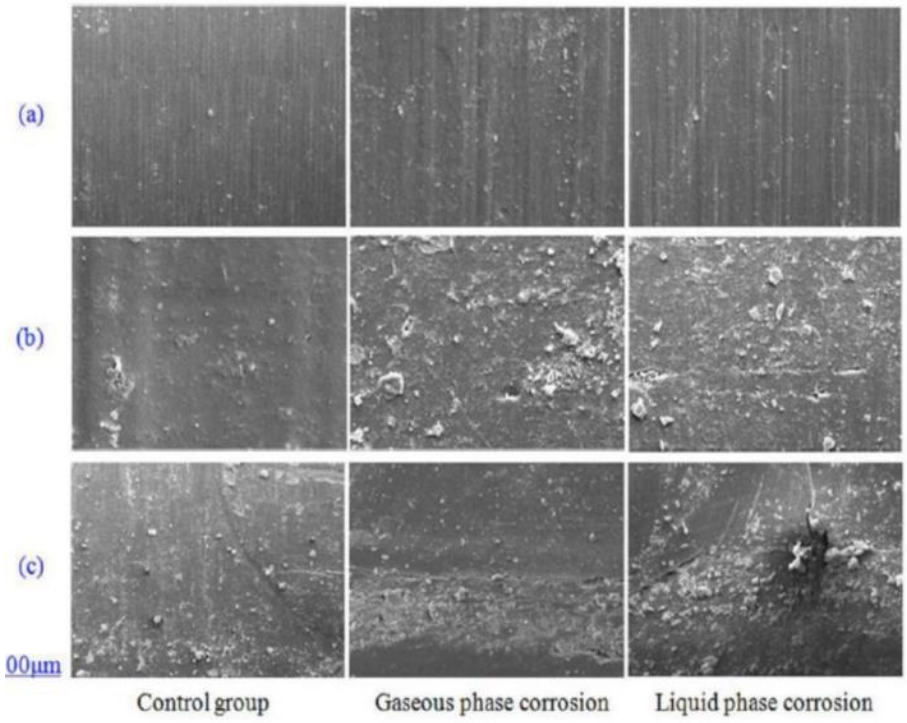

Figure 2.21: SEM image of HNBR samples aged in presence of gaseous and liquid CO_2 at different compression loads: 0 lbf (a), 1349 lbf (b), and 2698 lbf (c) (Dajiang et al. 2017)

2.3.3 Equipment Related Functional Failures

Deviations from recommended installation and relevant operational procedures and failure in equipment or structures that support the elastomer seal component are often responsible for loss of sealability or lack of seal energization. Unlike elastomer material failure, minimal research data is available in public domain that discusses operational, hardware or other peripheral failures affecting performance of seal assembly. Following are some of the important modes of functional failures gathered from literature.

Installation of conventional weight-set or mechanical set seal assembly often requires setting force in the range of 100,000 lbf to attain desired seal energization (Wiliford and Smith 2007). However, sometimes it is not possible to exert such force due to variety of reasons such as well deviations, drag forces, insufficient pipe weight etc. Such operational failures can significantly minimize seal performance.

Conventional liner hanger system consists of slip and cone components that provide mechanical anchoring to the liner and also act as support during seal energization. Concentration of excessive radial stress in slips can potentially collapse inner hanger mandrel (Zhong et al. 2017) and affect the energization process. Any compressive or tensile forces applied to the hanger body are permanently trapped between the slips (Fothergill 2002). The slips also damage casing and potentially increases risk of corrosion and other mechanical failure. Lack of centralization can also pose risk of non-uniform seal energization resulting in less than desired contact stress. Failure or anomalies in support components such as back-up ring or compression plate can result in extrusion of elastomer element (**Figure 2.22**). The back-up system is often designed to expand to the casing ID and fill the extrusion gap between seal and casing ID. Some of the major causes for back-up component failure are - excessive load, bending, shearing, or material strength reduction due to

chemical/temperature changes. One such failure in compression packer is shown in **Figure 2.23a**. Upton (2009) 22 incidents of failure in slip join packing system occurred between 2000 and 2008. It was observed that wear of seal element was the primary failure mechanism (**Figure 2.23b**). Some of the failure cases were caused by corrosion pitting of components.

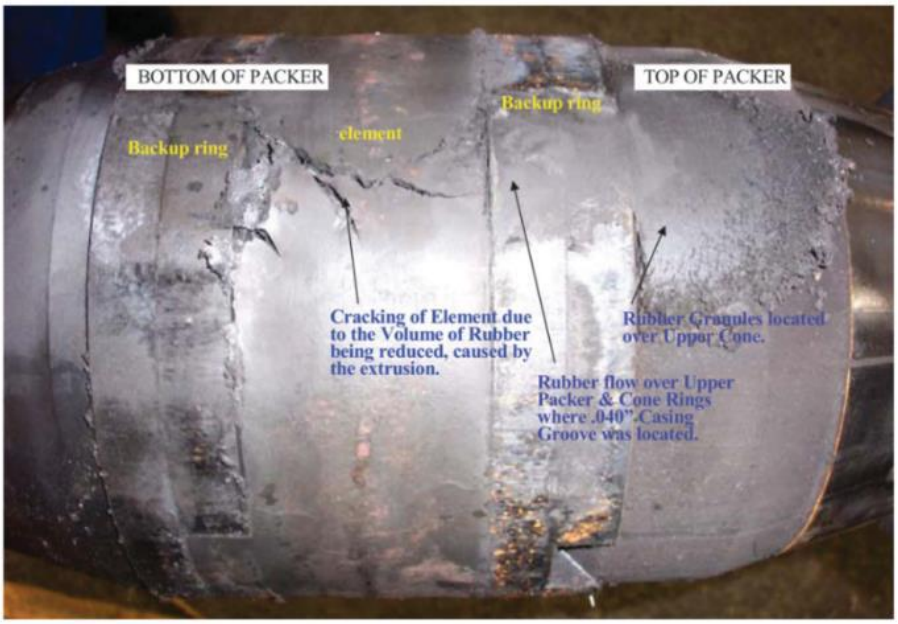

Figure 2.22: Failure in backup ring causing extrusion of elastomer element in packer equipment (Humphreys and Ross 2009)

(a) **(b)**

Figure 2.23: (a) Failure of shoulder drop in a compression packer (Hu et al. 2017), and (b) internal wear of packer element (Upton 2009)

Failure of hanger body is also a concern. The body of hanger assembly can collapse due to excessive stresses generated from above or below the seal element. Payne et al. (2016) presented inadequacy of traditional calculations such as two diameter rule, Barlow equation, Lame equation, API burst equation etc. for determining capacity of liner hanger body. They suggested to use computer models depicting actual complex geometry of hanger assemblies to determine true capacity.

Most of the hanger systems consist of many mechanical moving parts which can act as potential leakage paths. Exposed slips, hydraulic ports, and other moving components act as tortuous path and they are more prone to pack-off by solid particles. This can lead to slip hung up or failure in release of setting tool. The hanger and seal assembly may pre-set while running in the hole if the tripping is too fast or if the element is swabbed off (Walvekar and Jackson 2007). The cyclic effects of thermal expansion and contraction may lead to relative movements among the components and affect the sealability performance (Brown and Witwer, 2017).

2.4 Industry Standards and Gap Analysis

2.4.1 Overview of Relevant Standards

Comprehensive literature review indicates that all industry standards relevant to elastomer material and seal assemblies can be categorized into two groups. Majority of standards from API (American Petroleum Institute), ISO (The International Organization for Standardization), and NORSOK (Norsk Sokkels Konkuranseposisjon - Standards by Norwegian petroleum industry), provide guidelines for elastomer qualification testing specific to oil & gas industry equipment. Other reviewed standards such as ASTM (American Society for Testing and Materials), NACE (National Association of Corrosion Engineers), and ANSI (American National Standards Institute) include

protocols and guidelines primarily for laboratory-based testing of elastomer properties and failure characteristics.

2.4.1.1 API, ISO, and NORSOK Standards

The list of relevant API, ISO, and NORSOK standards is provided in **Table 2.6**. Some of the API and ISO standards are similar and cross-reference each other. For example, API 17D and ISO 13628 are similar.

API SPEC 6A (ISO 10423) contains specifications and recommendations for the performance, dimensional and functional interchangeability, design, materials, testing, inspection, etc. for wellhead and christmas tree equipment. API 17D (ISO 13628-4) is specifically deals with the subsea wellhead equipment and often refers to API 6A. Both these standards use the term "annulus seal assemblies" that encompass hanger seal assemblies. The annexure F of API6A contains information on elastomer validation testing via pressure and temperature cycles and also covers thermomechanical performance i.e. immersion testing of seals with an option for fixture testing using the actual seal design. API 17D does contain screening tests for material compatibility with various chemicals; comprising of three levels of screening depending on the complexity of testing. However, this section is listed as informative and not mandatory compliance. This standard requires that applied stresses to the seal structural components observe predetermined limitations as verified by either engineering calculations or finite element analysis. Both standard mainly aim to verify functionality of the sealing system rather than the material validation.

Table 2.6: List of API, ISO, and NORSOK standards relevant to elastomer seal assembly in wellhead and liner hangers

Standard	Description
API 6A	Specification for Wellhead and Christmas Tree Equipment
API 11D1	Packers and Bridge Plugs
API 17D	Design and Operation of Subsea Production Systems – Subsea Wellhead and Tree Equipment
API 17TR8	High-pressure High-temperature Design Guidelines
API 19LH	Specification for Liner Hangers
ISO 10423	Specification for Wellhead and Christmas Tree Equipment
ISO 13533	Petroleum and natural gas industries — Drilling and production equipment — Drill through equipment
ISO 13628	Design and Operation of Subsea Production Systems – Subsea Wellhead and Tree Equipment
ISO 14310	Petroleum and natural gas industries — Downhole equipment — Packers and bridge plugs
ISO 23936	Petroleum, petrochemical and natural gas industries – Non-metallic materials in contact with media related to oil and gas production – Part 2: Elastomers
NORSOK M-710	Qualification of non-metallic materials and manufacturers - polymers

The industry also uses standards developed for packer equipment - ISO 14310:2008E and API Specification 11D1. They provide guidelines for both manufacturers and end users in the selection, manufacture, design, and laboratory testing of the many types of packers available in today's market. ISO 14310/API 11D1 establish a minimum set of parameters with which the manufacturer must comply. The International Standard is structured with the requirements for both quality control and design verification in tiered rankings. There are three grades or levels established for quality control and six grades (plus one special grade) for design verification.

The quality standards range from grade Q3 to Q1, with grade Q3 carrying the minimum requirements and Q1 outlining the highest level of inspection and manufacturing verification

procedures. Provisions are also established to allow the end user to modify the quality plans to meet the specific application by including additional needs as supplement requirements.

The standard design-validation grades range from V6 to V1. V6 is the lowest grade and V1 represents the highest level of testing. A special grade (V0) was included to meet special acceptance criteria requirements. These six standard validation grades are – (i) V6: supplier/manufacturer-defined, (ii) V5: liquid test, (iii) V4: liquid test + axial loads, (iv) V3: liquid test + axial loads + temperature cycling, (v) V2: gas test + axial loads, (vi) V1: gas test + axial loads + temperature cycling, (vii) special validation grade V0: gas test + axial loads + temperature cycling + special acceptance criteria (V1 + zero bubble acceptance criterion)

ISO 14310 (Section 5.3.3.3) provides lists of material tests required for elastomer use in packers. These tests include tensile strength, elongation, and tensile modulus tests, as well as compression set and durometer hardness tests. Note that no minimum elastomer modulus properties are provided to guide elastomer selection in this standard.

API is recently published a standard for liner hanger equipment – API SPEC 19LH. This specification provides requirements for conventional and expandable liner systems including liner hangers, liner packers, liner hanger packers, tieback/polished bore receptacles, seal assemblies, setting adaptors/sleeves, and running/setting tools. The document mentions measurement of five elastomer material properties (tensile strength, elongation at break, elastic modulus at 50% and 100%, compression set, and hardness) and refers to ASTM standards for testing procedure. The standard does not provide any specific elastomer qualification guidelines or acceptance criteria for liner hanger applications. The document refers to ISO 23936 for qualification provisions for elastomer material and stats following as general sealing system requirements – “Chemical and

environmental effects shall be considered for nonmetallic sealing elements in order to determine selection of the seal material. Verification or validation shall establish that the nonmetal sealing element used is suitable for the specific configuration, environment, and application. The evaluations or tests shall ensure compatibility with the technical and functional requirements and shall consider mechanical loads, applied pressure, temperature range, design geometry, and sealing environment."

This specification provide three grades of design validation for seal assemblies: (i) V3 - Supplier/manufacturer defined validation method, (ii) V2 – Multiple engagements with static liquid pressure test plus temperature cycling, and (iii) V1 - Multiple engagements with static nitrogen pressure test plus temperature cycling. For dynamic seal assembly validation testing, the standard refers to API 19AC - Specification for Completion Accessories. For V2 grade, acceptance criteria of 1% pressure reduction over the holding period of 15 minutes is specified. For V1 grade, zero bubbles of nitrogen over 15 minutes of holding period is specified as the acceptance criteria.

NORSOK M-710 and ISO 23936-2 standards discuss qualification of elastomeric components for oil & gas service. They include tests for chemical compatibility, accelerated age evaluation, resistance to extrusion or creep under high pressures, resistance to change in chemical properties at high temperatures, and RGD. These standards acknowledge that elastomer selection can vary based on the end service environment and selection of appropriate material should be ensured.

2.4.1.2 ASTM and NACE Standards

NACE and ASTM standards discuss protocols and guidelines for laboratory-based tests to evaluate elastomer material properties and failure characteristics after exposure to various fluids,

temperatures, and pressures. The list of relevant ASTM and NACE standards is provided in **Table 2.7**. The description of each standards is self-explanatory.

Table 2.7: List of ASTM and NACE standards relevant to elastomer material testing for oil & gas application

Standard	Description
NACE TM0187	Evaluating Elastomeric Materials in Sour Gas Environments Test Temperature: 212, 302, 347°F Test Pressure: 1,000 ± 100 psig
NACE TM0192	Evaluating Elastomeric Materials in Carbon Dioxide Decompression Environments Test Temperature: 77 ± 9°F Test Pressure: 750 ± 50 psig
NACE TM0296	Evaluating Elastomeric Material in Sour Liquid Environments Test Temperature: 212, 250, 302, 347°F Test Pressure: 1,000 ± 100 psig
NACE TM0297	Effects of High-Temperature, High-Pressure Carbon Dioxide Decompression on Elastomeric Materials Test Temperature: 122-446°F Test Pressure: 1,000-5,500 psig
ASTM D575-91	Standard Test Methods for Rubber Properties in Compression Test Temperature: 73.4 ± 3.6°F Test Pressure: Atmospheric (14.7 psi)
ASTM D471-12a	Standard Test Method for Rubber Property— Effects of Liquids Test Temperature: -103 ± 4°F to 482 ± 4°F Test Pressure: Atmospheric (14.7 psi)
ASTM D6147-97	Standard Test Method for Vulcanized Rubber and Thermoplastic Elastomer – Determination of Force Decay (Stress Relaxation) in Compression Test Temperature: -103 ± 3.6°F to 572 ± 5.4°F Test Pressure: N/A
Other potentially useful standards	
ASTM D430-06	Standard Test Methods for Rubber Deterioration – Dynamic Fatigue

ASTM D573-04	Standard Test Method for Rubber— Deterioration in an Air Oven
ASTM D623-07	Standard Test Method for Rubber Property – Heat Generation and Flexing Fatigue in Compression
ASTM D926-08	Standard Test Method for Rubber Property – Plasticity and Recovery (Parallel Plate Method)
ASTM D945-06	Standard Test Methods for Rubber Properties in Compression or Shear (Mechanical Oscillograph)
ASTM D1349-14	Standard Practice for Rubber – Standard Conditions for Testing
ASTM D2632-15	Standard Test Method for Rubber Property – Resilience by Vertical Rebound
ASTM D7121-05	Standard Test Method for Rubber Property – Resilience Using Schob Type Rebound Pendulum

Overall, NACE standards provide test procedures along with protocols for test conditions, specimen preparation, equipment, and reporting of results. NACE standards focus on relative resistance measurements for O-rings or other elastomers to the specific test environments. Similarly, ASTM standards provide test procedures to determine chemical and physical properties of elastomers in laboratory environments.

2.4.2 Limitations and Gaps

Currently available standards provide valid benchmark and consistent testing methodologies for preliminary testing of seal assemblies. Although, there is always room for improvement, the standards cannot be made comprehensive that account for all types of applications. Additional layers of qualification testing at the manufacturer, service provides, and operators' side are essential. Following are some of the major limitations in the existing literature, that may help regulators and industry alike in improving reliability of elastomer seal assemblies:

NORSOK M-710 provides guidance to test a standard O-ring seal with a pre-determined cross-section and squeeze. API 6A uses molded slabs typically cut in form of bone or dumbbell geometry. They provide valid benchmark and consistent methodology for testing materials but material compliance to it does not reflect seal performance in the actual applications involving varying seal geometries (S seals, T-seals, MEC seals, etc.) and cross-sections with varying volume fill, squeeze, etc. parameters. For example, increasing volume fill beyond 85% can significantly increase RGD resistance for some applications (Groves et al. 2001). Another example is an observation that a larger seal cross section increases the probability of damage by decompression because of the longer gas diffusion path in comparison to a smaller seal (Morgan et al. 2008)

The NORSOK is based on a crack rating system for evaluating RGD failure. The criteria are not only subjective but also has two major limitations. First, a large seal may have cracks developed in localized areas that are not critical from the function point of view. A seal that passed functional pressure/temperature test can be deemed failed by stringent NORSOK criteria (Tu and Cheng 2016). Secondly, the cracks are evaluated after removing O-ring from the test fixture. In reality, the seal remains in the housing or fixture during the service and it has been shown that the RGD failure can remain contained under compressed loading state (Morgan et al. 2008).

As listed in **Table 2.8**, the acceptance criteria for the aging tests recommended by NORSOK M-710 are wide considering acceptance of ± 50% change in tensile properties, 20 point loss of hardness and 25% swell and may not be suitable for applications at high end of performance limits (Elhard et al. 2017, Slay and Ferrel 2008). Additionally, use of swelling may not be an appropriate criteria for quantifying or validation seal performance in some conditions. Volume swelling of seal in a closed fixture would result in higher contact stress and may in fact lead to better sealability provided that the stress value does not exceed structural stress limits of housing

or other surrounding mechanical components. ISO 14310 doesn't provide minimum elastomer modulus properties to guide elastomer selection.

Table 2.8: Acceptance criteria for elastomer aging tests as per ISO 23936-2 and NORSOK M-710 (Elhard et al. 2017, Slay and Ferrel 2008)

Measurement	ISO 2396-2	NORSOK M-710
Hardness	+10/-20 units	Not provided
Volume	+25%/-5%	+5%/-1%
Tensile	+/- 50%	+/- 50%

One of the major limitations identified is that the ISO, NACE and NORSOK standard tests do not cover the operating temperature/pressures of field applications. Specifically, as shown in **Table 2.9**, API standards with the exception of API 11D and API 14A do not reflect extreme HPHT conditions increasingly encountered in offshore wells (Elhard et al. 2017). ISO 23936 and NORSOK M-710 considers 2175 psi and 212°F as maximum pressure and temperature respectively for the material compatibility tests. These values are significantly less than the HPHT threshold of 1500 psi and 350°F. The maximum pressure and temperature required by API 6A to qualify wellhead is 20,000 psi at 121°C respectively. This is within the range of HPHT pressure conditions but falls short of qualifying the unit for high temperature service. To supplement this, API published API 17TR8 (HPHT Design Guidelines) to provide design information for service environments with temperatures exceeding 350°F and pressures exceeding 15,000 psi. Moreover, it should be noted that these temperature and pressure qualification levels are for the overall unit and not the elastomeric components explicitly. ASTM and NACE are focused on elastomer

material properties testing but as shown in **Table 2.9,** the test pressure/temperature requirements are not commonly intended for testing elastomers in HPHT environments

Table 2.9: Comparing scope of API standards against HPHT conditions (Elhard et al. 2017)

	HPHT Conditions	API 6A (12th Edition)	API 11D (3rd Edition)	API 14A (12th Edition)	API 14B 6th Edition	API 16A (3rd Edition)	API 17D** (2nd Edition)
Temperature (°F)	>350	Varies*	>350	>350	N/A	<350	<140***
Pressure (psi)	>15k	1k	>15k	>15k	N/A	<20k	<15k
Chemical Compatibility Issues	Yes	Yes	Yes	Yes	N/A	No	No
Rapid Gas Decompression Issues	Yes	No	Yes	Yes	N/A	No	No

*listed as the maximum specified temperature for the given application
**Identical to ISO 13628: Petroleum and natural gas industries -- Design and operation of subsea production systems -- Part 15: Subsea structures and manifolds
***End use temperature and pressure to be specified by user.

Another major gap is lack of storage requirement for elastomer material in reviewed standards. No maximum storage timeframes are provided in the standard, and no requalification criteria are defined for elastomers taken from storage prior to being installed in service. None of the API, ISO, and NORSOK standards provide guidelines related to appropriate protection during storing, shipping, handling, installation, etc. operations. No information is available on how logistical and operational conditions can affect elastomer performance or rating. Current standards can refer to aerospace industry's standard - ISO 27996 (Aerospace fluid systems --Elastomer seals -- Storage and shelf life) for elastomer components similar to the ones used in oil & gas industry. ISO 27996 recommends 112 months for NBR and HNBR, and 160 months for FKN, FFKM, and FEPM as maximum storage timeframes.

All standards discuss chemical compatibility with respect to pure hydrocarbon gases and liquids such as methane, heptane, carbon dioxide etc. No guidance is available on effects of

complex downhole chemicals such as drilling or completion fluids, hydrates, scale, corrosion inhibitors and other additives, etc.

Within API 6A, casing hangers are categorized into five groups depending on the complexity of their function – (i) absence of seal assembly, (ii) unidirectional and (iii) bidirectional hanging capability, (iv) presence of retention feature to hold hanger in place, and (v) without back pressure valve. However, the standard does not provide different qualification testing requirement for each of these groups.

As discussed in previous section, API 19LH and other API standards in general, refer to other standards such as ISO standards for specific elastomer qualification criteria which are not customized as per end application or equipment type. API standards require that the seal element and individual seal structural mechanisms be qualified to claimed ratings. However, there is no discussion on or requirement to prove cooperation of both material and functional aspects. Although structural components can be considered as rigid but small deflections within them can certainly change sealability across various ranges of temperature, pressures, and loads. As discussed and demonstrated for metallic seals by Brown and Witwer (2017), a system level validation or qualification testing where hanger and seal assembly react or have relative movement with each other similar to the actual field installation process is essential to validate performance of seal assembly in its entirety. Similarly, for finite element validation it becomes important to simulate installation process before pursuing simulations under pressure, temperature, and loading scenarios.

Elhard et al. (2017) presented a breakdown of development process of a well component or equipment. They reviewed and checked whether various standards relevant to elastomer

material testing provide guidance in all these steps of component design. As shown in the results (**Table 2.10**)

Table 2.10: Scope of guidance provided by various standard agencies to different steps in component design process (Elhard et al. 2017)

Process	Notes	API	ISO	NORSOK	NACE	ASTM	MIL-SPEC
System Design Guidance	Overall system/tool performance criteria	X	X				
Material Selection Guidance	Selection of most appropriate elastomer			X			X
Laboratory Material Qualification	Lab testing of material properties				X	X	X
HPHT Laboratory Qualification	HPHT laboratory testing of properties						
Chemical Compatibility Qualification	Lab chemical compatibility testing			X	X	X	X
Installed System Qualification	Performance testing of system/tool	X	X				
HPHT System Qualification	HPHT testing of system/tool						
Storage/Shipping Guidance	Packaging and storage considerations	X	X				X
Field Requalification	Evaluation of system components in field						X

To summarize, it can be concluded that no single family of standards provide complete guidance for elastomer seal selection, qualification of material, functional qualification of seal assembly, packaging, storage, etc. Some of the gaps can be filled by revisiting adjacent industry standards and consolidating them under one family of standards. Additional research is needed to customize qualification or acceptance criteria depending on end-application and equipment type. Moreover, there is also a need for understanding target seal energization criteria for complete sealability. Effect of functional failures in seal assembly and equipment level performance evaluation of elastomer seals are another two important areas of research.

2.5 Literature Review

2.5.1 Relevant Studies

Berger (2004) designed, built, and tested a retrievable 7 ¾-in. packer element for high pressure high temperature environment. The objective of the study was to examine various backup systems that provide support during energization. Different systems such as the carbon steel foldback ring, mesh rings, garter springs, and combination of these were evaluated at different temperatures and differential pressures. Sealing performance was tested by conducting ISO 14310 standard liquid and gas tests. A FEA study was also conducted to support the experimental work.

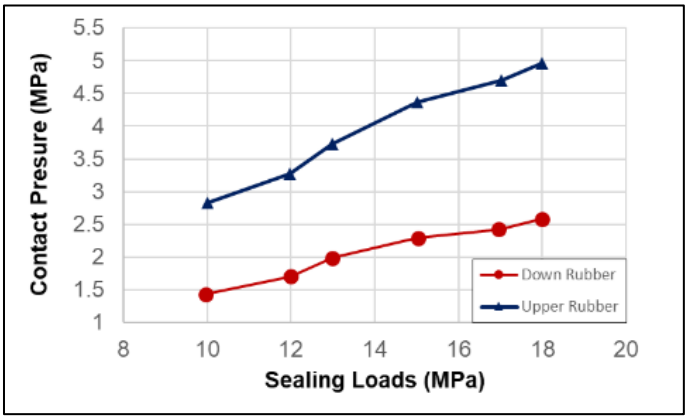

Figure 2.24: Contact pressure as a function of setting load (Recreated after Feng et al. 2010)

Feng et al. (2010) conducted two-dimensional finite element analysis on packer consisting of two elastomer elements separated by a metal ring. They examined the contact pressure in both seals for various setting loads and observed a relationship that was practically linear (**Figure 2.24**). The seal on the compression side (upper side in this case) had consistently higher contact pressure than the lower seal.

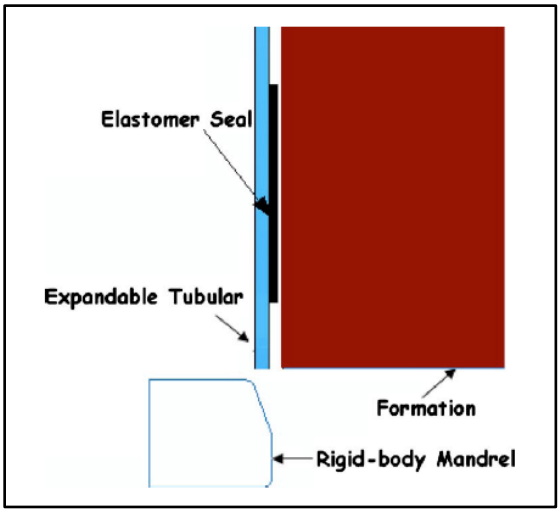

Figure 2.25: 2D axisymmetric finite element model of expandable liner hanger seal (Alzebdeh et al. 2010)

Alzebdeh et al. (2010) conducted finite element simulation of the compression of elastomeric seals in an open hole expandable type liner hanger (**Figure 2.25**). They modelled the formation in three different forms, as a rigid body, an elastic, and an elastic-plastic material. Two different boundary conditions (fixed-free and fixed-fixed) were employed depending on prevailing practices of oil operators in such applications. The effect of seal length and thickness, compression ratio, and type of formation behavior on the contact pressure were determined. Results demonstrated that the rigid formation provides the highest contact pressure compared to elastic and elastic-plastic type formation. Moreover, a thicker seal with a larger compression ratio was observed to yield higher contact stress (**Figure 2.26**). Furthermore, they observed that contact

pressure decreases with increase in seal length up to 200 mm and pressure remains practically constant thereafter. The effect of tubular end conditions was determined to be negligible. No theoretical or experimental validation was provided for the simulation results.

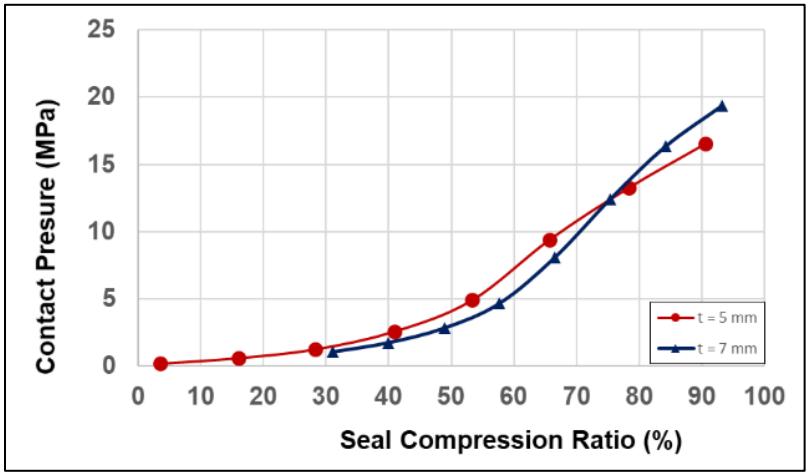

(a)

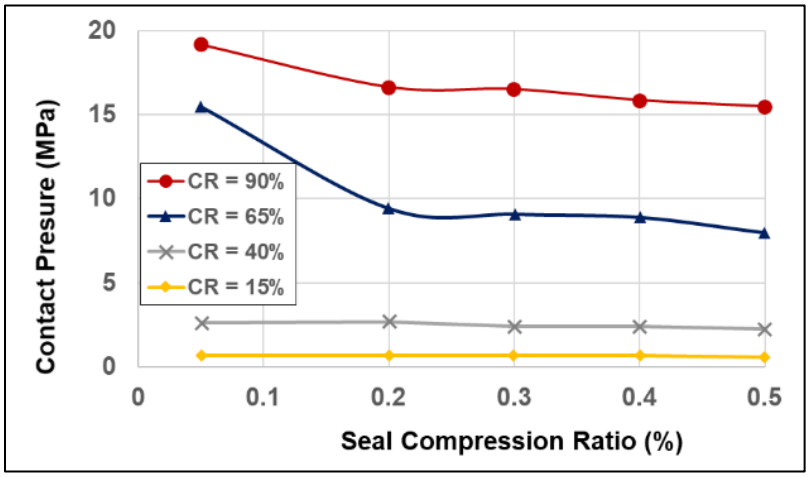

(b)

Figure 2.26: Effect of seal thickness (a) and seal length (b) on contact pressure at various compression ratio (Recreated after Alzebdeh et al. 2010)

Guo et al. (2011) used FEA to study a specific design of packer consisting of rubber tube, cone, central pipe, expansion sleeve, and casing pipe. They used nonlinear material properties for

the elastomer element and presented contact pressure variation as a function of applied load at different seal thickness. No validation for the FEA results was provided.

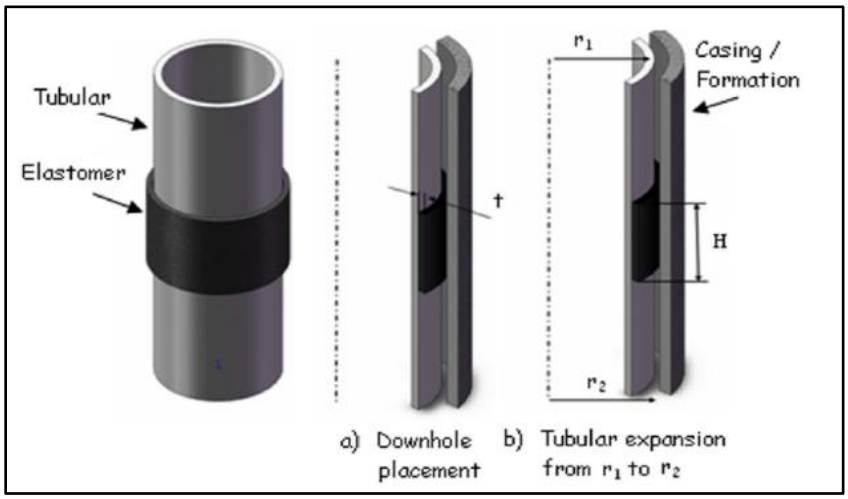

Figure 2.27: Elastomer seal radially confined between metal tubes with fluid pressures in axial direction (Al-Hiddabi et al. 2015)

Al-Kharusi et al. (2011) conducted a theoretical analysis on compression of elastomer seals in expandable tubular or liner hangers. They developed an analytical model for elastomer seal assuming linear elastic material property. The model was later refined and presented by Al-Hiddabi et al. (2015). This new model is based on elastomer seal that is radially confined between metal tubes with fluid pressures in axial direction (**Figure 2.27**). Originally developed for solid expandable tubular, this model can predict contact pressure along the contact length as a function of seal compression ratio, fluid pressures, and material properties. Besides developing the model, Al-Hiddabi et al. (2015) also performed parametric analysis using the model and investigated the effect of seal thickness, seal length, and compression ratio on contact pressure (**Figure 2.28**)

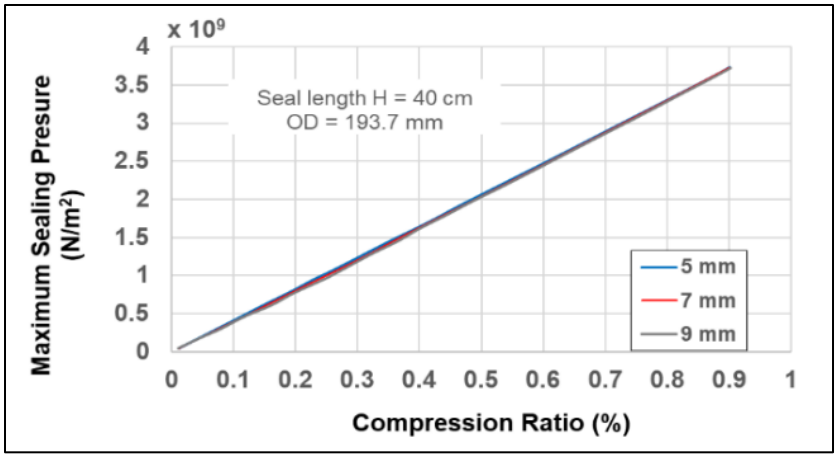

(a)

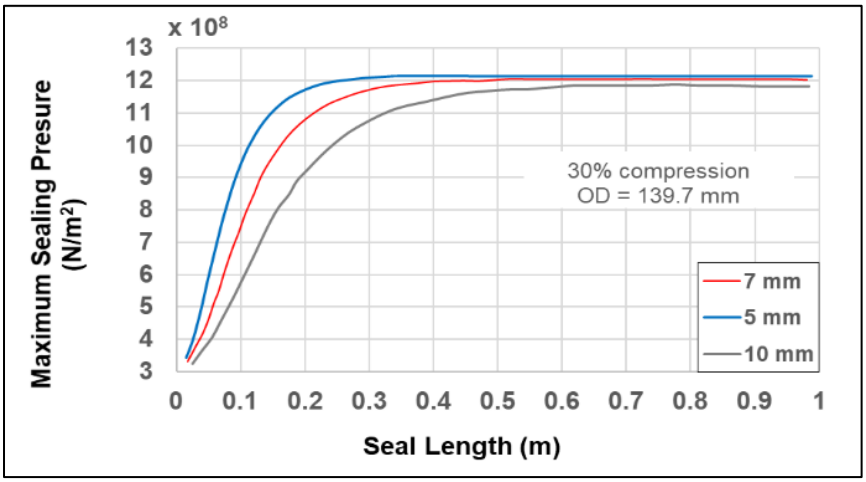

(b)

Figure 2.28: Maximum contact pressure in expandable tubular as a function of compression ratio (a) and seal length (b) for varying seal thickness (Recreated after Al-Hiddabi et al. 2015)

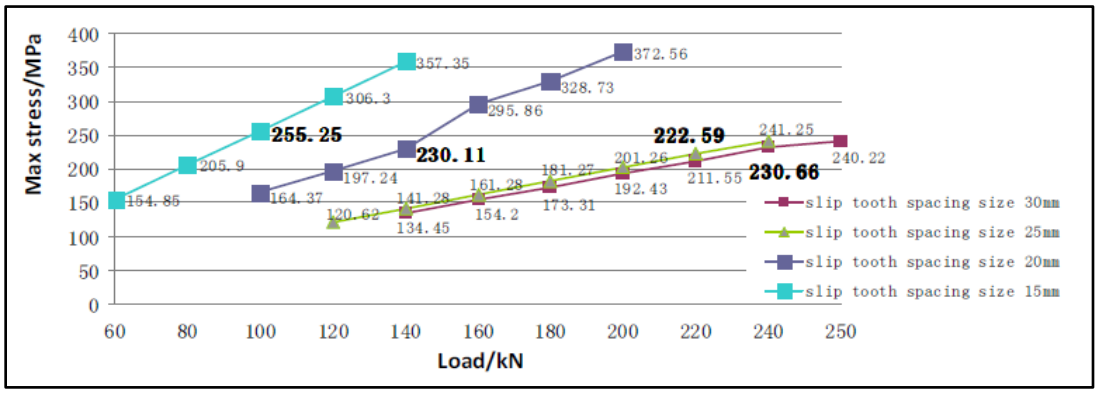

Figure 2.29: Maximum stress in slip element as a function of applied load (Lin 2013)

Lin (2013) conducted finite element structural analysis of slip element in packers. They examined stresses in slip element at different applied loads or setting pressures and observed almost linear correlation (**Figure 2.29**). They also studied the effect of spacing between the slip tooth on developed maximum stress in slip element. They performed a physical failure test on a slip element and confirmed its consistency with the simulation results.

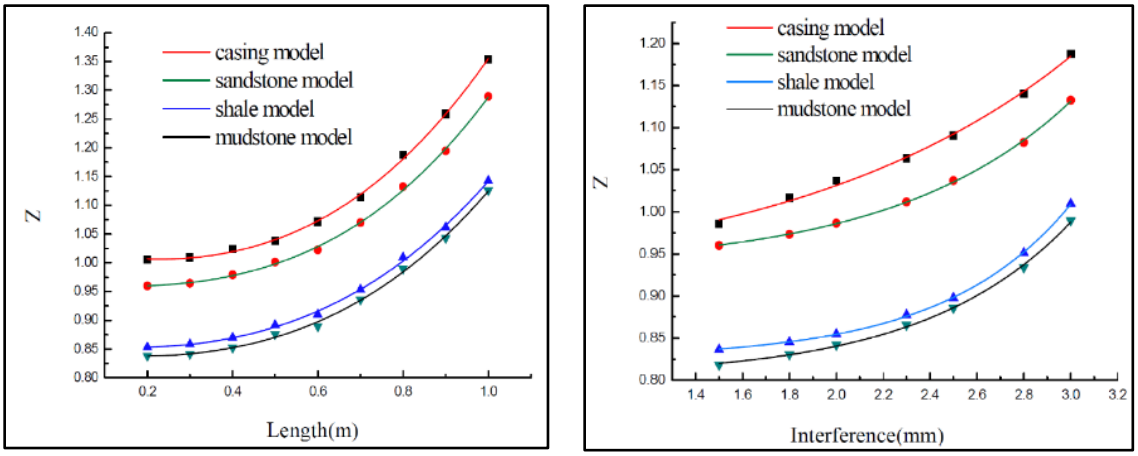

Figure 2.30: Sealing safety factor (contact pressure divided by operating fluid pressure) stress in slip element as a function of applied (Ma et al. 2014a)

Ma et al. (2014a) examined swellable elastomer packer element using two-dimensional finite element model with non-linear elastomer material properties. They modelled swellability by means of interference between seal thickness and annular space between casing and formation. Under the differential pressure of 20 MPa across the packer, they studied the maximum contact pressure for different seal length, interference thickness, and different formation. They evaluated the sealing performance in terms of sealing safety factors (Z) (**Figure 2.30**) which is calculated as contact pressure divided by packer differential pressure. No validation for simulation results is provided. They observed that upper seal element consistently provides higher contact pressures for the same applied load.

In a similar study with two elastomer seal elements, Ma et al. (2014b), investigated effect of different friction coefficient and concluded that contact pressure difference between upper and lower seal element can be manipulated by adjusting friction coefficient.

Wang et al. (2015) performed structural FEA of inner tube and setting sleeve of a packer equipment to identify zones of high stress concentration for design optimization. Validation of simulation results was not provided. Li et al. (2015) performed two dimensional FEA on rubber sealing ring for rotary liner hanger bearing. They studied maximum contact stress as a function of setting pressure at different temperature.

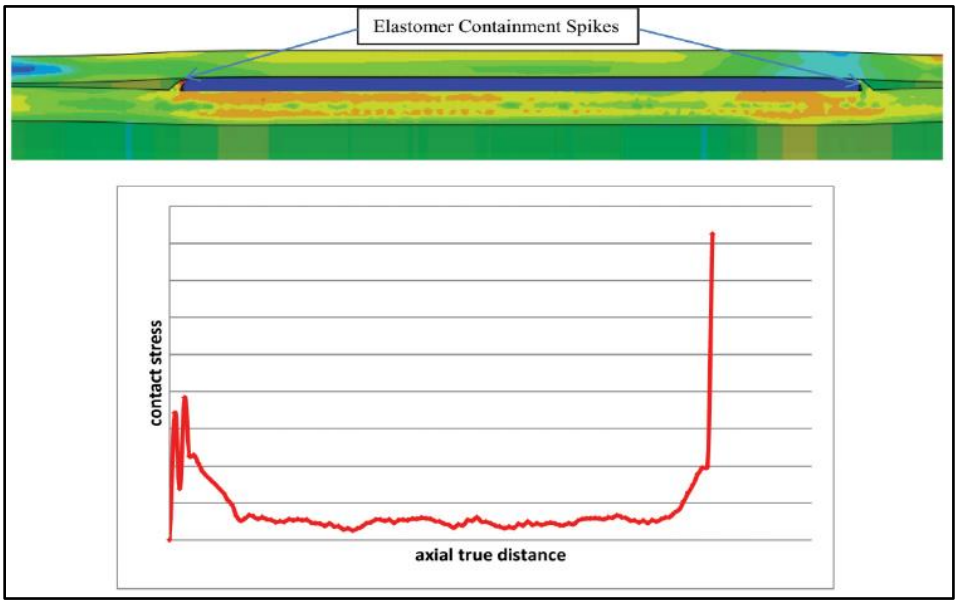

Figure 2.31: Contact stress along axial length of elastomer element in expandable liner hanger after the expansion (Zhong et al. 2015)

Zhong et al. (2015) used FEA to investigate performance of large bore expandable liner hanger. The authors studied expansions force, cone pull out force, contact pressure between elastomer and casing, and stress and deformations in hanger, casing, and cone body. Simulation demonstrated how deformation of elastomer containment spikes cause variation in contact stress

distribution (**Figure 2.31**). The upstream side spike deforms and loses contact to the casing and failing to provide good elastomer containment. The spike at downstream side maintains the contact with casing, prevents elastomer flow and provides higher contact stress compared to the upstream side.

Tu and Cheng (2016) reviewed current RGD and aging testing methodologies and proposed a new validation program for elastomer seals to bridge the gap between material and functional testing. The proposed testing philosophy is to validate a particular seal cross section and material in a representative test fixture that matches actual service conditions instead of only testing the material in isolation. This approach promises a more thorough validation program as testing pressure, temperature, fluid environment, fixture geometry, seal geometry, and cyclic conditions would be closer to the actual service conditions compared to current standard testing methodologies.

Payne et al. (2016) conducted three dimensional FEA of liner hanger body (no seal assembly) with validation from physical tests. They demonstrated that liner hanger capacity is sensitive to geometrical features and imperfections such as slots, grooves, ovality, and end effects. Inadequacy of traditional calculations such as two diameter rule, Barlow equation, Lame equation, API burst equation etc. for determining capacity of liner hanger body was also highlighted.

Wang et al. (2017) investigated extrusion, sliding, and rupture type failure modes of elastomer seals for packer application (**Figure 2.32**). The authors fabricated seals of various parameters in transparent chambers on a desktop, and watched the seals extrude, slide, rupture, and leak. They developed an analytical model that can predict the pressure-extrusion curves using material parameters (elastic modulus, sliding stress, and fracture energy) and geometric parameters

(thickness, length, and pre-compression). They also performed experimental validation (Liu et al. 2014; Wang et al. 2017).

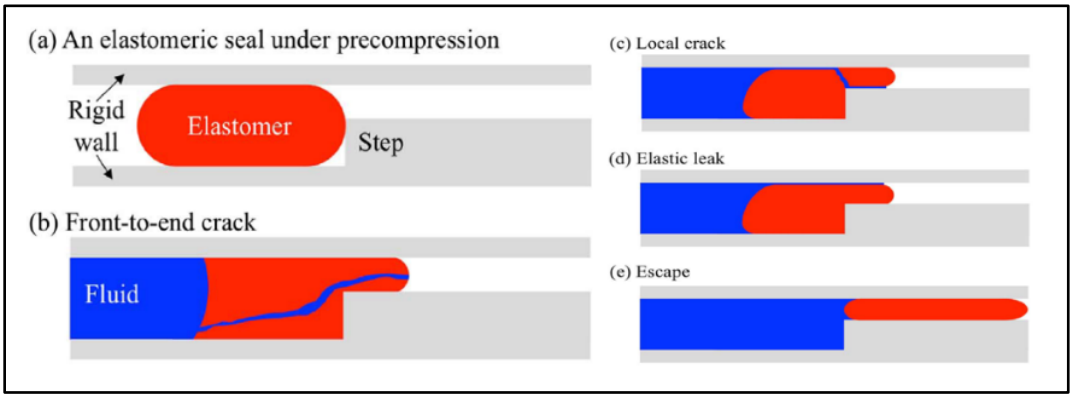

Figure 2.32: Extrusion failure and elastic leak of elastomer seal (Recreated from Wang et al. 2017)

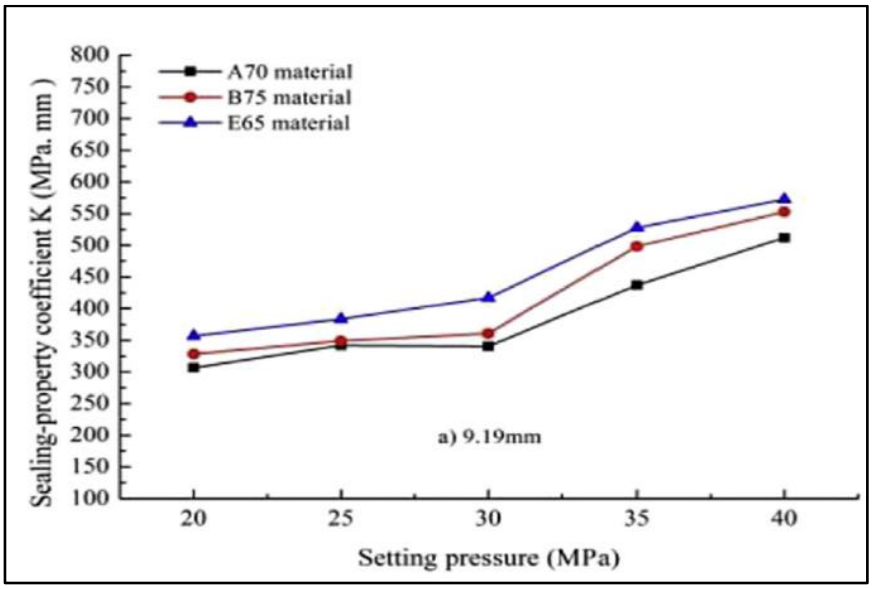

Figure 2.33: Sealing performance of elastomer packer element as a function of setting pressure (Hu et al. 2017)

Hu et al. (2017) studied the effect of elastomer material property on sealing performance of compression packer. They employed three NBR elastomers with different chemical formulation, measured uni-axial tension and compression data, and performed a 3-D finite element analysis

with a non-linear material property model. They measured sealing performance in terms of a coefficient K which can be obtained by multiplying the effective contact stress to the effective contact length. They observed that sealing performance increases almost linearly with increase in setting pressure (**Figure 2.33)**. No experimental or analytical validation was provided for contact stress.

Elhard et al. (2017) performed elastomer feasibility study for HPHT application. Based on comprehensive review of current industry standards and guidelines, they recommended to develop new or revise the current standards as they only provide guidance for elastomer use up to 5000 psi pressure. They conducted experimental study and FEA of O-rings to study elastomer material properties and six different failure mechanisms. For HPHT conditions, crack tear propagation via extrusion-initiated spiral failure was observed to be the dominant failure mechanism. The performance of seal material was determined to depend on critical tear pressure as a function of temperature. The authors emphasized use of FEA to expand testing beyond the seal O-ring to device and components level.

Table 2.11: Summary of studies related to performance evaluation of elastomer seal assemblies

Study	Type of study	Equipment / Model	Parameter(s) investigated	Results Validation
Berger (2004)	Experimental	Retrievable packer	Various backup systems such as foldback ring, mesh ring, garter springs etc.	FEA
Feng et al. (2010)	2D FEA	Packer with two elastomer elements	Setting load vs contact pressure	No
Alzebdeh et al. (2010)	2D FEA	Expandable tubular against formation	Contact pressure vs setting load for different seal length, seal thickness, and formation behavior	No

Guo et al. (2011)	2D FEA	Packer	Contact pressure vs setting load for different seal thickness	No
Al-Kharusi et al. (2011) and Al-Kharusi et al. (2011)	Analytical Model	Expandable tubular	contact pressure as a function of seal compression ratio, fluid pressures, and elastic modulus	FEA
Lin (2013)	2D FEA	Slip element of packer	Maximum stress in slip component vs applied load	No
Ma et al. (2014a and 2014b)	2D FEA	Swellable elastomer packer	Maximum contact pressure for different seal length, swelling amount, and different formation	No
Wang et al. (2015)	2D FEA	Inner tube and setting sleeve of packer	Identify zones of high concentration in equipment for design optimization	No
Li et al. (2015)	2D FEA	Rotary liner hanger bearing	Maximum contact stress vs setting load	No
Zhong et al. (2015)	2D FEA	Large bore expandable liner hanger	expansions force, cone pull out force, contact pressure at elastomer-casing interface, and stress/deformation in hanger, casing, and cone body	No
Payne et al. (2016)	3D FEA	Liner hanger body (no seal assembly)	Liner hanger mechanical capacity estimation	Physical tests
Liu et al. (2014) and Wang et al. (2017)	Experimental and Analytical	Elastomer element of packer	Extrusion, sliding, and rupture type failure of elastomer material	Experimental validation
Hu et al. (2017)	3D FEA	Packer	Setting pressure vs contact stress for different elastomers material with non-linear properties	No

Elhard et al. (2017)	Experimental and 2D FEA	O-ring extrusion	O-ring deformation, extrusion distance as a function of time and applied pressure,	FEA

2.5.2 Factors Influencing Sealability

Based on the literature review, list of potential factors affecting elastomer seal performance was prepared. The list along with brief description of each group of parameters is provided in **Table 2.12**.

Table 2.12: List of factors affecting elastomer seal performance

Parameter(s)	**Detail**
Seal material properties	Material properties define deformation behavior of the seal under loading and directly influences sealability. Material properties include – elastic modulus, poison's ratio, uniaxial, planer, biaxial stress behaviors, volumetric compression behavior etc.
Seal energization	Process of seal energization vary depending on manufacturer and type of equipment. The energization process can influence resultant contact stress profile and quality of seal. For example – in case of conventional liner hanger seal energization, contact stress profile decreases from the compression side towards support side. The seal in expandable hanger generates contact stress profile that peaks at the center of contact interface and reduces towards the ends.

Seal and housing dimensions	Seal and housing dimensions determine the amount of volume fill-in required by seal compression to establish contact and achieve desired contact stress. The dimensions also determine likelihood or severity of seal extrusion and energization failure.
Seal interface characteristics	Characteristics of contacting surface such as roughness, presence of lubrication, presence of solid debris, etc. can impact frictional factor, and also increase risk of abrasion/wear.
Operating conditions	Operating pressure, temperature, and chemical environment indirectly influence sealability by causing variation in material performance. Operational loads such as wellbore pressure and thermal stresses can cause relative movements or deformations of components in seal housing; resulting in change in contact stress.
Geo-mechanical factors	If seal is against formation such as in the case of open-hole packer, formation type and geo-mechanical stresses can impact seal performance. Seismicity can also impact structural stresses in tubular and wellbore impacting seal performance.

2.5.3 Analytical and Empirical Models

2.5.3.1 O-Rings

The standard elastomer seal geometry used for testing is O-ring. One of the earliest works on mathematical expression of stresses in compressed O-rings was presented by Lindley (1967). The author proposed that onset of leakage is when the pressure differential across the seal exceeds peak contact stress. The study demonstrated simplified expressions relating contact width to peak

contact stress assuming unrestrained loading and plain strain conditions (**Figure 2.34**). The peak contact stress P_{max} normalized with respect to modulus of elasticity is calculated as,

$$\frac{P_{max}}{E} = \left[\frac{16}{6\pi}(1.25\delta^{1.5} + 50\,\delta^{6})\right]^{0.5} \quad \text{.....(2.18)}$$

The contact width b normalized by cross-sectional diameter of O-ring is expressed as,

$$\frac{b}{d} = \left[\frac{6}{\pi}(1.25\delta^{1.5} + 50\,\delta^{6})\right]^{0.5} \quad \text{.....(2.19)}$$

Where δ is normalized compressive displacement (x/d). The first term on right hand side of the equation is based on Hertzian contact theory and the second term was added as adjustment based on empirical data.

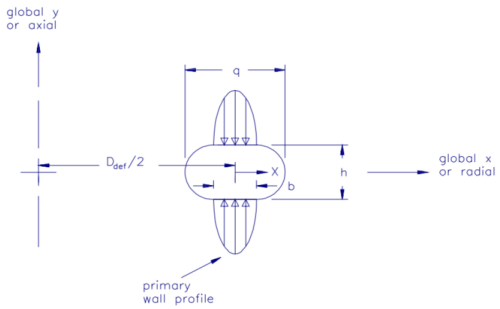

Figure 2.34: Unrestrained axial loading of O-ring (Green and English 1994)

Wendt (1971) examined compression of O-ring and x-rings with emphasis on grove design and proposed a notable contact width calculation for unrestrained axially loaded O-ring. Molari (1973) was one of the first researchers to investigate problem of restrained O-ring seals.

Strozzi (1986) presented a dimensionless stress parameter defined as Q = q/d (q shown in **Figure 2.34)** for calculation of peak contact stress and contact width. An empirical relationship

between Q and dimensionless compression (δ) was derived based on experimental data fitting. The expressions are as follows,

$$\frac{P_{max}}{E} = \sqrt{\frac{10}{3\pi}}\delta^{0.75} \quad \text{.....(2.20)}$$

$$\frac{b}{E} = \frac{3}{2}\delta^{0.67} \quad \text{.....(2.21)}$$

Where δ is defined as,

$$Q = 1 + 0.415\,\delta + 1.15\,\delta^2 = f(\delta) \quad \text{.....(2.22)}$$

Molari's work on one lateral restrain was extended by Dragoni and Strozzi (1988) to O-ring restrained between two lateral walls. They offered approximate analytical model for O-ring up to 15% compression. They developed expression for equivalent normalized squeeze δ_{ij} to be used in characterizing restrained O-ring. The notation ij was used to denote direction of perpendicular grove wall. For example, for restrained radial loading, the equivalent squeeze in the x direction (δ_{xy}) denotes compression associated partially to the squeeze directly applied in x direction and partially to constraints of the wall perpendicular to y direction.

$$\delta_{yx} = \frac{d\,f(S_{xy}) - h}{d} = f(\delta_{xy}) - \frac{h}{d} \quad \text{.....(2.23)}$$

$$\delta_{xy} = \frac{d\,f(S_{yx}) - l}{d} = f(\delta_{yx}) - \frac{l}{d} \quad \text{.....(2.24)}$$

Where f is the function given in equation (2.22). All other parameters are same as defined earlier and shown in **Figure 2.34.** Above relationships provide estimates for any groove dimensions.

All these researchers assumed plain strain conditions and did not tackle condition of axisymmetric loading. It implies that no distinction exists between axial and radial loading. This was found limited in some important loading conditions for the compression force and stiffness (Green and English, 1992). Green and English (1992, 1994) conducted finite element analysis and presented empirical correlations for the prediction of compression force and contact stress for O-ring under four different load cases – unrestrained radial loading, unrestrained axial loading, restrained radial loading, and restrained axial loading. Because of the lack of agreement to analytical work, Green and English (1994) presented empirical correlation based on FEA simulation data for determination of the peak contact stress. The second and third order correlations are as follows:

$$\frac{P_{max}}{E} = a\,\delta + b\,\delta^2 \quad \text{.....(2.25)}$$

$$\frac{P_{max}}{E} = c\,\delta + d\,\delta^2 + e\,\delta^3 \quad \text{.....(2.26)}$$

The correlation coefficients are defined in **Table 2.13.**

Table 2.13: Least square correlation coefficients for peak contact stress prediction in O-rings under different loading conditions

Loading Case	a	b	c	d	e
Unrestrained lubricated axial primary wall	2.0572	-3.1417	2.6296	-8.8589	12.8391
Unrestrained unlubricated axial primary wall	2.0090	-0.2211	2.8383	-8.5051	18.6031
Unrestrained lubricated radial primary wall	2.4891	-1.5967	3.4591	-11.2857	21.7583
Unrestrained lubricated plane strain primary wall	2.2340	-2.8961	3.0373	-10.9192	18.0171
Restrained axial primary wall	1.9715	3.1502	3.8295	-23.0013	82.6963
Restrained axial lateral wall	1.0497	6.4631	2.6584	-16.1793	71.5999
Restrained radial primary wall	2.1587	6.7729	4.9363	-32.3232	123.630
Restrained radial lateral wall	0.5844	8.7930	2.3003	-15.3593	76.3744
Restrained plane strain primary wall	1.9933	3.2711	4.0499	-25.6765	91.5384
Restrained plane strain lateral wall	0.9400	7.5182	2.6698	-16.8290	76.9908

2.5.3.2 Rectangular Seal

Strozzi et al. (2015) performed analytical evaluation of peak contact stress in a rectangular elastomeric seal with rounded edges. Older analytical work (Strozzi 1986, Ciavarella et al. 1998) work are mostly applicable to a rectangular rigid punch with rounded edges indenting a deformable half plane. It was shown that unrealities of analytical solutions can be corrected and finiteness of the indenter dimensions may be accounted for by combining analytical solution with fracture mechanics dealing with stress singularities at the tip of a transverse crack in a strip of finite width (Sackfield et al. 2003, and Banerjee et al. 2009). The work of Strozzi et al. (2015) uses this approach.

Because of the rounded edges of seal, the contact pressure exhibits Hertzian-type local bumps in lateral zones. The profile is almost flat at the center of contact interface and becomes zero at the end of either sides. Lateral bumps and the central flattish zone is termed as camel-backed profile (Strozzi et al. 2015)

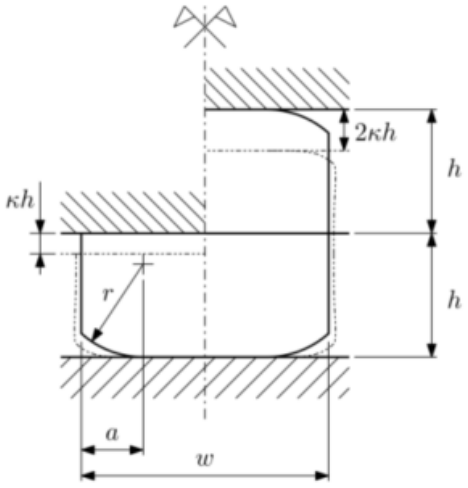

Figure 2.35: Schematic of rectangular elastomeric seal with rounded edges considered in analytical model by Strozzi et al. (2015)

The analytical contact stress expression presented by Strozzi et al. (2015) is as follows. The parameters are graphically defined in **Figure 2.35**.

$$P_{max} \cong 0.580\left(\frac{K_I^2 E^*}{r}\right)^{0.33} = 0.917E^{*\,3}\sqrt{\frac{ak^2}{r}}\,{}^{3}\sqrt{q^2\left(\frac{2a}{w},\frac{a}{h}\right)s^2\left(\frac{2a}{w},\frac{a}{h}\right)} \quad \text{..... (2.27)}$$

Where

$$q\left(\frac{2a}{w},\frac{a}{h}\right) = \frac{h}{w\int_0^h \frac{1}{w-2ae^{\frac{-xtan\emptyset}{a}}}dx} = \frac{tan\emptyset}{\frac{a}{h}\left[ln\left(e^{\frac{tan\emptyset}{a/h}}-\frac{2a}{w}\right)-ln\left(1-\frac{2a}{w}\right)\right]} \text{..... (2.28)}$$

$$s\left(\frac{2a}{w},\frac{a}{h}\right) = \frac{min\left(f\left(\frac{2a}{w}\right),g\left(\frac{a}{h}\right)\right)}{\sqrt{1-\frac{2a}{w}}} \text{..... (2.29)}$$

$$g\left(\frac{a}{h}\right) = 1.000 + 0.127\left(\frac{a}{h}\right) - 3.190\left(\frac{a}{h}\right)^2 + 4.958\left(\frac{a}{h}\right)^3 - 2.503\left(\frac{a}{h}\right)^4 \text{..... (2.30)}$$

$$f\left(\frac{2a}{w}\right) = 1.000 - 0.500\left(\frac{2a}{w}\right) - 0.183\left(\frac{2a}{w}\right)^2 + 0.420\left(\frac{2a}{w}\right)^3 - 0.169\left(\frac{2a}{w}\right)^4 \text{..... (2.31)}$$

2.5.3.3 Concentric Cylindrical Elastomer Seal

The elastomer seal components used in oil & gas well assemblies can often be approximated as concentric cylindrical. Assuming linear elastic material behavior, analytical model for elastomer seal perfectly fit between concentric cylinders can be easily derived based on Lamé's theory (Hearn 1997).

As shown in **Figure 2.36,** the liner-elastomer-casing system can be considered as composite thick cylinder system. Since the liner and casing are restrained in the z direction, the model can be considered as a plane strain axisymmetric problem. The contact pressure at the liner-seal and seal-casing interface can be calculated by following equations.

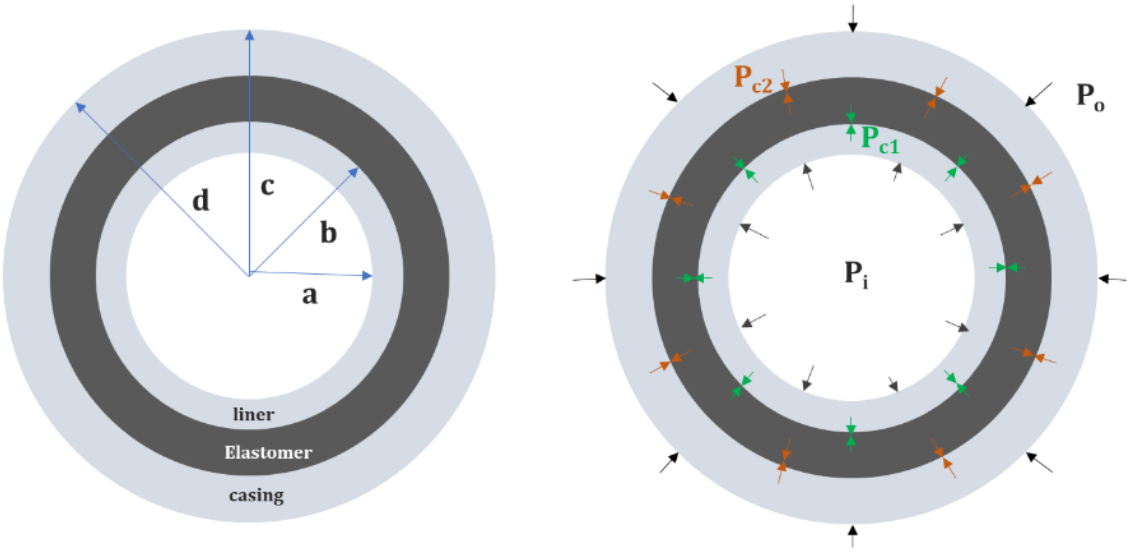

Figure 2.36: Schematic of liner-elastomer-casing system for derivation of analytical equations

$$P_{c1} = \frac{FB-KC}{DB-AK} \quad \text{..... (2.32)}$$

$$P_{c2} = \frac{C}{B} - \frac{A}{B}\left(\frac{FB-KC}{DB-AK}\right) \quad \text{..... (2.33)}$$

Where the parameters A, B, C, D, F, and K are defined as,

$$A = \frac{b}{E_c}\left[(1-\nu_e^2)\left(\frac{c^2+b^2}{c^2-b^2}\right) + (\upsilon_e + \nu_e^2)\right] + \frac{a}{E_l}\left[\frac{r_{ml}(1-\nu_l^2)}{t_l} + (\upsilon_l + \nu_l^2)\right] \quad \text{..... (2.34)}$$

$$B = -\frac{b}{E_c}\left[(1-\nu_e^2)\left(\frac{2c^2}{c^2-b^2}\right)\right] \quad \text{..... (2.35)}$$

$$C = \frac{aP_i}{E_l}\left[\frac{r_{ml}(1-\nu_l^2)}{t_l} + (\upsilon_l + \nu_l^2)\right] \quad \text{..... (2.36)}$$

$$D = -\frac{c}{E_e}\left[(1-\nu_e^2)\left(\frac{2b^2}{c^2-b^2}\right)\right] \quad \text{..... (2.37)}$$

$$K = \frac{c}{E_c}\left[(1-\nu_c^2)\left(\frac{d^2+c^2}{d^2-c^2}\right) + (\upsilon_c + \nu_c^2)\right] + \frac{c}{E_e}\left[(1-\nu_e^2)\left(\frac{c^2+b^2}{c^2-b^2}\right) - (\upsilon_e + \nu_e^2)\right]$$

..... (2.38)

$$F = \frac{cP_o}{E_c}\left[(1-\nu_c^2)\left(\frac{2d^2}{d^2-c^2}\right)\right] \quad \text{..... (2.39)}$$

P_o and P_i are casing external and liner internal pressure respectively. υ and E are Poisson's ratio and Young's modulus respectively. Subscript l, c, and e indicate properties related to liner, casing, and elastomer seal. Rest of the geometrical parameters are defined in **Figure 2.36.** The above analytical model predictions have been observed to match with FEA results.

2.5.3.4 Expandable Liner Hanger Seal

Very limited work has been done in the oil & gas industry to develop analytical model for elastomer seal assemblies.

The only work is conducted by Al-Kharusi et al. (2011) and Al-Hiddabi et al. (2015) for elastomer seal used in solid expandable tubular and liner hangers. Al-Kharusi et al. (2011) conducted a two-dimensional theoretical analysis on compression of elastomer seals in expandable tubular or liner hangers. They developed an analytical model for elastomer seal assuming linear elastic material property. The model was later refined and presented by Al-Hiddabi et al. (2015). This new model was based on elastomer seal that is radially confined between metal tubes with fluid pressures in axial direction (**Figure 2.37**). Originally developed for solid expandable tubular, this model can predict contact pressure along the contact length as a function of seal compression ratio, fluid pressures, and material properties.

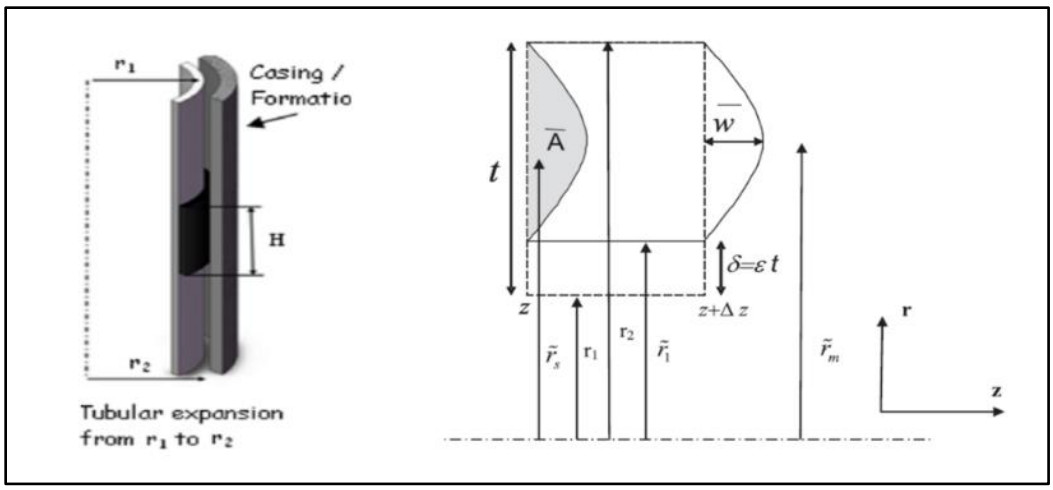

Figure 2.37: Schematic of elastomer seal volume element considered in analytical model development

$$P(z) = \frac{\left[-\left(P_0+\frac{2\pi\bar{r}_s\delta G}{\tilde{\lambda}_1\tilde{\lambda}^2}\right)+\left(P_b+\frac{2\pi\bar{r}_s\delta G}{\tilde{\lambda}_1\tilde{\lambda}^2}\right)cosh(\hat{\lambda})\right]}{sinh(\hat{\lambda})} sinh\left(\hat{\lambda}\left(\frac{z}{H}-1\right)\right) + \left(P_b+\frac{2\pi\bar{r}_s\delta G}{\tilde{\lambda}_1\tilde{\lambda}^2}\right) cosh\left(\hat{\lambda}\left(\frac{z}{H}-1\right)\right) - \frac{2\pi\bar{r}_s\delta G}{\tilde{\lambda}_1\tilde{\lambda}^2} \quad \text{(2.40)}$$

Definition of $\hat{\lambda}$ and $\tilde{\lambda}$ are provided in Al-Hiddabi et al. (2015). Above equation can be solved for different boundary conditions.

In case of zero fluid pressure on either side of the elastomer seal, the maximum contact stress can be estimated by,

$$P_{max} = \frac{\left[2\left(\frac{r_1}{t}\right)\left(\frac{\delta}{t}\right)+\left(\frac{\delta}{t}\right)^2\right]K}{\left[2\left(\frac{r_1}{t}\right)+1\right]}\left[1-\frac{3}{2}\frac{sinh\left(\frac{H}{2t}\zeta\right)}{sinh\left(\frac{H}{t}\zeta\right)}\right] \quad \text{(2.41)}$$

where

$$\zeta = \sqrt{\frac{8\left(2\left(\frac{r_1}{t}\right)+1\right)ln\left(\frac{\left(\frac{r_1}{t}\right)+1}{\left(\frac{r_1}{t}\right)+\left(\frac{\delta}{t}\right)}\right)G}{\left[\left(\frac{r_1}{t}+1\right)^4-\left(\frac{r_1}{t}+\frac{\delta}{t}\right)^4 ln\left(\frac{\frac{r_1}{t}+1}{\frac{r_1}{t}+\frac{\delta}{t}}\right)-\left\{\left(\frac{r_1}{t}+\frac{\delta}{t}\right)^2-\left(\frac{r_1}{t}+1\right)^2\right\}^2\right]K}} \quad \text{..... (2.42)}$$

Above equation can be simplified to

$$P_{max} = \frac{\left[2\bar{r}_1+\bar{\delta}\right]\bar{\delta}\,K}{\left[2\bar{r}_1+1\right]} \quad \text{..... (2.43)}$$

Provided that

$$\psi = \bar{H}\sqrt{\frac{\frac{12(2\bar{r}_1+1)(1-2\nu)}{1+2\nu}ln\left(\frac{\bar{r}_1+1}{\bar{r}_1+\bar{\delta}}\right)}{\left[\left((\bar{r}_1+1)^4-\left(\bar{r}_1+\bar{\delta}\right)^4\right)ln\left(\frac{\bar{r}_1+1}{\bar{r}_1+\bar{\delta}}\right)-\left\{(\bar{r}_1+1)^2-\left(\bar{r}_1+\bar{\delta}\right)^2\right\}^2\right]}} \geq 15 \quad \text{..... (2.44)}$$

In case of non-zero P_A and P_B i.e. presence of fluid pressure differential, the equation for maximum contact pressure changes to,

$$P_{max} = B\,cosh\left(\tanh^{-1}\frac{A}{B}\right) - A\,sinh\left(\tanh^{-1}\frac{A}{B}\right) - C \quad \text{..... (2.45)}$$

Where

$$A = \frac{\left[-\left(P_0-\frac{\left[2\bar{r}_1+\bar{\delta}\right]\bar{\delta}\,K}{\left[2\bar{r}_1+1\right]}\right)+\left(P_b-\frac{\left[2\bar{r}_1+\bar{\delta}\right]\bar{\delta}\,K}{\left[2\bar{r}_1+1\right]}\right)cosh(\psi)\right]}{sinh(\psi)} \quad \text{..... (2.46)}$$

$$B = \left(P_b - \frac{\left[2\bar{r}_1+\bar{\delta}\right]\bar{\delta}\,K}{\left[2\bar{r}_1+1\right]}\right) \quad \text{..... (2.47)}$$

$$C = \left(-\frac{\left[2\bar{r}_1+\bar{\delta}\right]\bar{\delta}\,K}{\left[2\bar{r}_1+1\right]}\right) \quad \text{..... (2.48)}$$

In the case when fluid pressure is acting on only on top or bottom of the seal, then the equation for maximum contact pressure becomes,

$$P_{bmax} = \left(\frac{[2\bar{r}_1+\bar{\delta}]\bar{\delta}\,K}{[2\bar{r}_1+1]}\right)\left[1-\frac{1}{cosh(\psi)}\right] \quad \text{..... (2.49)}$$

2.5.3.5 Conventional Hanger Seal

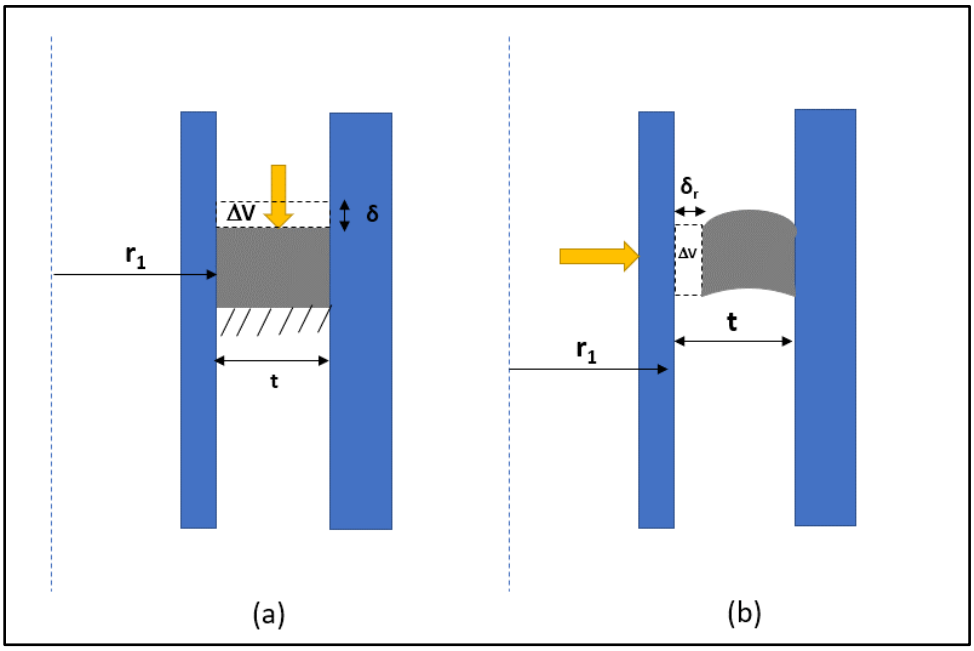

Figure 2.38: Comparison between (a) the analytical model (a) prepared in the present work for conventional liner hanger seal and (b) the analytical model of Al-Hiddabi et al. (2015) for expandable liner hanger

As shown in **Figure 2.38**, the geometry and boundary conditions for analytical model developed by Al-Hiddabi et al. (2015) has some similarities to the FEA model developed in this report. Hence, the original contact pressure equation provided in the reference (Al-Hiddabi et al. 2015) can be modified and used to provide approximate validation of contact pressures simulated in this work. After adjusting relevant input parameters, the maximum contact pressure in our model can be estimated by,

$$P_{max} = \frac{(2\bar{r}_1+\bar{\delta}_r)\bar{\delta}_r K}{(2\bar{r}_1+1)} \quad \text{..... (2.50)}$$

where

$$\bar{r}_1 = \frac{r_1}{t}\ ,\ \bar{\delta}_r = \frac{\delta_r}{t}\ ,\quad and \quad K = \frac{E}{3(1-2\nu)}$$

In the above equations, P_{max} is the maximum contact pressure, K is bulk modulus, and ν is Poisson's ratio. As shown in **Figure 2.38**, r_1 is the outer radius of the liner, t is the radial width of the seal, and δ_r is radial compression. δ_r is such that the change in volume is equivalent to the change in volume caused by the compression ratio δ in our FEA model. P_{max} and K are in consistent units.

Hyperelastic material behavior of elastomer seal combined with complex geometries and deformation restraints make analytical modelling highly challenging and limited. It is impractical to conduct physical tests because of high cost and time. Hence, finite element modelling validated by experiments and/or fundamental analytical equations has emerged as the go to solution for all types of engineering applications of seal.

2.5.4 Elastomer Alternatives

The industry has been exploring alternatives such as metal-to-metal (M2M) seals (Garfield and Mackenzie 2007; Dagle et al. 2016; Stautzenberger et al. 2016), particularly for applications in harsh chemical environment, and extreme temperature and pressure conditions. Metal seals offer several benefits such as greater temperature, pressure, and chemical resistance, robust mechanical properties, lack of porosity, and longer shelf life (Krishna and Lefrancois 2016). However, lack of ductility and elasticity is a major concern with metal seals. To alleviate this concern, researchers are exploring innovative seal designs such as spring energized metal O-rings and lattice seal with

thermoplastic matrix and metallic structure (Lamb 2014; Krishna and Lefrancois 2016; Yu et al. 2017). However, these newer seal designs are still in research and development stage. Additional challenges with the metal seals are higher costs, and limited selection of material grades.

Moreover, unlike elastomer seals, performance of metallic seal is significantly influenced by surface characteristics of the metal component (Patel et al. 2018). To predict the influence of surface roughness on sealability, Patel et al. (2018) proposed a modelling approach that can be used to model metal-to-metal seal at microscopic level. The model is able to predict contact stress and corresponding leakage rates considering surface characteristics of the metal seal. The authors concluded that leakage rates through M2M seal is primarily a function of surface finishing typically represented in terms of root mean square (RMS) value. The study also concluded that, for the same RMS, seal with randomly rough surface (e.g. manufactured by casting) would require higher contact stress to achieve zero leakage rate than a seal with more uniform distribution of surface asperities (e.g. machined component). Further research is necessary in this area to establish the true leakage criteria for metallic seals. In addition to surface characteristics, dynamic sealing and low effectiveness in presence of debris are other concerns for metallic seals (Krishna and Lefrancois 2016; Zhong 2016).

Overall, because of the various challenges discussed above, applications of metal seals are currently limited compared to elastomer seals. Elastomer is still widely used and preferred seal material primarily because of less cost, resilience, ability to seal against irregular and dynamic surfaces (Tu and Cheng 2016). With the increasing global energy demand and declining conventional resources, High-Pressure High-Temperature (HPHT) wells (>350°F and >15,000 psi) are becoming increasingly common. An industry survey (Oil & Gas iQ 2015) indicated that seals are one of the biggest technological challenges associated with HPHT oil & gas exploration.

2.6 Research Gaps

Until a more effective and commercially viable alternative is available, it is imperative to improve elastomer materials, seal design, and qualification process. Major knowledge gaps requiring extensive research are as follows:

1. It is not completely understood whether compliance with standard shaped laboratory scale elastomer material testing is representative of qualification of larger and varying seal geometries installed in the actual equipment (**Figure 1.3a**). It is understandable that testing true-scale seal geometries in laboratory environment may not be practically or economically feasible. However, the qualification criteria used to assess elastomer material can be customized as per end-application and equipment design.
2. Another major research gap is the unknown seal energization criteria. There is no consensus on whether contact pressure generated at seal-pipe interface due to seal energization indicates actual fluid pressure the seal can hold without permitting leakage (**Figure 1.3b**).
3. There is a lack of comprehensive database of elastomer material properties at HPHT conditions. Since, it is not practically possible to measure all available mechanical properties of elastomer, there is a need to identify critical material properties that are representative of elastomer behavior and must be tested. Development of sophisticated material models is another useful area of research.
4. There is no reliable technique to upscale the results obtained with standard elastomer samples and laboratory scale apparatus to larger and complex seal geometries used in field scale equipment.

5. Another important research gap is lack of reliable extrapolation technique that can use data from short term aging tests to predict elastomer performance over long-term service life spanning several years. There is also a need to identify appropriate test conditions for accelerated laboratory tests that are representative of downhole service conditions.
6. Research efforts in the direction of computational modelling tools can minimize the need for expensive and time intensive physical tests, and consequently, shorten research and development time.
7. Functional design of elastomer seal assemblies is an important area for further research. Specifically, some of the important questions that need to be answered are - which anti-extrusion mechanism is more resistant to failure? What are the strengths and limitations of various seal energization methods? How does pre-energization shape of seal impact seal energization? How influential is the dimensional tolerance or relative movements of components?
8. Majority of the seal assemblies are installed first and then energized in-situ using mechanical or hydraulic forces controlled from the surfaces. In certain conditions such as deviated wells, improper centralization of completion string, pipe buckling, etc., it may not be possible to exert enough force necessary to energize the seal. It would be useful to know the expected loss in sealability under such poor-quality seal energization conditions.
9. Significant research efforts are needed to understand the effects and consequences of functional failure modes of seal assemblies. Examples of such failures include – structural failure in support components like anti-extrusion ring, packer slips, elastomer containment spikes, etc., wear or tear of elastomer element, fluid leakage through the seal, etc.

10. Effects of pressure, temperature, chemical exposure, and gas penetration need to be investigated in terms of the influence on assembly level functional performance. For example, effect of high temperature should be discussed not only in terms of variation in material properties but also in terms of anticipated change in contact stress against pipe or formation.
11. Additional influential parameters that require further research are - dynamic wellbore loads, thermal stresses, contact characteristics (e.g. presence of debris, fluid film, friction, etc.), and geo-mechanical factors (e.g. formation properties, in-situ stresses, etc.).

2.7 Preliminary Work

Following is summary of the work conducted precursor to this dissertation work. Patel et al. (2019b) studied effect of various design parameters on performance of elastomer seal in conventional liner hanger assembly. The authors used analytically validated 3D FEA models to perform parametric analysis. The authors simulated contact stress as a function of seal compressions for different commonly used oil field elastomers. Analytically validated results indicated practically linear relationship between contact stress and amount of compression. The results can be used to quantify the loss in seal performance caused by insufficient mechanical load for seal energization. The authors also developed an empirical correlation from simulation data to predict contact stress as a function of various design parameters. The study indicated significant impact of Poisson's ratio and elastic modulus of seal on contact stress (**Figure 2.39**). The results emphasized the importance of using accurate values of material properties in seal design to avoid significant over-estimation or under-estimation of seal's performance.

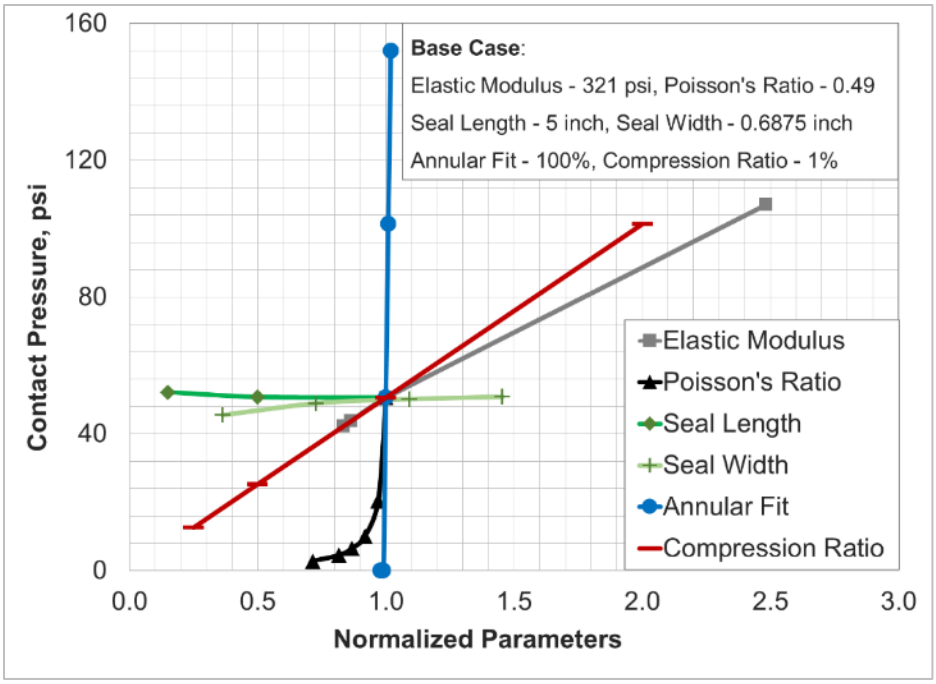

Figure 2.39: Sensitivity of contact pressure to various parameters (Recreated after Patel et al. 2019b)

Patel and Salehi (2019) developed three-dimensional finite element models of conventional and expandable type liner hanger seal assemblies. In one of the simulation cases, the authors compared contact stress predictions based on linear elastic and hyper-elastic material representation of FKM elastomer. Analytically validated simulation results indicated that the selection of material model does not impact the shape of contact stress profile generated at the seal-pipe interface. For the same amount of volumetric compression, hyper-elastic FKM yielded notably higher contact stress values than linear-elastic representation of FKM. This observation was attributed to the fact that hyper-elastic material model of FKM is able to capture material stiffening at higher strains.

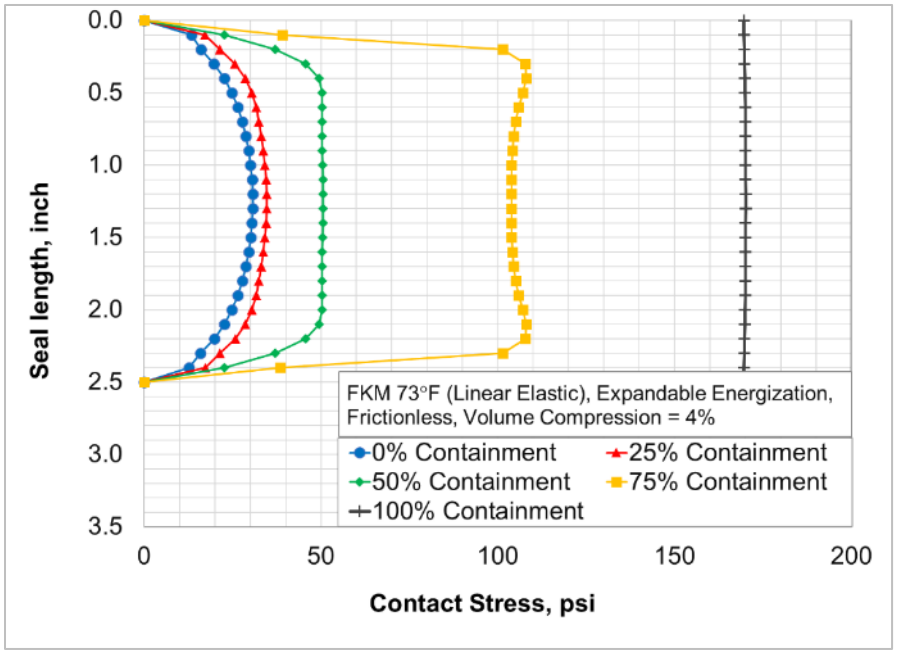

Figure 2.40: Contact pressure profile along axial length of elastomer element in expandable liner hanger (Recreated after Patel and Salehi 2019)

Simulation results illustrated that in case of conventional type axial energization, contact stress remains uniform along the contact length. In expandable type radial energization, contact stress peaks at the center of the seal length and declines towards either sides of the axial ends (**Figure 2.40**). In expandable assembly, if spikes are used on either side of the seal to contain the elastomer during compression, then the contact stress values increase. The contact stress profile becomes progressively flatter with increase in containment (**Figure 2.40**). The profile becomes similar to conventional seal assembly at 100% containment. In both assemblies, contact pressure was linearly dependent on amount of volumetric compression achieved during compression (**Figure 2.41**).

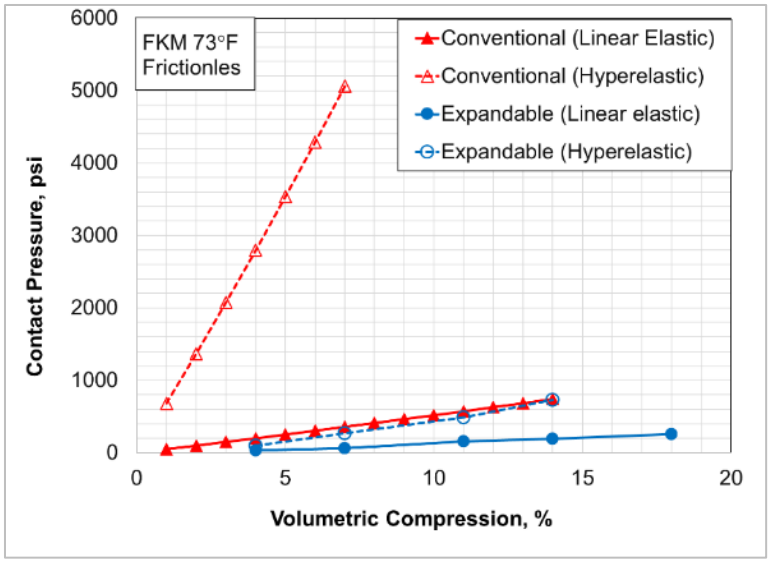

Figure 2.41: Contact pressure as a function of volumetric compression of elastomer seal in conventional and expandable liner hanger seal assemblies (Recreated after Patel and Salehi 2019)

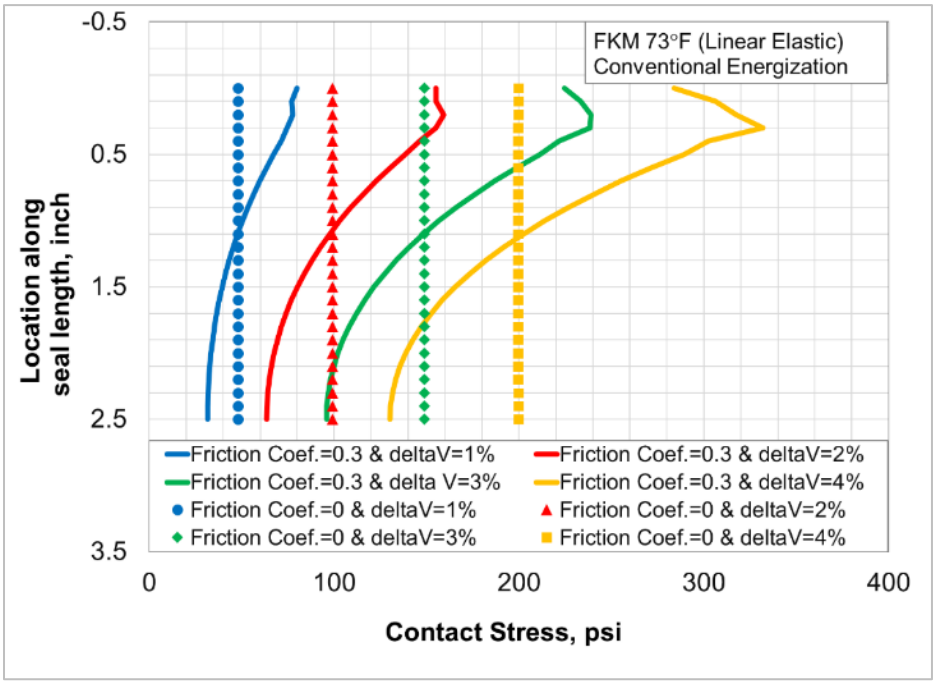

Figure 2.42: Effect of friction on contact pressure profile in conventional seal assembly (Recreated after Patel and Salehi 2019)

The authors also studied effect of friction on conventional and expandable type seal energizations. In presence of friction, contact pressure profile shape in the expandable type

energization remained the same as frictionless condition wherein it peaks at the middle of the contact length and declines towards the end. The contact pressure values increased with increase in friction coefficient. In conventional energization, frictional contact pressure rapidly peaks near the compression side and declines towards the opposite end (**Figure 2.42)**. This significant deviation can be detrimental as low contact pressure at the support end can increase chance of fluid penetration.

Chapter 3: Experimental Study

3.1 Material Properties Measurements

First of the three tasks conducted in experimental study was focused on measuring material behavior of elastomer samples to be investigated in this work. Specifically, the goal was to measure hardness and characterize stress-strain behavior of elastomer sample under compressive load for input into the FEA models. Four elastomers (NBR, EPDM, FKM, and PTFE) commonly used in the industry were selected for this work.

Elastomer component of liner hanger seal assembly undergoes energization under compressive load as discussed in **section 2.2**. Hence, uniaxial compression characterization is appropriate for input into FEA models. Sensitivity analysis of material properties is discussed later in results (**section 10.5**). Measurements were conducted as per ASTM D575-91 guidelines. As per the guidelines, cylindrical samples with height of 0.33-inch and 0.75-inch diameter were prepared for compression measurements (**Figure 3.1**). For hardness measurements, Shor A durometer was used as shown in the **Figure 3.1.** Samples used for hardness tests were 1-in thick with 0.75-in diameter.

Compressive strain was measured at six different compressive forces (15lbf, 30lbf, 45lbf, 60lbf, 75lbf, 90lbf). Each load was applied for 3 seconds before deflection on the dial gauge is read. The percent deflection or strain is calculated based on original height of the specimen. The stress is calculated using applied force and the area of top of elastomer sample. For each type of elastomer, three different samples were prepared to ensure reproducibility of the measurements. Each material property measured in this work (before or after degradation) is based on three samples. In total, more than 250 tests measurement tests were performed.

(a) **(b)**

Figure 3.1: Durometer (a) and digital force gauge (b) used for elastomer hardness and compression behavior characterization respectively

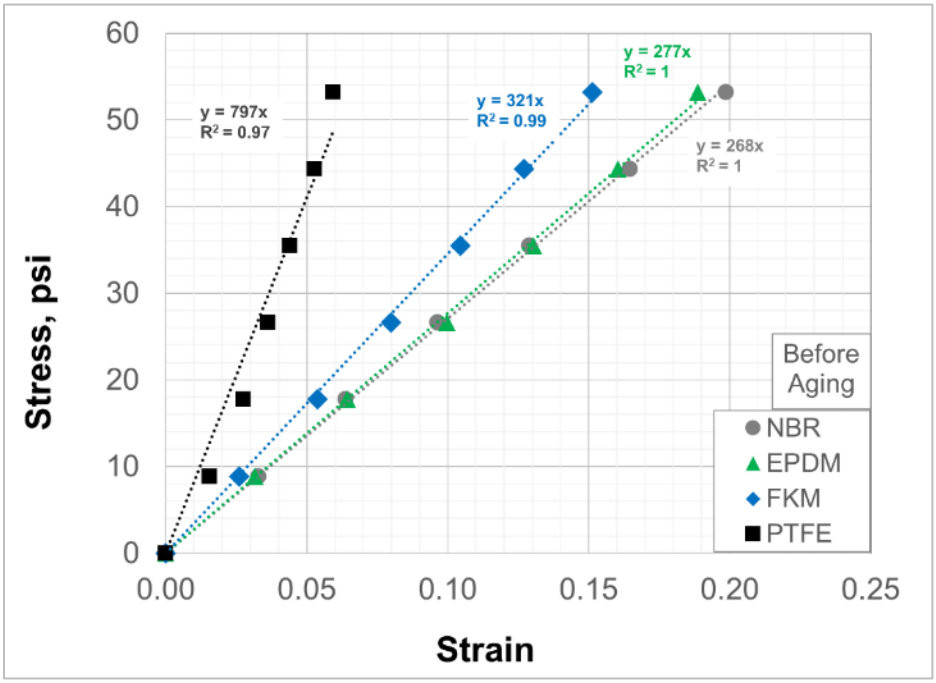

Figure 3.2: Elastomer compressive stress-strain behavior

Results from the compression tests are presented in **Figure 3.2.** It is clear that each of the four elastomer samples exhibited practically linear relationship between stress and strain. This indicates that elastomer samples can be modelled as liner elastic up to 20% strain. Beyond that, they may exhibit non-linear hyper-elastic behavior. The tests were restricted to 20% because of the instrument limit. Linear-elastic behavior exhibited by the elastomer samples enables characterizing their deformation behavior with a single constant elastic modulus. The value can be calculated as the slope of stress-strain curve. Calculated elastic moduli and hardness values are listed in **Table 3.1.**

Table 3.1: Table of elastic moduli and Shore A hardness of elastomer samples at room temperature before aging test

Elastomer	Elastic Modulus (E), psi	Hardness (H)
NBR	268	66
EPDM	277	70
FKM	321	75
PTFE	797	95

Additional characterization of these elastomer samples, such as chemical and morphological changes were investigated by colleagues and have been published earlier (Salehi et al. 2019). To achieve comprehensive understanding of elastomer material effects on seal assembly, three additional elastomer types (FKM, FEPM, and FFKM) were added in this investigation. Their material properties were sourced from another BSEE project (Elhard et al. 2017). The data included stress-strain behavior of elastomer under uniaxial, biaxial, and shear deformation. Various hyperelastic material models (discussed in **section 2.1.2.2**) were tried and Ogden 3rd order material model provided the best fit to all three tests data (Elhard et al. 2017). The material behavior curves for FKM elastomer are shown in **Figure 3.3.** Other two elastomers FEPM, and

FFKM also exhibited similar deformation behavior. Hyperelastic parameters of these three elastomers are listed in **Table 3.2.**

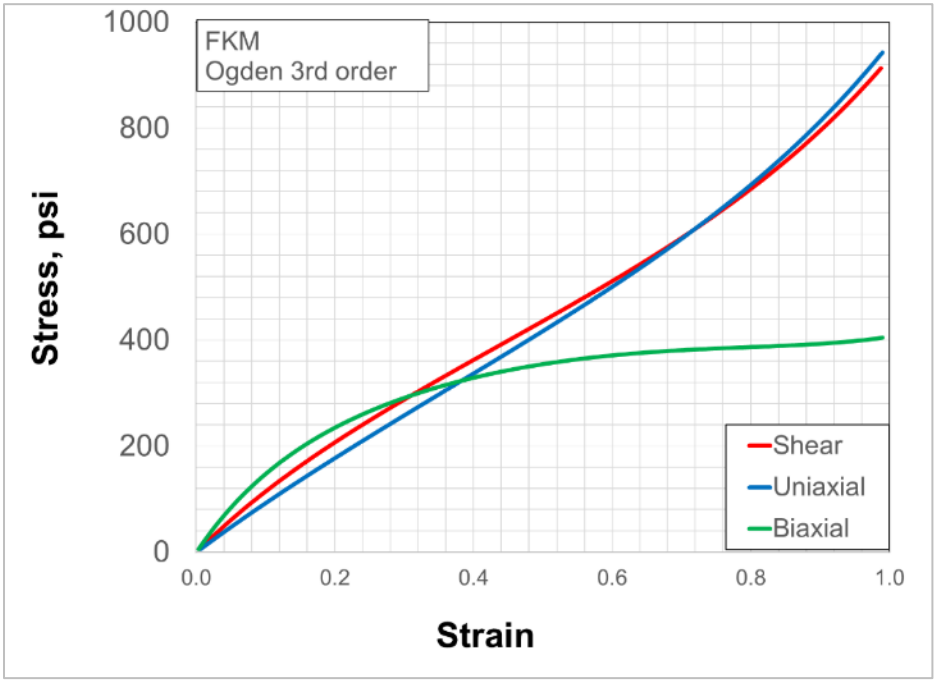

Figure 3.3: Hyperelastic characteristics of FKM elastomer

In summary, this dissertation work utilizes elastomer hardness and liner-elastic and hyper-elastic deformation behavior data for characterizing performance of seal assemblies at various operational, design, and downhole conditions. It is assumed that elastomer materials are homogenous and isotropic. It is also assumed that material properties measured with small scale samples also represent elastomer behavior at equipment-scale dimensions used in the FEA models. Other material properties (as discussed in section **2.1.1**) such as compression set, compression stress relaxation, torsion modulus, etc. have not been investigated and are beyond the scope of this work. Scenarios investigated in this work were carefully selected such that only measured properties would be relevant. Elastomers discussed in this work are divided into two groups. First group of elastomers whose material properties were measured in this work includes - NBR, EPDM,

FKM, and PTFE. The second group of elastomers whose material properties were sources from another project (Elhard et al. 2017) include - FKM, FEPM, and FFKM. For fair evaluation, direct inter-group comparisons of elastomers have not been performed in results analysis.

Table 3.2: Hyperelastic material parameters of elastomers (Additional data sourced from Elhard et al. 2017)

Hyperelastic parameter	FKM (212°F)	FKM (350°F)	FEPM (212°F)	FEPM (350°F)	FFKM (212°F)	FFKM (350°F)
μ_1, psi	278	250	196.3	190.0	192.7	189.2
μ_2, psi	32.31	29.04	15.81	15.30	94.19	92.44
μ_3, psi	0.198	0.178	0.797	0.771	0.555	0.544
α_1	2.661	2.661	3.151	3.151	3.469	3.469
α_2	-2.661	-2.661	-3.151	-3.151	-3.469	-3.469
α_3	10.79	10.79	8.559	8.559	13.32	13.32
D_1, 1/psi	1.40E-5	2.30E-5	1.85E-5	2.01E-5	3.04E-5	3.77E-5
D_2, 1/psi	2.70E-6	1.32E-5	7.74E-6	1.17E-5	1.43E-5	2.19E-5
D_3, 1/psi	0	0	0	0	0	0
Bulk modulus (K), psi	406000	229390	342635	455445	174870	188790
Shear modulus (G), psi	328	229	288	456	175	189
Poisson's ratio (ν)	0.4995	0.4995	0.4995	0.4995	0.4995	0.4995
Elastic modulus (E), psi	1218	688	1028	1366	525	566
Thermal expansion coefficient, 1/°F	1.29×10^{-4}	1.29×10^{-4}	1.36×10^{-4}	1.36×10^{-4}	2.39×10^{-4}	2.39×10^{-4}
Limiting Tresca stress, psi	5457	3582	4443	2351	6773	3175

3.2 Elastomer Aging Tests

To examine seal material failure, the elastomer samples were exposed to CH_4, CO_2, H_2S, and a mixture of all gases for 1 and 7 days at 120°F and 180°F. The aging tests were conducted as a part of project funded by the regulatory agency BSEE at our lab in well construction technology center. Downhole conditions used were prescribed by the agency and correspond to typical shallow depth liner hanger applications in Gulf of Mexico.

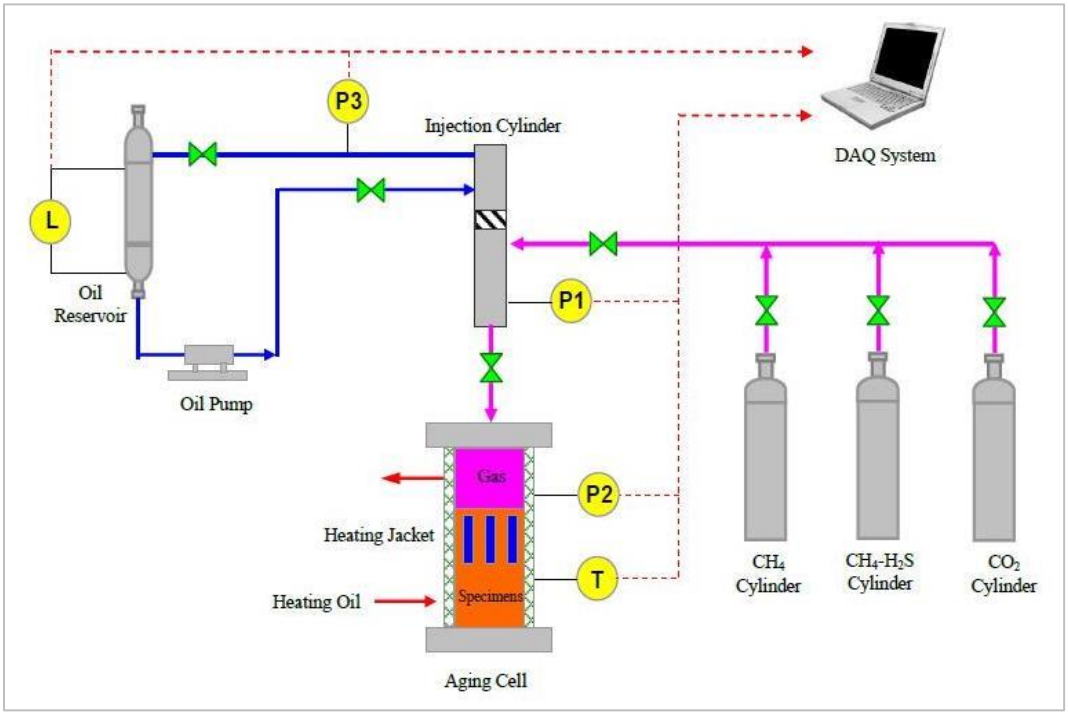

Figure 3.4: Schematic of autoclave setup for elastomer aging tests (courtesy: Dr. Ramadan Ahmed)

The schematic of the autoclave setup used for aging elastomers is shown in **Figure 3.4**. The aging cell wherein elastomer samples are put has 3-liter capacity. The cell is enclosed by heating oil circulating jacket for uniform heating of the cell. Gases were supplied from three pressurized cylinders (CO_2, CH_4, and H_2S with CH_4 carrier). The injection cylinder (250 ml capacity) was used for accurate control of the composition of the gas injected into the aging cell.

The upper chamber of the cylinder is connected to an oil pump and reservoir, while the lower chamber is used to meter and inject the gas phase into the aging cell. The hydraulic oil flows back to the oil reservoir when the lower chamber is refilled with gas coming from one of the test gas cylinders. The piston location is determined from the liquid-level measured in the oil tank. Whole process is controlled remotely using a data acquisition system. Elastomer samples were placed in the aging cell using a rack as shown in **Figure 3.5**.

Figure 3.5: Aging cell and elastomer sample rack

To examine effect of brine presence, the aging cell is partially filled with 2% NaCl brine. Some elastomer samples are immersed in brine while rest are exposed to vapor. Once the rack is lowered, the cell lid is put in place. The autoclave is sealed, and cell is heated to the desired temperature by circulating heating oil through the heating jacket. During temperature ramp-up, the

cell is flushed twice with nitrogen, 15 minutes for each flush. The purpose is to remove any trapped air within the system. When the autoclave temperature reaches the desired value, gas injection is initiated. Gas is injected into the cell repeatedly (in a selected sequence) until the cell pressure (P2) reaches the desired value which is 1000 psi. Gas compositions vary depending on the experiment being conducted. To simulate aging environment of 50% CO_2 and 50% H_2S (with CH_4 carrier), CO_2 is first injected up to 500psi (3.45PMa), followed by the H_2S with CH_4 carrier until target pressure of 1000psi (6.89MPa) is achieved.

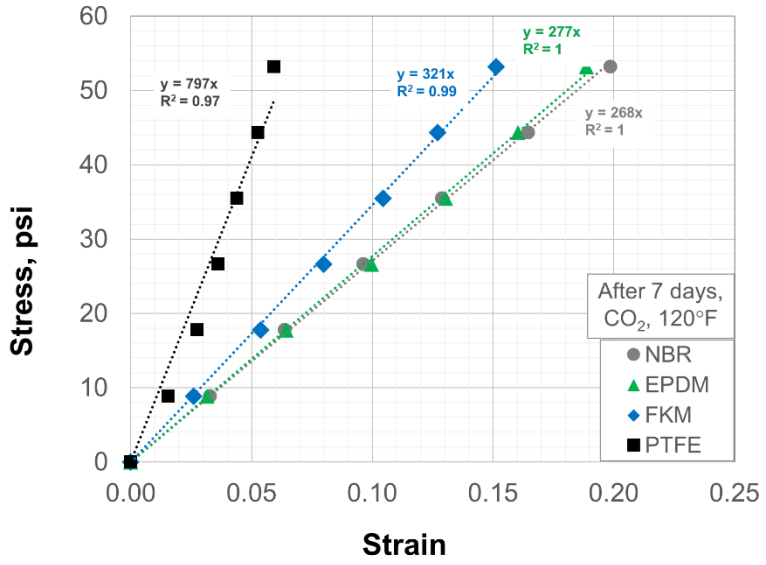

Figure 3.6: Elastomer compression behavior after aging in CO_2 at 120°F for 7 days

For each elastomer type, three samples were prepared for aging tests. After aging, the uniaxial compression and hardness data was acquired for each sample. The stress-strain data in the measured range was still practically linear as shown in **Figure 3.6**. Elastic moduli and hardness of elastomer samples after aging them in various conditions are listed in **Table** 3.3 and **Table 3.4** respectively**.** Detailed discussion on chemical effects on performance of seal assemblies are discussed later in results (section **7.2**).

Table 3.3: Table of elastic moduli after chemical exposure

Elastomer Type	All gases								CH_4		CO_2		H_2S	
	1 day, 120°F		7 days, 120°F		1 day, 180°F		7 days, 180°F		7 days, 120°F		7 days, 120°F		7 days, 120°F	
	V	B	V	B	V	B	V	B	V	B	V	B	V	B
NBR	158	166	173	178	172	185	190	195	221	227	161	168	228	236
EPDM	210	223	212	222	224	231	213	221	241	255	198	203	230	251
FKM	251	276	260	284	267	290	255	274	281	275	237	249	315	327
PTFE	737	744	723	746	708	763	749	779	812	814	802	778	747	792

V denotes vapor phase i.e. sample was not immersed in brine
B denotes that sample was immersed in brine

Table 3.4: Table of elastomer hardness after chemical exposure

Elastomer Type	Before Aging		All gases		CH_4		CO_2		H_2S	
			7 days, 120°F		7 days, 120°F		7 days, 120°F		7 days, 120°F	
	V	B	V	B	V	B	V	B	V	B
NBR	65.7	65.8	64.8	64.3	56.7	56.5	63.6	63.9	58.2	61.2
EPDM	70.2	69.8	66.4	66.4	61.8	63.6	67.0	67.0	63.6	64.6
FKM	75.2	75.4	72.6	72.2	64.2	66.9	72.2	72.6	69.9	71.6
PTFE	95.4	95.3	94.1	94.7	92.7	92.5	95.8	94.3	91.7	93.0

V denotes vapor phase i.e. sample was not immersed in brine
B denotes that sample was immersed in brine

3.3 Sealability Tests

A laboratory scale apparatus was constructed using two concentric transparent acrylic pipes with seal assembly consisting of two elastomer O-rings and three aluminum rings placed alternatively in annular space (**Figure 3.7**). The setup was created to mimic seal energization process of conventional liner hanger seal assembly. The setup consists of 10 in. outer acrylic pipe and 8 in. inner acrylic pipe. Transparent acrylic pipes were used to enable visual observation of seal energization and leakage. The annular space between the pipes is 0.7 in. The height of each pipe

is 3 ft. Two elastomer O-rings with cord thickness of 0.75 inch were placed alternatively between aluminum rings.

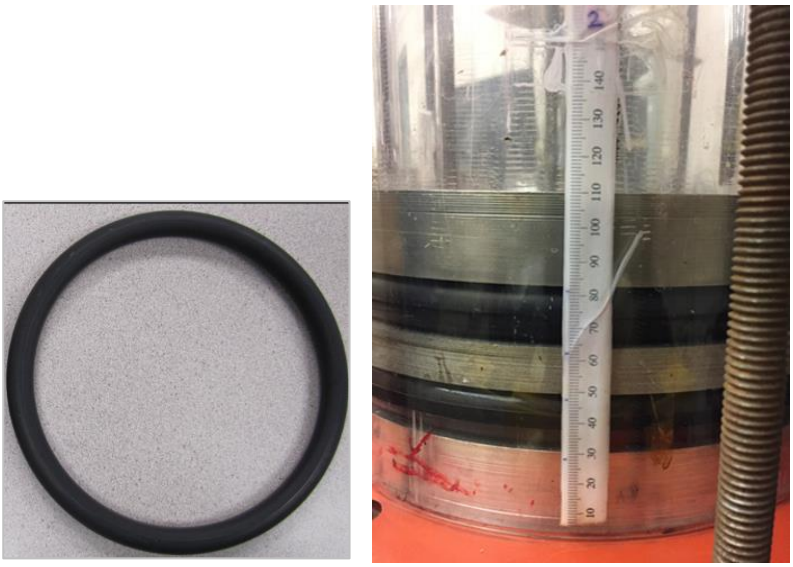

Figure 3.7: EPDM elastomer O-ring (left) and close-up of sealability test apparatus (right)

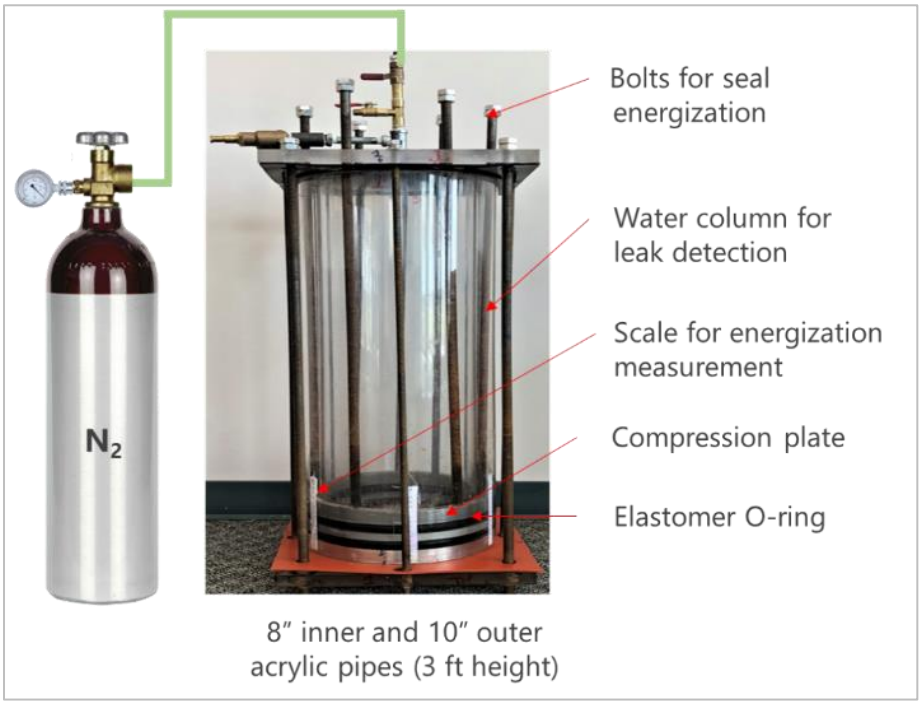

Figure 3.8: Elastomer sealability test apparatus

Photograph of the setup is shown in **Figure 3.8.** Seal energization was achieved by tightening six circumferentially equidistant threaded bolts using torque wrench (0, 120, and 180 in-lbf). Magnitude of seal energization was quantified by measuring axial compression of ring using measuring scale attached to the pipe (**Figure 3.7**). Sealability of elastomer was evaluated by injecting N_2 into the inner pipe and observing for leak through annulus at top of the setup. Water was poured on top of aluminum ring in annular space to enable visual detection of leakage. Because of the limited pressure rating of acrylic pipes, injection of N_2 was limited up to 40 psi. Gas was injected using an automatic regulator until constant 40 psi pressure was achieved inside the inner pipe. Then, injection was stopped, and setup was observed for 30 minutes for any sign of leakage.

Sealability tests were conducted with EPDM elastomer O-rings at three different energization (0, 120, and 180 in-lbf) before and after aging in CO_2. Nitrogen injection was restricted to up to 40 psi because of the pressure rating of the acrylic pipes. FEA model of the apparatus was also created to investigate additional scenarios not possible with the test setup. The primary goal of this sealability apparatus is to validate seal energization behavior and effect of material aging predicted by the FEA model.

Chapter 4: Finite Element Models

4.1 FEA Model of Conventional Assembly

Schematic of the axisymmetric FEA model developed to represent conventional liner hanger seal assembly is shown in **Figure 4.1**. The model consists of liner, casing, seal, and compression plates. The diameter of liner, and casing represents an actual offshore well construction design (BSEE 2014). Length of liner and casing components is 40 in. The length was kept long enough to avoid end effects on seal energization process. The axial length (or height) of the seal component is 2.5 in. and radial width is 0.6875 in. The initial clearance between seal and casing is 0.1 in. These three dimensions are realistic representation of an actual seal assembly. Seal length, width, and radial clearance were varied later as a part of assessing design scenarios.

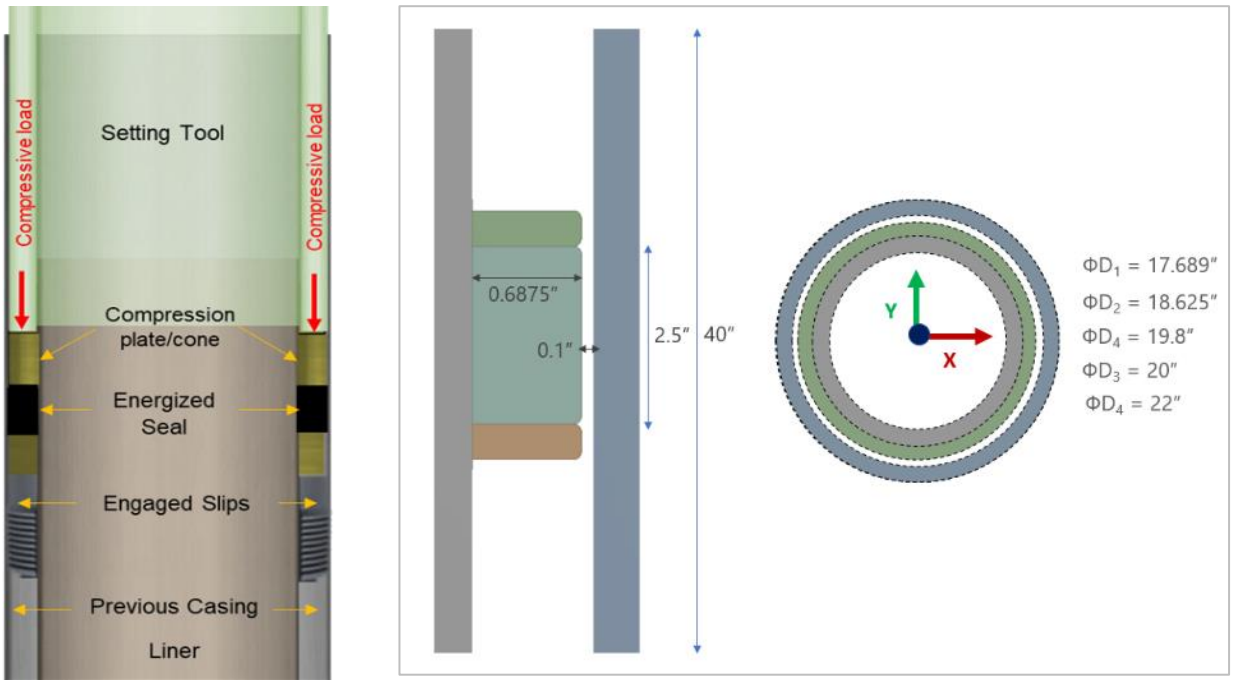

Figure 4.1: Conventional liner hanger seal assembly (left) and representative FEA model (right)

Conventional liner hanger is installed, and seal energized by engaging slips to previous casing and then applying compressive setting load on compression plate. This process has been mimicked in FEA model by assigning boundary conditions to the compression plates. Axial support boundary condition was assigned to the bottom compression plate. Liner and casing were also constrained axially at both ends. Seal was energized by applying fixed downward displacement boundary condition to the upper compression plate (**Figure 4.2)**. If the displacement is sufficiently large to overcome radial clearance between seal and casing, then compressed seal will generate contact pressure at the seal-casing interface. This contact pressure value is indicative of amount of fluid pressure the seal can withstand without leakage. There are two reasons for selecting a displacement type boundary condition instead of specifying a compressive load to the upper compression plate. First, displacement boundary conditions tend to provide faster and more controlled numerical convergence. ANSYS guidelines indicate that force type boundary conditions are difficult to converge and may not be accurate in some cases. Second reason is that displacement boundary condition is less susceptible to convergence failure than the load type boundary conditions.

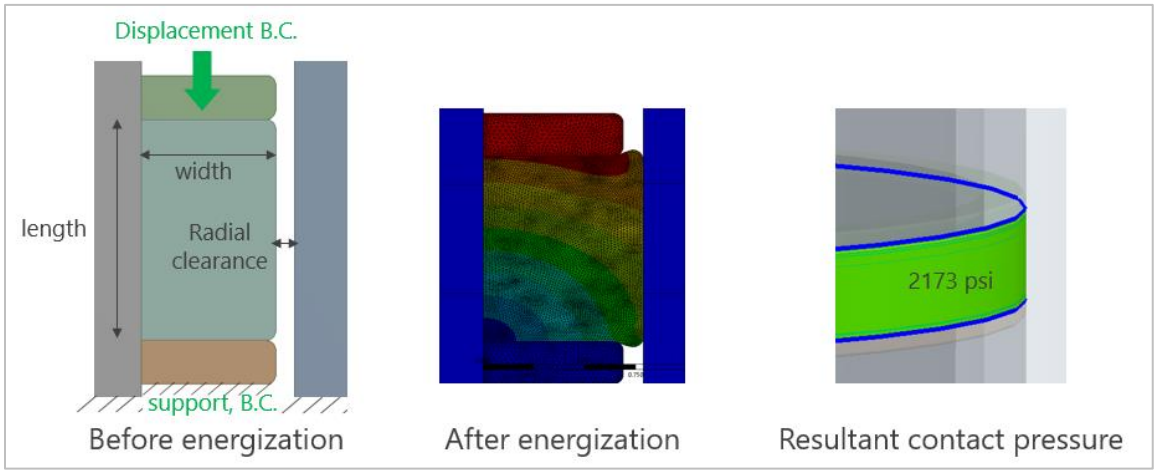

Figure 4.2: Seal energization and boundary conditions in FEA model of conventional seal assembly

4.2 FEA Model of Expandable Assembly

Schematic of the axisymmetric FEA model developed to represent expandable liner hanger seal assembly is shown in **Figure 4.3**. The model consists of liner, casing, and seal components. There are no compression plates like conventional liner hanger seal assembly. Dimensions of the base case model are same as the conventional assembly. The diameter of liner, and casing are from an actual offshore well construction design (BSEE 2014). Length of liner and casing components is 40 in. The length was kept long enough to avoid end effects on seal energization process. The axial length (or height) of the seal component is 2.5 in. and radial width is 0.6875 in. Seal length and width have been varied as a part of assessing design scenarios and have been discussed in results section.

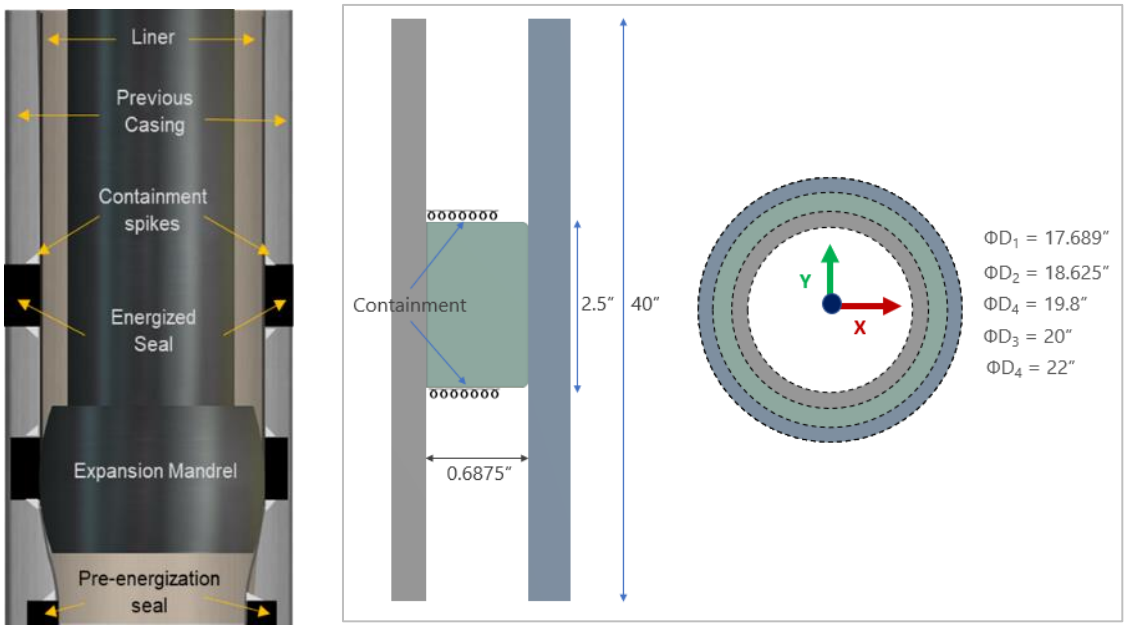

Figure 4.3: Expandable liner hanger seal assembly (left) and representative FEA model (right)

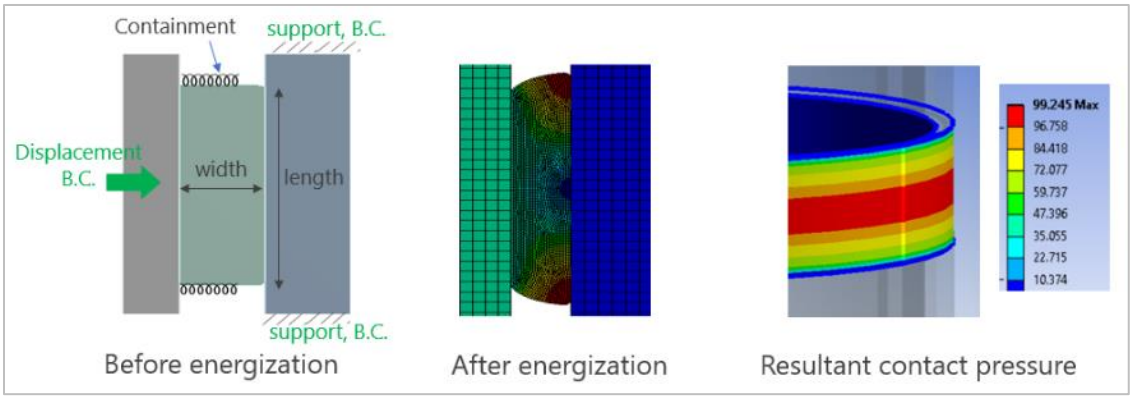

Figure 4.4: Seal energization and boundary conditions in FEA model of expandable seal assembly

Expandable liner hanger is installed, and seal is energized by reciprocating a solid mandrel through inner liner to plastically deform and expand it. Expansion of liner compresses seal element against host casing. Modern designs of hangers also have containment spikes on either side of the seal elements. The function of these spikes is to limit axial deformation of seal element and help achieve better seal energization and consequently higher contact pressure against host casing. This installation process of expandable liner hanger has been mimicked in FEA model by assigning boundary conditions to the liner, casing, and seal (**Figure 4.4**). Liner was assigned a radial displacement boundary condition. Host casing was restrained axially by applying support type boundary conditions. Containment spikes were represented by assigning a force support to axial ends of the seal. This force support is defined as pressure required for unit displacement of the boundary. For example, 5000 psi/in containment indicates that boundary of seal will deflect by an inch if 5000 psi stress is generated. The value of containment was varied to represent different quality of containment. Mandrel and plastic deformation of liner were not modelled to simplify the model and minimize computational time. Moreover, plastic deformation of liner is beyond the scope of this study and would require a separate study.

4.3 Material Properties

The liner and casing components were modelled as isotropic linear elastic material and their material properties are provided in **Table 4.1**. Seal was modelled as liner-elastic or hyperelastic material depending on the type of elastomer being modelled. The material properties of different elastomer studied are listed in **Table 3.1** and **Table 3.2.**

Table 4.1: Material properties used for liner and casing in FEA models

Property	P110 Liner	X80 Casing
Young's Modulus, psi	29×10^6 psi	29×10^6 psi
Poisson's ratio	0.3	0.3
Yield Strength, psi	110,000 psi	80,000 psi
Tensile Strength, psi	125,000 psi	90,000 psi

4.4 Meshing, Model Setup, and Contact Formulation

FEA models need to be carefully meshed and setup to achieve successful convergence. Achieving successful convergence with hyperelastic material behavior of seal is challenging. Some of the challenges in the FEA models of this study are – highly non-linear hyperelastic material behavior of seal element, incompressibility of elastomer, high computational requirement because of use of Ogden 3rd order material model, and non-linear contact formulation at seal-casing interface.

Element formulation is important for FEA modelling when analyzing hyperelastic elastomer seals where element locking could be a concern . Elastomers are nearly incompressible i.e. they have Poisson's ratio close to 0.5. This can cause numerical difficulties and lead to overly stiff behavior caused by volumetric locking. Various methods of dealing with incompressibility suggested by Harish (2018) were followed to fix convergence problems.

In FEA models of elastomers, shape and quality of mesh elements after deformation are more important than initial mesh elements. Therefore, it is often recommended to use low order mesh elements with triangular or tetrahedral elements. These elements are more stable and prevent excessive distortion. Finer mesh may not be useful in all scenarios as they are more prone to concentration of peak strain and extremely high distortions. Sometimes, auto rezoning and adaptive mesh controls are also needed in modelling high deformation scenarios. All these tricks were used as and when convergence issues arose in simulations. For majority of the cases, triangular elements with average size of 0.01 in were determined to be sufficient for meshing the FEA models (**Figure 4.5**).

Figure 4.5: Fine mesh elements (approx. 0.01 in.) used for discretizing FEA models

Contact between seal and casing is another challenging aspect of FEA modelling in this study. Contact is a changing status nonlinearity and its formulation can significantly affect simulation results. Therefore, it is the most critical aspect of this model. There are two contact surfaces in the model: seal-liner and the seal-casing interface. These contacting bodies can transmit compressive normal force and tangential frictional force but not tensile normal force. Realistically,

the contacting bodies do not penetrate each other. In finite element modelling, various contact formulations are available that enforce this contact compatibility to various degrees.

The most common contact formulations are pure penalty and augmented Lagrange. As shown in **Figure 4.6,** a contact stiffness (similar to spring constant) is assigned to the contact surfaces. The higher the contact stiffness, the lower the penetration. Ideally, for an infinite contact stiffness, one would get zero penetration. This is not numerically possible, but as long as penetration is small or negligible, the solution results will be accurate. Because of the additional parameter λ, the augmented Lagrange method is less sensitive to the stiffness constant. Normal Lagrange formulation adds an extra degree of freedom in the form of contact pressure to satisfy the contact compatibility. This eliminated the need for contact stiffness. This method provides excellent penetration control but takes a longer time to converge.

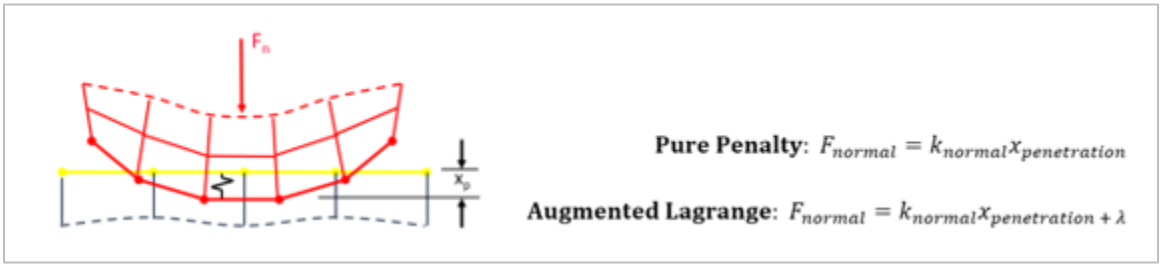

Figure 4.6: Pure penalty or augmented Lagrange contact formulation

Various contact formulation and their pros and cons were carefully considered. Detailed description of contact formulation is out of the scope of this dissertation. However, a summary of options used in contact modelling are as follows:

- Both contact surfaces (seal-liner and seal-casing) have been considered as frictionless unless otherwise mentioned.

- Because of significant difference between material properties of seal and casing/liner, asymmetric contact behavior has been selected. Based on ANSYS general guidelines, seal has been selected as contact body and the liner and casing as target bodies.
- Either Augmented Lagrange with an optimized stiffness factor or a normal Lagrange is selected as the contact formulation in this work.
- The nodal normal detection method has been selected as preferred method for contact detection as it provides less penetrations, particularly at the corners and edges.
- Pinball radius is a sphere surrounding each contact detection point within which the solver considers all nodes to be "near" contact and monitors the relationship. Its value is ensured to be sufficiently larger than seal interference or displacement.
- To ensure maximum accuracy, contact trimming - used for faster convergence, has been turned off. "Trim Contact" automatically reduces the number of contact elements generated within each pair, thereby speeding up processer time.

4.5 Model Verification and Validation

To improve reliability of the contact pressures simulated by the model, it is important to perform model verification and validation. Model verification is the process of confirming whether the finite element tool is solving the model correctly or not. Model validation is the process of confirming whether the model assumptions are true, and the results are representative of the reality.

Two steps were taken to verify the model. First, it was checked whether the displacement boundary conditions applied are indeed being observed in the simulation results. The second step was to perform a mesh sensitivity analysis. As mesh becomes finer, the numerical error reduces. However, it also increases computational requirements. To confirm that the results obtained in this

study are independent of mesh, contact pressures were examined as a function of mesh element size as shown in **Figure 4.7**.

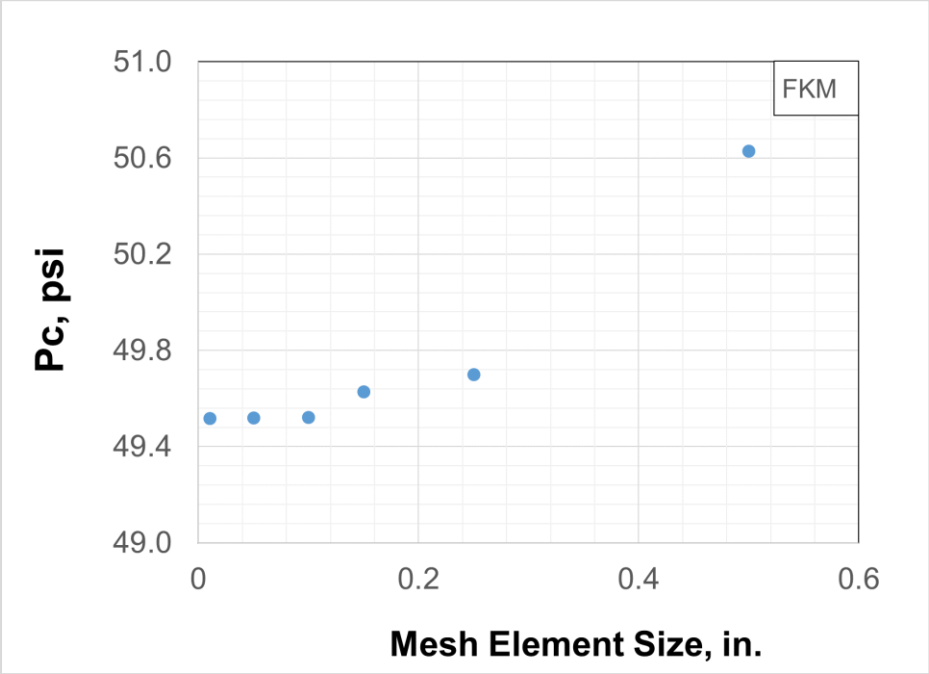

Figure 4.7: Contact pressure in middle of the seal-casing interface as a function of mesh element size

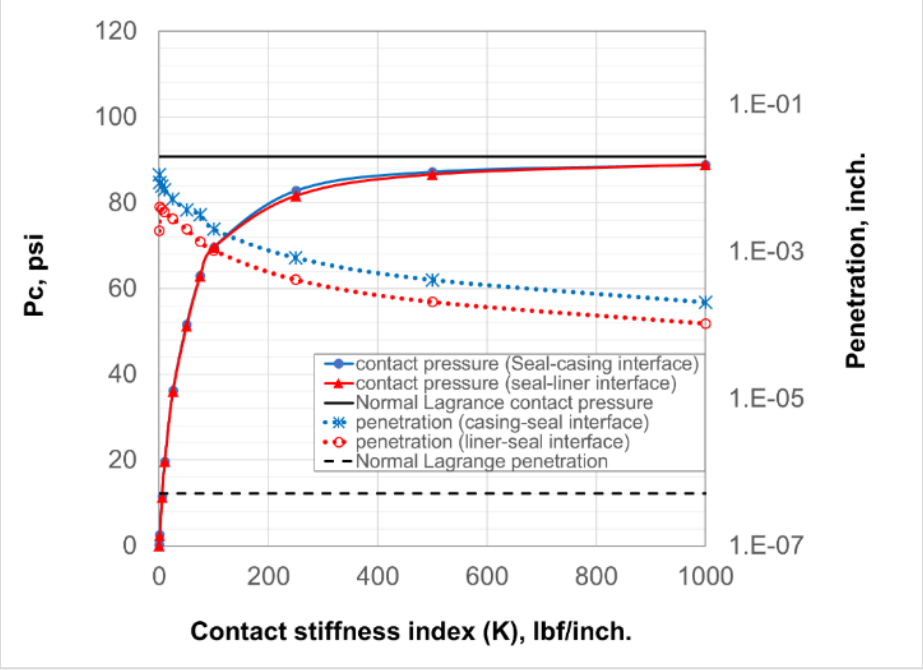

Figure 4.8: Sensitivity of contact pressure and residual penetration to contact stiffness index

The most crucial verification is that of contact pressure as it is the target output from the simulations. One way to increase the accuracy and reliability of contact pressure is to minimize penetration as much as possible by increasing the contact stiffness index. As shown in **Figure 4.8**, the stiffness index was varied from 0.1 to 1000. Penetration decreased 100-fold over this range. Contact pressure values plateaued near 90 psi at a higher stiffness index. Residual penetration of the order of 10-4 in. is practically negligible. Moreover, normal Lagrange method independently yielded contact pressure of 91 psi at significantly low penetration of the order of 10-7 in. Thus, it can be estimated with reasonable certainty that contact pressure is approximately 90 psi. This provides further validation of model results. It should be noted that increasing the stiffness index increased the time required for the solution to converge. Normal Lagrange was the most computationally intensive formulation as it has the most stringent requirement for contact penetration. In summary, various model verification techniques discussed in this section indicate that the model is setup correctly and should produce reliable results.

4.5.1 Analytical Validation

The simulated contact pressure values are the most important items that require validation. The contact pressure values were validated using two different analytical equations. It should be noted that only conventional liner hanger seal assembly with zero radial clearance could be verified analytically. For rest of the assembly configurations, no closely matching analytical solution is available.

To validate the FEA model, analytical relationship between bulk modulus, volumetric compression, and pressure can be used. As shown in the **Figure 4.9,** conventional hanger seal model is constrained in radial and axial direction after energization. The pressure generate at all

four frictionless contacting surfaces should be same. This situation is similar to how bulk modulus is defined i.e. application of equal external pressure over the surface of a three-dimensional body to achieve bulk volumetric compression.

$$\frac{\Delta V}{V} = -\frac{P}{K} \quad \text{..... (4.1)}$$

$$K = \frac{E}{3(1-2\nu)} \quad \text{..... (4.2)}$$

where P is pressure, K is bulk modulus, ν is Poisson's ratio, V is the original volume of elastomer seal, and ΔV is change in volume as shown in **Figure 4.9**. All variables have consistent unit.

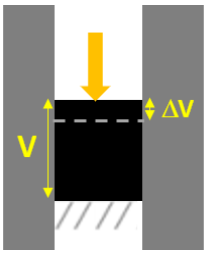

Figure 4.9: Use of analytical equation of bulk modulus to validate contact pressure

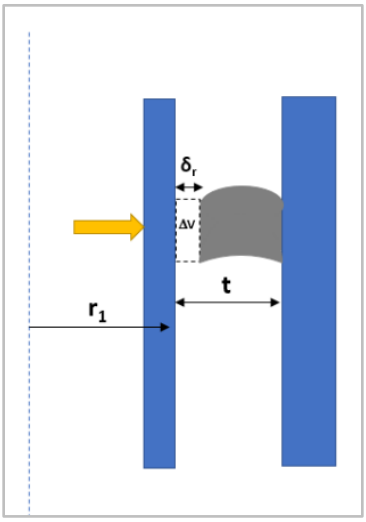

Figure 4.10: Schematic of the analytical model of Al-Hiddabi et al. (2015)

The second analytical equation that was used for validation was based on model developed by Al-Hiddabi et al. (2015) for predicting contact pressure in expandable liner hanger seals. This model is based on an elastomer seal that is radially confined between metal tubes with fluid pressures in an axial direction (**Figure 4.10**). Originally developed for a solid expandable tubular, this model assumes linear elastic material property and can predict contact pressure along the contact length as a function of the seal compression ratio, fluid pressures, and material properties. The model is discussed in detail in literature review (**section 2.5.3.4**).

The maximum contact pressure in can be estimated by,

$$P_{max} = \frac{(2\bar{r}_1+\bar{\delta}_r)\bar{\delta}_r K}{(2\bar{r}_1+1)} \quad \text{..... (4.3)}$$

where

$$\bar{r}_1 = \frac{r_1}{t}\ ,\ \bar{\delta}_r = \frac{\delta_r}{t}\ ,\quad and \quad K = \frac{E}{3(1-2\nu)}$$

In the above equations, P_{max} is the maximum contact pressure, K is bulk modulus, and ν is Poisson's ratio. As shown in **Figure 4.10**, r_1 is the outer radius of the liner, t is the radial width of the seal, and δ_r is radial compression.

Pressure calculated using above equations were compared with FEA simulated contact pressure for different compression ratio values. Compression ratio (CR) is defined as an axial compression of seal relative to axial length of the seal. For example, 0.25 inch of displacement relative to 2.5-inch seal length indicates CR of 10%. For the case of zero radial clearance, CR approximately equals volumetric compression. As shown in the **Figure 4.11,** good match was obtained between analytical and FEA predictions. Both analytical methods produced similar contact pressure results. Hence, separate datapoints have not been show for both methods.

Deviation from analytical calculation was 4% to 7% for low compression ratio (CR) of up to 5%. The deviation reduces to less than 3% at higher ends of compression ratio.

The deviation between FEA and analytical calculation can be primarily be attributed to the minor differences between the boundary conditions of the FEA model and the analytical models. The seal energization in conventional liner hanger assembly with zero radial clearance does not completely match with the first analytical equation which represents perfectly uniform volumetric compression of material. The difference arise due to slightly rounded edges of elastomer seal component in the FEA model and minor radial ballooning of liner-casing annulus caused by seal compression. The second analytical equation was derived from the model which was originally developed for radial compression of seal with axial fluid pressure. Modifying that equation for use in axial compression of seal with solid support instead of fluid pressure likely introduced the deviation.

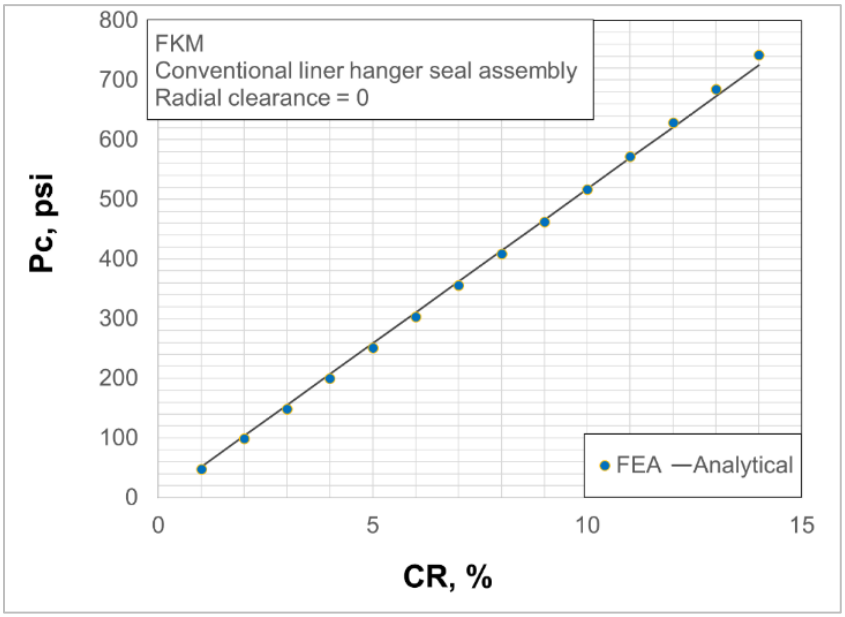

Figure 4.11: Comparison between FEA predicted contact pressure and analytical calculation (for conventional liner hanger seal assembly with zero radial clearance)

4.5.2 Experimental validation

As discussed in **section 3.3**, sealability test apparatus was used to validate finite element modelling approach. For this, a finite element model similar to experimental setup was developed. The schematic of the model with dimensions and boundary conditions is provided in **Figure 4.12.** The actual setup has two elastomer ring seals and three aluminum plates. Modelling that exact configuration would have resulted in too many contact regions and led to convergence issues. To mitigate the convergence issues, only one seal and two plates were used in the FEA model. This also helped reduce the simulation time.

As shown in the **Figure 4.12,** seal energization was performed by applying displacement boundary conditions to the top of the aluminum plate. The displacement values used in the simulation were obtained from the setup by measuring the axial compression of seal using the measurement scales attached to the pipe. **Figure 4.13** shows the FEA before and after seal energization process. Material properties used in the model are listed in **Table 4.2.**

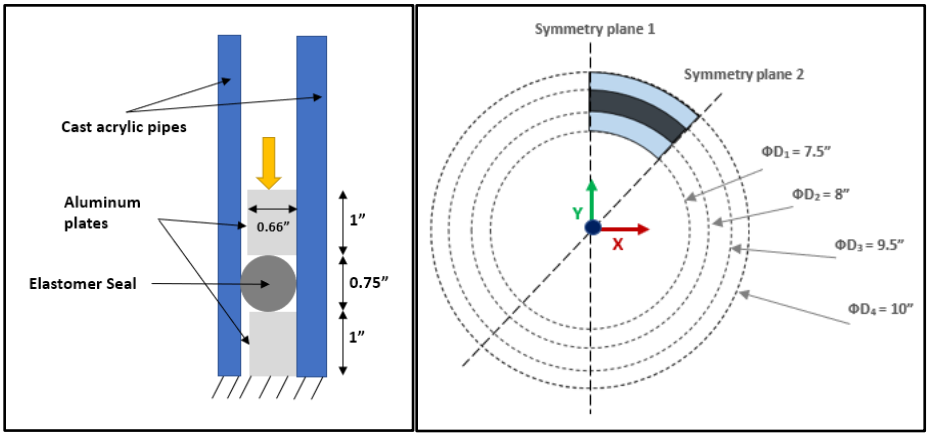

Figure 4.12: Schematic and dimension of FEA model of experimental setup in XZ plane (left) and top view of the model in XY plane

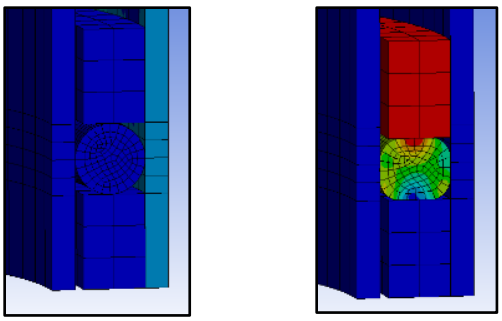

Figure 4.13: Graphical representation of FEA model of setup II before (left) and after (right) seal energization

Table 4.2: Material properties used in the FEA model of experimental setup

Property	Cast Acrylic Pipes	Aluminum Alloy NL Plates	EPDM elastomer	EPDM elastomer – after aging in CO_2
Young's Modulus / Elastic modulus	0.4 x 10^6 psi	10.29 X 10^6 psi	277 psi	194 psi
Poisson's ratio	0.37	0.33	0.49	0.49

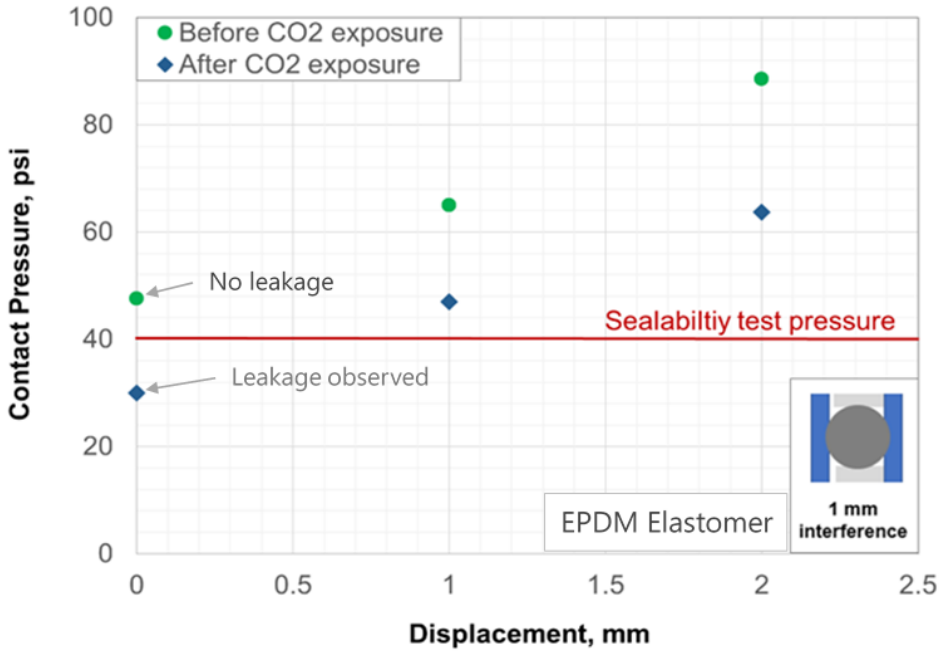

Figure 4.14: Confirmation of FEA predicted contact pressure using sealability tests

EPDM elastomer O-rings were placed in the setup to measure contact pressure as a function of displacement (i.e. compression). Nitrogen injection tests were conducted to estimate contact pressure between seal and pipe. Elastic modulus of EPDM was measured and input into the FEA model to simulate contact pressure at different displacement values. For second scenario, EPDM elastomer aged in CO_2 was used. The results of FEA simulation and sealability tests are summarized in **Figure 4.14**. As shown in the figure, FEA predicted contact pressure at zero displacement was approximately 48 psi. Sealability tests conducted at 40 psi did not indicate any leakage. For EPDM aged in CO_2 the contact pressure prediction was approximately 30 psi and as expected, leakage was observed when sealability test was conducted at 40 psi. Presence of contact pressure even at zero displacement (i.e. no external compression). This is because the cross sectional diameter of O-ring was 1 mm larger than the annulus space between pipes. Hence, installing the ring inside the setup resulted in compression of the seal due to interference. The upper limit of contact pressure could not be validated experimental because the pressure rating of the setup was determined to be 40 psi. A pilot test at high Nitrogen injection pressure had resulted in failure of the setup.

Overall, analytical and experimental validation of some assembly configurations and observations, combined with careful contact formulations and mesh sensitivity analysis, provide sufficient confidence in reliability of FEA modelling approach. Moreover, the major results discussed in this dissertation are based on relative comparison of contact pressure values. For making conclusions, only those observations have been considered that exhibit differences exceeding error margin of the FEA predictions as established by analytical validations.

Chapter 5: Leakage Model Development

5.1 Introduction

As discussed in previous section, sealability of liner hanger seal assembly or any other seal assembly for that matter can be quantified by contact pressure generated at the sealing interface. The contact pressure depends on various factors such as energization quality, method, seal dimensions, seal geometry, seal material behavior, operating pressure or thermal loads, etc. One major knowledge gap is lack of understanding of target seal energization. In other words, it is not fully understood how much seal energization is sufficient to seal variety of fluids at different operating conditions. The relationship between seal contact pressure, and actual fluid pressure it can hold without permitting leakage is not known.

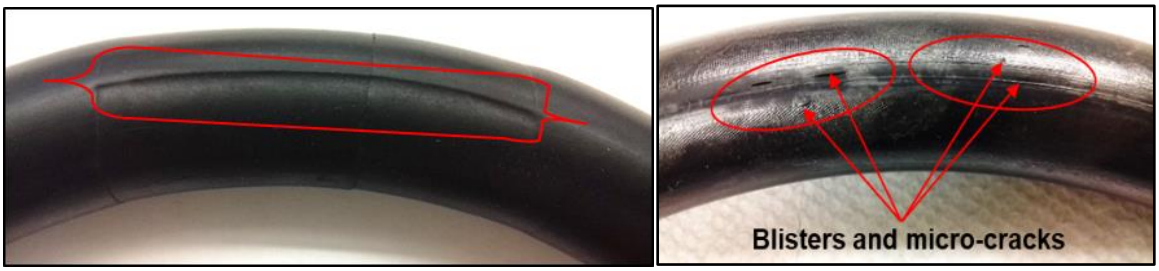

Figure 5.1: Surface defects on elastomer seal resulted in failed leakage tests (Ahmed et al. 2019)

Various evidences suggest that surface characteristics of seal element can also influence its performance. For example, various manufactures recommend surface finishing of 32 μinch for O-rings and elastomer components (Apple Rubber Products Inc. 2009). A recent study that employed the same experimental setup as used in this work, demonstrated that surface characteristics or defects on elastomer seal can impact its sealability (Ahmed et al. 2019b). For same elastomer material and energization conditions, elastomer O-rings (**Figure 5.1**) resulted in failure sealability tests whereas sample without any surface defects prevented leakage.

There have been many studies on microscopic seal modelling in the field of tribology. However, in Oil & Gas application, this research is very limited. Existing industry standards for seal equipment do not consider surface finishing in development of operating envelops for seal assemblies. For example, API TR 6AF2 (2013) contains operating envelopes for various sizes of API flange-gasket connections under various loading conditions. The operating curves were generated using finite element modelling in which the gasket seal was modelled only as a support, and face separation (or zero contact stress) was considered as the leakage criteria. It has already been recognized that the leakage criteria of contact lift-off or zero contact stress, as used in API6AF2, is not accurate because leakage can be observed even when a contact is maintained and contact stress is non-zero. There is no clear understanding on whether a certain contact pressure value is able to hold the same amount of fluid pressure. In other words, can 1000 psi of contact pressure at seal-pipe interface prevent penetration/leakage of fluid at 1000 psi pressure? Understand the relationship between contact pressure and leakage rate is essential to identify true leakage capacity of a seal assembly.

One way to address this research gap is to conduct real scale physical tests where surface topography of seal is also measured and monitored. However, it is often not physically possible and/or cost effective to conduct true scale experiments for various operating scenarios. Hence, use of verified computational modeling techniques is imperative. The existing FEA tools can accurately predict the contact pressure under various loading conditions. However, they assume perfectly smooth surfaces. The feature of simulating fluid penetration through contact nodes is also not accurate. It is not feasible for a macro scale FEA model to also consider microscopic characteristics of seal interfaces. Hence, it is necessary to develop an independent leakage modelling tool that can simulate fluid penetration at microscopic level. There have been some

studies on leakage modelling including the author's (Patel et al. 2018). However, that study was focused on metal-to-metal seals, where the impact of surface is arguably much higher than elastomer seals.

The objective of this task is to develop a leakage model that can consider surface characteristics of elastomer seal interface as an input and predict fluid penetration and leakage rates as a function of operating pressure, seal material properties, and fluid properties.

5.2 Technical Approach

The approach of developing the modelling tool was divided into three steps as shown in **Figure 5.2**. The first step is to model surface topography of elastomer and casing surfaces. Second step is to model microscopic interaction between the two surfaces as they are coming together at microscopic scale. Modelling this interaction is called contact mechanics modelling. The contact mechanics model should predict contact load distribution and apparent contact pressure as a function of deformation and separation between the surfaces.

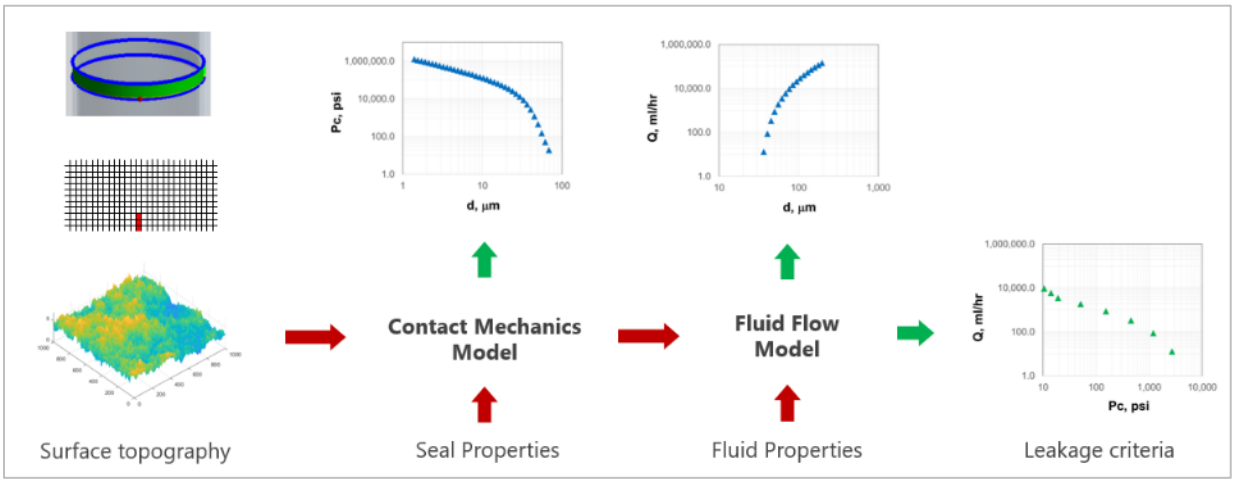

Figure 5.2: Technical approach used to develop leakage modelling tool

The third step is development of fluid flow model which can take microscopic contact separation information as an input, predict fluid flow through it, and calculate total flow rate i.e. leakage rate coming out from the contact boundary. This leakage rate is a function of separation which has a unique contact pressure value associated with it. The information of contact pressure and respective leakage rates can be used to determine target contact pressure and consequently, amount of seal energization needed to seal certain fluid at certain pressure. The seal assembly design and installation can then be tailored to meet this contact pressure requirement.

5.3 Surface Topography

As shown in **Figure 5.3** depending on the magnification, the surface topography of a seal comprises of complex features such as (i) out-of-flatness, (ii) crowning radius, (iii) waviness, and (iv) roughness (Pérez-Ràfols 2016). These features can greatly affect the way contact pressure is distributed. The microscopic gaps can facilitate leakage even when the sealing surfaces are in contact at macroscale. Out of flatness is also known as error of form which should generally be not present. This represents tilting in circumferential direction while crowning radius, as name suggests, represent tilting in radial direction. These two features can typically result from uneven energization of seal. Further magnification reveals waviness feature which is the often the result of turning process widely used in manufacturing these seals. The smallest features that are mostly random are termed as roughness. During examination of a surface, as magnification is increased smaller scales of roughness appear. It has been shown that roughness at smaller scales are similar to that of larger scale with only difference in length and height scales (Bora et al. 2005). This property is known as self-affinity. This self-affinity at different scales is a property exhibited by fractal surfaces. A fractal surface is difficult to describe in traditional geometric dimensions but it essentially has a structure that repeats itself throughout different scales.

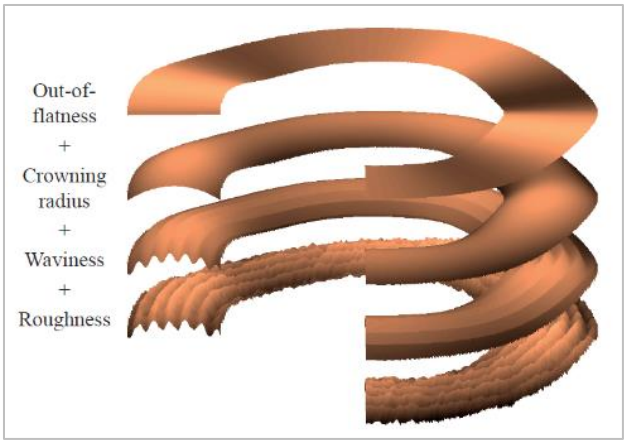

Figure 5.3: Various levels of surface features on a seal surface (Pérez-Ràfols 2016)

Since actual surface measurements of elastomer samples used in this work could not be measured, artificial surface topographies were generated, and parametric study was conducted to understand how surface feature influence leakage. Thorough literature review was conducted to develop or identify an appropriate function that can simulate various types of surface topographical characteristics depending on the scale and magnitude specified. The multivariate Weierstrass-Mandelbrot (W-M) function as adopted by Bora et al. (2005) was selected to be the most appropriate solution for creating artificial surfaces:

$$z(x,y) = C\sum_{m=1}^{M}\sum_{n=0}^{nmax}\gamma^{(D-3)n}\left\{cos\varphi_{m,n} - cos\left[\frac{2\pi\gamma^{n}(x^2+y^2)^{0.5}}{L}\cos\left(\tan^{-1}\left(\frac{y}{x}\right) - \frac{\pi m}{x}\right) + \varphi_{m,n}\right]\right\} \quad \text{.....(5.1)}$$

$$C = L\left(\frac{G}{L}\right)^{D-2}\left(\frac{ln\gamma}{M}\right)^{0.5} \quad \text{.....(5.2)}$$

Where equation (5.1) is constructed by taking two-dimensional fractal profile as a "ridge" and then superimposing a number of ridges at different angles to achieve randomization. φ is a random number to generate random phase and profile angles. M is number of ridges. G is roughness coefficient that determines surface RMS. L is the length of surface domain being constructed. γ determines frequency and amplitude ratio of successive cosine shapes which indirectly represents relative frequency separation of successive terms in the function. L_{max} is the sample size. n_{max} is the total number of cosine shapes added to generate the surface. For perfectly fractal surface, n_{max} would be infinite. However, for practical purposes, finite value of n_{max} is used such that cosine waves with periods large than L and smaller than L_{min} are not required.

D is fractal dimension of the surface. One of its definitions is a ratio of number of self-repeating units to magnification factor. In simple terms, fractal dimension is an index that measures how details in a surface or pattern changes with the scale at which it is measured. For example, one counter-intuitive real-world example is measurement of coastline. As the length of scale used to measure the coastline reduces, the total length of coastline will increase (Mandelbrot 1967).

$$\text{D: Fractal dimension} = \frac{\log(\text{No of self repeating units})}{\log(\text{magnification factor})} \quad \text{.....(5.3)}$$

Equations (5.1) and (5.2) were coded into MATLAB. **Figure 5.4** shows various types of surfaces that can be generated by the function. In the figure, bottom two surface have smaller fractal dimension compared to the top two surfaces. The upper two figures have more roghness, lower minimum frequency, and more number of superimposed ridges.

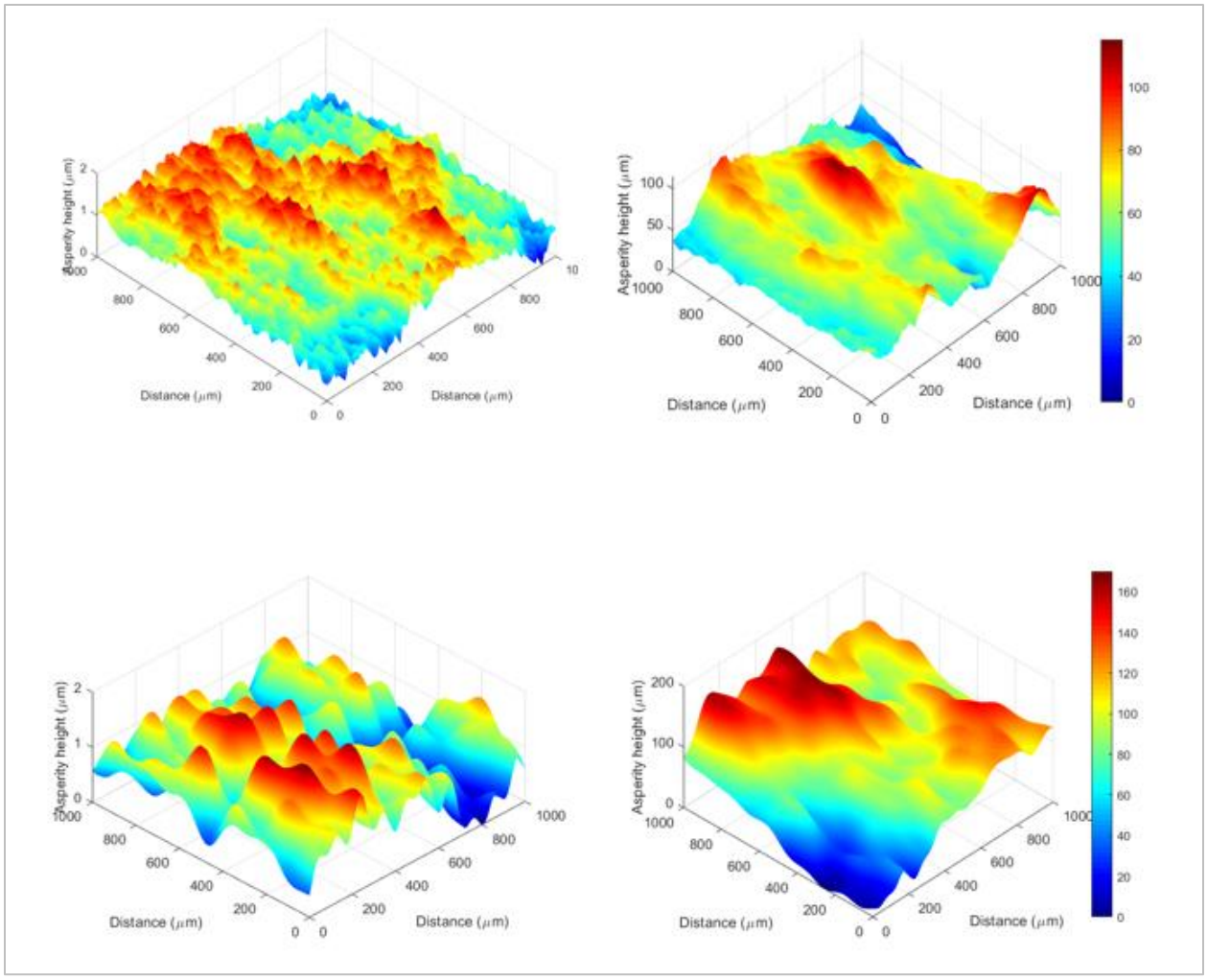

Figure 5.4: Examples of various artificial surfaces generated by W-M function

5.4 Contact Mechanics Model

Contact mechanics is study of deformation of solids that touch each other at one or more points. In the field of tribology, a variety of contact mechanics model exists but mainly they can be classified into asperity based analytical models, fractal-based model, and fully numerical models (Pérez-Ràfols 2016).

The basic idea behind asperity based analytical models is to describe a surface as a collection of discrete asperities of certain shape and solving individual contact problem at each of

the asperities. There are two types of asperity-based models: deterministic and statistical. Statistical models as name suggests only requires the asperity height distribution as an input and hence can be computationally faster and can also incorporate different scale of surface topography i.e. roughens, waviness, out of roundness etc. Some of the latest development in statistical model are discussed in Pérez-Ràfols (2016). Deterministic model on the other hand takes into consideration locations of asperities. Since, the goal of present work is to understand effect of surface topography on leakage, it becomes essential to consider the location information. Therefore, deterministic approach has been employed in the present work.

A semi-analytical model such as one presented by Persson (2006) assumes isotropic surfaces which is not valid in case of a typical surface topography of a metal-to-metal seal. Commonly employed numerical models are computational structural mechanics (CSM) approach which is based on finite element method. This approach makes the fewest approximation but is extremely expensive in terms of computational power and memory. For these reasons, semi-analytic and fully numerical approaches are out of the scope of the presented work.

The oldest analytical model in contact mechanics is Hertz theory (Hearn 1997). Hertz considered only elastic contact between regular shapes such as spheres, cylinders and flat surfaces. The author considered a smooth frictionless surface and the model was only applicable to small strain values. The contact area is considered small and flat in comparison with radius of curvature of undeformed contact bodies. The Hertzian pressure is then solved as a contact of two spherical bodies.

Greenwood and Williamson (1966) first introduced a model for nominally rough surfaces. The Greenwood and Williamson (G-W) model describes asperities as spheres with fixed radius

and Gaussian distribution for heights. Since then, various researchers have improved the original model and have led to increasingly better predictions of contact area and contact separation between two surfaces. Greenwood and Tripp (1970) later extended the G-W model to contact between two rough surfaces. Whitehouse and Archard (1970) introduced variable radius of curvature. Chang, Etsion, and Bogy or CEB model (1987) introduced concept of volume conservation of asperities and were able to provide accurate predictions of contact area. Zhao et al (2000) improved the G-W model further with incorporation of elastic-plastic deformation of asperities.

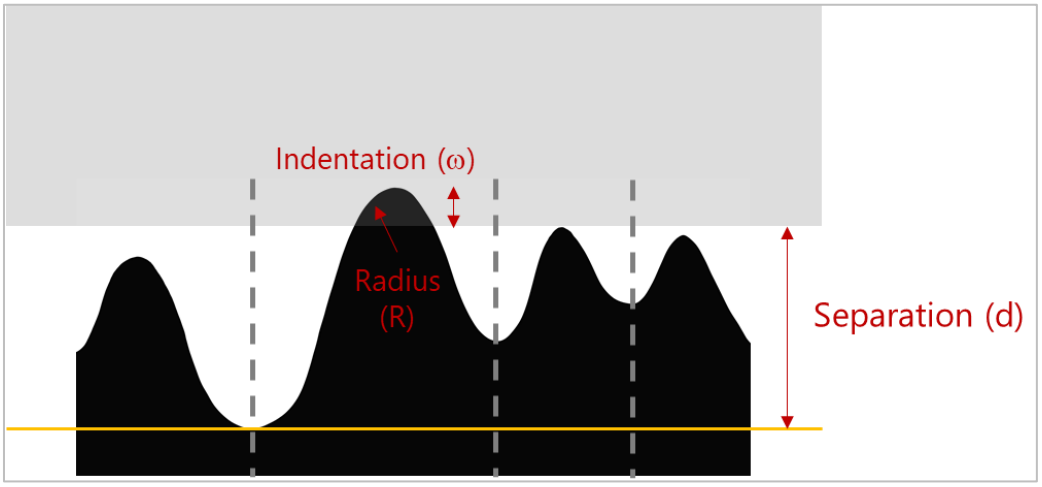

Figure 5.5: 2D representation of elastic interactions between elastomer seal (black) and smooth casing surface

The contact mechanics model developed in this model is a deterministic model. Height distribution of each asperity was calculated based on W-M function discussed in previous section. The model algorithm is as follows:

1. As shown in **Figure 5.5**, the model assumes that casing surface is perfectly smooth. Separation between seal and casing surface is defined as distance between the lowest valley on seal surface

to casing surface. Initial separation or would be equal to the height of highest peak on elastomer seal surface.

Initial separation $d_0 = h_{max}$ ……..……..……(5.4)

Where h_{max} is the height of the highest peak on elastomer seal surface and d_0 is separation at initial time.

2. Separation is reduced gradually at a user-defined rate. At each separation case, location of asperities that have been contact are determined. For each contacted asperity, amount of indention is determined.

Asperity i contacted if $h_i > d_t$ ……..……..……(5.5)

Asperity indentation $\omega_{it} = h_i - d_t$ ……..……...……(5.6)

Where h_i is the height of asperity i, d_t is separation at current load step, and ω_{it} represents indentation of asperity i at load step t.

3. Each asperity can be represented by an ellipsoid and its tip can be characterized as spherical and represented by a radius of curvature. For each contact asperity, contact load and contact area can be calculated using Hertz theory.

Contact load at asperity i $F_{it} = \frac{4}{3} E^* R_i^{0.5} \omega_{it}$ ……..……(5.7)

Contact area at asperity i $A_{it} = \pi R_i \omega_{it}$ ……..……(5.8)

Where F_{it} is the load needed to deform asperity i at load step t. R_i is radius of curvature at the tip of asperity i. It is calculated based on second order derivative of heights of adjecent

asperities. A_{it} is the contact area generated by deformation of asperity i at load step t. E^* is equvalent Young's modulus of interacting surface. It is defined as,

$$E^* = \frac{E_e E_s}{E_e(1-\nu_s^2)+E_s(1-\nu_e^2)} \quad \text{.....(5.9)}$$

Where E_e and E_s are Young's modulus of elasomer and steel casing respectively. ν_e and ν_s are Poisson's ratio of elastomer and steel respectively. Apparent contact pressure can then be calculated by summing all contact load values across contacted asperities and dividing it by apprent contact area.

4. Now next step is to calculate porosity or porous volume between the elastomer and steel surfaces. It is assumed that volume of each asperity is being conserved while it is being crushed. Another assumption is lack of interaction between adjacent asperities. In other words, deformation of an asperity doesn't exert additional loads on adjacent asperities.

Porosity at asperity i and load step t: $\phi_{it} = 4d_i b^2 - \frac{2}{3}\pi h_i b^2$ .....(5.10)

Where b is the radius of asperity base as shown in **Figure 5.6.**

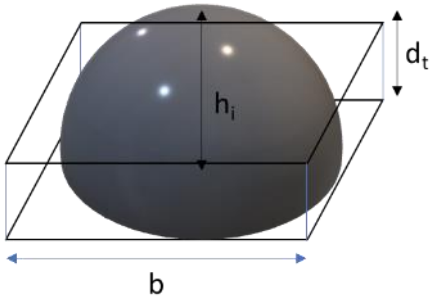

Figure 5.6: Ellipsoid shape assumed for individual asperity

5. Once porosity becomes zero, then the contact load is calculated based on volumetric compression and bulk modulus equation. Moreover, the cell is no longer active for fluid flow model discussed in the next section.

5.5 Fluid Flow Model

The function of leakage model or flow mechanics model is to calculate the flow rate or leakage rate for a particular contact separation value. Leakage depends on many factors which can be classified into three primary categories: (i) properties of porous path, (ii) fluid properties, and (iii) operating parameters. Flow mechanics model is governed by Navier-Stokes equations which is simplified based on various assumptions.

The leakage phenomena is similar to fluid flow in porous medium as studies in reservoir engineering. Using the same concepts as reservoir simulation, a leakage model was developed with following assumptions:

- Fluid doesn't deform porous medium (Fluid pressure << contact pressure)
- No surface effects- surface tension, adsorption, drag
- 100% saturation and single fluid
- Steady state laminar flow
- Isothermal flow
- Incompressible Newtonian fluid

For an incompressible Newtonian and laminar fluid flow, the Navier stokes equation can be simplified to,

$$\nabla \cdot [v] = 0 \quad \text{……...…(5.11)}$$

For a laminar flow, the velocity can be computed by a Darcy's equation. Hence the above equation can be written as,

$$\nabla \cdot \left[\left(\frac{KA}{\mu}\right)\nabla p_f\right] = 0 \quad \text{.....(5.12)}$$

Where K is hydraulic conductivity, A is area, μ is Newtonian viscosity, and P_f is fluid pressure gradient. Above equation in two dimensions can be written as

$$\frac{\partial}{\partial x}\left(\frac{A_x K_x}{\mu}\left(\frac{\partial p_f}{\partial x}\right)\right)\Delta x + \frac{\partial}{\partial y}\left(\frac{A_y K_y}{\mu}\left(\frac{\partial p_f}{\partial y}\right)\right)\Delta y = 0 \quad \text{.....(5.13)}$$

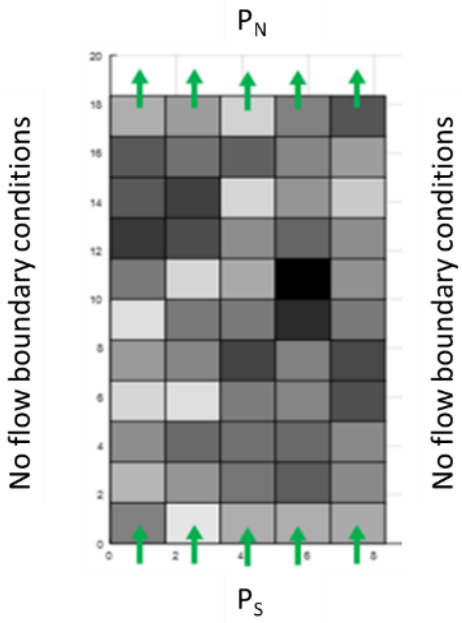

Figure 5.7: Boundary conditions for fluid flow calculations

The boundary conditions used for fluid flow calculations are shown in **Figure 5.7**. Fluid flow direction is from south to north. The south and north boundaries are constant pressures boundaries - P_S and P_N respectively. The east and west boundary conditions are no-flow boundary conditions. This assumption should not affect the total flow rate calculation over the contact area

because even if fluid traverses in circumferential direction, eventually, it has to come out in axial direction.

To solve the governing equation (5.13), information on hydraulic conductivity is required. Porosity values output by the contact mechanics model can be used to estimate the hydraulic conductivity value. For this, the simplest form of Carman-Kozeny equation has been used,

$$\text{Hydraulic conductivity (K)} = \frac{r^2 \emptyset}{8\tau} \quad \text{.....(5.14)}$$

Where r is hydraulic radius, Φ is porosity, and τ is tortuosity which is assumed to be 1. All variables are in consistent unit. The hydraulic radius r is calculated by assuming that the asperity when deformed is being packed downwards in form of a rectangular rhombohedral. The pore volume is then compared to the same volume of a cylinder (**Figure 5.8**) and the radius of that cylinder becomes the hydraulic radius (r) to be used in the equation (5.14).

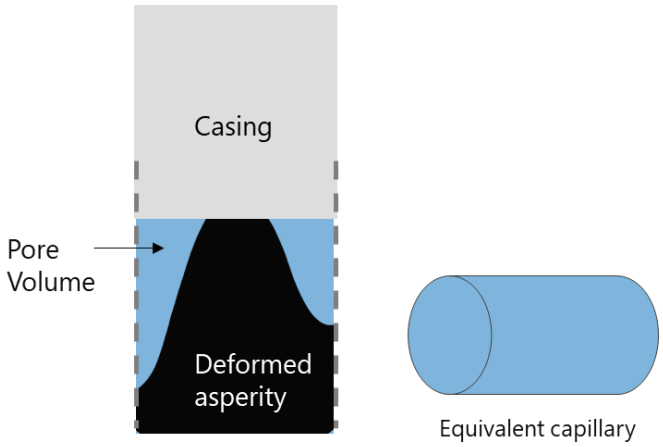

Figure 5.8: Pore space between casing and deformed asperity is assumed to be made of capillaries

Additionally, hydraulic conductivity should also depend on the flow capacity of adjacent cells. This has been achieved by calculating four different types of hydraulic conductivity for each

cell: North, south, west, and east. Each K is evaluated at the corresponding boundary by harmonic average of connecting cells K. For example, as shown in **Figure 5.9**, for block 5, K at the north boundary (K_N) is harmonic average of K of cell 1 and cell 5. Because of harmonic averaging the resultant K would be dictated by the smaller K. Additionally, if one of the connected cells has zero K then the K at the boundary would be zero as well.

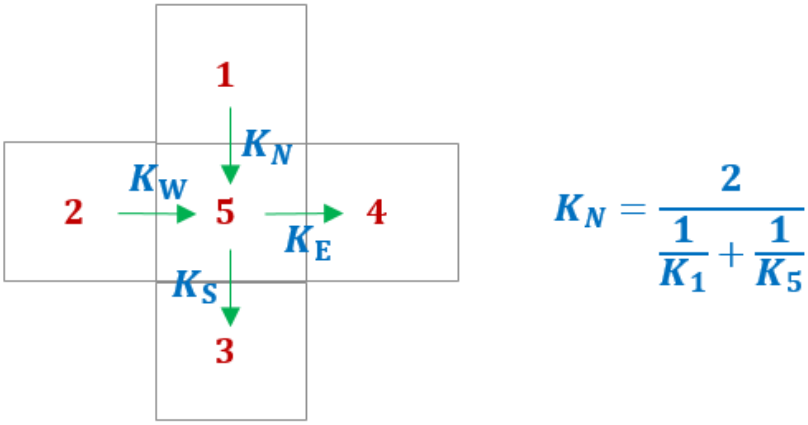

Figure 5.9: Flow path selection through harmonic hydraulic conductivity estimation at asperity boundaries

To calculate the leakage rate, information of fluid pressure distribution is required. This is achieved by solving equation (5.13). To solve the equation, finite different approximation was used.

$$\text{For, } A_x = A_y\,, \Delta x = \Delta y, \text{and } \mu = \text{constant}$$

$$\frac{\partial}{\partial x}\left(K_x\left(\frac{\partial p_f}{\partial x}\right)\right) + \frac{\partial}{\partial y}\left(K_x\left(\frac{\partial p_f}{\partial y}\right)\right) = 0 \qquad \text{.....(5.15)}$$

For a certain gridblock x, the finite different approximation of x component of equation (5.15) can be written as,

$$\frac{\partial}{\partial x}\left(K_x\left(\frac{\partial p_f}{\partial x}\right)\right)=\frac{\left\{K_x\left(\frac{\partial p_f}{\partial x}\right)\right\}_{x+1/2}-\left\{K_x\left(\frac{\partial p_f}{\partial x}\right)\right\}_{x-1/2}}{\Delta x}$$

$$=\frac{\{K_x\}_{x+1/2}\left\{\left(\frac{\partial p_f}{\partial x}\right)\right\}_{x+1/2}-\{K_x\}_{x-1/2}\left\{\left(\frac{\partial p_f}{\partial x}\right)\right\}_{x-1/2}}{\Delta x} \quad \ldots\ldots\ldots\ldots\ldots\ldots\ldots\ldots\ldots\ldots\ldots(5.16)$$

First derivatives can be approximated by,

$$\left\{\left(\frac{\partial p_f}{\partial x}\right)\right\}_{x+\frac{1}{2}}=\frac{P_{fE}-P_{fc}}{\Delta x} \quad \text{and} \quad \left\{\left(\frac{\partial p_f}{\partial x}\right)\right\}_{x+\frac{1}{2}}=\frac{P_{fW}-P_{fc}}{\Delta x} \quad \ldots\ldots\ldots\ldots\ldots\ldots\ldots\ldots(5.17)$$

As discussed in previous section, the hydraulic conductivity is calculated as,

$$\{K_x\}_{x+\frac{1}{2}}=K_E=\frac{2}{\frac{1}{K_{x+1}}+\frac{1}{K_x}} \quad \text{and} \quad \{K_x\}_{x-\frac{1}{2}}=K_W=\frac{2}{\frac{1}{K_{x-1}}+\frac{1}{K_x}} \quad \ldots\ldots\ldots\ldots\ldots\ldots(5.18)$$

Simplifying,

$$K_W\left(P_{fW}^{n+1}-P_{fc}^{n+1}\right)+K_E\left(P_{fE}^{n+1}-P_{fc}^{n+1}\right)=0 \quad \ldots\ldots\ldots\ldots\ldots\ldots\ldots\ldots\ldots\ldots(5.19)$$

Where P_{fE} and P_{fW} are pressures in east and west side block respectively. P_{fc} is pressure in current block for which the equation is being written. Unknown values are represented by superscript $n+1$ which is a common annotation used in numerical schemes.

Simplifying the above equation for two dimensions,

$$K_W\left(P_{fW}^{n+1}-P_{fc}^{n+1}\right)+K_E\left(P_{fE}^{n+1}-P_{fc}^{n+1}\right)+K_N\left(P_{fN}^{n+1}-P_{fc}^{n+1}\right)+K_S\left(P_{fS}^{n+1}-P_{fc}^{n+1}\right)=0$$

$$\ldots\ldots\ldots\ldots\ldots\ldots\ldots\ldots\ldots\ldots\ldots\ldots\ldots\ldots\ldots\ldots\ldots\ldots\ldots\ldots\ldots\ldots\ldots\ldots\ldots\ldots\ldots\ldots(5.20)$$

Equation (5.20) is written for all cells in the model domain and then all the equations are solved simultaneously to obtain the pressure values.

Once the pressure distribution is known, the leakage rate can be easily calculated using the Darcy's equation. As shown in the **Figure 5.7**. Total leakage rate is the summation of individual flow rates calculated at either north (or south) boundary of the domain.

$$Q_{total} = \sum_{i=1}^{n} \frac{AK_{Ni}}{\mu}\left(\frac{P_{fi} - P_N}{\Delta y}\right) \qquad \ldots\ldots\ldots\ldots\ldots\ldots\ldots\ldots (5.21)$$

Where n is number of gridblocks at the north boundary of the domain.

Chapter 6: Assembly Design Results

6.1 Overview

This chapter discusses results related to seal assembly design. Specifically, it discusses differences in conventional and expandable type assembly, and effects of - energization method, seal dimensions, elastomer material, and seal geometry. Performance of seal assembly has been evaluated in terms of contact pressure generated at the seal-casing interface.

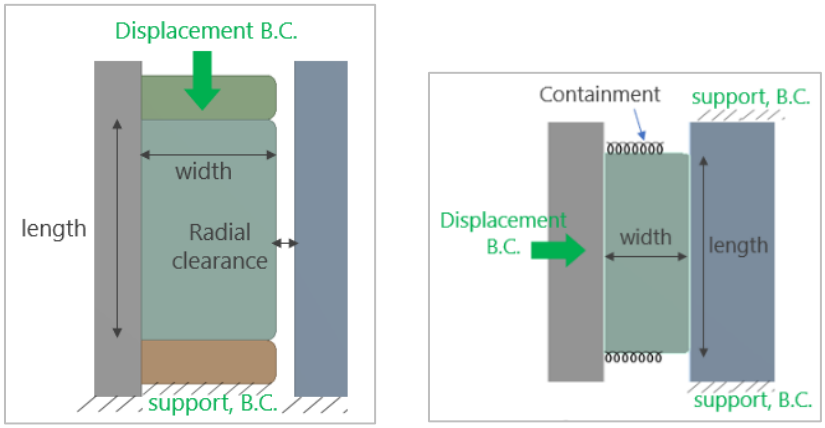

(a) **(b)**

Figure 6.1: Boundary conditions and terminology used for conventional (a) and expandable (b) seal assembly model

Following are definitions of important variables frequently used in this chapter:

- **Compression Ratio (CR, %)**: This term is relevant only for conventional seal assembly. It is defined as an axial compression (displacement in **Figure 6.1a**) of seal relative to length of the seal. For example, 0.25 inch of displacement relative to 2.5-inch seal length indicates CR of 10%.
- **Radial clearance (R_c, inch)**: This term is only applicable to conventional seal assembly. It is defined as initial annular space between seal and casing before energization (**Figure 6.1a**).

- **Expansion Ratio (ER, %):** This term is relevant for expandable seal assembly. It is the amount of radial compression of seal (or amount of displacement of liner) relative to initial radial width of the seal (**Figure 6.1b**). For example, 0.1-inch displacement of liner relative to 0.6875-inch seal width indicates ER of 14%. Typically, expandable tubular can have ER up to 20% to 30%.
- **Containment (C, psi/in):** This term is only applicable to expandable seal assembly. It is defined as the amount of pressure needed for a unit deflection of axial boundaries of seal (**Figure 6.1b**). For example, containment of 5000 psi/in indicate that during seal energization if 1000 psi stress is generated at the axial boundary of seal, then the boundary would deflect by 0.2 in. Higher containment represents better seal containment in axial direction. This will consequently generate higher seal compression against host casing.
- **Energization coefficient (E_c, psi):** This term is applicable to both conventional and expandable type assemblies. It is defined as contact pressure generated per unit CR (or ER in case of expandable assembly). It is the slope of contact pressure vs CR or ER curve once contact between seal and casing has been establish.

6.2 Equipment and Energization

In this section, differences in various configurations of conventional and expandable type seal assemblies are compared. Specifically, contact pressure profile generated at seal-casing interfaces have been examined for various magnitude of energization (CR vs ER). Relevant variables and the range of values investigated are listed in **Table 6.1**.

.

Table 6.1: Simulation cases for studying effect of equipment design and seal energization method

Variable	Values	
	Conventional assembly	**Expandable assembly**
Elastomer	FKM	FKM
Seal radial width	0.6875 in	0.6875 in
Seal axial length	2.5 in	2.5 in
Radial clearance (R_c,in)	0, 0.025, and 0.1 in	-
Compression ratio (CR)	0 to 20%	-
Containment (C)	-	0, 5, and 10 ksi/in
Expansion ratio (ER)	-	0 to 20%
Temperature	212°F	212°F
Chemical exposure	-	-

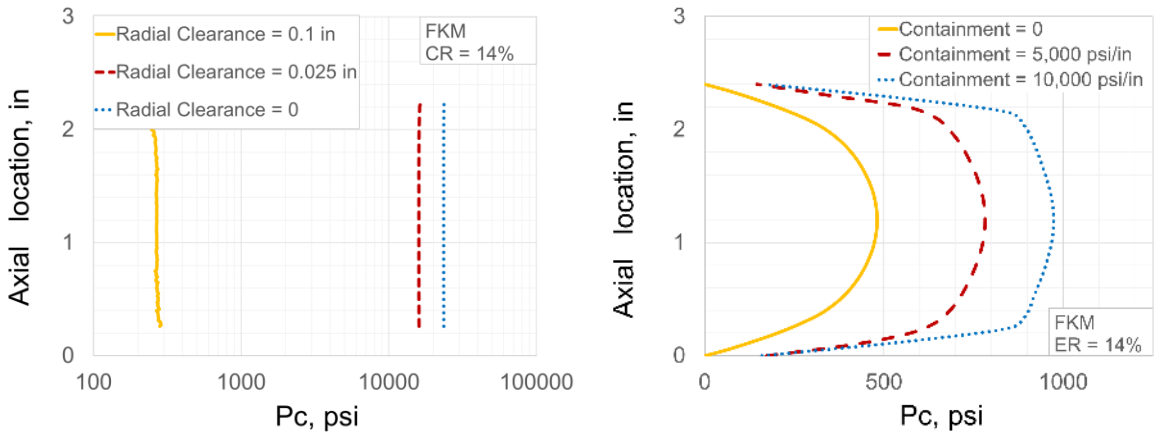

(a) **(b)**

Figure 6.2: Shape of contact pressure profile in (a) conventional and (b) expandable seal assembly

Distribution of contact pressure profile generated due to seal energization in both types of assemblies is shown in **Figure 6.2**. Both assemblies have distinct shape of contact pressure profile. In conventional assembly (**Figure 6.2a**), contact pressure remains practically constant along the seal-casing interface regardless of radial clearance. This flat shape can be attributed to two factors – (i) frictionless assumption of seal and casing surfaces, and (ii) energization method of compressing seal axially while constraining it on either side by compression plates. In case of expandable assembly, the profile is elliptical with a peak in the middle of the contact length (**Figure 6.2b**). The shape here depends on quality of seal containment. Increasingly stiffer containment spikes (0 to 10,000 psi/in) yield flatter contact pressure profiles. Elliptical shape can be attributed to the fact that the seal is not completely restrained in axial direction as in the case of conventional assembly.

If seal-casing interface is considered as a frictional contact then the shape of contact pressure profiles notably changes (**Figure 6.3)**. The profile in conventional assembly is no longer flat. It peaks near compression side and drastically reduces towards supporting plate. This indicates that because of friction, axial compression load is not effectively transferred along the length of the seal. It can be extrapolated that longer seal further magnifies the impact of friction. Higher CR also increases the deviation in profile due to friction (**Figure 6.3a)**. This dip in contact pressure near support side could increase the risk of fluid penetration (further discussed in **Chapter 9**). Unlike conventional assembly, expandable assembly retains the general shape of contact profile. With increase in friction coefficient, the peak contact pressure increases, and the profile becomes narrower at the middle (**Figure 6.3b)**.

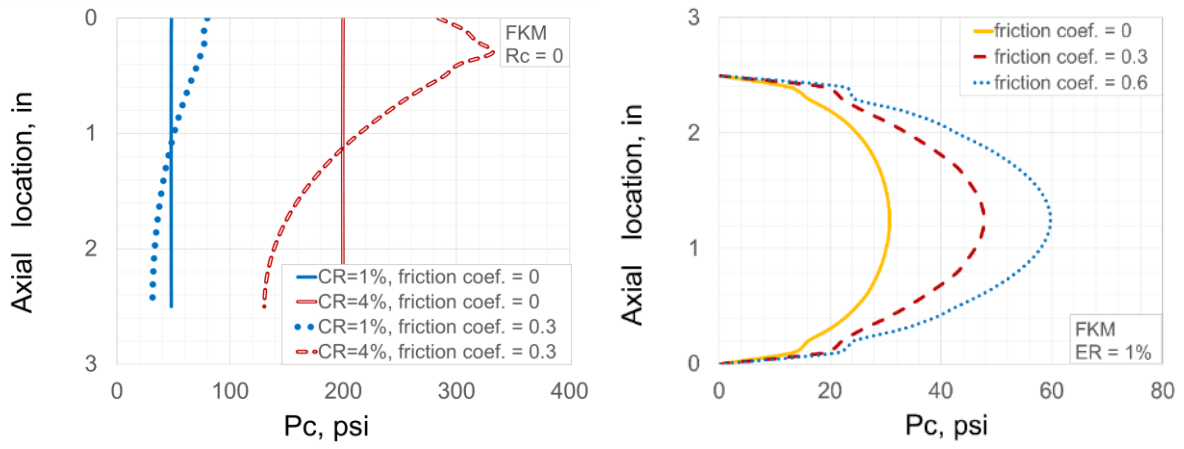

(a) **(b)**

Figure 6.3: Change in contact pressure profile due to friction in (a) conventional and (b) expandable seal assembly

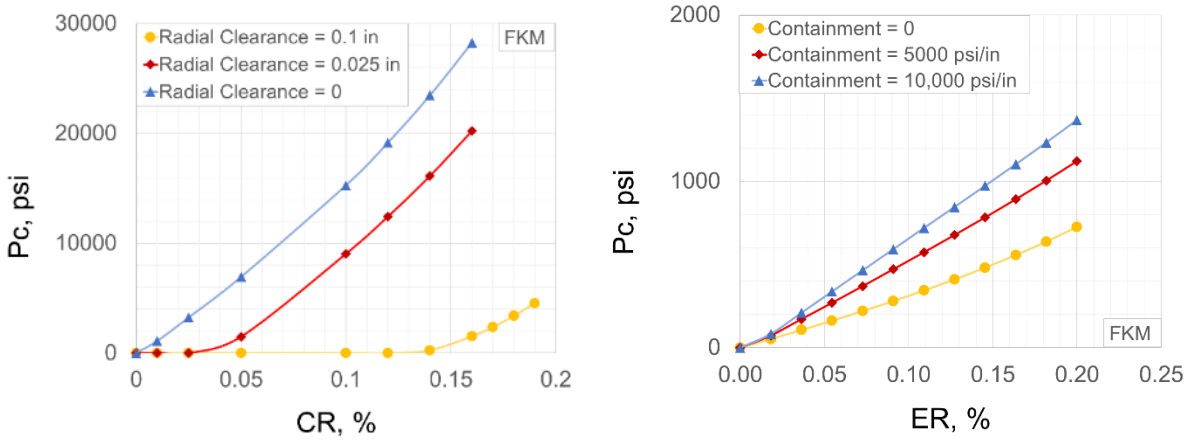

(a) **(b)**

Figure 6.4: Seal energization curves in (a) conventional and (b) expandable assembly

Next, effect of energization magnitude on the contact pressure was assessed. The energization curves in conventional and expandable assemblies are compared in **Figure 6.4**. Contact pressure shown in Y axis is the peak contact pressure measured at the middle of contact length. In both types of assembly, the relationship between peak contact pressure and energization magnitude (CR or ER) is practically linear. Contact pressure increases with increase in seal compression. In case of conventional assembly, the onset of contact pressure depends on the radial

clearance (R_c) of the assembly. For example, assembly design with clearance of 0.025 in (or 4% relative to seal width) and 0.1 in (or 14% relative to seal width) require approximately 4% and 14% compression ratio to first establish the contact with casing (**Figure 6.4a)**. Thereafter, the energization curve is a straight line. In case of expandable assembly, since there is no radial clearance, the energization curves build up from the beginning (**Figure 6.4b)**. Regardless of containment magnitude, energization curves can be considered linear in practical application range of 0 to 20% ER. It is clear that these assemblies differentiate from each other in terms of the slop of energization curves i.e. energization coefficient.

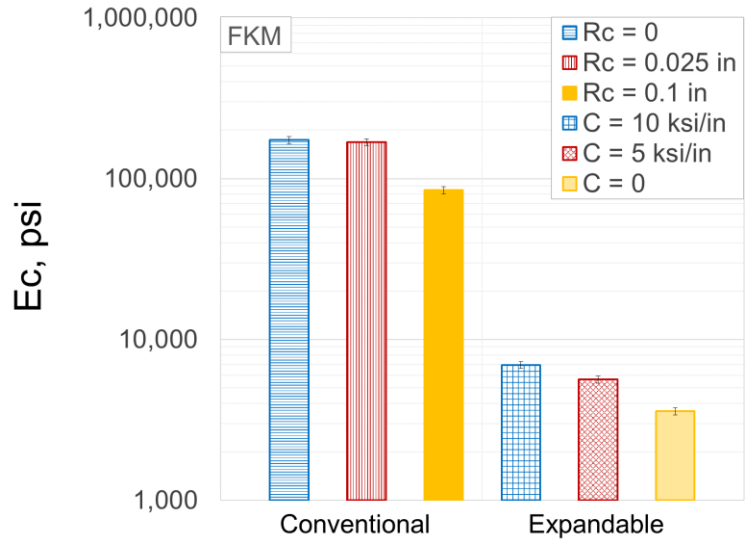

Figure 6.5: Effect of assembly design on energization coefficient

Difference in energization coefficient of different assembly designs is summarized in **Figure 6.5**. It is clear that regardless of specific configuration, conventional type assembly is likely to exhibit significantly higher energization coefficient than expandable type assembly. Improving quality of seal containment by reducing radial clearance (in conventional) or increasing stiffness of containment spikes (in expandable) can improve energization coefficient of the assembly.

Higher energization coefficient would generate higher contact pressure at a given seal compression and consequently provide better sealability. If seal-casing interface has high friction coefficient, then conventional assembly may not provide robust contact pressure distribution despite higher contact pressure values as shown in **Figure 6.3a**.

6.3 Seal Dimensions

In this section, effects of seal dimensions in various configurations of conventional and expandable assemblies are discussed. Specifically, contact pressure and energization coefficients have been evaluated at different seal lengths and widths. Relevant variables and the range of values investigated are listed in **Table 6.2.**

Table 6.2: Simulation cases for studying effect of seal dimensions

Variable	Values	
	Conventional assembly	**Expandable assembly**
Elastomer	FKM	FKM
Seal radial width, in	0.25, 0.68, and 1 in	0.25, 0.68, and 1 in
Seal axial length, in	1.25, 2.5, and 5 in	2.5, 5, and 10 in
Radial clearance (R_c,in)	0, 0.025, and 0.1 in	-
Compression ratio (CR, %)	0 to 20%	-
Containment (C, psi/in)	-	0, 5, and 10 ksi/in
Expansion ratio (ER, %)	-	0 to 20%
Temperature, °F	212°F	212°F
Chemical exposure	-	-

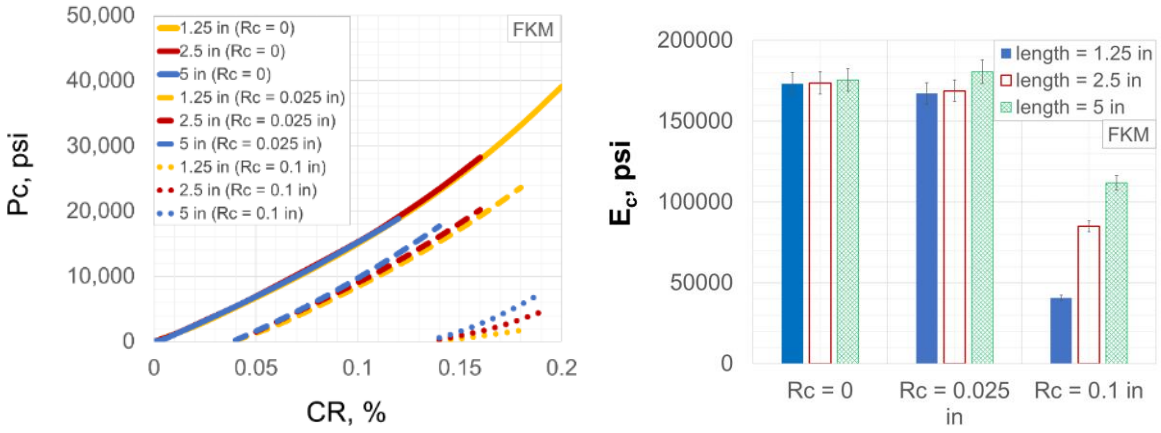

(a) **(b)**

Figure 6.6: Effect of seal length on (a) seal energization curve (a) and energization coefficient (b) in conventional assemblies

Energization curve and energization coefficient of conventional assemblies with different seal lengths are shown in **Figure 6.6**. The linear nature of energization curves is retained despite of changing seal lengths (**Figure 6.6a)**. Interestingly, the onset of seal energization has not been influenced by change in seal length. In other words, increasing the seal length does not provide early establishment of contact with casing. The slope of curves i.e. energization coefficient is certainly influenced by seal length. The influence is more pronounced in case of assembly with high radial clearance (R_c) of 0.1 in compared to 0.025 in and 0 in (**Figure 6.6b)**. At high R_c, increase in seal length results in higher energization coefficient and consequently better sealability. This can be attributed to the fact that longer seal can compensate seal extrusion through high radial clearance and hence, provide better seal containment. For complete volumetric constraint i.e. case of zero clearance, the influence of seal length can be considered significant as the variations are within FEA error margin (**Figure 6.6b)**.

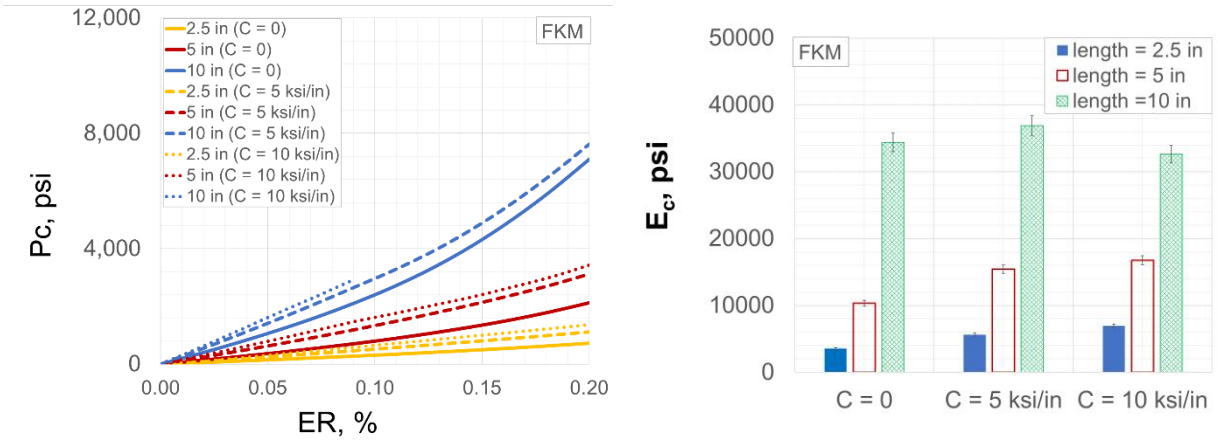

(a) **(b)**

Figure 6.7: Effect of seal length on seal energization curve (a) and energization coefficient (b) in expandable assemblies

Energization curve and energization coefficient of expandable assemblies with different seal lengths are shown in **Figure 6.7**. For the realistic range of ER up to 20%, energization curves are linear. Unlike conventional assembly, the influence of seal length is distinctly clear here. As shown in **Figure 6.7b**, higher seal length results in significantly higher energization coefficient and hence, better sealability. Similar to conventional assembly, the influence of length slightly diminishes for assembly with better containment. The influence remains significant, nonetheless.

Energization curve and energization coefficient of conventional assemblies with different seal widths are shown in **Figure 6.8.** As indicated in **Figure 6.8a,** unlike seal length, change in seal width changes the onset of seal energization. This is because radial clearance is changing relative to the seal width and consequently, different amount of volumetric fill is required to establish contact of seal with casing. The onset of energization curve occurs at CR equal to radial clearance as a percentage of seal width. For example, in case of radial clearance of 0.025 in, energization curve initiates at 2.5% CR, 4% CR, and 10% CR for seal width of 1 in, 0.6875 in, and 0.25 in respectively. This is because 0.025 in clearance is equal to 2.5%, 4%, and 10% of seal

widths of 1 in, 0.6875 in, and 0.25 in respectively. Expectedly, in case of zero radial clearance, the energization curves of different seal widths originate at the same point i.e. 0% CR.

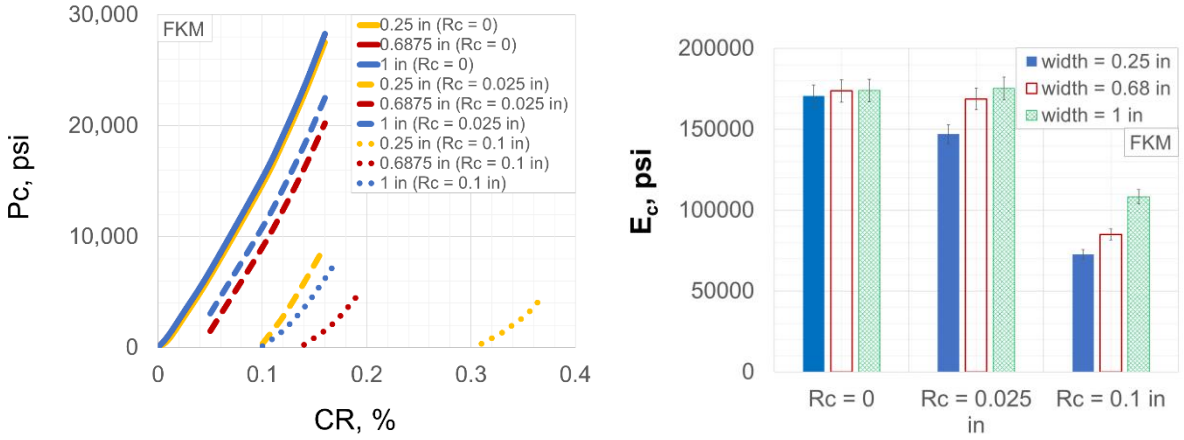

(a) **(b)**

Figure 6.8: Effect of seal width on seal energization curve (a) and energization coefficient (b) in conventional assemblies

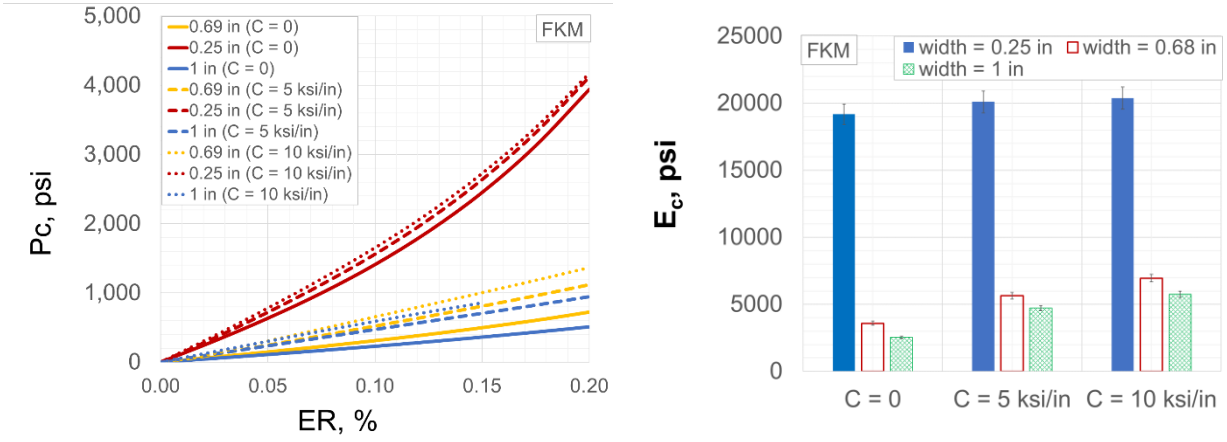

(a) **(b)**

Figure 6.9: Effect of seal width on seal energization curve (a) and energization coefficient (b) in expandable assemblies

Comparison of energization coefficient (**Figure 6.8b)** indicates similar trend as variation in seal lengths. For the same radial clearance, increase in seal width increases the energization coefficient and consequently improves sealability. The influence of seal width is more pronounced

in high radial clearance scenario of 0.1 in. For complete volumetric constraint i.e. in the case of zero clearance, the influence of seal width is not significant as the variation is within FEA error margin (**Figure 6.8b)**.

Energization curve and energization coefficient of expandable assemblies with different seal widths are shown in **Figure 6.9**. Energization curves retain their linearity in practical range of ER (up to 20%) despite changing seal width (**Figure 6.9a**). The slopes of energization curves have certainly changed. As presented in **Figure 6.9b**, for the same containment design, thinner seal element yields significantly higher energization coefficient. This means that at a given expansion of liner, a thin seal will provide higher contact pressure compared to a thick seal. This is because despite of same ER, the effective volumetric containment of seal is more effective in case of thin seal compared to a thick seal. To confirm this, an example simulation cases were run where perfect containment (i.e. no axial movement of seal), similar to conventional assembly with zero clearance, was applied. The effects of seal width were observed to be negligible.

6.4 Elastomer Material

In this study, different type of elastomer materials were input into various conventional and expandable seal assemblies to understand the influence of elastomer material properties. Total six different commonly used elastomer were studied – NBR, EPDM, FKM, FEPM, FFKM, and PTFE. As discussed in material properties measurement (**section 3.1**), these elastomers were categorized into two groups based on availability of various tests data. Fist group of elastomers (NBR, EPDM, FKM, and PTFE) were modelled as liner elastic material since their compressive stress-strain behavior was linear up to 20% strain (**section 3.1**). For second group of elastomers (FKM, FEPM, and FFKM, uniaxial, biaxial, and shear test data was available and hyperelastic characterization

was possible. They were modelled as Ogden 3rd order hyperelastic material. In addition to changing elastomer material type, a sensitivity analysis was performed on elastomer bulk modulus and shear modulus. Purpose of this analysis was to understand which parameter is more important for designing/selecting elastomer material appropriate for liner hanger applications. List of variables and range of values investigated are listed in **Table 6.3**.

Table 6.3: Simulation cases for studying effect of elastomer material

Variable	Values	
	Conventional assembly	**Expandable assembly**
Elastomer (Linear elastic)	NBR, EPDM, FKM, and PTFE	NBR, EPDM, FKM, and PTFE
Elastomer (Hyperelastic)	FKM, FEPM, and FFKM	FKM, FEPM, and FFKM
Elastomer (Bulk modulus)	174, 342, and 406 ksi	174, 342, and 406 ksi
Elastomer (Shear modulus)	174, 287, and 328 psi	174, 287, and 328 psi
Seal radial width, inch	0.6875 in	0.6875 in
Seal axial length, inch	2.5 in	2.5 in
Radial clearance (R_c,in)	0, 0.025, and 0.1 in	-
Compression ratio (CR, %)	0 to 20%	-
Containment (C, psi/in)	-	0, 5, and 10 ksi/in
Expansion ratio (ER, %)	-	0 to 20%
Temperature, °F	212	212
Chemical exposure	-	-

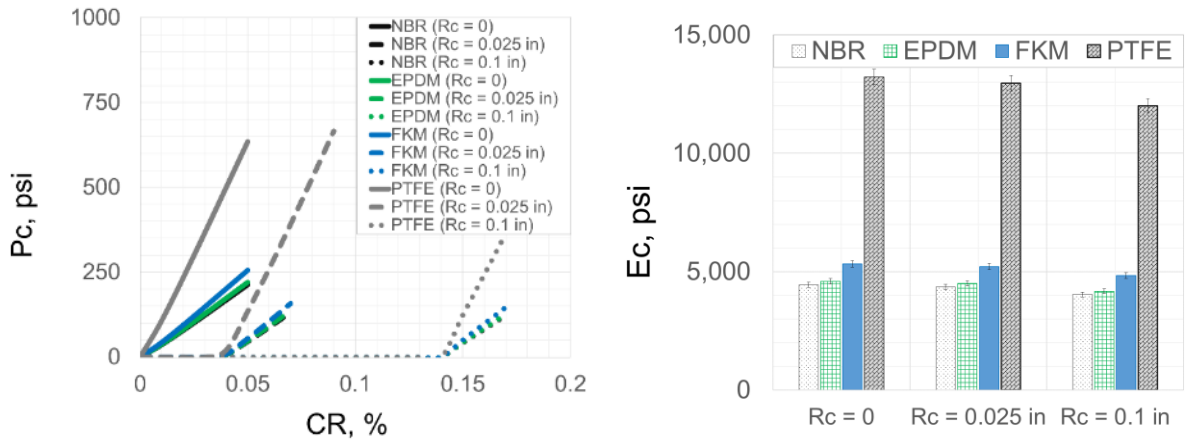

(a) **(b)**

Figure 6.10: Seal energization curves (a) and energization coefficient (b) for NBR, EPDM, FKM, and PTFE elastomers in conventional assemblies

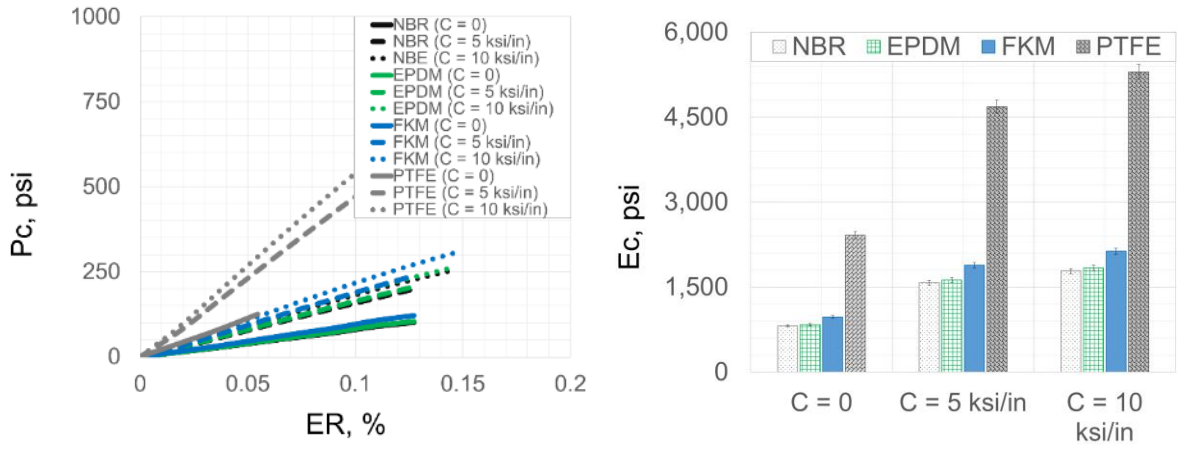

(a) **(b)**

Figure 6.11: Seal energization curves (a) and energization coefficient (b) for NBR, EPDM, FKM, and PTFE elastomers in expandable assemblies

Seal energization curves and energization coefficient for the first group of elastomers (NBR, EPDM, FKM, and PTFE) in conventional assembly is presented in **Figure 6.10**. The energization curves exhibit linear relationship with CR and the onset of curve depends on radial clearance. As demonstrated in **Figure 6.10b**, PTFE exhibits the highest energization coefficient indicating that it would provide highest contact pressure compared to other elastomer for the same assembly and energization conditions. NBE and EPDM do not have significantly different

performance. For expandable assembly, energization curves and coefficients of this group of elastomers (**Figure 6.11**) display similar trends as conventional assembly. The only difference is in magnitude of P_c and E_c.

Seal energization curves and energization coefficients for the second group of elastomers (FKM, FEPM, and FFKM) in conventional and expandable assemblies are presented in **Figure 6.12** and **Figure 6.13** respectively. Despite hyperelastic (Ogden 3rd order model) representation of these elastomers, the energization curves exhibit linear relationship with CR or ER. As expected, the onset of curves in conventional assembly is dependent on radial clearance. Comparing **Figure 6.12b** and **Figure 6.13b**, it can be concluded that FKM elastomer provides the highest contact pressure followed by FEPM and FFKM. The difference among these three elastomers decreases as seal containment during energization is improved (i.e. radial clearance is reduced in conventional assembly or containment stiffness improved in expandable assembly).

Compared to first group of elastomers (**Figure 6.10** and **Figure 6.11)**, these hyperelastic elastomer materials exhibit significantly higher contact pressure values. This is probably due to more realistic modelling of incompressibility in hyperelastic models. Elastomer material tend to exhibit nearly perfect incompressibility i.e. Poisson's ratio close to 0.5. However, the first group of elastomers were modelled using Poisson's ratio of 0.49. This can significantly impact contact pressure values as a portion of energization load gets wasted in compression of the seal component and volume change. Hyperelastic model used 3rd order Ogden characterization. The equivalent Poisson's ratio for all three elastomer sis close to 0.4995. Hence, hyperelastic material yields high contact pressure values. This can be further confirmed by the observation that when seal assembly had better volume containment (e.g. no radial clearance in conventional or 10 ksi/in containment in expandable), the difference in performance among these elastomers slightly reduces.

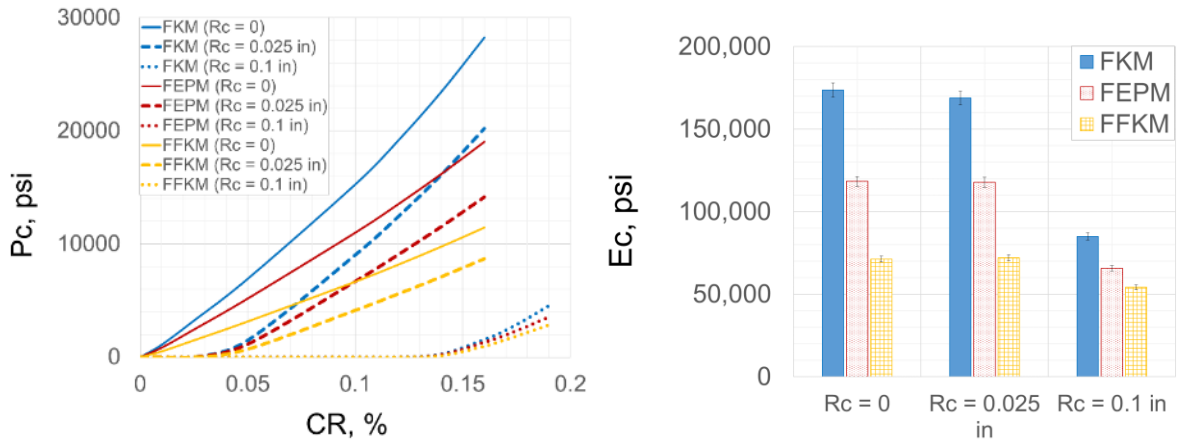

(a) **(b)**

Figure 6.12: Seal energization curves (a) and energization coefficient (b) for FKM, FEPM, and FFKM elastomers in conventional assemblies

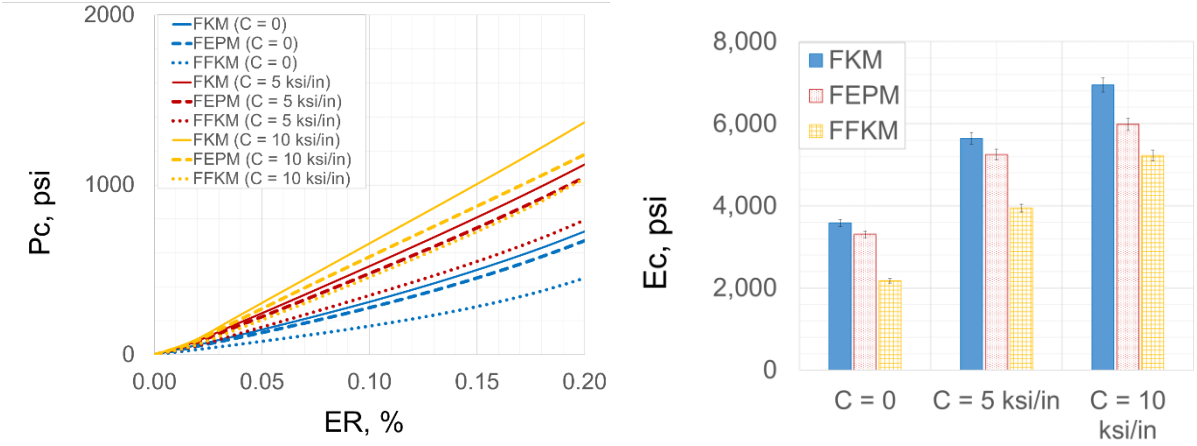

(a) **(b)**

Figure 6.13: Seal energization curves (a) and energization coefficients (b) for FKM, FEPM, and FFKM elastomers in expandable assemblies

The difference in performance of elastomers could be because of one or more of their specific properties such as bulk modulus, shear modulus, incompressibility, etc. Hence, to identify which material property is the dominant predictor of elastomer's performance, bulk modulus (K) and shear modulus (G) of elastomers were individually varied keeping the other parameter constant. Fixing these two parameters also fix elastic modulus and incompressibility or Poisson's

ratio of the elastomer. Hyperelastic FKM was considered as the base case, and its bulk modulus was varied from 174 ksi to 406 ksi keeping its shear modulus constant. Next, keeping its bulk modulus constant, shear modulus was varied from 174 psi to 328 psi. The equations for calculating K and G for hyperelastic Ogden 3rd order model is discussed in **section 2.1.2.2**.

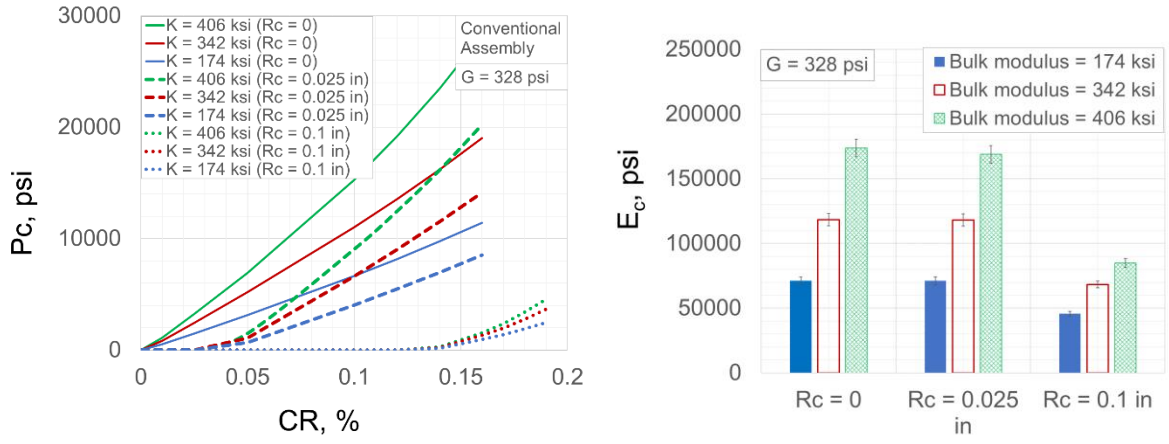

(a) **(b)**

Figure 6.14: Effect of elastomer bulk modulus on seal energization curve (a) and energization coefficient (b) in conventional assemblies

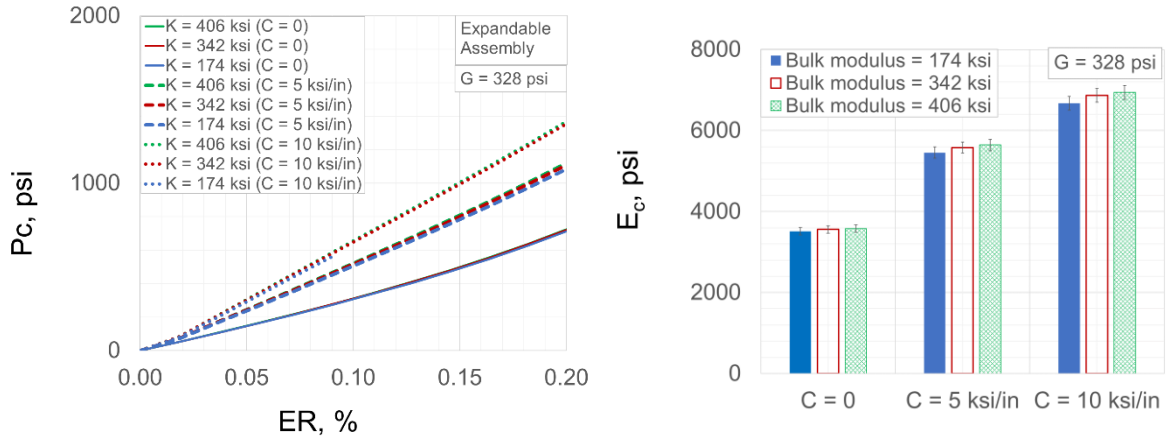

(a) **(b)**

Figure 6.15: Effect of elastomer bulk modulus on seal energization curve (a) and energization coefficient (b) in expandable assemblies

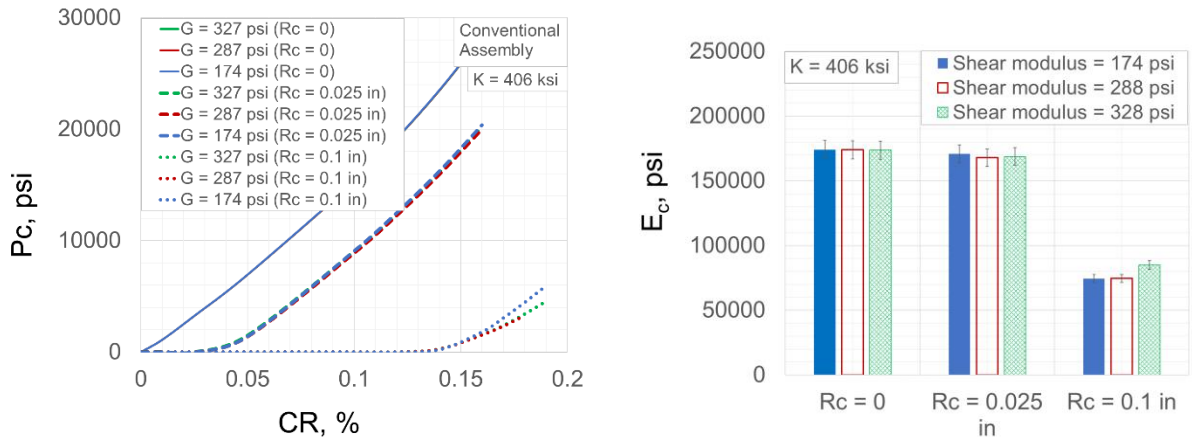

(a) **(b)**

Figure 6.16: Effect of elastomer shear modulus on seal energization curve (a) and energization coefficient (b) in conventional assemblies

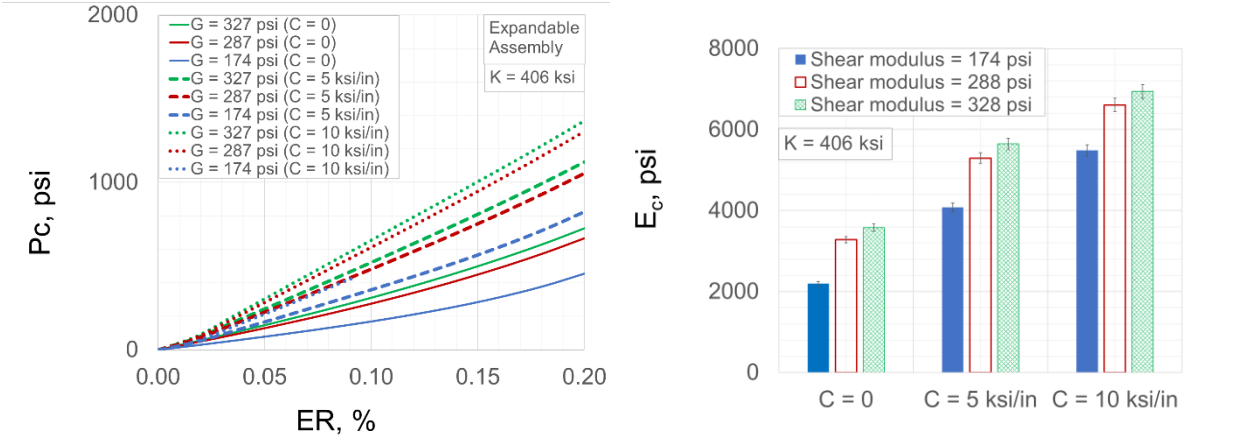

(a) **(b)**

Figure 6.17: Effect of elastomer shear modulus on seal energization curve (a) and energization coefficient (b) in expandable assemblies

Effect of bulk modulus on performance of conventional and expandable seal assemblies are presented in **Figure 6.14** and **Figure 6.15**. As shown in **Figure 6.14b**, increasing bulk modulus while keeping shear modulus constant, significantly increases energization coefficient of conventional assembly. However, for expandable assembly (**Figure 6.15b)**, the change in E_c caused by variation in bulk modulus is outside accuracy of FEA models, indicating that the

conclusion cannot be made. The energization curves of different bulk moduli (**Figure 6.15a)** also overlap with each other.

Effect of shear modulus of elastomer on performance of conventional and expandable seal assemblies are presented in **Figure 6.16** and **Figure 6.17**. Opposite to the influence of bulk modulus, influence of shear modulus is negligible in case of conventional seal assembly (**Figure 6.16b)**. But for expandable seal assembly, effect of changing shear modulus is notable. Importance of bulk modulus in conventional assembly can be attributed to a restrained seal housing where elastomer component undergoes volumetric compression except near the extrusion gap. On the other hand, in expandable assembly, despite of containment spikes, seal is not as restrained in axial direction as conventional assembly. Hence, shear behavior of elastomer become more important.

In summary, to achieve high contact pressure, the first group of elastomers can be ranked in decreasing order of preference as - PTFE > FKM > EPDM ≈ NBR. Similar ranking for second group of elastomers is – FKM > FEPM > FFKM. Considering that FKM is the common elastomer in both groups, if properties of these elastomers are scaled accordingly, then the elastomer material can be ranked as – PTFE > FKM > FEPM > FFKM > EPDM ≈ NBR. Bulk modulus of elastomer is critical for conventional type assembly while shear modulus is important for expandable seal assembly. Additionally, it was observed that hardness values do not always provide accurate indication of contact pressure or sealability. Although the ranking of fluoroelastomers in terms of energization coefficient was observed to be FKM > FEPM > FFKM, their ranking in terms of hardness values was FFKM > FEPM > FKM. This indicates that hardness measurements alone are not sufficient for elastomer selection or qualification. Deformation behavior is important to measure for accurate prediction of elastomer's equipment level performance.

6.5 Seal and Housing Geometry

Elastomer components in liner hanger seal assembly are typically rectangular with rounded edges as modelled in this work. Sometimes, they can also have tapered edges. Use of O-rings is almost not common in such high pressure seal equipment. However, O-rings type samples are frequently used in laboratory scale standard tests. The sealability test apparatus used in this work also utilized O-ring shaped elastomer samples. Hence, it is important to understand the difference between seal energization and contact pressure generated by rectangular vs O-ring type elastomer components.

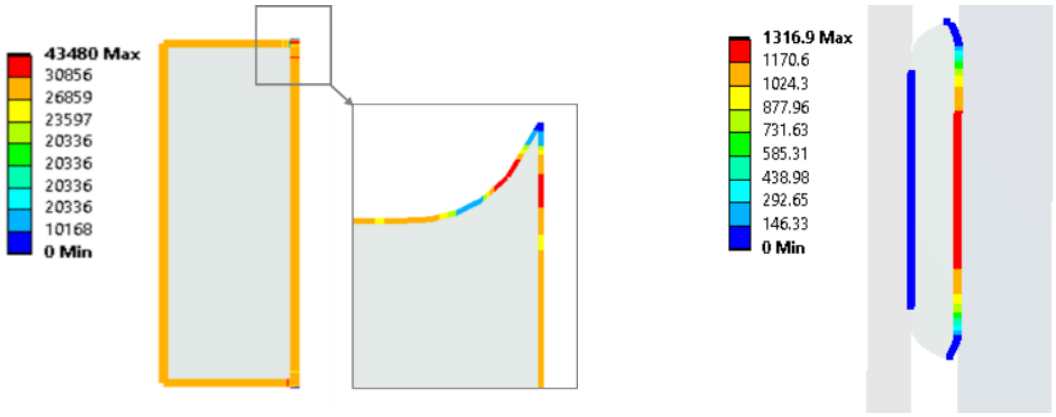

Figure 6.18: Contact pressure distribution along seal boundary in (a) conventional and (b) expandable liner hanger seal assemblies

Contact pressure distribution along rectangular seal components of conventional and expandable liner hanger seal assemblies are shown in **Figure 6.18.** The seal component has better overall fit within the conventional assembly and hence, seal energization generates uniform contact pressure along seal-casing, seal-compression plate, and seal-liner boundaries. Only near extrusion gap, the contact pressure varies and reduces to zero at the tip of extruded portion (**Figure 6.18a)**. Overall, conventional seal assembly has robust profile with low risk of fluid pressure penetration. In expandable assembly (**Figure 6.18b)**, contact pressure only exists at seal-casing interface. Seal-liner boundary is bonded interface and should theoretically be free from the risk of fluid

penetration. The seal component is not restrained in axial direction and free to deform. Hence, towards the axial ends of seal component, contact pressure decreases to zero and it can pose risk of fluid penetration.

For O-ring type seal component, as used in scaled laboratory tests, contact pressure profile along the seal geometry is presented in **Figure 6.19**. It should be noted that there are four contact interfaces with the seal – two with compression plates and one each with liner and casing. The X-axis in the figure, represents the location on seal in terms of degree angle 0°, 90°, 180°, 270°, and 360° which corresponds to seal-casing, seal-bottom plate, seal-liner, and seal-upper plate interfaces respectively. The Y-axis represents the corresponding contact pressure.

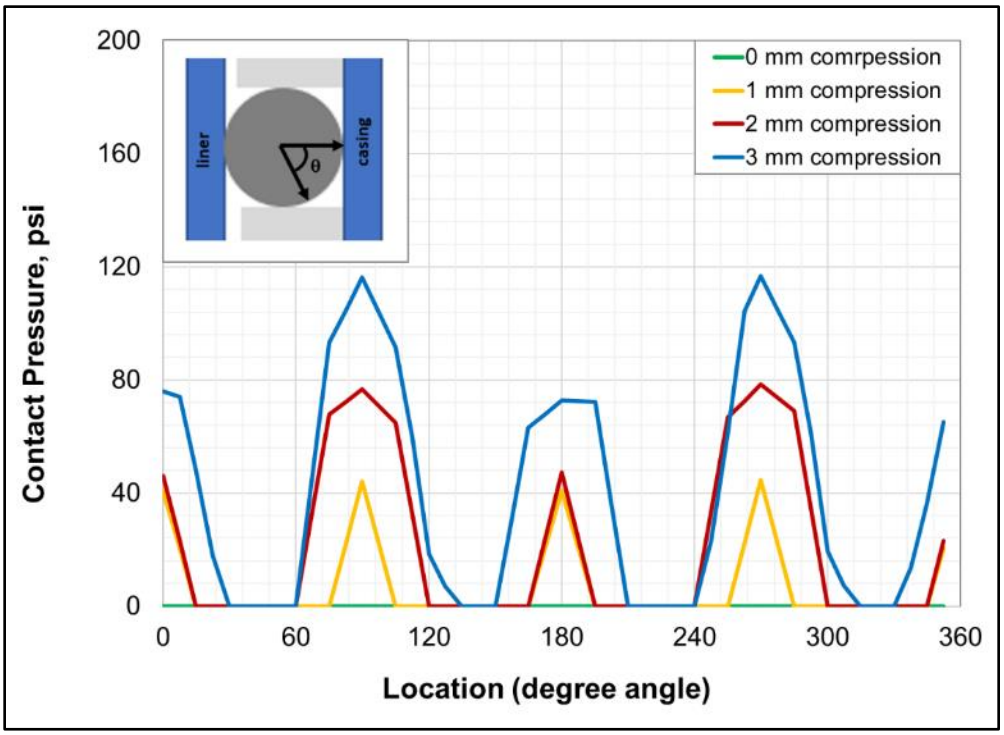

Figure 6.19: Contact pressure distribution along circular cross section for EPDM seal at various amount of compression

It is clear from the distribution that contact is not established along the entire seal boundary. Zero contact pressure locations can pose risk of fluid pressure penetration and compromise the sealability. Contact pressure at all points may only establish at extremely high compression which is not likely to be achieved because of risk of compression-set failure.

Based on the comparison among conventional, expandable, and O-ring seal assemblies, it can be concluded that conventional assembly has the most robust contact pressure distribution followed by expandable assembly. O-ring type seal component would theoretically pose the highest risk of fluid penetration.

As discussed in **section 6.2**, the rectangular seal component in both conventional and expandable assemblies generate linear energization curves i.e. peak contact pressure is linearly dependent on compression ratio. However, with the O-ring type seal assembly, the relationship may not be linear as shown in **Figure 6.20**. The energization curve for seal with perfect fit to housing appears to be linear (red points in **Figure 6.20**). However, at higher compression ratio, contact pressure appears to increase exponentially with increase in CR.

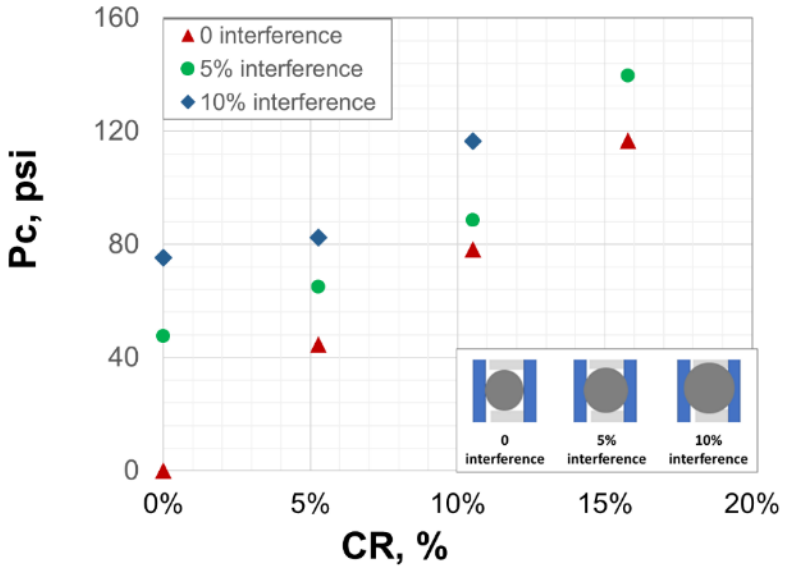

Figure 6.20: Effect of compression and interference on contact pressure in O-ring type seal assembly

Cross sectional diameter of molded EPDM elastomer O-rings used in setup II were identified to have diameter approximately 1 mm greater than the annulus gap. Hence, the effect of seal interference or seal annular fit on contact pressure was examined. The presence of interference leads to pre-stress condition and results in an intercept value at zero displacement. Inserting the seal into the setup led to a pre-stress condition and the system was observed to be gas tight when a 40 psi injection test was performed in the absence of an external displacement application via bolts. This is confirmed by the FEA model which predicts contact pressure of 48 psi for the EPDM seal with 1 mm interference and 0 mm displacement application (**Figure 6.20**).

Chapter 7: Failure Scenarios Results

7.1 Extrusion and Energization Failure

Extrusion of elastomer seal component is a common failure mode for seal assemblies. Extrusion can be caused by various factors such as over-energization of the seal during assembly installation, thermal expansion of seal, swelling of seal due to chemical absorption, softening of the seal due to temperature or chemical exposure, etc.

Table 7.1: Simulation cases for studying effect of extrusion/over-energization failure

Variable	Values	
	Conventional assembly	**Expandable assembly**
Elastomer	FKM, FEPM, and FFKM	FKM, FEPM, and FFKM
Seal radial width	0.6875 in	0.6875 in
Seal axial length	2.5 in	2.5 in
Radial clearance (R_c,in)	0, 0.025, and 0.1 in	-
Compression ratio (CR)	0 to 30%	-
Containment (C)	-	0, 5, and 10 ksi/in
Expansion ratio (ER)	-	0 to 60%
Temperature	212°F	212°F
Chemical exposure	-	-

In this study, extrusion of elastomer was studied by applying high energization condition to the model. Different simulation scenarios investigated are listed in **Table 7.1**. The failure of seal due to extrusion or over-energization was determined based on Tresca shear stress criteria. According to the criteria, when maximum shear stress at any location within seal component

exceeds the limiting strength of elastomer, the seal is considered as failed. The limiting Tresca stress of FKM, FEPM, and FFKM elastomers are listed in **Table 7.2**.

Table 7.2: Limiting Tresca shear stress of elastomers. Values obtained from Elhard et al. 2017

Elastomer	Critical Tresca Stress, psi
FKM	5457
FEPM	4443
FFKM	6773

FEA simulation results indicated that regardless of energization amount, for conventional assembly, the highest Tresca shear stress occurs near the extrusion gap and compression plate region as highlighted in **Figure 7.1a**. In case of expandable assembly, the concentration of Tresca shear stress occurs at the edges of seal-liner bond (**Figure 7.1b**).

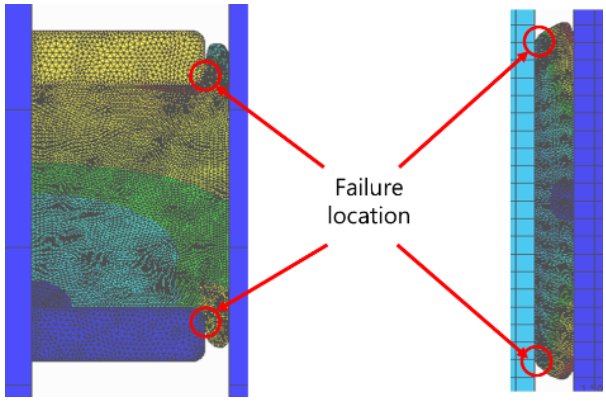

(a) **(b)**

Figure 7.1: Distribution of Tresca stress in conventional (a) and expandable assembly designs

Tresca stress at these high failure-risk locations were monitored for various seal energization as listed in **Table 7.1**. The seal was termed failed when the maximum Tresca stress in the failure prone region exceeded limiting strength of the elastomer listed in **Table 7.2**. Seal

energization as represented by CR or ER was increased until the failure point was reached. The limit of seal energization until extrusion failure occurs for various conventional and expandable assemblies is presented in **Figure 7.2** and **Figure 7.3**. It is difficult to provide a general recommendation regarding elastomer material selection based on the results. Appropriate selection of elastomer would depend on contact pressure requirement (P_{cmax}) and/or maximum energization load available (CR_{max} or ER_{max}).

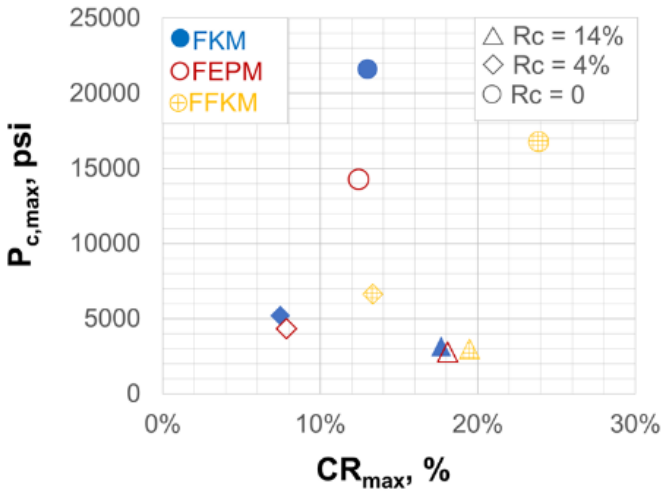

Figure 7.2: Limits of seal energization in conventional liner hanger seal assemblies

For conventional assembly, if achieving high contact pressure is the selection criteria, then FKM elastomer provides the highest amount of contact pressure before energization failure occurs. This is despite the fact that FFKM has highest limiting strength. If achieving high compression ratio or robustness to over-energization is the selection criteria then FFKM should be the preferred material, followed by FKM and FEPM which have practically similar energization limits. These observations are true for assembly with low clearance (R_c = 0). For assembly with high radial clearances, the differences in performance of these three elastomers diminish. For the highest radial clearance (Rc = 14%), all three elastomers have practically similar energization limits and any one of them could be selected.

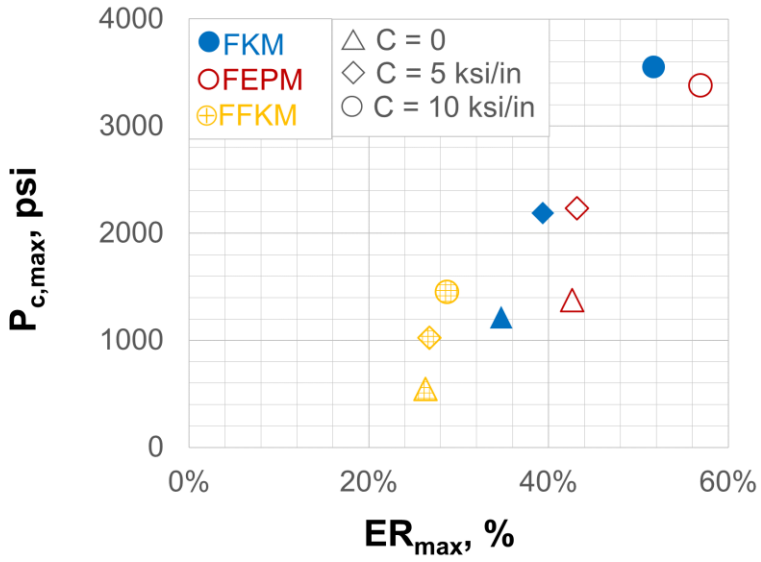

Figure 7.3: Limits of seal energization in expandable liner hanger seal assemblies

For expandable assembly, as shown in **Figure 7.3**, if robustness to high expansion ratio is the selection criteria, then FEPM provides the highest amount of ER before extrusion failure occurs. FFKM fails at low expansion ratios. This is despite the fact that FFKM has the highest limiting strength. This discrepancy is likely due to different shear deformation behavior of the elastomer materials. If achieving highest contact pressure is the selection criteria then the elastomer material can be ranked as FKM ≈ FEPM > FFKM. Above observations are true regardless of seal containment quality.

7.2 Chemical Exposure

Exposure to downhole chemicals is expected to be one of the most detrimental factors causing failure of seal assemblies. Using the aging tests data and material properties measurements discussed in **section 3.2**, simulations were run to understand degradation in performance of seal assemblies after exposure to various chemical conditions. The conditions and simulation scenarios investigated are listed in **Table 7.4**. The temperature, exposure period, and gaseous conditions studied were prescribed by the regulatory agency BSEE (project# E17PC00005). Degradation in

seal's performance has been discussed in terms of change in energization coefficient. For both conventional and expandable assemblies, similar percentage reduction in E_c were observed and hence, following results are independent of assembly design.

Table 7.3: Simulation cases for studying effect of downhole chemical conditions

Variable	Values	
	Conventional assembly	**Expandable assembly**
Elastomer	NBR, EPDM, FKM, and PTFE	NBR, EPDM, FKM, and PTFE
Seal radial width	0.6875 in	0.6875 in
Seal axial length	2.5 in	2.5 in
Radial clearance (R_c,in)	0, 0.025, and 0.1 in	-
Compression ratio (CR)	0 to 20%	-
Containment (C)	-	0, 5, and 10 ksi/in
Expansion ratio (ER)	-	0 to 20%
Temperature	120°F and 180°F	120°F and 180°F
Chemical exposure	1 day and 7 days CH_4, CO_2, H_2S, and their mixture	1 day and 7 days CH_4, CO_2, H_2S, and their mixture

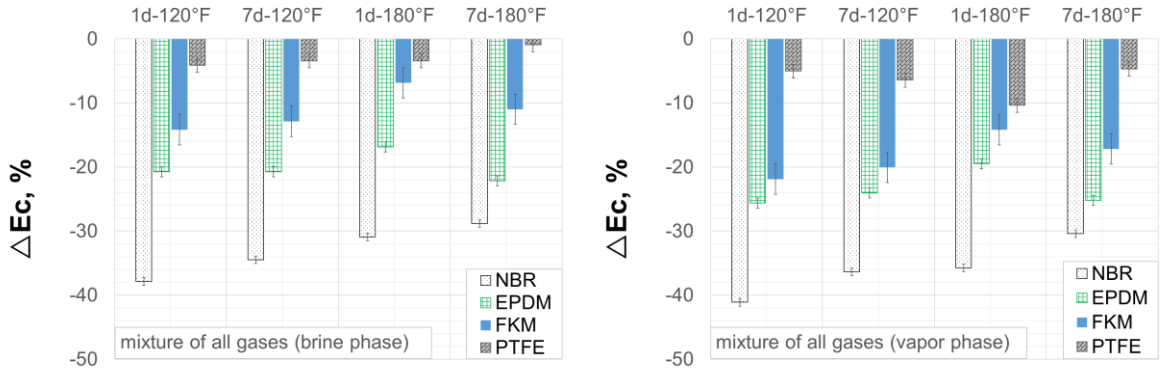

(a) **(b)**

Figure 7.4: Change in energization coefficient of conventional and expandable seal assemblies after exposure to mixture of CO_2, CH_4, and H_2S with brine (a) and without brine (b)

Figure 7.4 prsents the effect of mixture of gases (50% CH_4 with 500 ppm H_2S + 50% CO_2) with and without presence of brine on energization coefficient of seal assemblies. Elastomer materials were exposed to the gases for two different exposure period (1 and 7 days) at two different temperatures (120°F and 180°F). The results indicate that regardless of the aging condition, in general, NBR elastomer had the highest deterioration in performance followed by EPDM, and FKM. The highest chemical resistance was exhibited by PTFE. Degradation in assembly level performance of the seal ranged from about 40% in case of NBR to as low as 3% in case of PTFE. No clear trend can be established regarding the influence of exposure duration and temperature. Interestingly, elastomers submerged in brine seemed to exhibit slightly less degradation than samples exposed to just gas (**Figure 7.4a vs Figure 7.4b)**.

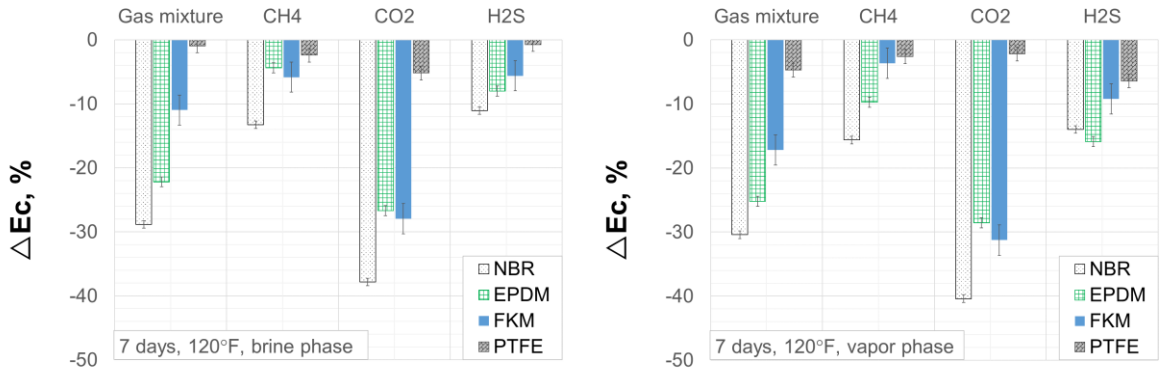

(a) **(b)**

Figure 7.5: Change in energization coefficient of conventional and expandable seal assemblies after individual exposure to CO_2, CH_4, and H_2S with brine (a) and without brine (b)

Figure 7.5 presents comparisons among individual gases and mixture. It is clear that CO_2 exerts the highest amount of degradation in seal's performance followed by mixture of gases. Next is H_2S, and the least effect was observed in case of CH_4. However, it should be noted that the concentrations of each gas was not equal and hence, it is difficult to comment on rank the gases in

terms of impact on elastomer. Change in energization coefficients due to various downhole conditions are summarized in the **Table 7.4**.

Table 7.4: Average percentage reduction in energization coefficient of conventional and expandable seal assemblies after exposure to various downhole conditions. Reference for degradation is room condition.

Elastomer Type	All gases								CH_4		CO_2		H_2S	
	1 day, 120°F		7 days, 120°F		1 day, 180°F		7 days, 180°F		7 days, 120°F		7 days, 120°F		7 days, 120°F	
	V	B	V	B	V	B	V	B	V	B	V	B	V	B
NBR	-41%	-38%	-36%	-35%	-36%	-31%	-30%	-29%	-16%	-13%	-40%	-38%	-14%	-11%
EPDM	-26%	-21%	-24%	-21%	-19%	-17%	-25%	-22%	-10%	-4%	-29%	-27%	-16%	-8%
FKM	-22%	-14%	-20%	-13%	-14%	-7%	-17%	-11%	-4%	-6%	-31%	-28%	-9%	-6%
PTFE	-5%	-4%	-6%	-3%	-10%	-3%	-5%	-1%	-3%	-2%	-2%	-5%	-6%	-1%

V denotes vapor phase i.e. sample was not immersed in brine
B denotes that sample was immersed in brine

Difference in the degradations can be attributed to various physico-chemical conditions. In presence of brine, CO_2 and H_2S can create acids and react chemically with elastomers. H_2S can dissociate into H^+ and HS^- ions. H+ causes hydrolysis of the C≡N group in NBR while HS- attacks C=O. This results in C=S and C-C=S groups. In homolysis, mercapto radicals from H2S (H• and HS•) causes reaction with elastomer polymer and results in macromolecule radical. This radical then reacts with another mercapto radical. This chain reaction continues, dissociates triple and double bonds, and eventually results in saturated C-S-C bonds. These processes notably alters physical properties of elastomer.

CO_2 can form carbonic acid in presence of brine. In large quantities, this weak acid can become corrosive and cause chemical reactions with elastomers. This irreversible reaction is caused by dissociation of weak C≡N bond in NBR and results in amine groups. The C=C double bond in EPDM exhibits relatively higher resistance to dissociation. The C-F bond in Fluorocarbon

elastomer is highly stable bond with very high dissociation energy and hence, FKM exhibits more resistance to CO_2 degradation.

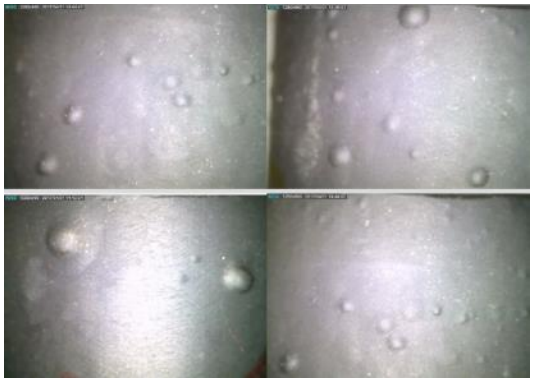

Figure 7.6: Blistering on FKM elastomer sample after aging tests (Salehi et al. 2019)

Effect of H_2S and CO_2 on elastomer samples not submerged in brine can be attributed to predominantly physical interaction in form of molecular invasion. Influence of CH_4 can also be attributed to physical interaction rather than chemical reaction. All elastomer samples, regardless of whether they are submerged in brine or not, exhibited volumetric swelling as well. The swelling was higher in case of vapor phase compared to brine phase (Salehi et al. 2019). Moreover, some samples (including FKM) also demonstrated blistering on the surface. These two factors could further influence the equipment level performance of the seal.

Table 7.5: Average percentage reduction in elastomer hardness after exposure to various gases at 7 days, 120°F. Reference for degradation is room conditions.

Elastomer Type	Gas Mixture		CH_4		CO_2		H_2S	
	vapor	brine	vapor	brine	vapor	brine	vapor	brine
NBR	-11.4%	-7.0%	-1.4%	-2.3%	-13.7%	-14.1%	-3.2%	-2.9%
EPDM	-9.4%	-7.4%	-5.4%	-4.9%	-12.0%	-8.9%	-4.6%	-4.1%
FKM	-7.0%	-5.0%	-3.5%	-4.2%	-14.6%	-11.3%	-4.0%	-3.7%
PTFE	-3.9%	-2.4%	-1.4%	-0.6%	-2.8%	-2.9%	-0.4%	-1.0%

The hardness changes in elastomers due to these aging tests are listed in **Table 7.5**. It can be observed that degradations trend in elastomer hardness do not correlate with degradation trends in assembly level performance of seal discussed in this section. For example, degradation of 10% in hardness does not necessarily indicate 10% reduction in energization coefficient of seal assembly. This observation shows that hardness measurements alone may not provide accurate indication of elastomer performance degradation in downhole environment. Measurements of elastic moduli or deformation characteristics of elastomers need to be performed for reliable estimation of loss of sealability.

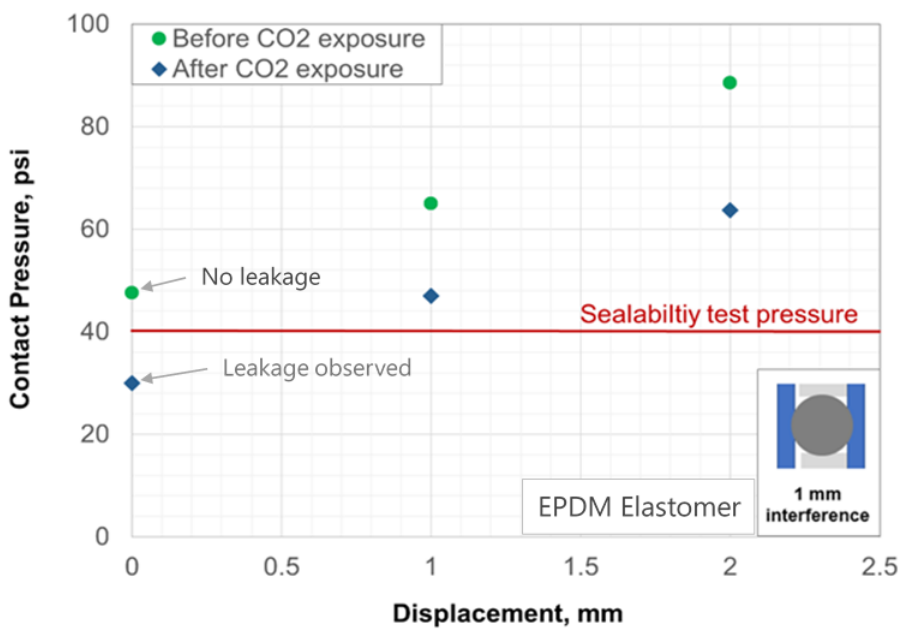

Figure 7.7: Contact pressure as a function of compression as simulated by finite element model

Reliability of the FEA model in predicting aging effect was verified by sealability test apparatus. As discussed in section **4.5.2** and reiterated in **Figure 7.7,** aging test and FEA predictions matched with the experimental sealability tests. With un-aged EPDM O-ring the

system was observed to be gas tight when a 40 psig pressure injection test was performed. This is confirmed by the FEA model which predicts contact pressure of 48 psi for the EPDM seal with same energization condition as experimental test (1 mm interference and 0 mm displacement). However, after exposure to CO_2, as per the FEA model, EPDM seal generated 30 psi contact pressure. This is in line with the experimental observation where leak was observed at 40 psi injection pressure.

7.3 Thermal Degradation

In previous discussion, the effect of temperature could not be isolated because of the presence of gases and 100 psi pressure. In this discussion, effects of temperature on performance of both conventional and expandable liner hanger seal assemblies are presented. The material properties used are discussed in experimental setup (section **3.1**). As listed in the simulation matrix (**Table 7.6**), performance of FKM, FEPM, and FFKM elastomers were compared at 212°F and 350°F. Additionally a third scenario where elastomer transitions from 212°F to 350°F was also examined. The transition would result in thermal expansion of elastomer in addition to changes in material deformation behavior. This scenario is represented as 350°F with thermal expansion.

Tresca failure criteria was employed to evaluate energization limit and failure of seal assemblies. Critical Tresca stress or limiting strength of FKM, FEPM, and FFKM elastomers are listed in **Table 7.7**. As shown in the table, increasing temperature from 212°F to 350°F causes 35%, 48%, and 54% reduction in limiting strengths of FKM, FEPM, and FFKM respectively.

Table 7.6: Simulation cases for studying effect of downhole temperature

Variable	Values	
	Conventional assembly	**Expandable assembly**
Elastomer	FKM, FEPM, and FFKM	FKM, FEPM, and FFKM
Seal radial width	0.6875 in	0.6875 in
Seal axial length	2.5 in	2.5 in
Radial clearance (R_c,in)	0, 0.025, and 0.1 in	-
Compression ratio (CR)	0 to 20%	-
Containment (C)	-	0, and 10 ksi/in
Expansion ratio (ER)	-	0 to 20%
Temperature Scenarios	212°F, 350°F, and 212°F to 350°F transition (with thermal expansion)	212°F, 350°F, and 212°F to 350°F transition (with thermal expansion)
Chemical exposure	-	-

Table 7.7: Limiting Tresca stress and thermal expansion coefficients of elastomer material. Values obtained from Elhard et al. (2017).

Elastomer	Critical Tresca Stress, psi			Thermal expansion coefficient (1/°F)
	212°F	350°F	% change	
FKM	5457	3582	35%	1.29×10^{-4}
FEPM	4443	2351	48%	1.36×10^{-4}
FFKM	6773	3175	54%	2.39×10^{-4}

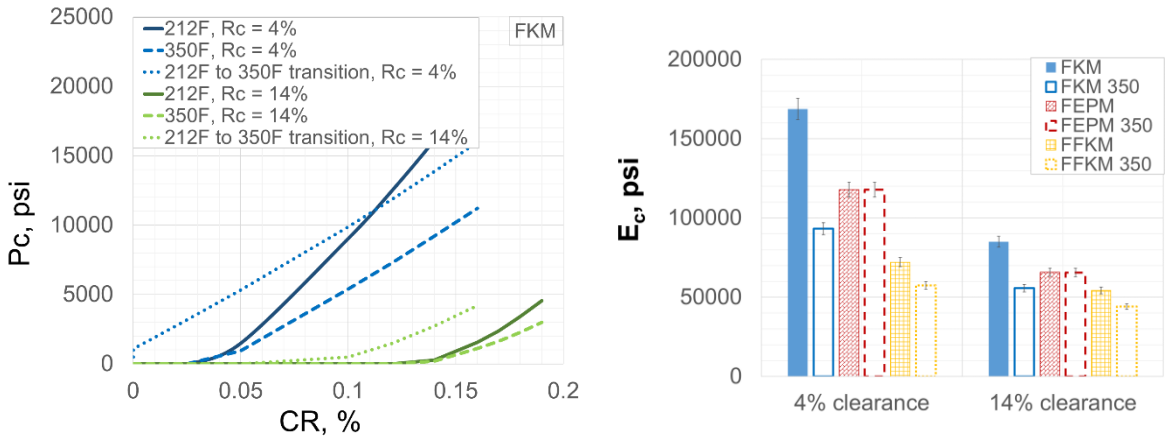

(a) **(b)**

Figure 7.8: Effect of temperature on seal energization curve of FKM (a) and comparison of energization coefficients of FKM, FEPM, and FFKM (b) in conventional assemblies

Energization curves for the three elastomer samples in conventional seal assemblies at three thermal scenarios are presented in **Figure 7.8**. It is clear from **Figure 7.8a** that energization curve maintains linearity regardless of thermal conditions. For a specific assembly design, at high service temperature of 350°F, slope of the energization curve (i.e. energization coefficient) is lesser compared to low operating temperature of 212°F (compare solid lines with dashed lines in **Figure 7.8a**). However, the onset of seal energization remains the same. The reduction in energization coefficient is significant for FKM elastomer compared to FFKM while FEPM elastomer remains practically unaffected by the temperature hike. Rank of elastomers in terms of contact pressure changes from FKM > FEPM > FFKM at 212°F operating temperature to FEPM > FKM > FFKM at 350°F operating temperature. If elastomer temperature changes from 212°F to 350°F during service then thermal expansion of seal component also needs to be considered. As shown in **Figure 7.8a** (dotted curves), thermal expansion shifts the energization curve up with a positive intercept on y axis. This means that because of thermal expansion of elastomer, contact pressure would be generated even in absence of external energization load. The slope of this new energization curve remains same as the curve for 350°F which means energization coefficient is not affected.

Effect of temperature on expandable seal assembly is presented in **Figure 7.9**. Similar to conventional assembly, the only difference between energization curve at 212°F and 350°F is slope i.e. energization coefficient. Unlike conventional assembly, here, FKM retains highest energization coefficient even at 350°F. The thermal degradation in energization coefficient for FEPM and FFKM is within error margins of FEA prediction while for FKM degradation is notable but significantly less compared to conventional assembly. In the third scenario of temperature transition, the energization curve shifts up to reflect volumetric swelling of elastomer component. The energization coefficient however remains unaffected.

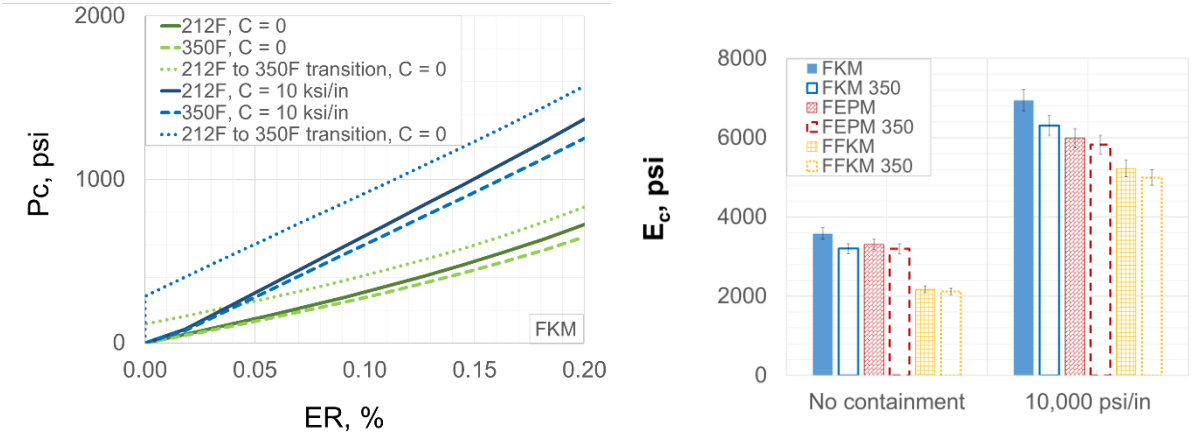

(a) **(b)**

Figure 7.9: Effect of temperature on seal energization curve of FKM (a) and comparison of energization coefficients of FKM, FEPM, and FFKM (b) in expandable assemblies

It is important to consider degradation in limiting strength of elastomer and corresponding energization limits while evaluating effects of temperature. Comparison of energization coefficients alone may not provide the true performance capabilities of the elastomer seal assemblies. **Figure 7.10** presents energization limits of elastomers in conventional liner hanger assemblies at studied temperature conditions. An important observation is that at 350°F, the maximum CR permissible and corresponding maximum P_c are lesser compared to 212°F. For

example, in assembly with Rc = 4%, at 212°F, FFKM elastomer has energization limit of 13% CR and corresponding P_c of 6600 psi. However, at 350°F, the limits reduce to 10% CR and 3400 psi. That is about 3% reduction in CR and 46% reduction in maximum achievable contact pressure. For temperature transition scenario of 212°F to 350°F, the limits further reduce to 8.5% CR and 1600 psi. It is difficult to provide general ranking for elastomer material based on robustness to thermal degradation. The selection of appropriate elastomer would depend on assembly design, service temperature, likelihood of temperature changes during service, desired contact pressure values, and operational constraints on energization.

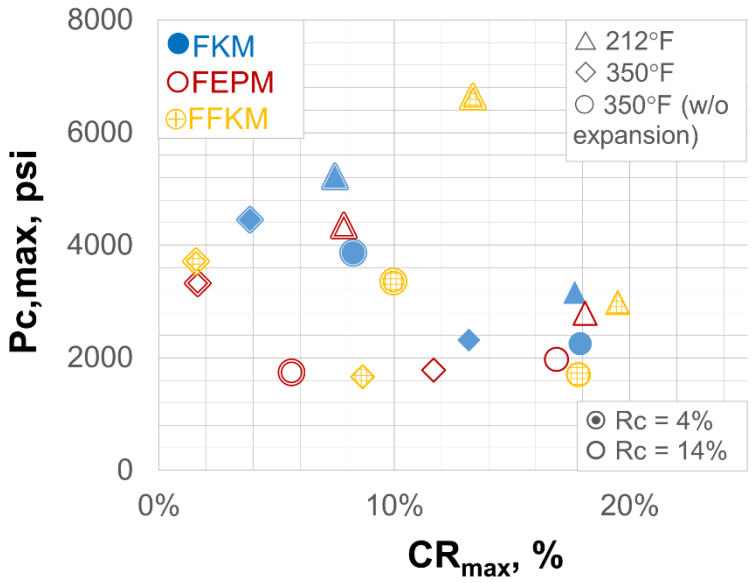

Figure 7.10: Seal energization limits of conventional liner hanger seal assemblies at different thermal conditions

Figure 7.11 presents energization limits of elastomers in expandable liner hanger assemblies at different temperature conditions. Similar to conventional assembly, robustness to energization failure reduces at 350°F compared to 212°F. For example, FKM elastomer in an assembly with 10 ksi/in containment and at 212°F has energization limits of 52% ER, and 3500

psi P_c. At high temperature of 350°F, the limits reduce to 45% and 2900 psi. For temperature transition from 212°F to 350°F, the limits further reduce to 39% and 2700 psi. Similar reduction trends are observed for FEPM and FFKM elastomers and other containment design. Unlike conventional assembly, the trends are clear, and a general ranking of elastomers can be determined. In general, FKM has the highest energization limit for any given condition, followed by FEPM and FFKM.

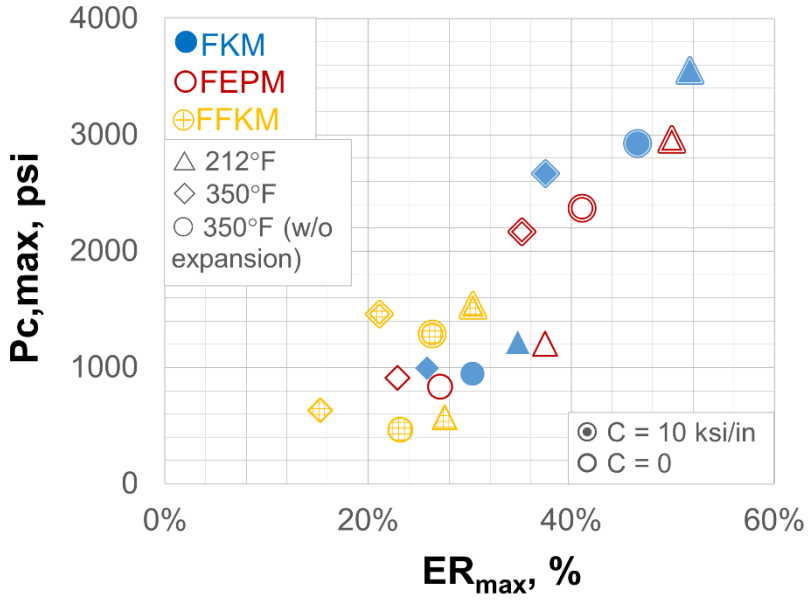

Figure 7.11: Seal energization limits of expandable liner hanger seal assemblies at different thermal conditions

7.4 Equipment Failure

Conventional liner hanger assembly has many moving parts such as slips, compression plates, energization mandrel, etc. Function of slip is to restrain compression plates axially and maintain seal under compression. However, due to various factors (such as excessive mechanical/pressure/thermal loads, corrosion, lack-of centralization, extrusion, shearing, etc.) slips and compression plates may get damaged. The movement in slips or a partial failure in compression plate can reduce seal energization. For example, as shown in **Figure 7.12**, localized

failure in compression plate can lead to varying contact pressure distribution along circumferential direction of the seal-casing contact. Lower contact pressure along failed region (position A in **Figure 7.12b**), can be a potential risk for fluid pressure penetration. **Figure 7.13**, shows percentage reduction in energization coefficient for varying partial support provided by the compression plate. If compression support fails completely, then contact pressure would effectively reduce to zero resulting in complete lack of seal.

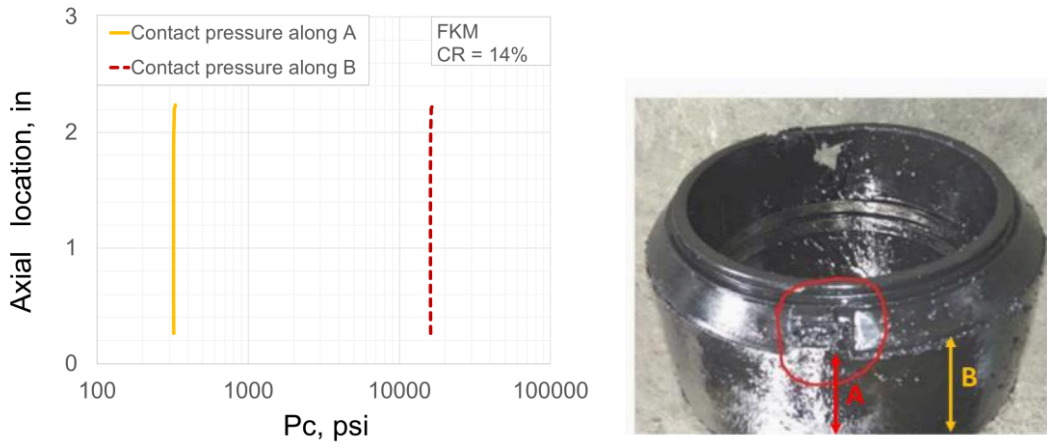

(a) **(b)**

Figure 7.12: Example of (a) non-uniform contact pressure distribution caused by (b) failure in support component (image courtesy Hu et al. 2017)

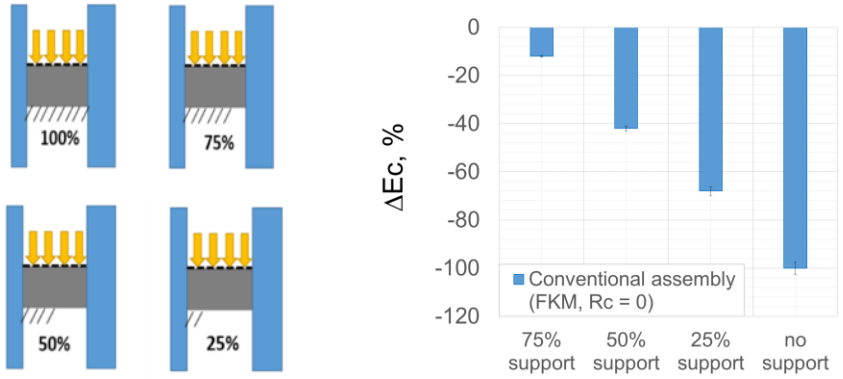

Figure 7.13: Change in seal energization coefficient of conventional hanger assembly due to failure in support component

Unlike conventional seal assembly, expandable assembly has no complex moving parts. Hence, it is less prone to structural failure compared to conventional liner hanger assembly (Walvekar and Jackson 2007). However, it is still prone to failure in seal containment. The spikes designed to contain elastomer axially, may get deformed during installation, lack of centralization, or excessive load concentration causing plastic deformation. However, as shown in **Figure 7.14**, even if complete seal containment is lost, the assembly will still maintain about 50% of original energization coefficient. Thus, although conventional assembly provides higher energization coefficient and consequently better sealability (**section 6.2**), expandable assembly is more robust to equipment related failure.

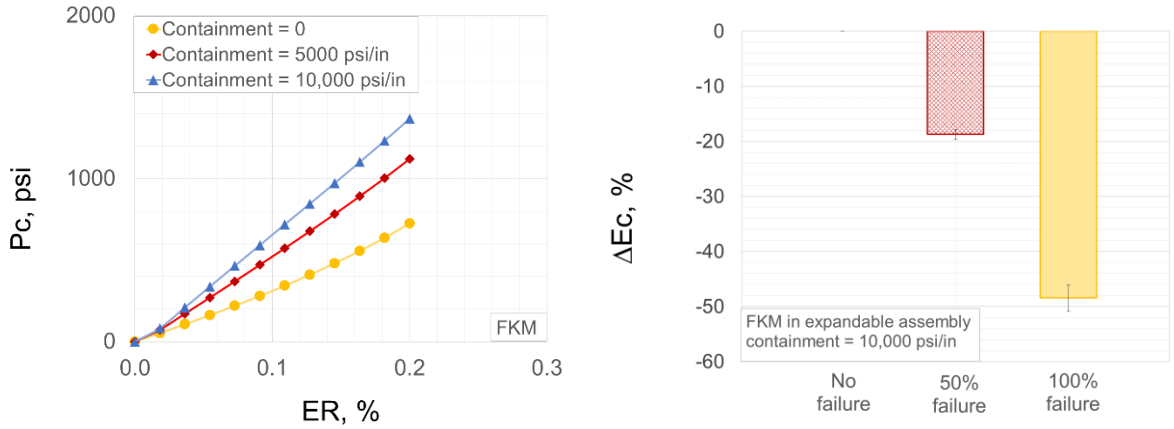

(a) **(b)**

Figure 7.14: Change in (a) energization curve and (b) energization coefficient due to failure in seal containment in expandable assembly

Chapter 8: Sensitivity Analysis

8.1 Overview

Sensitivity analysis was conducted on different configurations of conventional and expandable assembly to identify major performance predictors. Design parameters varied and the range of values investigated are listed in **Table 8.1**. For each assembly configuration, sensitivity of energization coefficient to seal dimension, material properties, and temperature were investigated.

Table 8.1: Simulation cases for sensitivity analysis

Variable	Values	
	Conventional assembly	**Expandable assembly**
Elastomer (Bulk modulus)	174, 342, and 406 ksi	174, 342, and 406 ksi
Elastomer (Shear modulus)	174, 287, and 328 psi	174, 287, and 328 psi
Seal radial width, inch	0.25, 0.68, and 1 in	0.25, 0.68, and 1 in
Seal axial length, inch	1.25, 2.5, and 5 in	2.5, 5, and 10 in
Radial clearance (R_c,in)	0, 0.025, and 0.1 in	-
Containment (C, psi/in)	-	0, 5, and 10 ksi/in
Temperature, °F	212°F and 350°F	212°F and 350°F
Chemical exposure	-	-

8.2 Conventional Assembly

Results from sensitivity analysis for conventional liner hanger assembly are presented in **Figure 8.1**, **Figure 8.2**, and **Figure 8.3**. As shown in **Figure 8.1**, for conventional assembly with no radial clearance, bulk modulus of elastomer has the highest influence on energization coefficient.

Temperature is the next important parameter. Seal dimensions (width and length) and shear modulus of elastomer have practically negligible influence.

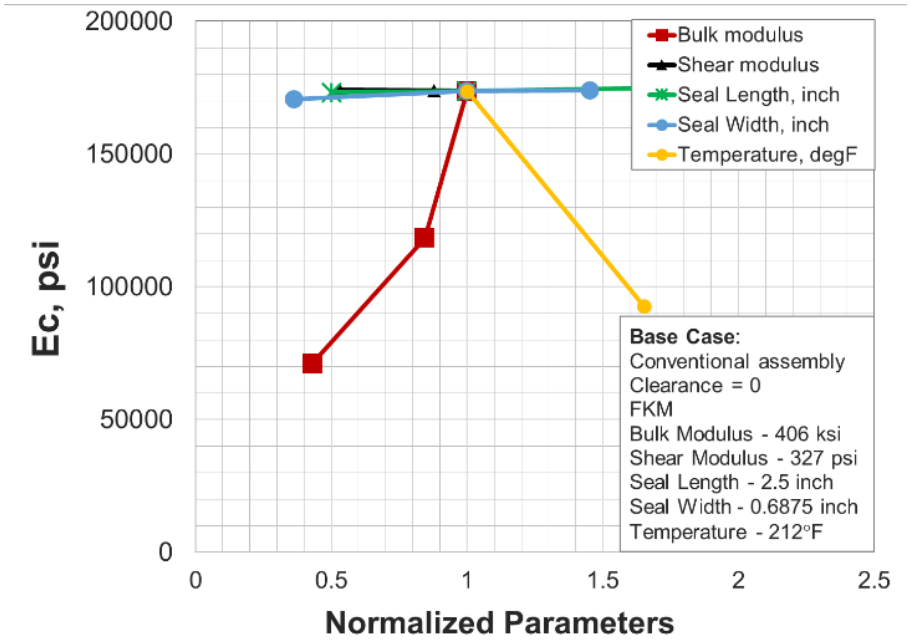

Figure 8.1: Sensitivity analysis of conventional assembly with no radial clearance

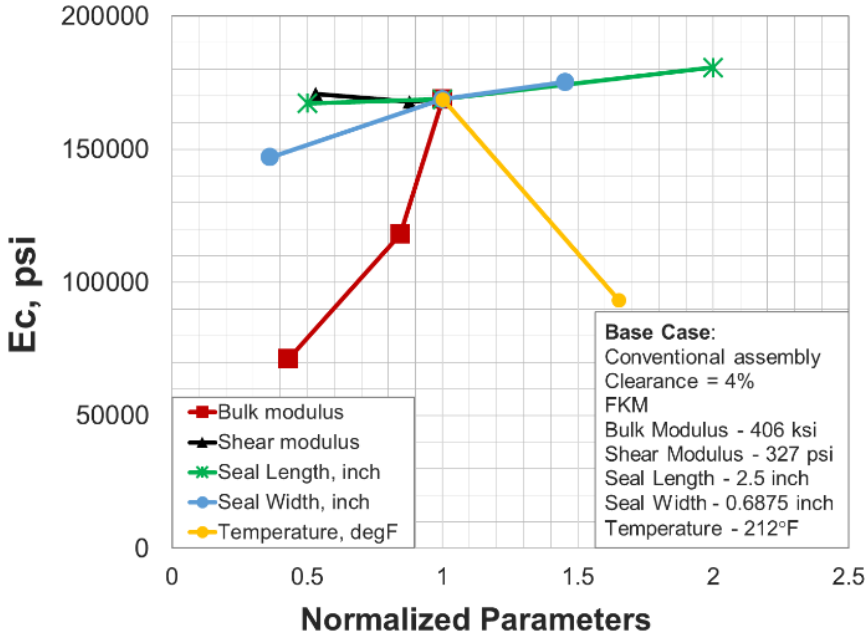

Figure 8.2: Sensitivity analysis of conventional assembly with 4% radial clearance

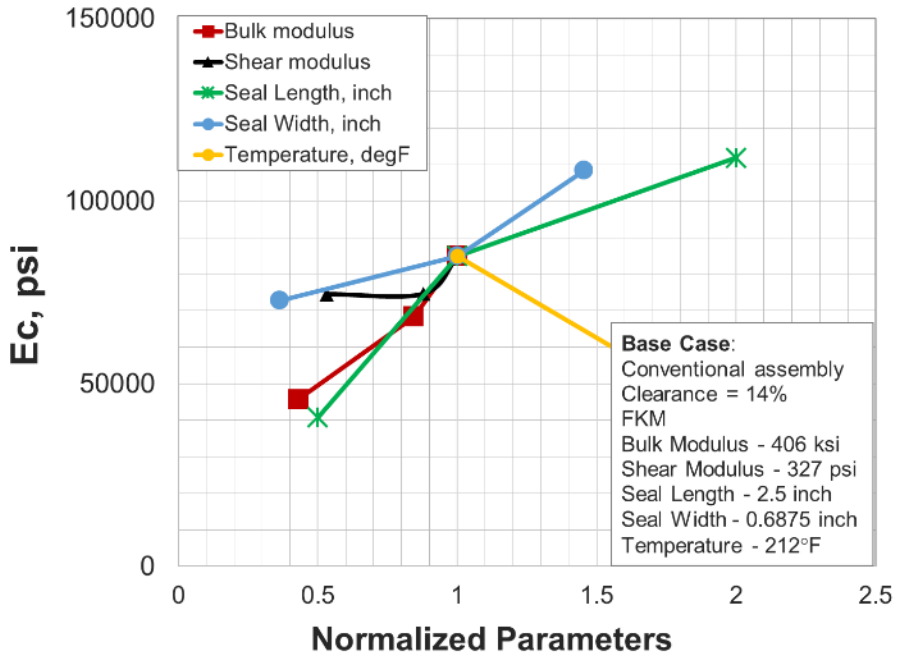

Figure 8.3: Sensitivity analysis of conventional assembly with 14% radial clearance

Table 8.2: Summary of sensitivity analysis of conventional liner hanger seal assembly

Seal assembly configuration	Influence of Parameters
Conventional (R_c = 0)	K > T >>> (w ≈ l ≈ G ≈ insignificant)
Conventional (R_c = 4%)	K > T > w > l >> (G ≈ insignificant)
Conventional (R_c = 14%)	l ≈ K ≈ G ≈ T > w

G: shear modulus of elastomer, K = bulk modulus of elastomer
l: axial length of seal element, T: operating temperature
w: radial width of seal element

Sensitivity plot for conventional assembly with 4% radial clearance is shown in **Figure 8.2**. Bulk modulus closely followed by temperature are the most dominant predictors of energization coefficient. However, unlike previous assembly configuration, seal dimensions have notable influence on assembly performance. This is likely due to the presence of extrusion gap

which makes seal dimensions and volume-fill important factors. Shear modulus of elastomer has negligible influence on seal performance.

Sensitivity plot for conventional assembly with 14% radial clearance is presented in **Figure 8.3**. Increase in radial clearance compared to previous two cases have significantly increased sensitivity to seal dimensions. For this assembly, bulk modulus, seal length, and temperature are approximately equally dominant performance predictors. Next important parameter is shear modulus and seal width. Increased importance of shear modulus compared to previous assembly configurations can be attributed to high extrusion gap making shear behavior important. Ranking of variables in terms of their influence on energization coefficient of conventional assemblies is listed in **Table 8.2**.

8.3 Expandable Assembly

Results from sensitivity analysis for conventional liner hanger assembly are presented in **Figure 8.4**, **Figure 8.5**, and **Figure 8.6**.

Sensitivity plots for all three expandable assemblies exhibit similar trends except few minor differences. The base case energization coefficient increases with increase in containment (3500 psi in **Figure 8.4** vs 7000 psi in **Figure 8.6**). This is because of reduced extrusion and consequently better compression as discussed in **section 6.2**. Slopes of seal length and seal width curves also increases slightly with increase in containment (**Figure 8.4** vs **Figure 8.6**). This indicates diminishing influence of seal dimensions as seal containment improves (detailed discussion in **section 6.3**).

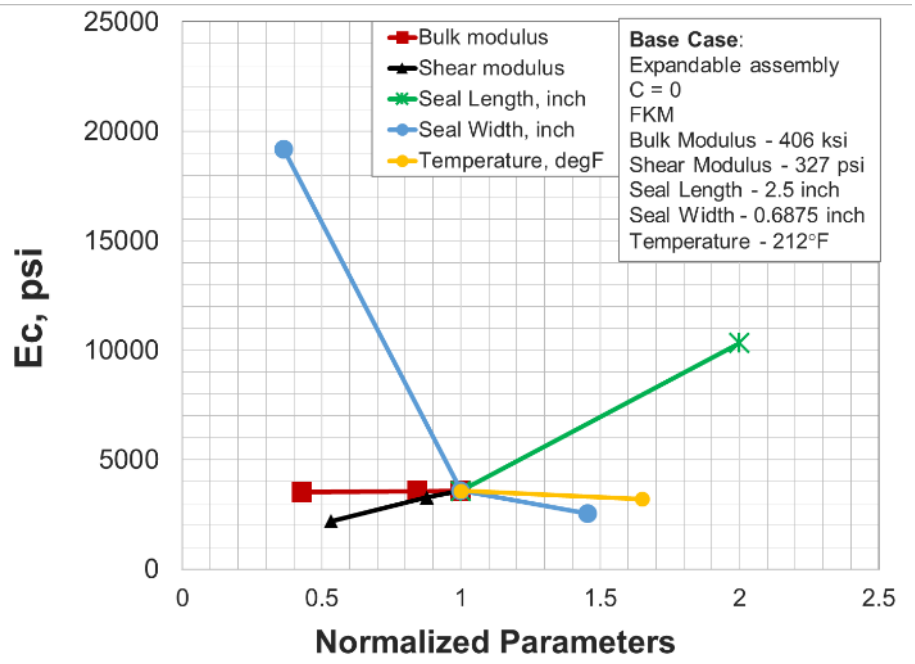

Figure 8.4: Sensitivity analysis of expandable assembly with no seal containment

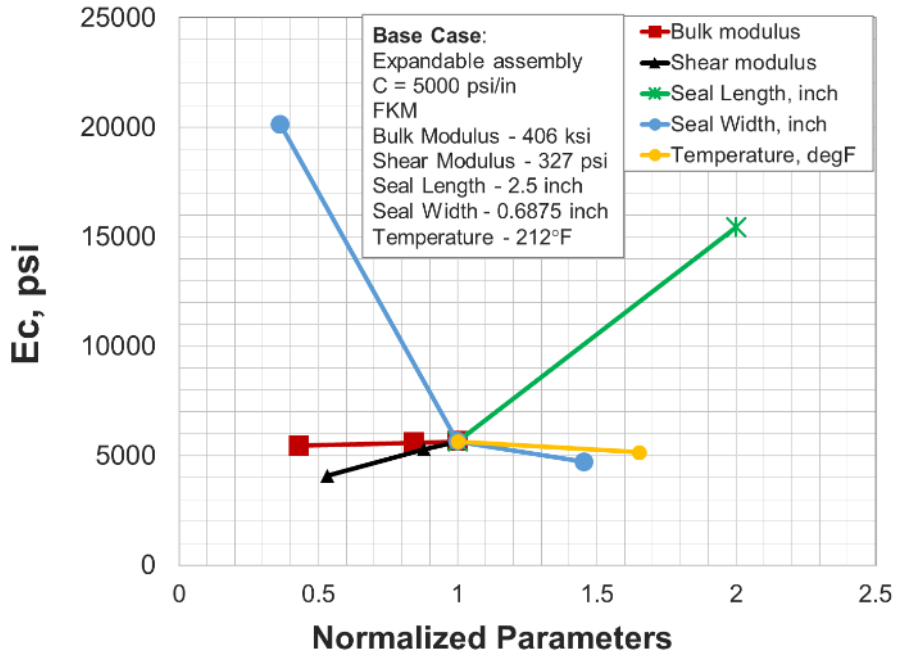

Figure 8.5: Sensitivity analysis of expandable assembly with 5000 psi/in containment

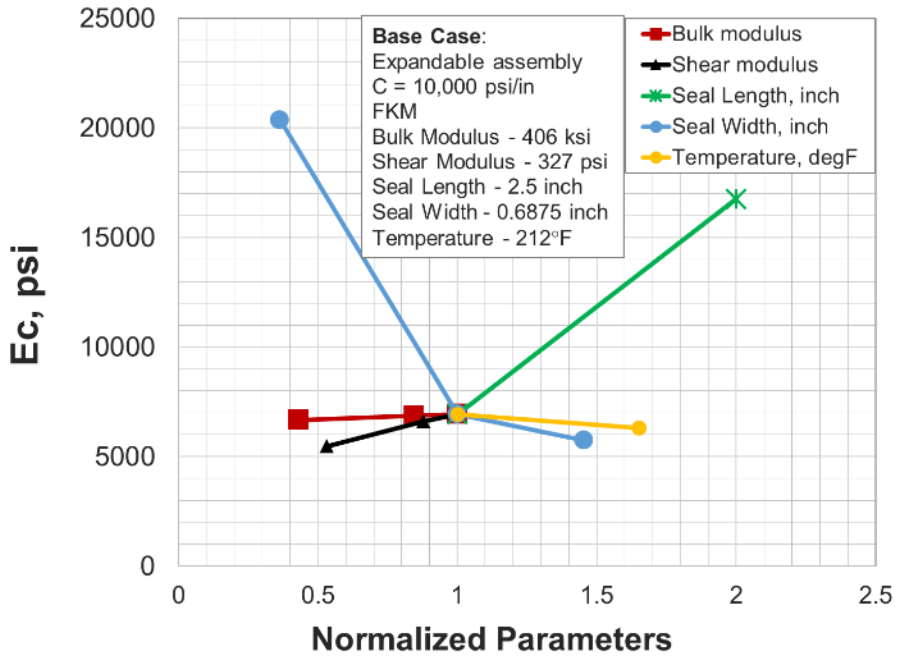

Figure 8.6: Sensitivity analysis of expandable assembly with 10,000 psi/in containment

Table 8.3: Summary of sensitivity analysis of expandable liner hanger seal assembly

Seal Assembly	Influence of Parameters
Expandable (C = 0)	w > l > G > T (K ≈ insignificant)
Expandable (C = 5000 psi/in)	w > l > G > T (K ≈ insignificant)
Expandable (R_c = 10,000 psi/in)	w > l > G > T (K ≈ insignificant)

G: shear modulus of elastomer, K = bulk modulus of elastomer
l: axial length of seal element, T: operating temperature
w: radial width of seal element

The sensitivity plots of expandable assemblies are different from conventional assembly. In expandable assembly, seal element is not restrained completely in axial direction and the energization load comes from liner expansion in radial direction. Hence, shear modulus of elastomer material is more important in determining assembly's performance compared to bulk

modulus. This is opposite from conventional assembly where bulk modulus is dominant predictor. Seal width followed by seal length have the highest influence on expandable assembly's performance. They have higher influence than even shear modulus and operating temperature. This is in stark contrast to conventional assembly where importance of seal dimensions depend on amount of extrusion gap. The ranking of parameters in terms of importance in performance prediction is summarized for all three expandable assembly configurations in **Table 8.3**.

Chapter 9: Leakage Modelling Results

9.1 Base Case

A novel leakage model was developed to simulate fluid penetration and leakage through elastomer-casing interface. The model algorithm details are discussed in **Chapter 5**. The goal of this modelling tool is to correlate contact pressure predicted by FEA model with leakage rates for given contact characteristics and operating conditions. The model is capable of taking surface finishing of elastomer seal as an input. The input parameters for the model are listed in **Table 9.1**. As shown in the table, elastomer material, seal surface finishing as represented by root-mean-squared (RMS) value, and microscopic surface features were varied and their impact on leakage rates were examined. The data presented in this chapter is scheduled for publication (Patel and Salehi 2020).

Table 9.1: Input parameters used for leakage modeling simulations

Parameter	Value
Seal assembly	9-5/8" liner hanger
Elastomer material	NBR, FKM-75*, FKM-90
Elastomer Poisson's ratio	0.499
Surface RMS, μinch	16, 32*, 64
Surface type	Roughness dominant* waviness dominant I, waviness dominant II
Target surface Young's modulus, psi	3×10^7
Target surface Poisson's ratio	0.3
Differential fluid pressure, psi	1000
Fluid type	water

* values used in base case simulation

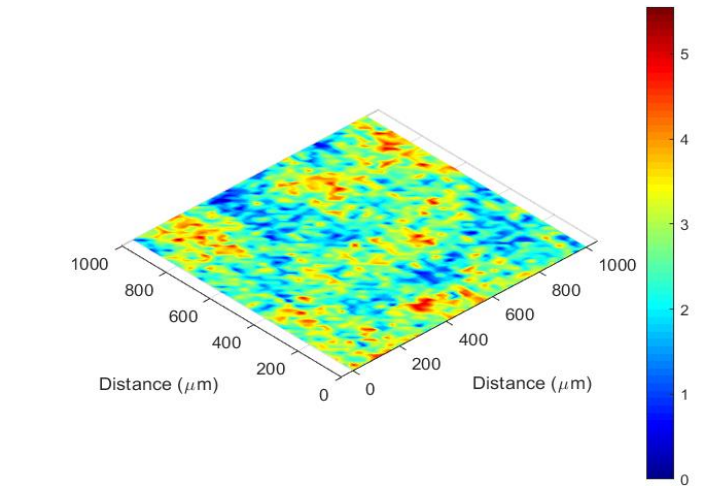

(a)

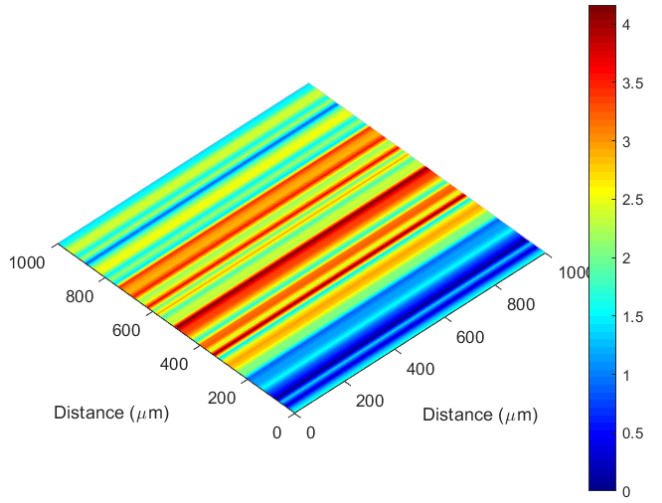

(b)

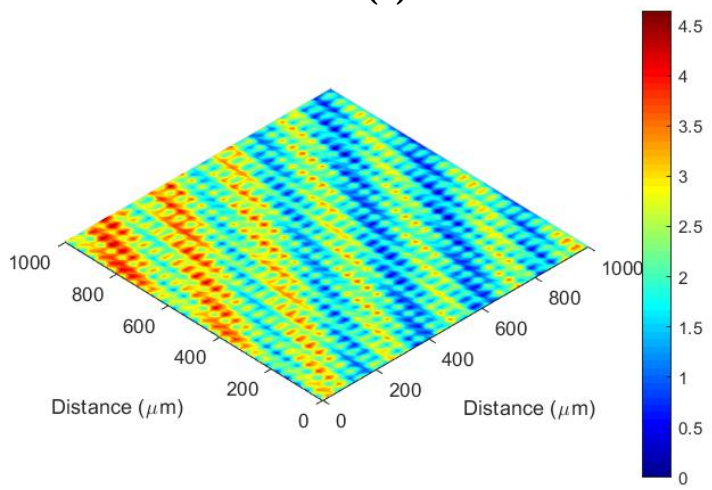

(c)

Figure 9.1: Surface topography used in simulations: (a) roughness dominant, (b) waviness dominant I, (c) waviness dominant II. Z-axis represent height in micron

Three types of seal surface topographies considered in this study are shown in **Figure 9.1**. First surface (**Figure 9.1a**) has roughness dominant features and lack higher scale waviness. This surface represents elastomer component manufactured by molding. The other two surface types (**Figure 9.1b and Figure 9.1c**) exhibits patterns and waviness features on surface. Such surface characteristics are representative of machined seal components.

9.2 Effect of Elastomer Type

Effect of elastomer material on leakage curves was examined by keeping the surface topography of seal constant. NBR and FKM elastomer material were compared. In case of FKM, two samples having different durometer shore A hardness (75 and 90) were compared. Leakage rates as a function of contact pressure at seal-casing interface are plotted in **Figure 9.2**. As shown in the figure, leakage rate rapidly decreases as contact pressure (i.e. seal compression) increases. Eventually complete seal i.e. zero leakage rate is achieved at a certain critical contact pressure.

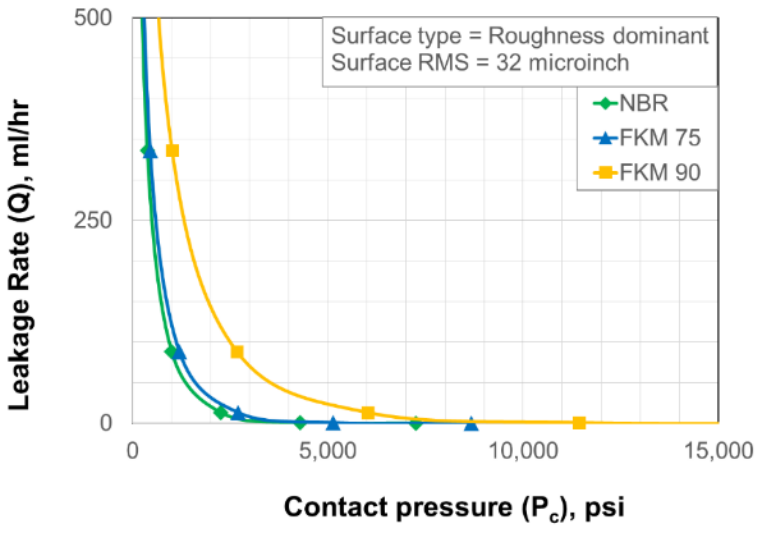

Figure 9.2: Leakage rate as a function of contact pressure for different elastomer material but same surface

The results indicate practically similar critical contact pressure for NBR and FKM despite the fact that FKM has 20% higher elastic modulus than NBR. Comparison between FKM 75 and FKM 90 indicate that higher hardness elastomer requires significantly higher contact pressure to achieve complete seal. FKM-90 required greater than 15,000 psi contact pressure to achieve sealability while FKM-75 achieved sealing at approximately 9000 psi contact pressure.

9.3 Effect of Surface RMS

Next, influence of seal surface finishing as represented by RMS was investigated. Commercially available seal components often have roughness of approximately 32 µinch (API 6AF2). Keeping the surface topography and asperities distributions constant, surface RMS was varied from 16 to 64 µinch. FKM 75 was selected as the elastomer material in the simulations. Influence of surface RMS on leakage curve is presented in **Figure 9.3.**

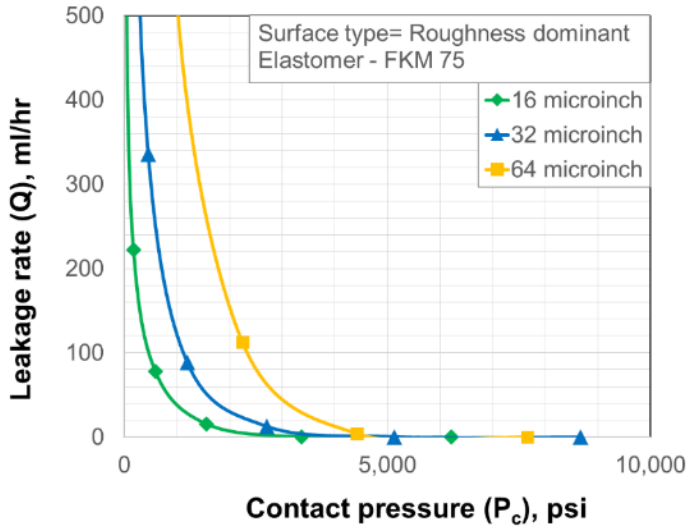

Figure 9.3: Leakage rate as a function of contact pressure for surfaces with different RMS but similar topographical characteristics

As shown in the figure, the critical contact pressure needed to achieve complete seal is practically similar in all three cases. However, the leakage rates values at a given contact pressure are significantly higher for a surface with higher surface RMS. This can be better visualized in **Figure 9.4** which presents leakage rates as a function of contact area. The contact area needed to achieve complete seal are same regardless of surface RMS but leakage rates at a given contact area is higher for surface with high surface RMS. This is an expected trend because higher surface RMS indicate higher differences between peaks and valleys and consequently provide more contact gaps for fluid to leak through.

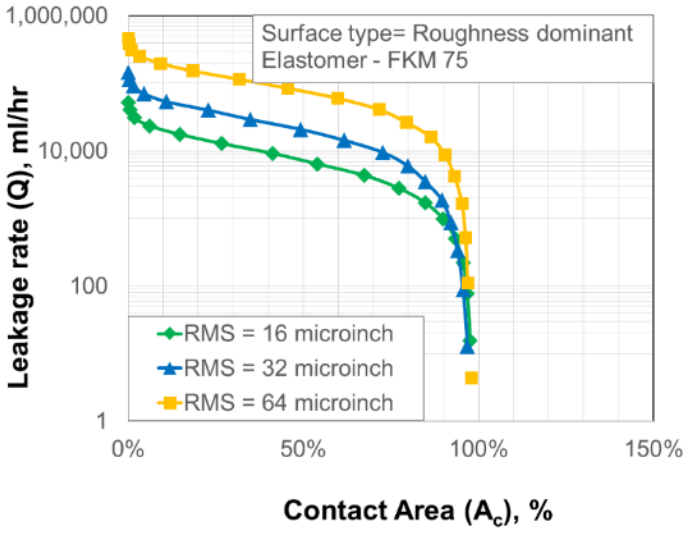

Figure 9.4: Leakage rate as a function of contact area for surfaces with different RMS but similar topographical characteristics

9.4 Effect of Surface Type

In this simulation scenario, three surface types (shown in **Figure 9.1**) were compared keeping the surface RMS and elastomer material properties constant. These surfaces are representative of different manufacturing processes and surface characteristics.

As shown in **Figure 9.5**, these surfaces requires significantly different critical contact pressure to achieve complete seal. Roughness dominant surface (**Figure 9.1a)** had random distribution of peaks and valleys. Therefore, it requires higher contact pressure than waviness surface I, to achieve complete seal (**Figure 9.5**). As shown in **Figure 9.1b,** Waviness dominated surface I has uniform bands of peaks and valleys that lie perpendicular to the flow direction. Therefore, even at low contact area and contact pressure, the peaks are able to block the fluid flow (**Figure 9.5**). In case of waviness dominant surface II (**Figure 9.1c**), the bands of peaks and valleys are located oblique to the fluid penetration direction. Hence, significantly high compression of seal (i.e. contact pressure) is needed to achieve zero leakage rate (**Figure 9.5**). These observations can be further confirmed by evaluation leakage rates as a function of seal contact area (**Figure 9.6**).

Another interesting observation from **Figure 9.5**, is that these surfaces do not exhibit significantly distinct leakage rates at a given contact pressure. This is likely due to the fact that the three surfaces despite of different topographic features, have similar surface finishing as represented by same RMS values.

Sealing process in these surfaces is visually presented in **Figure 9.7**, **Figure 9.8**, and **Figure 9.9**. These figures show distribution of porosity over the contact surface at different level of seal compression i.e. contact pressure. The plots can also be used to understand leakage path of the fluids.

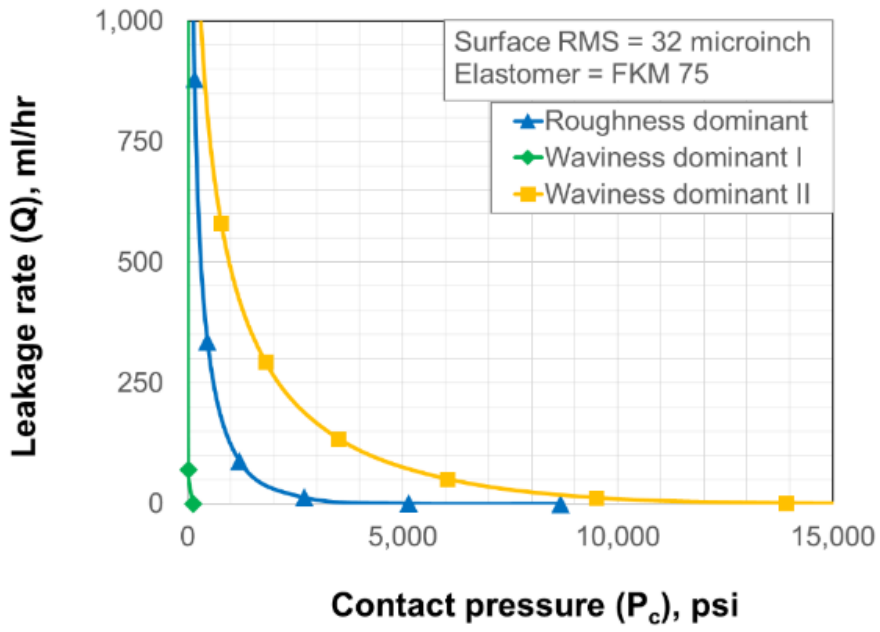

Figure 9.5: Leakage rate as a function of contact pressure for different types of surfaces with similar RMS

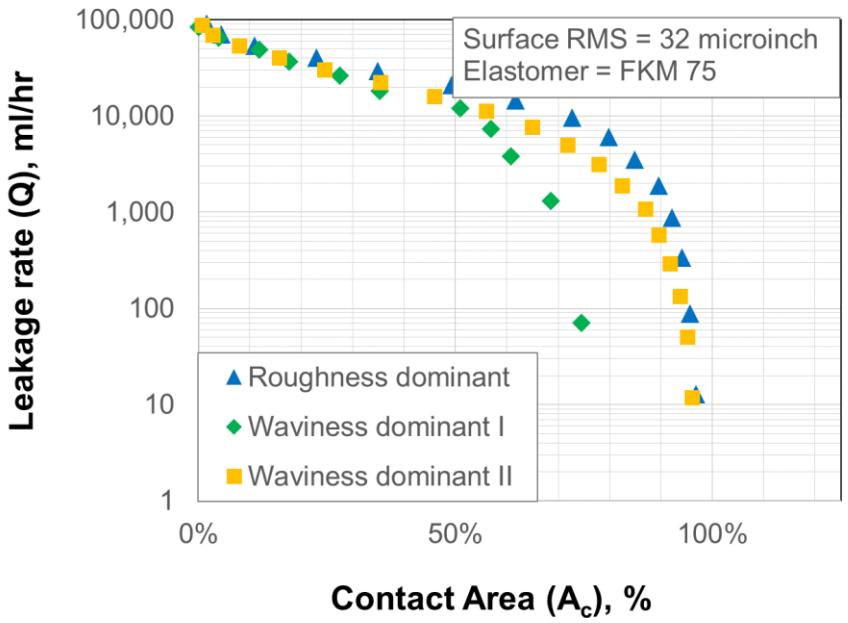

Figure 9.6: Leakage rate as a function of contact area for different types of surfaces with similar RMS

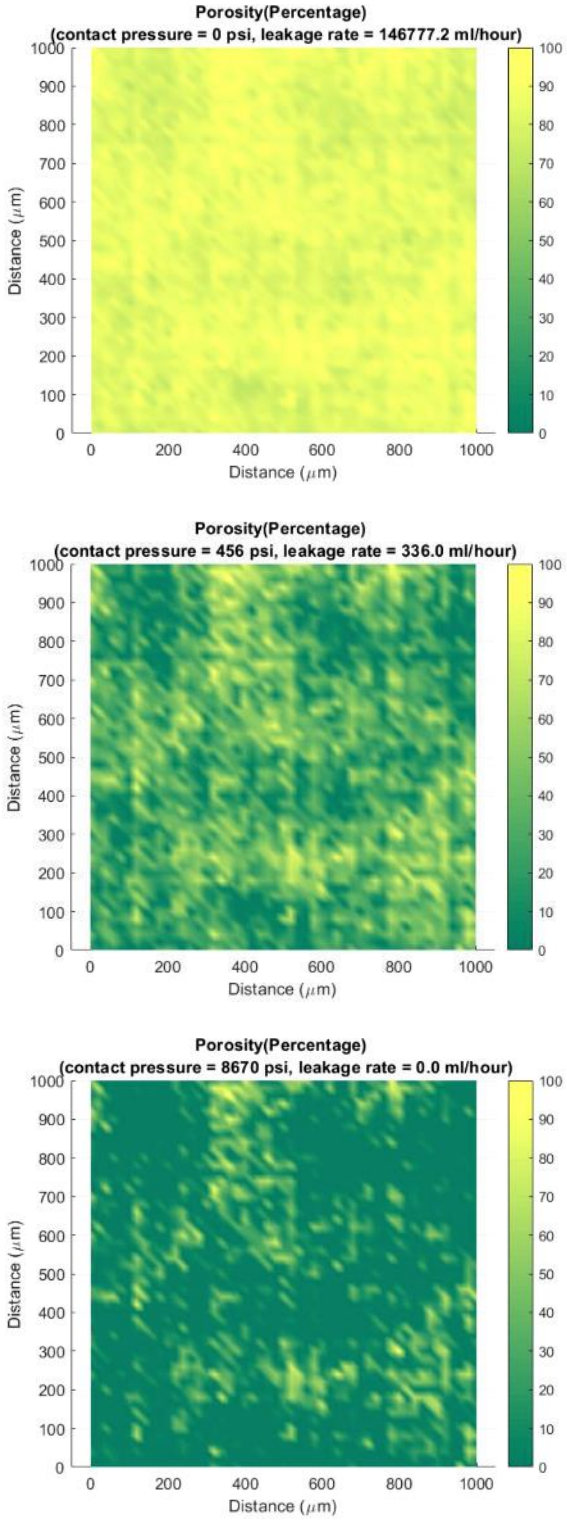

Figure 9.7: Roughness dominant surface: evolution of contact gap distribution with increasing contact pressure. Flow direction is bottom to top.

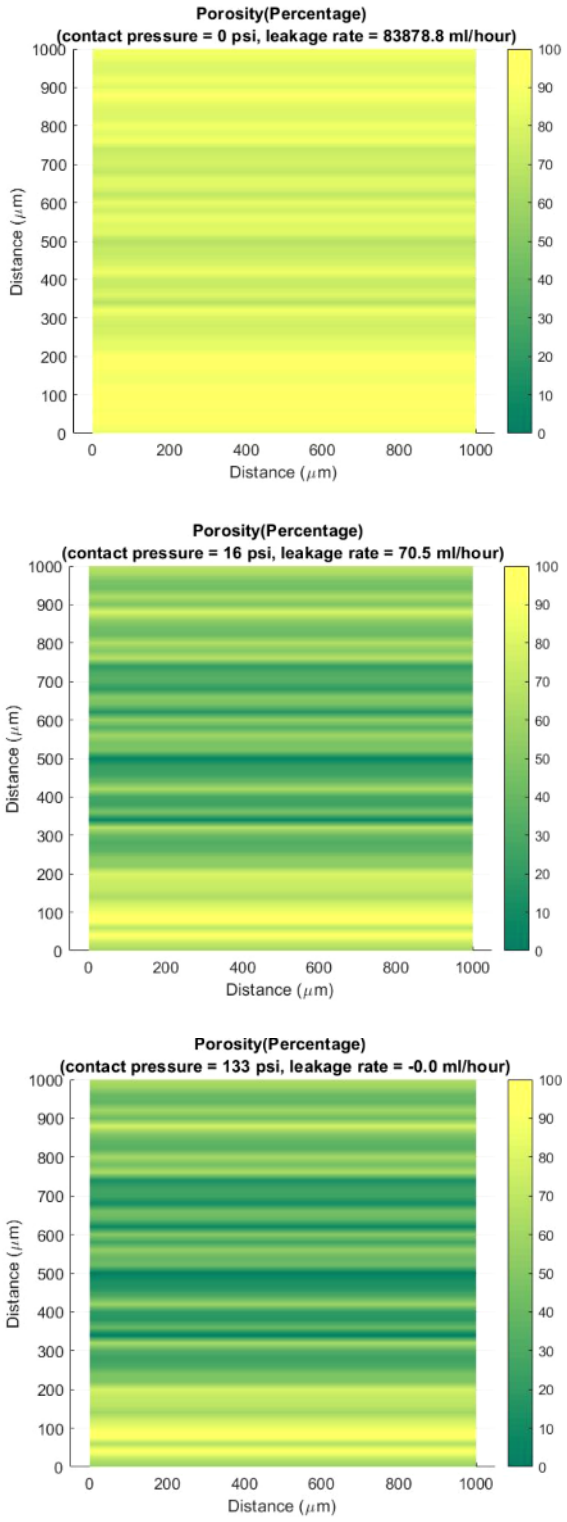

Figure 9.8: Waviness dominant surface I: evolution of contact gap distribution with increasing contact pressure. Flow direction is bottom to top.

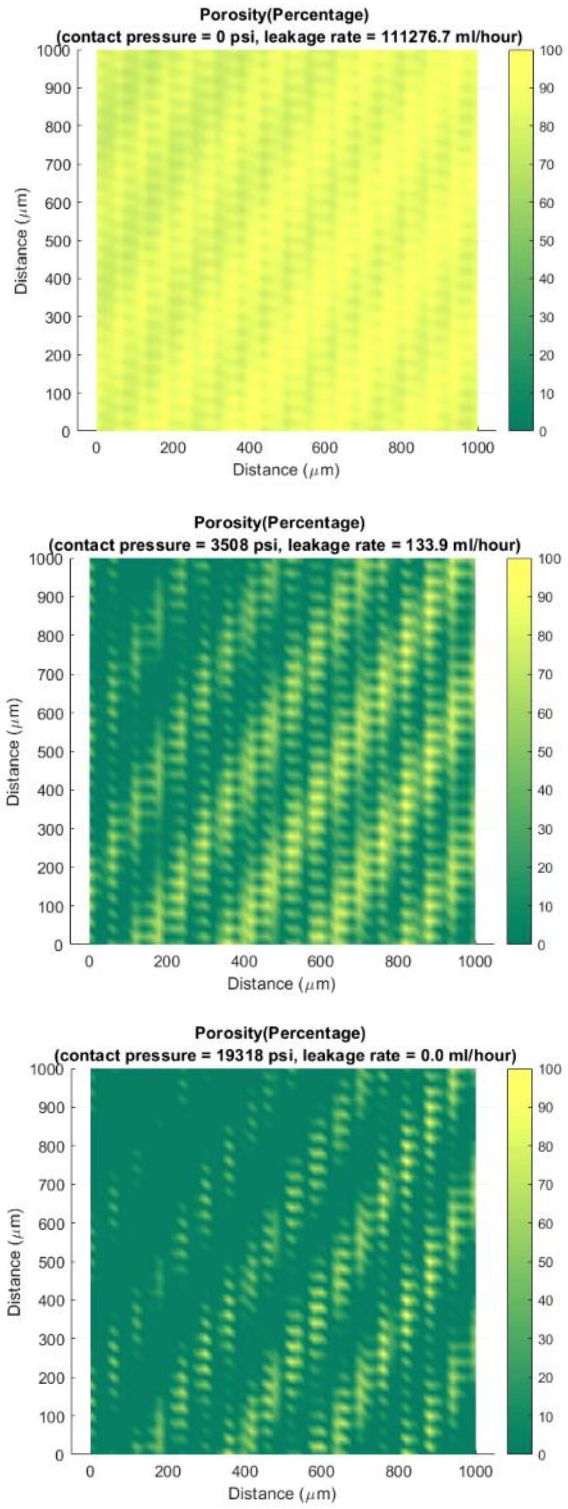

Figure 9.9: Waviness dominant surface II: evolution of contact gap distribution with increasing contact pressure. Flow direction is bottom to top.

Chapter 10: Summary

This dissertation work investigates six elastomer materials commonly used in the oil & gas well construction. This includes – NBR, EPDM, FKM, FEPM, FFKM, and PTFE. Hardness and elastic moduli of the elastomers were measured in variety of downhole conditions. Both linear elastic and hyperelastic type material behavior were examined. Material data includes variations with temperature (75°F, 212°F, and 350°F), and effect of chemicals exposure (CO_2, CH_4, H_2S, and mixture of the gases; with and without presence of brine, 1 and 7 days, 120°F, and 180°F, 1000 psi).

Performance of the elastomers were investigated at equipment level using FEA models of conventional and expandable liner hanger seal assemblies. Analytical calculations were performed to validate contact pressures at seal-pipe interface as predicted by the FEA models. Sealability tests were conducted using a scaled laboratory setup to further verify FEA observations. Validated FEA models were used to investigate performance of elastomer seals in various design, operational, and failure scenarios. Sensitivity analysis was conducted to identify critical parameters influencing the performance of elastomer seal assemblies.

A novel modelling tool was developed to predict fluid leakage rate through elastomer seal interface as a function of surface characteristics, seal properties, and operating fluid conditions. Parametric analysis was performed to examine effects of surface characteristics and elastomer properties on leakage rates.

Following is the summary of important results and observations from this dissertation work:

10.1 Energization Design

- In conventional seal assembly, contact pressure value remains constant along the seal length. For frictional condition, contact pressure value decreases along the seal length from the compression side towards the support side. In expandable seal assembly, regardless of friction condition, contact pressure peaks at the center of the seal length and declines towards either sides of the axial ends. The profile becomes flatter with increase in elastomer seal containment. For both assemblies, above profile observations remain true regardless of elastomer type and material behavior (linear-elastic or hyper-elastic).
- Regardless of assembly design (energization method, geometry, and elastomer material) the relationship between contact pressure generated by seal energization and compression/expansion ratio is practically linear. The slope of this linear energization curve, termed as energization coefficient, is a unique value for each assembly design.
- For the same elastomer material, regardless of geometric design, energization coefficient of conventional seal assembly will always be higher than energization coefficient of expandable seal assembly.

10.2 Seal Dimensions and Geometry

- For conventional assembly, importance of seal dimensions depends on the initial radial clearance or extrusion gap of the assembly. Effect of seal dimensions on energization coefficient diminishes as radial clearance or extrusion gap reduces. In presence of extrusion gap, longer and thicker seal yields higher energization coefficient and consequently better sealability.

- For expandable assembly, seal dimensions are important design considerations regardless of assembly configuration. Thicker and longer seal elements produce higher energization coefficient and consequently higher contact pressure at a given expansion ratio.

10.3 Elastomer Material

- For similar assembly design, studied elastomer materials can be ranked in terms of increasing order of energization coefficient as – NBR < EPDM < FFKM < FEPM < FKM < PTFE.
- Regardless of assembly design, type of material model used for elastomer characterization does not impact the shape of contact pressure profile. However, hyper-elastic characterization yielded significantly higher energization coefficient than the linear elastic representation. Therefore, it is important to measure true elastomer material behavior over the range of operating strains and use appropriate model in simulations.
- For conventional assembly, bulk modulus of elastomer material is the dominant predictor of energization coefficient and consequently, sealability. Shear modulus of elastomers has relatively insignificant influence on contact pressure.
- For expandable assembly, energization coefficient is not dependent on bulk modulus of elastomer. However, shear modulus has some influence on contact pressure. Both moduli are not as important as they are in case of conventional assembly.

10.4 Failure Scenarios

- Expandable energization is more robust to energization failure than the conventional assembly. Even if both elastomer containment spikes completely fail, the expandable seal assembly would still maintain about 50% contact pressure. However, in conventional

assembly, complete failure in slips or compression plate will result in complete loss of contact pressure.

- Conventional seal assembly generates significantly higher Tresca stress and consequently it is more prone to failure compared to expandable assembly.
- To minimize the risk of failure by over-energization, radial clearance should be minimized in case of conventional assembly and quality of containment spikes should be improved in expandable assembly.
- Although ranking of elastomers in terms of limiting Tresca stress is - FFKM > FKM > FEPM, it is difficult to rank them in terms of risk of extrusion failure. Selection of appropriate elastomer depends on type of assembly, type of geometry, and target compression ratio or expansion ratio.
- Based on chemical aging tests, and corresponding energization coefficients for seal assemblies, elastomers can be ranked in decreasing order of chemical resistance as – PTFE > FKM > EPDM > NBR.
- Simulation results and experimental observation indicate that degradation in energization coefficient of seal assembly due to chemical exposure can be approximated by degradation in elastic properties of elastomer. Hardness alone is not an accurate indicator of elastomer performance in downhole conditions.
- Comparison between performance at 212°F and 350°F indicate that FKM exhibits highest reduction of sealability at higher temperature. Change in performance of FEPM, and FFKM due to increase in temperature was insignificant. However, it is difficult to recommend elastomer based on thermal resistance alone. Elastomer selection depends on

assembly design, temperature induced changes in limiting Tresca stresses, thermal expansion, and operating constraints.

10.5 Sensitivity Analysis

- For conventional assembly, bulk modulus of elastomer seal is the primary predictor of energization coefficient followed by temperature and seal dimensions. Having small radial clearance or extrusion gap reduces the effect of seal dimensions. Shear modulus of elastomer seal is not an important factor.
- For expandable assembly, seal radial width followed by seal axial length are the dominant predictors of energization coefficient. Next important parameters are shear modulus of elastomer and temperature. Bulk modulus of elastomer has negligible influence on energization coefficient.

10.6 Leakage Model

- Contact pressure generated by seal energization does not represent fluid pressure that it can withstand without permitting fluid leakage. Microscopic surface characteristics of seal interface determines the target contact pressure required to seal various fluids at different operating pressures.
- For same surface characteristics, elastomer material with higher elastic modulus and higher hardness require higher contact pressure to achieve complete sealability or target leakage rates.
- Target contact pressure required to achieve zero leakage rate is primarily dependent on type of surface topography of seal. Surface topography i.e. asperities distribution does not have notable influence on amount of leakage rate at a given microscopic separation.

- Roughness of seal surface (as represented by RMS) determines the amount of leakage rate at a given contact pressure. However, surface RMS does not have significant impact on the target contact pressure required to achieve zero leakage rate.

Chapter 11: Conclusions, Recommendations, and Future Work

This dissertation work investigates performance of six elastomer materials commonly used in the oil & gas industry. Hardness and elastic moduli of the elastomers were measured in variety of downhole conditions and input into FEA models of conventional and expandable liner hanger seal assemblies. The FEA models were verified by analytical calculations and scale laboratory tests. Validated models were used to investigate performance of elastomers in various design, operational, and failure scenarios. A novel modelling tool was developed to predict leakage through elastomer seal interface considering surface characteristics, seal properties, and operating fluid parameters. Following are the major conclusions and recommendations from this research work:

11.1 Conclusions

1. Appropriate selection of elastomer for a given application not only depends on downhole conditions but also on equipment type, seal design, and installation and operational constraints.
2. Hardness alone is not an accurate indicator of elastomer's performance in downhole conditions. It is essential to measure elastomer deformation behavior (i.e. elastic, bulk ,and shear moduli) for accurate prediction of sealability.
3. In general, bulk modulus of elastomer is important for conventional seal assembly design while shear modulus is important for expandable seal assembly. In general, elastomers studied can be ranked in decreasing order of chemical resistance as - PTFE > FKM > EPDM > NBR.

4. Dimensions of elastomer component are important for expandable assembly. For conventional assembly, importance of seal dimensions depends on extrusion gap in housing design.
5. Surface characteristics of elastomer and target surface significantly influence contact pressure required to seal various fluids at different operating conditions.
6. Elastomer with higher elastic modulus and higher hardness require higher target contact pressure to seal same fluid pressure.
7. Surface finishing as represented by RMS determines the absolute values of leakage rate at a given contact pressure. For same surface RMS, target contact pressure needed to achieve zero leakage rate primarily depends on the surface topographical features or patterns.
8. Conventional liner hanger seal assembly outperforms expandable liner hanger seal assembly in terms of magnitude of sealing contact pressure. However, expandable seal assembly is more robust to failure by extrusion, over-energization, and faulty supporting components compared to conventional seal assembly.

11.2 Recommendations

1. Elastomer seal qualification criteria should vary depending on end-application, and design of seal component and equipment. Hardness alone is not an accurate indicator of elastomer's performance. Qualification testing should also include other material properties (e.g. elastic modulus, bulk modulus, shear modulus, etc.) depending on end-application. For example, as identified in this work, bulk modulus of elastomer is critical for conventional liner hanger seal assembly design while elastomer dimensions and shear modulus are important for expandable liner hanger seal assembly.

2. Fitness-for-service assessment of elastomer seal should not be limited to material testing. The assessment process should also leverage true scale FEA models and leakage modelling tools to evaluate actual equipment level performance of elastomer material.
3. Surface characteristics or defects on elastomer material and target surface can have notable impact on seal quality. Hence, surface finishing or damage should be considered as an important parameter during seal design, selection, evaluation, and installation processes.
4. Seal design and selection workflow should include microscopic leakage modelling studies. Leakage modelling tool can help in determining target contact pressure needed to seal various fluids at different operating pressures. Seal assembly should be designed to provide sufficient energization to achieve this target contact pressure.
5. Expandable seal assembly is typically more robust to failure than conventional assembly. Hence, it should be preferred unless significantly high contact pressure is required which can only be achieved through conventional type energization method.

11.3 Future Work

1. Lab scale experiments are needed to validate the developed leakage model.
2. Leakage model is currently only applicable to Newtonian and incompressible fluid. Further upgrades are needed to model flow of compressible and non-Newtonian fluids such as gases, oil, drilling fluids, etc.
3. Interactions between adjacent asperities were ignored in the contact mechanics model. Additionally, fluid mechanics and contact mechanics models have been assumed to be decoupled. Eliminating these two assumptions will be an important future upgrade to the leakage modelling tool.

4. Additional influential parameters that require further investigation using sophisticated modelling techniques are – effect of dynamic loads, chemical interactions, geo-mechanical factors, transient leakage and failure modes, etc.
5. More research should be directed at developing database of elastomer material properties at various HPHT downhole conditions. Such material library is essential for fitness-for-service evaluation of elastomer seals in various downhole applications.
6. Another important area of future research work is development of reliable models/techniques that can use accelerated aging tests data and predict elastomer performance over service life spanning several years. Identifying appropriate conditions for accelerated laboratory aging tests is also an important research gap.
7. Research should also advance in the area of alternative sealing solutions such as metal-to-metal seals, spring loaded seal elements, swelling elastomer material, pressure sensitive seal materials, composites materials, etc.

Nomenclature

Acronyms

ALT	:	Accelerated Life Testing
API	:	American Petroleum Institute
ASTM	:	American Society of Testing and Materials
BOP	:	Blowout Preventer
BSEE	:	Bureau of Safety and Environmental Enforcement
CR	:	Compression ratio, %
DfR	:	Design for Reliability
EPDM	:	Ethylene Propylene Diene Monomer
ER	:	Expansion ratio, %
FEA	:	Finite Element Analysis
FEPM	:	Tetrafluoroethylene Propylene
FFKM	:	Perfluorocarbon Elastomer
FEA	:	Finite Element Analysis
FKM	:	Fluorocarbon Elastomer
HPHT	:	High Pressure High Temperature
HNBR	:	Hydrogenated Nitrile Butadiene Rubber
ID	:	Internal Diameter
ISO	:	The International Organization for Standardization petroleum industry
LOWC	:	Loss of Well Control
M2M	:	Metal-to-Metal
MIL-SPEC	:	Military Specifications

NACE : National Association of Corrosion Engineers

NBR : Nitrile Butadiene Rubber

NORSOK : Norsk Sokkels Konkuranseposisjon (Standards by Norwegian Petroleum Industry)

PTFE : Polytetrafluoroethylen

RGD : Rapid Gas Decompression

RMS : Root Mean Square

SEM : Scanning Electron Microscope

SSSV : Subsurface Safety Valve

Symbols

b : Radius of asperity base, L, m

d : Contact gap or separation, L, m

d_0 : Initial contact gap or separation, L, m

h : Height of asperity, L, m

h_{max} : Height of highest asperity, L, m

r : Hydraulic radius, L, m

A : Contact area (contact mechanics model) / flow area (leakage model), L^2, m^2

D : Fractal dimension, dimensionless

E* : Equivalent Young's modulus of contact pair (gasket and flange), m/Lt^2, Pa

E_e : Elastic modulus of elastomer, m/Lt^2, Pa

E_s : Young's modulus of casing or target surface, m/Lt^2, Pa

F : Contact load, mL/t^2, N

H : Gasket hardness, m/Lt^2, Pa

K : Hydraulic conductivity, L^2, m^2

P_i : Flange internal pressure, m/Lt^2, Pa

P_e : Flange external pressure, m/Lt^2, Pa

P_f : Fluid pressure at a given location in model domain, m/Lt^2, Pa

R : Radius of curvature at the tip of asperity, L, m

v : Fluid velocity, L, m

Greek Symbols

μ : Fluid Newtonian viscosity, m/Lt, Pa.s

ν_e : Poisson's ratio of elastomer, dimensionless

ν_s : Poisson's ratio of steel casing, dimensionless

τ : Tortuosity, dimensionless

ω : Indentation of asperity, L, m

ϕ : Porosity, dimensionless

References

Abubakar, I. J., Myler, P. and Zhou, E. 2016. Constitutive Modelling of Elastomeric Seal Material under Compressive Loading. Modeling and Numerical Simulation of Material Science: 06(02), 28–40. http://dx.doi.org/10.4236/mnsms.2016.62004.

Ahmed, S., Salehi, S., Ezeakacha, C. P., and Teodoriu, C. 2019a. Evaluation of liner hanger seal assembly and cement sheath as a dual barrier system: Implications for industry standards. Journal of Petroleum Science and Engineering, 178, 1092–1103. http://dx.doi.org/10.1016/j.petrol.2019.04.017.

Ahmed, S., Salehi, S., Ezeakacha, C. P., and Teodoriu, C. 2019b. Experimental investigation of elastomers in downhole seal elements: Implications for safety. Polymer Testing, 76, pp.350–364. http://dx.doi.org/10.1016/j.polymertesting.2019.03.041.

Ahmed, S., Patel, H., Ahmed, S., Salehi, S., and Teodoriu, C. 2020. Numerical and Experimental Evaluation of Liner Dual Barrier System in Geothermal Wells. Presented at 45th Workshop on Geothermal Reservoir Engineering, Stanford University, February 10-12, CA, USA. https://pangea.stanford.edu/ERE/db/GeoConf/papers/SGW/2020/Ahmed.pdf

Akhtar, M., Qamar, S. Z., Pervez, T., and Al-Jahwari, F. K. 2013. FEM Simulation of Swelling Elastomer Seals in Downhole Applications. Proc. of the ASME 2013 International Mechanical Engineering Congress and Exposition, November 15-21, 2013, San Diego, California, USA. http://dx.doi.org/10.1115/imece2013-64312

Al-Hiddabi, S. A., Pervez, T., Qamar, S. Z. et al. 2015. Analytical model of elastomer seal performance in oil wells. Applied Mathematical Modelling: 39(10-11), 2836–2848. http://dx.doi.org/10.1016/j.apm.2014.10.028

Al-Kharusi, M. S. M., Qamar, S. Z., Pervez, T. et al. 2011. Non-Linear Model for Evaluation of Elastomer Seals Subjected to Differential Pressure. Presented at SPE/DGS Saudi Arabia Section Technical Symposium and Exhibition, 15-18 May, Al-Khobar, Saudi Arabia. SPE-149032-MS. https://doi.org/10.2118/149032-MS

Al Ramadan, M., Salehi, S., Kwatia, G., Ezeakacha, C., and Teodoriu, C. 2019a. Experimental investigation of well integrity: Annular gas migration in cement column. Journal of Petroleum Science and Engineering. http://dx.doi.org/10.1016/j.petrol.2019.04.023.

Al Ramadan, M., Salehi, S., Teodoriu, C. 2019b. Robust Leakage Modeling for Plug & Abandonment Applications. ASME 38th International Conference on Ocean, Offshore and Arctic Engineering, Glasgow, Scotland, UK, 9-14 June. OMAE2019-95612.

Al-Yami, A. S., Nasr-El-Din, H. A., Al-Saleh, S., Al-Humaidi, A. S., & Al-Arfaj, M. K. 2008. Lab Investigation of Oil Swelling Elastomers for Smart Well Completions. Europec/EAGE Conference and Exhibition, 9-12 June 2008, Rome, Italy. http://dx.doi.org/10.4043/19403-ms.

Al-Yami, A., Nasr-El-Din, H. A., Al-Humaidi, A. S., Al-Arfaj, M. K., & Al-Saleh, S. H. 2010. Effect of HCl Acid and Brines on Water-Swelling Packers. SPE Drilling & Completion: 25(03), pp.322–327. http://dx.doi.org/10.2118/114812-pa.

Alzebdeh, K., Pervez, T., and Qamar, S.Z. 2010. Finite Element Simulation of Compression of Elastomeric Seals in Open Hole Liners. Journal of Energy Resources Technology: 132(3). 031002. http://dx.doi.org/10.1115/1.4002244

Ansys®, 2018. Workbench 18.2 User Manual

API 6A, Specification for Wellhead and Christmas Tree Equipment, 20th Edition. 2010. Washington, DC: API

API 11D1, Packers and Bridge Plugs, Third Edition. 2015. Washington, DC: API

API Spec 17D, Specification for Design and Operation of Subsea Production Systems—Subsea Wellhead and Tree Equipment, Second Edition. 2011. Washington, DC: API

API Spec 19LH, Liner Hanger Equipment, First Edition. 2019. Washington, DC: API

API 17TR8, High-pressure High-temperature Design Guidelines, First Edition, 2015. Washington, DC: API

API TR 6AF2, Technical Report on Capabilities of API Integral Flanges Under Combination of Loading—Phase II, fifth Edition, April 2013. Washington, DC: API

Apple Rubber Products Inc. 2009. Seal Design Guide. http://www.applerubber.com/src/pdf/seal-design-guide.pdf (Accessed 8 October 2018)

Apple Rubber Products Inc. 2017. Material selection guide. http://www.applerubber.com/src/pdf/section6-material-selection-guide.pdf (Accessed 10 October 2018)

ASTM D430-06, Standard Test Methods for Rubber Deterioration—Dynamic Fatigue. 2018. ASTM International, West Conshohocken, PA, USA.

ASTM D471-12a, Standard Test Method for Rubber Property—Effect of Liquids. 2012. ASTM International, West Conshohocken, PA, USA.

ASTM D573-04, Standard Test Method for Rubber—Deterioration in an Air Oven. 2015. ASTM International, West Conshohocken, PA, USA

ASTM D575-91, Standard Test Methods for Rubber Properties in Compression. 2018. ASTM International, West Conshohocken, PA, USA.

ASTM D623-07, Standard Test Methods for Rubber Property—Heat Generation and Flexing Fatigue In Compression. 2014. ASTM International, West Conshohocken, PA, USA.

ASTM D926-08, Standard Test Method for Rubber Property—Plasticity and Recovery (Parallel Plate Method). 2008. ASTM International, West Conshohocken, PA, USA.

ASTM D945-06. Standard Test Methods for Rubber Properties in Compression or Shear (Mechanical Oscillograph). 2012. ASTM International, West Conshohocken, PA, USA.

ASTM D1349-14, Standard Practice for Rubber—Standard Conditions for Testing, ASTM International, West Conshohocken, PA, USA.

ASTM D2632-15, Standard Test Method for Rubber Property—Resilience by Vertical Rebound. 2015. ASTM International, West Conshohocken, PA, USA.

ASTM D6147-97, Standard Test Method for Vulcanized Rubber and Thermoplastic Elastomer—Determination of Force Decay (Stress Relaxation) in Compression. 2014. ASTM International, West Conshohocken, PA, USA.

ASTM D7121-05. Standard Test Method for Rubber Property—Resilience Using Schob Type Rebound Pendulum. 2018. ASTM International, West Conshohocken, PA, USA.

Banerjee, N., Hills, D.A. and Dini, D., 2009. The derivation and application of a semi-infinite flat and rounded asymptotic frictionless contact. International Journal of Mechanical Sciences: 51(9-10), 662–666. http://dx.doi.org/10.1016/j.ijmecsci.2009.07.003.

Berge, T., Mathisen, K. D., Storebo, O. et al. 2013. Expandable Liner Hanger Milling: North Sea Case Histories. Presented at SPE/IADC Drilling Conference, 5-7 March, Amsterdam, The Netherlands. http://dx.doi.org/10.2118/163568-ms.

Berger, S. 2004. Experimental and Finite Element Analysis of High Pressure Packer Elements. MS Thesis, Massachusetts Institute of Technology, Cambridge, Massachusetts (September 2004)

Bora, C. K., Flater, E. E., Street, M. D. et al., 2005. Multiscale roughness and modeling of MEMS interfaces. Tribology Letters, 19(1), pp.37–48.http://dx.doi.org/10.1007/s11249-005-4263-8.

Bosma, M. G. R., Cornelissen, E. K., and Schwing, A., 2000. Improved Experimental Characterisation of Cement/Rubber Zonal Isolation Materials. Presented at SPE Asia Pacific Oil and Gas Conference and Exhibition, 16-18 October, Brisbane, Australia. SPE-64395-MS. http://dx.doi.org/10.2118/64395-ms

Brown, L. and Witwer, B., 2017. Next Generation HP/HT Wellhead Seal System Validation. Presented at Offshore Technology Conference, 1-4 May, Houston, Texas, USA. http://dx.doi.org/10.4043/27738-ms.

BSEE. 2014. QC-FIT Evaluation of Seal Assembly & Cement Failures Interim Summary of Findings. Internal QC-FIT Report #2014-02, Bureau of Safety and Environmental Enforcement, Washington, DC.

Campion, R. P., Thomson, B., and Harris, J. A. 2005. Elastomers for fluid containment in offshore oil and gas production: Guidelines and review. Research report (RR 320) prepared by MERL Ltd for the Health and Safety Executive, U.K. http://www.hse.gov.uk/research/rrpdf/rr320.pdf

Cantu, J., Smith, P., and Nida, R. 2004. Expandable Liner Hanger Application in Arduous Well Conditions Proves Reliability: A Case History. Presented at SPE Asia Pacific Oil and Gas Conference and Exhibition, 18-20 October, Perth, Australia. SPE-88510-MS. https://doi.org/10.2118/88510-MS

Carroll, T. 2016. Successful selection of oil and gas seals. World Pumps: 2016(9), 28–30. http://dx.doi.org/10.1016/s0262-1762(16)30235-8.

Chang W. R., Etsion, I. I., and Bogy, D. B. 1987. An Elastic-Plastic Model for the Contact of Rough Surfaces. *ASME Journal of Tribology*: **109**(2), 257-263. http://dx.doi.org/10.1115/1.3261348.

Chen, X., Bartos, J., Salem, H., et al. 2016. Elastomers for High Pressure Low Temperature HPLT Sealing. Presented at Offshore Technology Conference, 2-5 May, Houston, Texas, USA. http://dx.doi.org/10.4043/27227-ms.

Ciavarella, M., Hills, D.A. and Monno, G. 1998. The influence of rounded edges on indentation by a flat punch. Proceedings of the Institution of Mechanical Engineers, Part C: Journal of Mechanical Engineering Science: 212(4), 319–327. http://dx.doi.org/10.1243/0954406981521259

Cong, C., Cui, C., Meng, X. et al. 2013. Degradation of hydrogenated nitrile-butadiene rubber in aqueous solutions of H2S or HCl. Chemical Research in Chinese Universities: 29(4), 806–810. http://dx.doi.org/10.1007/s40242-013-2401-7

Daemar Inc. 2015. Causes of O-Ring Failure. Retrieved from http://daemar.com/o-rings_causesoffailure_117.html/ (Accessed on August 3, 2018

Dagle, O., Johnson, J., and Moeller, D. 2016. Metal-to-Metal Sealing and Anchoring Expandable Hanger in Gulf of Mexico: Development, Collaboration, and Execution. Presented at SPE Deepwater Drilling and Completions Conference, 14-15 September, Galveston, Texas, USA. SPE-180304-MS. https://doi.org/10.2118/180304-MS

Dajiang, Z., Yuanhua, L., Huali, Z. et al. 2017. Experimental studies on CO2 corrosion of rubber materials for packer under compressive stress in gas wells. Engineering Failure Analysis: 80, 11-23. https://doi.org/10.1016/j.engfailanal.2017.01.012

Daou, F., de Miranda, C. R., de Oliveira, J. L., Engelke, B., Borman, C., Le Roy-Delage, S., and Lungwitz, B. 2014. Swelling of Elastomers in CO2 Environment: Testing Methodology and Experimental Data. Presented at SPE Latin America and Caribbean Petroleum Engineering Conference, 21-23 May, Maracaibo, Venezuela. http://dx.doi.org/10.2118/169277-ms.

Denison, C.R., Fiore, C.J. & Krakowski, F.J. 2018. Application of Wear-Resistant Elastomer to Significantly Improve Service Life of Telescopic Joint Packers. Presented at Offshore Technology Conference, 30 April - 3 May, Houston, Texas, USA. http://dx.doi.org/10.4043/28918-ms.

Dolog, R., Ventura, D., Khabashesku, V., and Darugar, Q. 2017. Nano-Enhanced Elastomers for Oilfield Applications. Presented at Offshore Technology Conference, 1-4 May, Houston, Texas, USA. http://dx.doi.org/10.4043/27609-ms.

Dragoni, E. and Strozzi, A. 1988. Analysis of an Unpressurized, Laterally Restrained, Elastomeric O-Ring Seal. Journal of Tribology: 110(2), 193. http://dx.doi.org/10.1115/1.3261583.

Edmond, K., Ho, E., Flitney, R. et al. 2001. Comparison of Explosive Decompression Test Protocols for Elastomer Seals in High Pressure Gas Service. Presented at NACE International CORROSION 2001, 11-16 March, Houston, Texas. https://www.onepetro.org/conference-paper/NACE-01109

Elhard, J. D., Duguid, A., and Heinrichs, M. 2017. Research on Safety Technology Verification for Materials and Pressure High Temperature (HPHT) Continental Shelf (OCS), High Corrosions in the U.S. Outer Material Evaluation. Technical Assessment Program Report (TAP 767AA) prepared for Bureau of Safety and Environmental Enforcement. https://www.bsee.gov/tap-technical-assessment-program/research-on-safety-technology-verification-for-materials-and

Era polymers. 2019. Elastomer Properties. http://www.erapol.com.au/technical/elastomer/properties/ (Accessed on 10 June 2019)

Fakoya, M.F., Patel, H. and Shah, S.N. 2018. Nanotechnology: Innovative Applications in the Oil and Gas Industry. International Journal of Global Advanced Materials and Nanotechnology.

Fernández, C., and Castaño, P. 2016. Compatibility Behavior of Elastomers for PCP Applications. NACE International: NACE-2016-7106. https://www.onepetro.org/conferencepaper/NACE-2016-7106

Feng, D., Yuan, Y., Tan, B. et al. 2010. Finite Element Analysis of The Packer Rubbers on Sealing Process. Presented at 2010 International Conference on Mechanic Automation and Control Engineering, 26-28 June, Wuhan, China. 11461585. http://dx.doi.org/10.1109/mace.2010.5535502

Feng, Y., Podnos, E., and Gray, K. 2016. Well Integrity Analysis: 3D Numerical Modeling of Cement Interface Debonding. Presented at 50th U.S. Rock Mechanics/Geomechanics Symposium, 26-29 June, Houston, Texas, USA. ARMA-2016-246.

Fothergill, J. 2003. Ratings Standardization for Production Packers. Presented at SPE Production and Operations Symposium, 23-26 March, Oklahoma City, Oklahoma. SPE-80945-MS. https://doi.org/10.2118/80945-MS

Garfield, G. L., and Mackenzie, G. 2007. Recent Metal-To-Metal Sealing Technology for Zonal Isolation Applications Demonstrates Potential for Use in Hostile HPHT Environments. SPE/IADC Drilling Conference. http://dx.doi.org/10.2118/105854-ms.

Green, I. and English, C. 1992. Analysis of Elastomeric O-Ring Seals in Compression Using the Finite Element Method. Tribology Transactions: 35(1), 83–88. http://dx.doi.org/10.1080/10402009208982093.

Green, I. and English, C. 1994. Stresses and Deformation of Compressed Elastomeric O-ring Seals. Presented at 14th International Conference on Fluid Sealing, April 6-8, Firenze, Italy.

Greenwood, J. A., and Williamson, J. B. P. 1966. Contact of nominally flat surfaces. *Proc. of the Royal Society of London*: **A**(295), 300–319. https://doi.org/10.1098/rspa.1966.0242

Greenwood, J. A., and Tripp, J. H. 1970. The contact of two nominally flat rough surfaces. *Proc. of the Institution of Mechanical Engineers*: **185**(1), 625-634. https://doi.org/10.1243/PIME_PROC_1970_185_069_02

Groves, S., Page, N., & Embury, P. 2001. Seal Life Prediction for Critical Offshore Service. Presented at NACE International CORROSION 2001, 11-16 March, Houston, Texas. https://www.onepetro.org/conference-paper/NACE-01108

Guo, Z., Li, Q., Wang, Y. et al. 2011. Analysis and structural improvement of the rubber part in packer in a way of non-linearity finite element. 2011 Second International Conference on Mechanic Automation and Control Engineering, 15-17 July, Hohhot, China. 12242645. https://dx.doi.org/10.1109/mace.2011.5986860

Harish, A. 2018. Modeling Elastomers Using FEM: Do's and Dont's. https://www.simscale.com/blog/2016/08/tips-modeling-elastomers-using-fem/ (Accessed 4 October 2019)

Hearn, E. J. 1997. Mechanics of Materials I: An Introduction to the Mechanics of Elastic and Plastic Deformation of Solids and Structural Materials, Third Edition. Jordan Hill, Oxford: Butterworth-Heinemann.

Hogan, M., Gunderson, R. H., and Stevenson, A. 1997. Seal Life Prediction for Critical Offshore Service. Presented at NACE International Corrosion97, 9-14 March, New Orleans, Louisiana. https://www.onepetro.org/conference-paper/NACE-97079

Holand, P. 2017. Loss of Well Control Occurrence and Size Estimators, Phase I and II. Report prepared for Bureau of Safety and Environmental Enforcement. Report #ES201471/2, Washington, DC.

Hu, G., Zhang, P., Wang, G. et al. 2017. The influence of rubber material on sealing performance of packing element in compression packer. Journal of Natural Gas Science and Engineering: 38(Feb 2017), 120–138. https://doi.org/10.1016/j.jngse.2016.12.027

Humphreys, A. T., and Ross, R. C. 2009. Delivering a Fully Qualified HP/HT Production Packer Following Field Failure. SPE Drill & Compl: 24(01). SPE-105736-PA. https://doi.org/10.2118/105736-PA

ISO 10423:2009. Petroleum and natural gas industries -- Drilling and production equipment -- Wellhead and christmas tree equipment, fourth edition, 2009. Geneva, Switzerland.

ISO 13533:2001. Petroleum and natural gas industries -- Drilling and production equipment -- Drill-through equipment, first edition, 2001. Geneva, Switzerland.

ISO 13628-4:2010. Petroleum and natural gas industries -- Design and operation of subsea production systems -- Part 4: Subsea wellhead and tree equipment, second edition, 2010. Geneva, Switzerland.

ISO 14310:2008. Petroleum and natural gas industries -- Downhole equipment -- Packers and bridge plugs, second edition, 2008. Geneva, Switzerland.

ISO 23936-2:2011. Petroleum, petrochemical and natural gas industries -- Non-metallic materials in contact with media related to oil and gas production -- Part 2: Elastomers, first edition, 2011. Geneva, Switzerland.

Izon, D., Danenberger, E. P., and Melinda, M. 2007. Absence of fatalities in blowouts encouraging in MMS study of OCS incidents 1992-2006. Drilling Contractor: July/August 2017, 84-90. http://drillingcontractor.org/dcpi/dc-julyaug07/DC_July07_MMSBlowouts.pdf

Jakel, R. 2010. Analysis of Hyperelastic Materials with MECHANICA – Theory and Application Examples. Presented at the 2nd SAXSIM, 27 April, Technische Universität Chemnitz, Germany. http://qucosa.de/fileadmin/data/qucosa/documents/5995/data/Analysis_of_Hyperelastic_Materials_with_MECHANICA.pdf (Accessed 12 October 2018)

James Walker. 2017. Elastomer Engineering Guide. https://www.jameswalker.biz/de/pdf_docs/148-elastomer-engineering-guide (Accessed 28 August 2018)

John, H. 1997. Elastomers in Mud Motors for Oil Field Applications. Presented at NACE International Corrosion97, 9-14 March, New Orleans, Louisiana. https://www.onepetro.org/conference-paper/NACE-97085

Jimenez, C., Soto, S., Leon, A. et al. 2009. New Liner-Hanger Technology Improves Safety and Reduces Non-Productive Time in Deviated High-Temperature Wells in South Central Venezuela. Presented at SPE Annual Technical Conference and Exhibition, 4-7 October, New Orleans, Louisiana. SPE-124396-MS. https://doi.org/10.2118/124396-MS

K C Seals Inc. 2018. Compression set. Image retrieved from https://kcseals.ca/blog/10-blog/165-compression-set-and-why-its-important.html (Accessed 11 October 2018)

Kiran, R., Teodoriu, C., Dadmohammadi, Y. et al. 2017. Identification and evaluation of well integrity and causes of failure of well integrity barriers (A review). Journal of Natural Gas Science and Engineering, 45: 511-526. http://dx.doi.org/10.1016/j.jngse.2017.05.009.

Krishna, C. and Lefrancois, M. 2016. Metal Seal Technologies in Subsea Applications. Presented at Offshore Technology Conference, 2-5 May, Houston, Texas, USA. http://dx.doi.org/10.4043/26912-ms.

Kwatia, G., Al Ramadan, M., Salehi, S, and Teodoriu, C. 2019. Enhanced Cement Composition for Preventing Annular Gas Migration. ASME 38th International Conference on Ocean, Offshore and Arctic Engineering, Glasgow, Scotland, UK, 9-14 June. OMAE2019-95589.

Lamb, K. 2014. Metal Seals for Critical Valve Applications. Valve World: 19(9), 125-127. Available at https://cdn.thomasnet.com/ccp/30155420/237602.pdf (Accessed on March 1st 2019).

Lehr, D. and Furlan, W. 2017. Seal Life Prediction and Design Reliability in Downhole Tools. Presented at SPE Annual Technical Conference and Exhibition, 9-11 October, San Antonio, Texas, USA. http://dx.doi.org/10.2118/187133-ms.

Li, W., Wang, Y., and Miao, D. 2015. Finite Element Analysis on Rubber Sealing Ring of the Rotary Liner Hanger Bearing. Proc. of the 2015 International Conference on Modeling, Simulation and Applied Mathematics, 23-24 August 2015, Phuket, Thailand. http://dx.doi.org/10.2991/msam-15.2015.52.

Lin, Z. C. 2013. The Strength Analysis and Structure Optimization of Packer Slip Based on ANSYS. Applied Mechanics and Materials: 423-426, 1967–1971. https://doi.org/10.4028/www.scientific.net/AMM.423-426.1967

Lindley PB. 1967. Compression characteristics of laterally–unrestrained rubber O-rings. J. Inst. Rubber Ind: 1(4), 209–213.

Liu, Q., Wang, Z., Lou, Y., and Suo, Z. 2014. Elastic leak of a seal. Extreme Mechanics Letters: 1, 54–61. http://dx.doi.org/10.1016/j.eml.2014.10.001

Lohoefer, C. L., Mathis, B., Brisco, D. et al. 2000. Expandable Liner Hanger Provides Cost-Effective Alternative Solution. Presented at IADC/SPE Drilling Conference, 23-25 February, New Orleans, Louisiana. SPE-59151-MS. https://doi.org/10.2118/59151-MS

Ma, M., Jia, W., Bu, Y. et al. 2014a. Study on Rubber Seal Design of a Swellpacker in Oil Well Cementing. Open Access Library Journal: 01(09), 1–8. http://dx.doi.org/10.4236/oalib.1101082

Ma, W., Qu, B., and Guan, F. 2014b. Effect of the friction coefficient for contact pressure of packer rubber. Proc. of the Institution of Mechanical Engineers, Part C: Journal of Mechanical Engineering Science: 228(16), 2881–2887. http://dx.doi.org/10.1177/0954406214525596

Mackenzie, G. and Garfield, G. 2007. Wellbore Isolation Intervention Devices Utilizing a Metal-to-Metal Rather Than an Elastomeric Sealing Methodology. Presented at SPE Annual Technical Conference and Exhibition, 11-14 November, Anaheim, California, U.S.A. http://dx.doi.org/10.2523/109791-ms.

Mandelbrot, B. 1967. How Long Is the Coast of Britain? Statistical Self-Similarity and Fractional Dimension. Science, 156(3775), pp.636–638. http://dx.doi.org/10.1126/science.156.3775.636.

Marco Rubber & Plastic Inc. 2018. O-Ring Failure Analysis Guide. https://www.marcorubber.com/o-ring-failure.htm (Accessed on August 3 2018)

Mccormick, J., Matice, M., and Cramp, S. 2012. Big Bore Expandable Liner Hangers for Offshore and Deepwater Applications Reduces Cost and Increases Reliability : Global Case History. Presented at SPETT 2012 Energy Conference and Exhibition, 11-13 June, Port-of-Spain, Trinidad. SPE-158856-MS. https://doi.org/10.2118/158856-MS

Mohamed, A.O. and Al-Zuraigi, A. 2013. Liner Hangers Technology Advancement and Challenges. Presented at SPE Middle East Oil and Gas Show and Conference, 10-13 March, Manama, Bahrain. http://dx.doi.org/10.2118/164367-ms

Molari, P.G. 1973. Stresses in O-ring Gaskets. Proc. 6th Int. Conf. on Fluid Sealing BHRA.

Moore, M.J., Campo, D.B., Hockaday, J. et al. 2002. Expandable Liner Hangers: Case Histories. Presented at Offshore Technology Conference, 6-9 May, Houston, Texas. OTC-14313-MS. https://doi.org/10.4043/14313-MS.

Morgan, G., Martin, R., and Thomson, B. 2008. Improvements to Materials Qualification Testing – Updating NORSOKM710. Presented at Oilfield Engineering With Polymers, 7-8 October, London, U.K.

Mullins, F. 2016. Metal-Formed Liner Hanger Avoids High-Setting-Pressure Requirements. Journal of Petroleum Technology: 68(01), 4-8. https://doi.org/10.2118/0116-0022-JPT

NACE TM0187-2011. Evaluating Elastomeric Materials in Sour Gas Environments, 2011. NACE International, Houston, TX, USA.

NACE TM0192-2012. Evaluating Elastomeric Materials in Carbon Dioxide Decompression Environments, 2012. NACE International, Houston, TX, USA.

NACE TM0296-2014-SG. Evaluating Elastomeric Materials in Sour Liquid Environments, 2014. NACE International, Houston, TX, USA.

NACE TM0297-HD1997-SG. Effects of High-Temperature, High-Pressure Carbon Dioxide Decompression on Elastomeric Materials, 1997. NACE International, Houston, TX, USA.

NORSOK M-710, Qualification of non-metallic materials and manufacturers – Polymers, Revision 2, 2001. Lysaker, Norway: Standards Norway.

NORSOK D-010, Well integrity in drilling and well operations, Revision 4, 2013. Lysaker, Norway: Standards Norway

Oil & Gas iQ. 2015. High Pressure High Temperate, High Costs, High Stakes? https://www.oilandgasiq.com/content-auto-download/5b04c1b543dfd0385d3c7c22 (Accessed 4 October 2018)

Parco Inc. 2013. Elastomer selection guide. http://www.parcoinc.com/pdfs/Elastomer-Selection-Guide.pdf (Accessed on 21 May 2018)

Patel, H., Hariharan, H., Bailey, G., and Jung, G. 2018. Advanced Computer Modelling for Metal-to-Metal Seal in API Flanges. Presented at SPE Annual Technical Conference and Exhibition, 24-26 September, Dallas, Texas, USA. http://dx.doi.org/10.2118/191636-ms

Patel, H., Salehi, S., Ahmed, R., and Teodoriu, C. 2019a. Review of elastomer seal assemblies in oil & gas wells: Performance evaluation, failure mechanisms, and gaps in industry standards. Journal of Petroleum Science and Engineering, 179, pp.1046–1062. http://dx.doi.org/10.1016/j.petrol.2019.05.019.

Patel, H., Salehi, S., Teodoriu, C., and Ahmed, R. 2019b. Performance evaluation and parametric study of elastomer seal in conventional hanger assembly. Journal of Petroleum Science and Engineering: 175, 246–254. http://dx.doi.org/10.1016/j.petrol.2018.12.051.

Patel, H., and Salehi, S. 2019. Investigation of Elastomer Seal Energization: Implications for Conventional and Expandable Hanger Assembly. Energies 2019: 12(4), 763; https://doi.org/10.3390/en12040763

Patel, H. and Salehi, S. 2020. A Novel Approach For Modelling Leakage Through Elastomer Seals. Paper # OTC-30491-MS to be presented at Offshore Technology Conference, May 4-8, Houston, TX, USA.

Payne, C. W., Warneke, J. S., and Kaculi, J. T. 2016. Liner Hanger Rating Methodologies Validated with Physical Testing. Presented at Offshore Technology Conference, 2-5 May, Houston, Texas, USA. OTC-26945-MS. http://dx.doi.org/doi:10.4043/26945-MS

Perez Rafols, F. 2016. Modelling and numerical analysis of leakage through metal-to-metal seals. Thesis. Luleå University of Technology, Luleå, Sweden.

Persson, B. N. J. 2006. Contact mechanics for randomly rough surfaces. *Surface Science Reports*: **61**(4), 201–227. http://dx.doi.org/10.1016/j.surfrep.2006.04.001.

Pervez, T., Qamar, S. Z., Siddiqui, R. A., and Van de Velden, M. 2009. Effect pf exposure on material response of a swelling elastomer. International Scientific Journal: 37(2), 77-84.

Qamar, S. Z., Al-Hiddabi, S. A., Pervez, T., and Marketz, F. 2009. Mechanical Testing and Characterization of a Swelling Elastomer. Journal of Elastomers & Plastics: 41(5), 415–431. http://dx.doi.org/10.1177/0095244309105248

Rodriguez, F., Cohen, C., Ober, C. K., and Archer, L. A. 2003. Principles of Polymer Systems, Fifth Edition. Taylor and Francis. http://dx.doi.org/10.1201/b12837

Ruddock, D. 2006. Completion Systems. In: Petroleum Engineering Handbook, Vol. 4, ed. Lake, L.W. Chap. 2, 41-103. Richardson, Texas: Society of Petroleum Engineers.

Sackfield, A., Mugadu, A., Barber, J., et al. 2003. The application of asymptotic solutions to characterizing the process zone in almost complete frictionless contacts. Journal of the Mechanics and Physics of Solid: 51(7), 1333–1346. http://dx.doi.org/10.1016/s0022-5096(03)00020-6.

Salehi, S.; Ezeakacha, C.P.; Kwatia, G.; Ahmed, R.; Teodoriu, C. 2019. Performance verification of elastomer materials in corrosive gas and liquid conditions. Polym. Test. 75, 48–63. http://dx.doi.org/10.1016/j.polymertesting.2019.01.015.

Salehi, S., and Patel, H. 2019. Assessing Mechanical Integrity of Expanding Cement. Presented at SPE Oklahoma City Oil & Gas Symposium, April 9-10, Oklahoma City, OK, USA. https://doi.org/10.2118/195225-MS

Shadravan, A. & Amani, M., 2012. HPHT 101: What Every Engineer or Geoscientist Should Know about High Pressure High Temperature Wells. SPE Kuwait International Petroleum Conference and Exhibition. Available at: http://dx.doi.org/10.2118/163376-ms.

Slay, J. B., & Ray, T. W. 2003. Fluid Compatibility and Selection of Elastomers in Oilfield Completion Brines. NACE International CORROSION 2003, 16-20 March, San Diego, California. https://www.onepetro.org/conference-paper/NACE-03140

Slay, B. 2008. Performance Testing of Seals for Oilfield Service. Presented at Oilfield Engineering with Polymers, 7-8 October, London, U.K.

Slay, J.B. and Ferrell, K. 2008. Proper Performance Testing to Maintain Seal Integrity in Deepwater Completions. Presented at Offshore Technology Conference, 5-8 May, Houston, Texas, USA. http://dx.doi.org/10.4043/19626-ms.

Smith, P., and Williford, J. 2006. Case Histories : Liner-Completion Difficulties Resolved With Expandable Liner-Top Technology. Presented at Canadian International Petroleum Conference, 13-15 June, Calgary, Alberta. PETSOC-2006-103. https://doi.org/10.2118/2006-103

Speer, M. 2006. Introduction to Wellhead Systems. In: Petroleum Engineering Handbook, Vol. 2, ed. Lake, L.W. Chap. 8, 344-369. Richardson, Texas: Society of Petroleum Engineers.

Stautzenberger, A., Baird, S., and Lundgård, G. 2016. Expandable Liner Hanger Technology Provides Metal-to-Metal Sealing and Improved Anchoring Solution for ERD Wells : Case History in North Sea. Presented at SPE Bergen One Day Seminar, 20 April, Grieghallen, Bergen, Norway. SPE-180012-MS. https://doi.org/10.2118/180012-MS

Strozzi, A. 1986. Experimental Stress-Strain Field in Elastomeric O-Ring Seals. Experimental Stress Analysis: 613–622. http://dx.doi.org/doi:10.1007/978-94-009-4416-9_67

Strozzi, A. 1986. Static Stresses in an Unpressurized, Rounded, Rectangular, Elastomeric Seal. A S L E Transactions: 29(4), 558–564. http://dx.doi.org/10.1080/05698198608981720.

Strozzi, A., Bertocchi, E., Mantovani, S., et al. 2015. Analytical evaluation of the peak contact pressure in a rectangular elastomeric seal with rounded edges. The Journal of Strain Analysis for Engineering Design: 51(4), 304–317. http://dx.doi.org/10.1177/0309324715612300.

Substech. 2018. Shore (Durometer) hardness test. Image retrieved from http://www.substech.com/dokuwiki/doku.php?id=shore_durometer_hardness_test (Accessed 15 October 2018)

Tu, B. and Cheng, H.L. 2016. Alternative Methodology for Elastomeric Seal RGD and Aging Testing Validates Long-Term Subsea Seal Performance and Integrity. Presented at Offshore Technology Conference, 2-5 May, Houston, Texas, USA. http://dx.doi.org/10.4043/27125-ms.

Tynan, C. 2016. Successful selection of oil and gas seals. World Pumps: 2016(9), 28-30. ISSN 0262-1762. http://dx.doi.org/10.1016/S0262-1762(16)30235-8

Upton, T. L. 2009. Improving the Reliability of Slip Joint Packer Systems. Presented at SPE/IADC Drilling Conference and Exhibition, 17-19 March, Amsterdam, The Netherland. SPE-119292-MS. https://doi.org/10.2118/119292-MS

Van Dort, R. 2009. Metal-to-Metal Seals Meet Downhole Hazard Demands. Journal of Petroleum Technology. 61(01), 24–26. SPE-0109-0024-JPT. https://doi.org/10.2118/0109-0024-JPT

Walvekar, S., and Jackson, T. 2007. Development of an Expandable Liner-Hanger System To Improve Reliability of Liner Installations. Presented at Offshore Technology Conference, 30 April-3 May, Houston, Texas, USA. OTC-18730-MS. https://doi.org/10.4043/18730-MS

Wang, X., Sadana, A.K. and Mathur, V. 2015a. Water-Swellable Elastomers for Heavy Brine Environments. Presented at SPE Annual Technical Conference and Exhibition, 28-30 September, Houston, Texas, USA. http://dx.doi.org/10.2118/174825-ms.

Wang, J., Han, X., Wang, J. et al. 2015b. Research on Packer Material Stress Analysis. Proc. of the 2015 Asia-Pacific Energy Equipment Engineering Research Conference, 13-14 June, Zhuhai, China. https://doi.org/10.2991/ap3er-15.2015.47

Wang, Z., Chen, C., Liu, Q. et al. 2017. Extrusion, slide, and rupture of an elastomeric seal. Journal of the Mechanics and Physics of Solids: 99, 289–303. https://doi.org/10.1016/j.jmps.2016.12.007

Welch, J. C., Newman, C. R., Gerrard, D. P., Mazyar, O. A., Mathur, V., and Thieu, V. 2012. Nano-enhancement of Elastomers for Improved Downhole Barrier Performance. Presented at SPE Deepwater Drilling and Completions Conference, 20-21 June, Galveston, Texas, USA. http://dx.doi.org/10.2118/147409-ms.

Wendt, G. 1971. Investigation of Rubber O-ring and X-rings, 1. Stress Distributions, Service and Groove Design. BHRA Fluid Engineering, Internal Report T1115.

Whitehouse, D.J. and Archard, J.F. 1970. The Properties of Random Surfaces of Significance in their Contact. Proceedings of the Royal Society A: Mathematical, Physical and Engineering Sciences, 316(1524), pp.97–121. http://dx.doi.org/10.1098/rspa.1970.0068.

Williford, J. W., and Smith, P. E. 2007. Expandable Liner Hanger Resolves Sealing Problems and Improves Integrity in Liner Completion Scenarios. Presented at Production and Operations Symposium, 31 March-3 April, Oklahoma City, Oklahoma, USA. SPE-106757-MS. https://doi.org/10.2118/106757-MS

Yu, C., Xu, Z., Shyu, G. D., and Prieto, C. 2017. Development of Advanced Seal Material and Downhole Packer for High Temperature Applications. Presented at Offshore Technology Conference, 1-4 May, Houston, Texas, USA. http://dx.doi.org/10.4043/27538-ms.

Zhao, Y., Maietta, D. M., and Chang, L. An Asperity Microcontact Model Incorporating the Transition from Elastic Deformation to Fully Plastic Flow. *Journal of Tribology*: **122**(1), 86. http://dx.doi.org/10.1115/1.555332

Zhong, A., Johnson, M., Kohn, G., et al. 2015. Performance Evaluation of a Large Bore Expandable Liner Hanger for Field Operations in the Gulf of Mexico. Presented at Offshore Technology Conference, 04-07 May, Houston, Texas, USA. http://dx.doi.org/10.4043/25995-ms

Zhong, A., 2016. Challenges for High-Pressure High-Temperature Applications of Rubber Materials in the Oil and Gas Industry. Conference Proceedings of the Society for Experimental Mechanics Series, 65–79. http://dx.doi.org/10.1007/978-3-319-21765-9_10.

Zhong, A., Moeller, D. and Maddux, S. 2017. Development of a High Hang Weight Expandable Liner Hanger for Deepwater Applications. Presented at Offshore Technology Conference, 1-4 May, Houston, Texas, USA. http://dx.doi.org/10.4043/27542-ms

Appendix A: Biography

Harsh Patel is a PhD graduate in Petroleum Engineering from The University of Oklahoma, USA. He also holds MS and BTech degrees in petroleum engineering from The University of Oklahoma and Pandit Deendayal Petroleum University (India) respectively.

During graduate studies, Harsh successfully executed 14 research projects sponsored by DOE, BSEE, BP, Schlumberger, Halliburton, API, and few other leading organizations. He also has industry experience of working at Shell, McDermott, and ONGC during his academic journey. His research portfolio includes variety of areas - well construction and integrity, fluids and cement, elastomer/metallic seals, flow assurance, and hydraulic fracturing. His expertise is computational modelling research for solving interdisciplinary engineering problems related to fluid flow, contact mechanics, fluid-solid interactions, particles transport, mechanical integrity, etc.

As a graduate student, Harsh published more than 20 technical papers, 1 SPE book chapter, and 10 international conference presentations (LinkedIn, Google scholar). He has received 14 prestigious national and university level awards which include - best research assistant in the university, dissertation fellowship award across all disciplines at the university, distinguished PhD student award for two consecutive years, 1st place in national level research presentation competition, gold medal for highest academic excellence, and few other scholarships from different organizations and government. He is an active member of SPE, AADE, and also serves as technical reviewer for leading journals by Elsevier, SPE, MDPI, ASME, SAGE etc.